



UNIVERSITI PUTRA MALAYSIA

***BROKEN ROTOR BAR FAULT DETECTION IN LINE START-
PERMANENT MAGNET SYNCHRONOUS MOTOR***

MOHAMMAD REZAZADEH MEHRJOU

FK 2016 162



**BROKEN ROTOR BAR FAULT DETECTION IN LINE START-
PERMANENT MAGNET SYNCHRONOUS MOTOR**

By

MOHAMMAD REZAZADEH MEHRJOU

**This thesis Submitted to the School of Graduate Studies, Universiti Putra
Malaysia, in Fulfillment of the Requirements for the Degree of
Doctor of Philosophy**

October 2016

© COPYRIGHT UPM



COPYRIGHT

All Material contained within the thesis, including without limitation text, logos, icon, photographs and all other artwork, is copyright material of Universiti Putra Malaysia unless otherwise stated. Use may be made of any material contained within the thesis for non-commercial purposes from the copyright holder. Commercial use of material may only be made with the express, prior, written permission of Universiti Putra Malaysia.

Copyright © Universiti Putra Malaysia



DEDICATION

To my Parents: Ail and Iran
my Parents in law: Amrolah, Afsar
my lovely Wife, Firoozeh Danafar,
my caring Son: Radin, and
my Family



Abstract of thesis presented to the Senate of Universiti Putra Malaysia in fulfillment of the requirement for the degree of Doctor of Philosophy

**BROKEN ROTOR BAR FAULT DETECTION IN LINE START-
PERMANENT MAGNET SYNCHRONOUS MOTOR**

By

MOHAMMAD REZAZADEH MEHRJOU

October 2016

Chairman : Professor Norman Mariun, PhD, PEng
Faculty : Engineering

High efficiency motors are being gradually exerted in many industrial applications because of their positive impacts on the environment by reducing energy consumption and CO₂ emission. In this regard, Line Start Permanent Magnet Synchronous Motors (LS-PMSMs) have been introduced to the market recently. Due to the unique configuration, LS-PMSMs are allowed to reach Super Premium Efficiency levels accompanied with high torque and power factor. However, since the use of LS-PMSMs in industry is in its infancy, no efficient scheme has been reported for faults detection in this type of motor. Online monitoring and setting of preventive maintenance programs in the industries is one of the important issues. Therefore, in order to classify different indices of motor under fault condition, the electrical behavior of LS-PMSMs motor under broken rotor bar should be considered and the electrical parameters should be characterized. The main aim of this research is to investigate the effects of broken rotor bar fault on LS-PMSMs performance, and also to find reliable fault-related feature for this fault. The proposed detection strategy for broken rotor bar in LS-PMSM is based on monitoring of startup current signal. In this regard, a simulation model and experimental setup for investigation of broken rotor bar in LS-PMSM is obtained. The current signal is used to extract the fault-related features using three different signal processing method. Finally, the ability of these features is validated for detection of broken rotor bar in LS-PMSM through statistical analysis. This study can be beneficial for the industry by using the online monitoring systems where the motor fault can be detected during its operation. Therefore, the proposed method can be used in the preventive maintenance programs.

This research indicates the importance of load effects on broken bar detection in LS-PMSMs. The current signal is collected at different load levels of starting torque within four steps, which increases from 0% to 65%. The experimental and simulation results substantiate that increasing the load, will also increase the starting time duration. The time duration of machine with one broken rotor bar also increases compared to healthy

condition. The value of starting torque drops in the presence of broken rotor bar fault. In the time domain analysis, three features, namely peak to peak, shape factor and impulse factor cannot distinguish faulty state of motor from healthy state based on upward or downward trend. Skewness also fails to detect broken bar when the starting torque is high. In time domain analysis using of envelop signal, four features, namely RMS, RSSQ, Energy and Variance cannot distinguish faulty state of motor from healthy state at low level load. The variance feature also fails to detect the fault based on upward or downward trend. When the starting torque is high, Kurtosis feature is not a suitable feature to detect broken rotor bar. In the time-frequency domain analysis, Log Energy Entropy feature has satisfactory performances for broken rotor bar detection compare to Shannon Entropy feature. The result also presents that the most effective sub-band frequency is Detail of level 7 that includes the frequency band ranges of [39.06-19.53]Hz. The simulation results were validated with an experimental work to confirm the effectiveness of proposed methods.



Abstrak tesis yang dikemukakan kepada Senat Universiti Putra Malaysia sebagai memenuhi keperluan untuk ijazah Doktor Falsafah

**PENGESANAN KEROSAKAN BAR ROTOR PECAH DALAM MOTOR
SEGERAK MAGNET KEKAL MULA TALIAN**

Oleh

MOHAMMAD REZAZADEH MEHRJOU

Oktober 2016

Pengerusi : Profesor Norman Mariun, PhD, PEng
Fakulti : Kejuruteraan

Motor kecekapan tinggi sedang digunapakai secara berperingkat dalam pelbagai aplikasi industri kerana kesan positifnya terhadap alam sekitar dengan mengurangkan penggunaan tenaga dan pelepasan CO₂. Dengan itu, Motor Segerak Magnet Kekal Mula Talian (LS-PMSMs) telah diperkenalkan baru-baru ini. Oleh kerana konfigurasi yang unik, LS-PMSMs membolehkan motor untuk mencapai tahap kecekapan super premium dengan disertai tork dan faktor kuasa yang tinggi. Walau bagaimanapun, sejak penggunaan LS-PMSMs dalam industri di peringkat awal, tidak ada lagi sistem cekap yang dilaporkan untuk mengesan kerosakan motor ini. Pemantauan dalam talian dan penetapan program penyelenggaraan pencegahan dalam industri adalah salah satu isu penting. Oleh itu, untuk mengelaskan indeks motor yang berbeza dalam keadaan rosak, tingkah laku elektrik motor LS-PMSMs di bawah bar rotor pecah perlu dipertimbangkan dan parameter elektrik harus dicirikan. Matlamat utama kajian ini adalah untuk mengkaji kesan kerosakan bar rotor pecah pada prestasi LS-PMSMs, dan untuk mencari ciri-ciri kaitan kerosakan ini. Strategi pengesanan untuk bar rotor pecah pada LS-PMSM dicadangkan di sini di mana ianya adalah berdasarkan pemantauan isyarat semasa permulaan. Dalam hal ini, model simulasi dan persediaan eksperimen untuk siasatan bar rotor pecah dalam LS-PMSM diperolehi. Isyarat semasa digunakan untuk mengekstrak ciri yang berkaitan dengan kerosakan menggunakan tiga kaedah pemprosesan isyarat yang berbeza. Akhir sekali, keupayaan ciri-ciri ini disahkan untuk mengesan bar rotor pecah dalam LS-PMS motor melalui analisis statistik. Kajian ini boleh memberi manfaat kepada industri dengan menggunakan sistem pemantauan dalam talian di mana kerosakan motor boleh dikesan semasa operasinya. Oleh itu, kaedah yang dicadangkan boleh digunakan dalam program-program penyelenggaraan pencegahan.

Kajian ini menunjukkan betapa pentingnya kesan beban pada pengesanan bar rotor pecah dalam LS-PMSMs. Isyarat semasa dikumpulkan dalam tahap beban yang berbeza pada tork yang bermula dalam empat langkah, yang meningkat dari 0% hingga

65%. Keputusan eksperimen dan simulasi mengesahkan bahawa peningkatan beban akan juga meningkatkan tempoh masa permulaan. Tempoh masa mesin dengan satu bar rotor pecah juga meningkat jika berbanding keadaan normal. Selain itu, bar rotor pecah juga memberi kesan pada kejatuhan nilai permulaan tork. Dalam analisis domain masa, tiga ciri, iaitu puncak ke puncak, faktor bentuk dan faktor dorongan tidak dapat membezakan kerosakan nyata motor dalam keadaan normal berdasarkan trend ke atas atau ke bawah. Kepencongan juga gagal untuk mengesan bar rotor pecah apabila permulaan tork tinggi. Dalam analisis domain masa menggunakan isyarat envelop, empat ciri, iaitu RMS, RSSQ, Tenaga dan Varians tidak dapat membezakan kerosakan nyata motor pada keadaan normal yang berada pada tahap rendah beban. Ciri varians juga gagal untuk mengesan kerosakan berdasarkan trend ke atas atau ke bawah. Apabila tork permulaan yang tinggi, ciri Kurtosis adalah tidak sesuai untuk mengesan bar rotor pecah. Dalam analisis domain masa-frekuensi, ciri Log Tenaga Entropy mempunyai prestasi yang memuaskan bagi pengesanan bar rotor pecah jika dibandingkan dengan ciri Shannon Entropi. Keputusan juga menunjukkan sub-band frekuensi yang berkesan adalah Perincian Tahap 7 yang merangkumi julat jalur frekuensi bagi [39,06-19,53] Hz. Oleh itu, keputusan eksperimen dan simulasi menyokong antara satu sama lain dan mengesahkan kerja-kerja secara keseluruhan.

ACKNOWLEDGEMENTS

In the Name of Allah, Most Gracious, Most Merciful, all praise and thanks are due to Allah, and peace and blessings be upon His Messenger. I would like to express the most sincere appreciation to those who made this work possible; family, supervisory members and friends.

I would like to express my great gratitude to my respected supervisor Professor Ir. Dr. Norman Mariun for his invaluable advice and comments, constant encouragement, guidance, support and patience all the way through my study work. Equally the appreciation extends to the supervisory committee members Professor Dr. Norhisam Misron and Associate Professor Dr. Mohd. Amran Mohd. Radzi for providing me the opportunity to complete my studies under their valuable guidance.

I would also like to thank and appreciations my friends: Dr. Mahdi Izadi, Mr. Suleiman musa and other my colleagues for their constant support and help through the work.

I would also like to acknowledge the Electrical Engineering Department of Universiti Putra Malaysia for providing the numerous facilities and support for this research work and to Ministry of High Education Malaysia for financial support through grant number FRGS-5524356.

I certify that a Thesis Examination Committee has met on 14 October 2016 to conduct the final examination of Mohammad Rezazadeh Mehrjou on his thesis entitled "Broken Rotor Bar Fault Detection in Line Start-Permanent Magnet Synchronous Motor" in accordance with the Universities and University Colleges Act 1971 and the Constitution of the Universiti Putra Malaysia [P.U.(A) 106] 15 March 1998. The Committee recommends that the student be awarded the Doctor of Philosophy.

Members of the Thesis Examination Committee were as follows:

Ishak bin Aris, PhD

Professor
Faculty of Engineering
Universiti Putra Malaysia
(Chairman)

Hashim bin Hizam, PhD

Associate Professor
Faculty of Engineering
Universiti Putra Malaysia
(Internal Examiner)

Mohammad Hamiruce Marhaban, PhD

Professor
Faculty of Engineering
Universiti Putra Malaysia
(Internal Examiner)

Martin Moreno Francisco, PhD

Professor
Malaga University
Spain
(External Examiner)



NOR AINI AB. SHUKOR, PhD
Professor and Deputy Dean
School of Graduate Studies
Universiti Putra Malaysia

Date: 28 February 2017

This thesis submitted to the Senate of Universiti Putra Malaysia and has been accepted as fulfilment of the requirement for the degree of Doctor of Philosophy. The members of the Supervisory Committee were as follows:

Norman Mariun, PhD, Ir

Professor
Faculty of Engineering
Universiti Putra Malaysia
(Chairman)

Norhisam Misron, PhD

Professor
Faculty of Engineering
Universiti Putra Malaysia
(Member)

Mohd. Amran b. Mohd. Radzi, PhD

Associate Professor
Faculty of Engineering
Universiti Putra Malaysia
(Member)

ROBIAH BINTI YUNUS, PhD

Professor and Dean
School of Graduate Studies
Universiti Putra Malaysia

Date:

Declaration by graduate student

I hereby confirm that:

- this thesis is my original work;
- quotations, illustrations and citations have been duly referenced;
- this thesis has not been submitted previously or concurrently for any other degree at any other institutions;
- intellectual property from the thesis and copyright of thesis are fully-owned by Universiti Putra Malaysia, as according to the Universiti Putra Malaysia (Research) Rules 2012;
- written permission must be obtained from supervisor and the office of Deputy Vice-Chancellor (Research and Innovation) before thesis is published (in the form of written, printed or in electronic form) including books, journals, modules, proceedings, popular writings, seminar papers, manuscripts, posters, reports, lecture notes, learning modules or any other materials as stated in the Universiti Putra Malaysia (Research) Rules 2012;
- there is no plagiarism or data falsification/fabrication in the thesis, and scholarly integrity is upheld as according to the Universiti Putra Malaysia (Graduate Studies) Rules 2003 (Revision 2012-2013) and the Universiti Putra Malaysia (Research) Rules 2012. The thesis has undergone plagiarism detection software.


Signature: _____ Date: _____


Name and Matric No: Mohammad Rezazadeh Mehrjou, (GS31472)

Declaration by Members of Supervisory Committee


This is to confirm that:

- the research conducted and the writing of this thesis was under our supervision;
- supervision responsibilities as stated in the Universiti Putra Malaysia (Graduate Studies) Rules 2003 (Revision 2012-2013) are adhered too.

Signature: 
Name of
Chairman of
Supervisory
Committee: Professor Ir. Dr. Norman Mariun

Signature: 
Name of
Member of
Supervisory
Committee: Professor Dr. Norhisam Mison

Norhisam Mison, Dr. Eng.
Professor
Department of Electrical and Electronic Engineering
Faculty of Engineering, Universiti Putra Malaysia
43400 UPM Serdang, Selangor

Signature: 
Name of
Member of
Supervisory
Committee: Associate Professor Dr. Mohd Amran Mohd Radzi

DR. MOHD AMRAN MOHD RADZI
Associate Professor
Department of Electrical and Electronic Engineering
Faculty of Engineering
Universiti Putra Malaysia
43400 UPM Serdang

TABLE OF CONTENTS

	Page
ABSTRACT	i
ABSTRAK	iii
ACKNOWLEDGEMENTS	v
APPROVAL	vi
DECLARATION	viii
LIST OF TABLES	xii
LIST OF FIGURES	xiii
LIST OF ABBREVIATIONS	xv

CHAPTER

1	INTRODUCTION	1
	1.1 General Background	1
	1.2 Problem Statement	2
	1.3 Aim and Objectives	3
	1.4 Thesis Scope	3
	1.5 Contribution of the Thesis	4
	1.6 Thesis Layout	4
2	LITERATURE REVIEW	6
	2.1 Introduction	6
	2.2 Line Start Permanent Magnet Motor	8
	2.2.1 Structure	8
	2.2.2 Operation	9
	2.3 Motor Fault	11
	2.3.1 Rotor Fault	13
	2.3.2 Secondary Failures Caused by Broken Rotor Bar	13
	2.4 Condition Monitoring Techniques	14
	2.4.1 Acoustic Noise Monitoring	16
	2.4.2 Air Gap Torque Monitoring	17
	2.4.3 Stator Current Monitoring	19
	2.4.4 Electromagnetic Field Monitoring	24
	2.4.5 Instantaneous Angular Speed Measurement	25
	2.4.6 Power Analysis	26
	2.4.7 Motor Circuit Analysis	27
	2.4.8 Vibration Monitoring	28
	2.4.9 Voltage Monitoring	28
	2.5 Signal Processing Techniques	30
	2.5.1 Time Domain Analysis	30
	2.5.2 Frequency Domain Analysis	32
	2.5.3 Time-Frequency Domain Analysis	33
	2.6 Broken Rotor Bar Fault Detection in Induction Machine	34
	2.7 Research Trends in LS-PMSM	43
	2.8 Summary	44

3	METHODOLOGY	46
3.1	Introduction	46
3.2	Simulation of Electrical Motor with Finite Element Method	47
3.3	Experimental Design	50
3.3.1	Experimental Devices	51
3.3.2	PicoScope and MATLAB Software	58
3.4	Sampled Signals Procedure	59
3.5	Signal Processing Procedure	60
3.5.1	Time Domain Analysis	60
3.5.2	Time-Frequency Domain Analysis	64
3.6	Statistical Analysis	72
3.7	Summary	73
4	RESULT AND DISCUSSION	74
4.1	Introduction	74
4.2	Performance of LS-PMSM with presence of fault	74
4.2.1	Simulation Result	74
4.2.2	Experimental Result	78
4.3	Data Processing for Fault Detection	79
4.3.1	Time Domain Analysis	80
4.3.2	Time-Frequency Domain Analysis	97
4.4	Summary	99
5	CONCLUSION AND FUTURE RECOMMENDATIONS	103
5.1	Conclusion	103
5.2	Future works and Recommendations	105
	REFERENCES	106
	APPENDICES	123
	BIODATA OF STUDENT	144
	LIST OF PUBLICATIONS	145

LIST OF TABLES

Table		Page
2.1	Rotor Assembly Stresses	12
2.2	The correlations proposed for estimation of rotor fault severity	24
2.3	Summary of published paper with the aim of broken rotor bar detection in IM	35
3.1	Specification of YSB-2.5	53
3.2	Wavelet functions	69
3.3	Frequency ranges for wavelet decomposition of signal	70
4.1	Analysis of variance for dimensional parameter features in time domain analysis	83
4.2	P-value calculation from post- hoc test procedure for dimensional parameter features in time domain analysis	83
4.3	Analysis of variance for non-dimensional parameter features in time domain analysis	88
4.4	P-value calculation from post-hoc test procedure for non-dimensional parameter features in time domain analysis	88
4.5	Analysis of variance for dimensional parameter features in envelope analysis	92
4.6	P-value calculation from post- hoc test procedure for dimensional parameter features in envelope analysis	92
4.7	Analysis of variance for non-dimensional parameter features in envelope analysis	96
4.8	P-value calculation from post-hoc test procedure for non-dimensional parameter features in envelope analysis	97
4.9	Analysis of variance for Entropy features using “dmey” mother wavelet in Detail of level 7	98
4.10	P-value calculation from post-hoc test procedure for Entropy features using “dmey” mother wavelet in Detail of level 7	98
4.11	P-value signification from post-hoc test procedure for features in approximation of level 6	100
4.12	P-value signification from post-hoc test procedure for features in Detail of level 7	101
4.13	P-value signification from post-hoc test procedure for features in approximation of level 7	102

LIST OF FIGURES

Figure		Page
2.1	Two broken rotor bars at the end rings	7
2.2	The structure and configuration of the LS-PMSM (Four Pole)	8
2.3	Torque components of an LS-PMSM	10
2.4	Rotor Faults in Electrical Machines	12
2.5	Illustration of rotor bar current and magnetic flux in the existence of a broken rotor bar	20
2.6	Effect of broken rotor bar in MMF of rotor	21
2.7	Time–frequency propagation of the rotor fault components	44
3.1	Methodology Employed in Research Design	46
3.2	The geometry of the LS-PMSM with one Broken Rotor Bar	48
3.3	Cross-Section of LS-PMSM with Mesh Plotting	48
3.4	The detailed process of model solving in Maxwell 2-D	49
3.5	Illustration of experimental set up	51
3.6	Experimental test rig	51
3.7	(a) LS-PMSM used in this research and (b) its nameplate	52
3.8	Demonstration of the rotor with one broken bar	52
3.9	Electromagnetic Power Brake Model YSB-1.2	54
3.10	Lovejoy coupling	54
3.11	Demonstration of the current measurement board	55
3.12	Torque sensor and its indicator	56
3.13	Demonstration of the magneto-type detector (MODEL MP-981)	56
3.14	PicoScope 4424	57
3.15	Voltage differential probe model TA041	58
3.16	PicoScope 6 environment	58
3.17	The transient stator current signals that selected for processing	59
3.18	Figure 3.17: The transient current signal and its envelope a) healthy motor, b) faulty motor	63
3.19	Illustration of the principle of Time–Frequency resolution for wavelet transform and STFT approach	65
3.20	Dyadic Wavelet Decomposition Algorithm	68
3.21	Filtering Process	69
3.22	Behavior f_{LSH} during the start-up	70
3.23	Theoretical behavior of f_{LSH} as a function of slip	71
4.1	(a) The symmetrical magnetic flux distribution in the healthy motor, (b) The asymmetrical magnetic flux distribution in the faulty motor	75
4.2	Rotating Magnetic Field produces a Force on Squirrel Cage Rotor	76
4.3	Magnetic Force in Starting Torque (a) Healthy and (b) Faulty Motor	76
4.4	The Comparison of Maximum Starting Torque [2.3 Nm] for (a) Healthy and (b) Faulty Motor	77
4.5	Simulation Current signal in four-load condition for Healthy and Faulty motor	78
4.6	Comparison the result of starting time in different load	78

4.7	Experimental current signal in four-load condition for Healthy and Faulty motor	79
4.8	Comparison the result of starting time in different load based on the mean value of 40 Samples for each load	79
4.9	Trend and Boxplot for dimensional features in time domain analysis (a) Mean, (b) RMS, (c) RSSQ, (d) Peak to Peak and (e) Energy	82
4.10	Trend and Boxplot for non-dimensional features in time domain analysis a) Shape Factor, b) Impulse Factor, c) Crest Factor, d) Margin Factor, e) Peak-to-average power ratio, f) Variance, g) Skewness and h) Kurtosis	86
4.11	Trend and Boxplot for dimensional features in envelope analysis a) Mean, b) Root Mean Square (RMS), c) RSSQ, d) Peak to Peak and e) Energy	91
4.12	Trend and Boxplot for non-dimensional features in envelope analysis a) Shape Factor, b) Impulse Factor, c) Crest Factor, d) Margin Factor, e) Peak-to-average power ratio, f) Variance, g) Skewness and h) Kurtosis	95



LIST OF ABBREVIATIONS

a	Wavelet scale
$A_{m0,n}$	Approximate coefficients
AC	Alternative current
b	Wavelet position
B_{ag}	Air-gap flux density
CWT	Continuous wavelet transform
c_1	T_{Cage} correction factor
$D_{m,n}$	Detail coefficients
DC	Direct current
DFT	Discrete Fourier transform
DWT	Discrete wavelet transform
f_{brb}	Broken rotor bar frequency feature
f_{jbrb}	Fluctuating frequency related to broken rotor bar
f_{LSH}	Left Sideband Harmonic Frequency
f_r	Rotor frequency
f_s	Sampling frequency
f	Fundamental frequency
f_{sh}	Rotor slot harmonic frequency
$f_{T\pm}$	Frequency related to electromagnetic torque
f_{Tbrb}	Frequency related to the broken rotor bar fault in torque spectrum
FFT	Fast Fourier transform
GUI	Graphical Interface Unit
$i(t)$	Instantaneous stator current
$i_A, i_B, \text{ and } i_C$	Three-phase line currents
$I_{(1-2ks)f}^K$	Amplitude for harmonic component $f_{(1-2ks)f}$
$I_{(1+2ks)f}^K$	Amplitude for harmonic component $f_{(1+2ks)f}$
I_f	Amplitude of stator current at fundamental frequency
I_{PN}	Primary nominal RMS
I_p	Primary current
J	Total moment of inertia
k	$k = 1,2,3, ..$
$k' = 1 \text{ or } 0$	When exists or not effect of saturation
LS-PMSM	Line start permanent magnet motor
l_x	Length of the rotor
$l = 1,2,3, ...$	The rotor slot related harmonic rank number
MCSA	Motor current signature analysis
MMF_{ag}	Air-gap magneto-motive force
μ	The rotor harmonic rank number
N_R	The number of rotor bars
m	Stator phases
N_{BRB}	The number of broken rotor bar
n	Rotor speed
n'	A sum or difference of any two integers $n'=2,-1, 0, 1, 2, ...$
n_{sys}	Synchronous speed

n_{RATED}	Rated asynchronous speed
p	Number of pole pairs
P_{ag}	Air-gap permeance
R	Half of the line-to-line resistance
R_c	The contact resistance between the bar and the rotor core
R_b	Number of broken bars
RMS	Root mean square
RSH	Rotor slot harmonics
R_1	Stator resistance
R'_2	Rotor resistance referred
s	Slip
S_{RF}	Severity of the fault
STFT	Short-time Fourier transform
T_{Break}	Dynamic braking torque
T_{Cage}	Cage torque
T_{Load}	Load torque
T_{Sync}	Synchronous torque
v	The stator harmonic rank number
v_{AB}, v_{BC}, v_{CA}	Line to Line voltages
V_{ph}	rms phase voltage
W	Window position
W_{cwt}	Continuous wavelet coefficient
ω_{bMMF}	Speed of the backward MMF with respect to the stator
ω_m	Rotor speed
ω_{syn}	Synchronous speed
X_1	Stator leakage reactance
X'_2	Rotor leakage reactance referred
Z_b	The bar impedance
ψ	Mother wavelet or wavelet functions
ω	Angular frequency
ω_s	Electrical synchronous speed
ϕ	Scaling functions or scaling functions
ϕ_s	Stator angular position
ϕ	Main phase shift angle of stator current
$\phi_{(1-2ks)f}^k$	Phase shift angle of harmonic component $f_{(1-2ks)f}$
$\phi_{(1+2ks)f}^k$	Phase shift angle of harmonic component $f_{(1+2ks)f}$
θ_m	Mechanical rotor position
δ	Load angle (rad)

CHAPTER 1

INTRODUCTION

In this chapter, after presenting the research problem statement, the aim and objectives and scopes of this dissertation are presented. A short background about the extent of this research work is discussed and the contribution to the knowledge is specified. This chapter ends with the layout of the thesis.

1.1 General Background

Electrical machines facilitate and expedite production processes and related services leading to immense changes in the human life style. They are extensively employed in the entire aspects of domestic, industrial, commercial, utility and special-purpose commercial markets. The rugged configuration of squirrel-cage electrical machines (induction machine) with reasonable price and size make them suitable for all these applications. The other desired characteristics of squirrel-cage electrical machines are their adaptability and operation with an easily available power supply because of using squirrel-cage bars. However, induction machines suffer from low efficiency and low power factor that means the loss of energy is high. This issue is viewed as an important disadvantage because of the energy cost and global energy concerns.

The improvement of induction machine efficiency was examined through an optimal design of these motors. However, due to several inherent limitations, it is difficult to improve the efficiency of its significantly. An option is to substitute induction machine by high efficiency permanent magnet Synchronous motors (PMSMs). An important obstacle for ordinary PMSMs is they need inverter to start, which is not economical for single speed applications. To overcome this problem, the permanent magnet motors equipped with squirrel-cage bars, called Line Start Permanent Magnet Synchronous motors (LS-PMSMs), have been introduced. LS-PMSMs also allow reaching Super Premium Efficiency levels [1,2]. A LS-PMSM consists of a stator (single or poly-phase) and a hybrid rotor comprising electricity conducting squirrel cage and pairs of permanent magnet poles. Squirrel-cage bars in electrical machine produce adequate high starting torque when the motor is run from standstill. Similar to asynchronous motors, squirrel-cage bars in LS-PMSM develop the startup performance during motor run up by enabling the rotor to have direct-on-line movement. When the load situation is unbalanced or the rotation speed is fluctuated, an important role of squirrel-cage bars is to lessen the counter-rotating fields of the air gap, which otherwise would lead to significant losses [3].

In the practical applications, LS-PMSMs are subjected to unavoidable stresses, such as electrical, environmental, mechanical and thermal stresses. These stresses produce some failures and imperfections in different parts of the LS-PMSMs. The created faults disturb the safe operation of the LS-PMSMs, threaten the normal manufacturing, and therefore result in the substantial cost penalties. An efficient fault

detection technique can reduce the maintenance costs by preventing the high expense failures and unscheduled downtimes.

Breakage of the rotor bars is usually the serious failure in the squirrel cage motors, because it progressively increase different stresses and also brings possible secondary failures in machine. These failures will also reduce the motor efficiency, threaten its safe operation, shorten its lifetime and thus increase the operational cost. Broken rotor bar generates unbalanced currents and torque pulsation, and as a result reduces the developed torque and increases the speed fluctuations of the motor [4]. Changes in the rotor current distribution due to bar breakage progressively deteriorates the condition of the neighboring bars. For instance, once a bar breaks, the current in the neighboring bars increases up to 50% of rated current and overheat them [5,6]. The overheated bars bow and cause the rotor bends over that results an eccentricity, which causes basic rotor unbalance and a greater unbalanced magnetic pull [7]. Broken rotor bar may also cause a shaft vibration that results failures in bearing and eccentricity in the air gap [8]. In permanent magnet motor, the extra heat can also demagnetize the permanent magnets [9]. During operation of the motor, the broken rotor bar may rise out itself, or broken pieces of the rotor bar may exit the slot due to the centrifugal force and damage the stator windings or laminations [10]. Broken rotor bar is mainly accounted for noise during the motor start-up as well as destructive sparking that threatens the operation safety [11]. Accordingly, diagnosis of broken bars in electrical machine can preserve its good performance and its normal lifetime [12]. As the LS-PMSMs have a hybrid rotor with squirrel-cage bars and permanent magnets, it is not distinct from this part, broken rotor bars can also occur in this motor.

Manufacturing companies are making great efforts to ensure proper condition of the motors by predicting motors imperfection and failures using machinery maintenance plan. The maintenance plans are relied on observation of the machines operating condition for diagnosing the existent failure at an early stage, *i.e.* before it causes the machines to stop. An operative condition monitoring technique that can manifest the situation of electrical machine in order to detect the fault is a key requirement of maintenance. This system should be able to detect any change in the machine quantities to predict the necessity of maintenance before major breakdown occurs. Hitherto, a variety of condition monitoring techniques, which monitor a certain parameter of the electrical machines allowing its health to be determined, have been developed [13].

1.2 Problem statement

The most recent global motor market survey and forecast assumes that the number of low voltage motors sold between 2014 and 2019 will increase by 11% and IE4 appears on the horizon with 1.5% of the global market share of motors by 2019 [14]. The LS-PMSMs are the latest electrical machine selection of researchers owing to their high efficiency and power density, quiet operation and compact size. The LS-PMSMs provide efficiency close to NEMA Super Premium Efficiency standard

(IE4). As the number of LS-PMSMs used in different fields is increasing, presence of maintenance scheme for fault detection in this type of motor becomes important and vital. Early detection of irregularity in the motor with a proper fault diagnosis scheme will help to prevent high cost failures and hence reduces maintenance costs and more importantly prevents unexpected downtimes that cease the production and cause loss of financial income. Since, the productivity of LS-PMSM for various applications is in its infancy; the lack of an accurate broken rotor bar fault detection technique does not exist and also no research work is reported in this case. Accordingly, this research intends to investigate the ability of fault-related features for broken rotor bars fault in LS-PMSMs in different signal processing methods.

1.3 Aim and Objectives

The main aim of this dissertation is to study the effects of broken bars that may occur in LS-PMSMs on motor performance and propose a fault-related feature indicative of this failure in LS-PMSMs. In this respect, relevant papers were accurately surveyed and studied to select suitable methods for condition monitoring and signal processing. Research methodology was then designed and conducted according to the objectives of this dissertation. This study embarks on the following objectives:

- to obtain and simulate a three-phase, 4-pole LS-PMSM with different starting torque of case study machine using finite element method in order to procure the stator current signal for both healthy and faulty conditions,
- to investigate the machine performance in the presence of fault,
- to investigate and validate the statistical fault-related features extracted from startup current signal using time domain analysis in order to identify the broken rotor bars fault in simulation and experimental study,
- to investigate and validate the statistical fault-related features extracted from the startup current signals using time domain envelope analysis in order to identify the broken rotor bars fault in simulation and experimental study, and
- to investigate and validate the features extracted from the startup current signals using Wavelet analysis (Time-frequency domain analysis) in order to identify the broken rotor bars fault in simulation and experimental study.

1.4 Thesis Scope

This dissertation provides a comprehensive study on broken rotor bars fault condition monitoring in electrical machine. The main focus is given to introduce features for detection of broken rotor bars fault in three-phase, 4-pole LS-PMSM during the startup operation condition. Accordingly, the effect of broken rotor bars in case study motor is investigated. The accuracy of research outcomes are examined through a professional laboratory examination in addition to a simulation performance. The influence of starting load on fault-related features is investigated and data acquisition has been collected while the motor running at 0%, 21.7%, 43.47% and 65.21% of its rated starting torque. Motor current signature analysis has been selected for condition

monitoring of the motor during its startup operation. The signals acquired through this method are processed using Time and Time-frequency domain to find the feature related to the fault detection in LS-PMSM. At the last stage, statistical analysis is used to validate the method that proposed for fault detection.

A three-phase, 4-pole LS-PMSM is simulated based on finite element method (FEM) using Maxwell 2-D software. The specifications of simulated LS-PMSM and the motor used in the laboratory test exactly match. Three phase sinusoidal voltages are applied to the motor terminals as windings excitation. To obtain the startup current signal of LS-PMSM, a transient solver with time integration method based on backward Euler is employed. In the simulation method, starting loads are obtained and set equal to the load percentages implemented in the experimental activities. Either the current signals of stator obtained through simulation or experiment is then analyzed to extract the fault-related features for fault detection. The obtained features are compared to validate the results and determine the most reliable fault-related features.

The area of current research is limited to the objectives mentioned above in order to investigate the effect of broken rotor bar in three-phase, 4-pole LS-PMSM. Accordingly, investigation on other types of faults, application of further condition monitoring methods and other signal processing techniques are beyond the objectives of this thesis.

1.5 Contribution of the Thesis

- This work is a new research in broken rotor bar detection in LS-PMSM and none of the previous researches published has attempted to detect this fault. The reason is LS-PMSM was launched to the market recently, and its application is growing gradually. The other reason may be the complexity of broken rotor bar detection in LS-PMSM. Detection of broken rotor bar in LS-PMSM is one of the major contributions of this dissertation.
- This research attempts to investigate the effects of broken bar on the performance of machine through simulation and experimental analyses.
- The reliable features are proposed for broken rotor bar detection in three-phase 4-pole LS-PMSM based analysis of transient current signal. The reason for monitoring of stator current is its accessibility, being cost effective and having noninvasive characteristics.
- Finally, this research provides remarkable outcomes for further research in the area of fault detection techniques in LS-PMSMs.

1.6 Thesis Layout

Chapter one presents a brief introduction on the research background of current study. The research requirements are stated as the problem statement to define the key research aspects used. The aim and objectives of the study are listed to

present the focus of the research. Afterward, the scope of research work and relevant contributions are highlighted.

Chapter Two provides an extensive literature review related to the dissertation topic. The general structure of LS-PMSM is described. The broken rotor bars fault and its effects on Squirrel-cage electrical machine are described. Different methods for signal acquisition and signal processing with the purpose of fault detection in electrical machines are comprehensively documented. The chapter ends with research trends in broken rotor bar detection for LS-PMSM.

Chapter three presents the research methodology designed and conducted according to the objectives of this dissertation. In the first section of Chapter three, the simulation of LS-PMSM with finite element method software is introduced. In the second section, full demonstration of experimental set up, devices, instruments is explained. In the final section of this chapter, signal-processing methods implemented in this case study and features used as fault signature are introduced. At the end of chapter, statistical analysis is explained for features validation.

Chapter four presents the results and discussions on the effect of broken rotor bar on startup current captured from LS-PMSM. Different features with three methods of signal processing are discussed and statistical analysis is used to validate the ability of each methods. The relevant explanations and interpretations on the results and observations presented provide a promising conclusion.

Chapter Five finally presents conclusion drawn from this research for broken rotor bar detection in three-phase, 4-pole LS-PMSM, as well as recommendations for future study that can be implemented in the field of fault detection in LS-PMSM.

CHAPTER 2

LITERATURE REVIEW

The aim of this chapter is to presents a comprehensive literature review on various subjects pertaining to the research activities. First, general principles of line-start permanent magnet motors (LS-PMSMs) are described. The focus is then shifted to explanations on failures usually observed in different parts of electrical machine. Since broken rotor bar detection is the aim of this research, different condition monitoring techniques utilized for diagnosis of this failure are introduced and detail description on these techniques are presented. The raw signal obtained from condition monitoring of electrical machine needs to be analyzed to extract the features related to the fault that presents in the machine. Accordingly, the literature review section also contains description of signal processing techniques utilized to interpret the information obtained from condition monitoring.

2.1 Introduction

In every plant or in any service field that offers advantage to the society, there is an electrical machine contributing to the production or services. Electrical machines account for 95% of all prime movers in industrialized nations [15]. A major portion of supplied energy has been provided to generate electric energy whereas nearly 50% of the end-use electricity is consumed by electrical motors [16]. Among various types of the electrical machines, induction machines are consist about 68%, including fans, pumps, air compressors, mixers, conveyors and many other industrial applications [16]. Despite of their wide range of use, induction machines have efficiency and power factor, which are not desired.

An option to address these problems (low efficiency and power factor) is replacing induction machines with permanent magnet synchronous motors (PMSMs). However, a PMSM have several drawbacks including: they lack the starting torque capability comparing to induction machines [17], and they require a variable frequency driver (VFD) system to start. Since VFD is generally expensive, this requirement makes usage of PMSMs uneconomical for those applications where the speed is constant, like fans, pumps and compressors. Noting that constant speed applications form more than 70% of electrical motor applications, however presence of VFD also reduces the overall efficiency and increases the price of using the PMSMs. Taking into account the mentioned drawbacks of PMSMs, replacing induction machines with this type of motor is not considered as an acceptable solution. On the other hand, employing electrical machines of high efficiency is obligatory as the new standards introduced by national electrical manufacturers association (NEMA) and institute of electrical and electronics engineers (IEEE) for electric motors restrict the use of low efficiency electrical motors [17].

In order to have high efficiency electrical motor, which does not suffer from those problems related to PMSMs, as mentioned above, line start permanent magnet

synchronous motors (LS-PMSMs) have been developed. This type of motor have a stator similar to induction machines but its rotor involves an electricity conducting squirrel-cage and pairs of permanent magnet poles. Such structure makes LS-PMSMs as the best alternative to overcome problems pertaining to both induction machines and PMSMs. It is worth mentioning that, LS-PMSMs provide efficiency close to NEMA super premium efficiency (IE4) standard and it is a candidate to reach IE4 standard [2].

Although the electrical machines are robust, failures may happen in some parts of the machines. Electrical machines are often operated in an antagonistic environment, where is corrosive and dusty, and exposed to undesirable situations or miss operations. These conditions make several progressive failures in motor and most of the time put the motor in an unserviceable condition. One of the failures in the electrical machine is those faults generated in different parts of rotor, rotor bars, end rings, rotor bow, and laminations problem. The effects of faulted rotor in electrical machine can be observed as torque fluctuations, unbalanced motor currents, loss increasing, degradation of transient performance and larger thermal pressures [18]. The rotor faults seriously deteriorate the performance of the electrical machines and their efficiency. Figure 2.1 shows a real broken rotor bar in electrical machines. Several case studies were carried out for in situ detection of broken rotor bar in electrical machine in industry [10,19-21].

The percentage of motor failures attributed to rotor problems is not large, but among various defects may occur in electrical machines, rotor failures are of significant importance as they bring about secondary failures and eventually lead to a serious malfunction of motor [13]. Diagnosis of rotor failures has long been an important but complicated task in the area of faults detection in electrical motors.



Figure 2.1: Two broken rotor bars at the end rings [21].

2.2 Line-start permanent magnet motor

The idea of combining the high efficiency permanent magnet synchronous motor with simplicity and starting ability of induction machines results in advent of new generation known as a LS-PMSM. The design of LS-PMSM has been introduced in 1955 [22]. In 1984, Miller presented a study describing the starting process of line-start permanent magnet AC motors [23]. It was stated that “the line start PM motor is a very high efficiency synchronous motor designed to operate at a fixed voltage and frequency from the same power supply as induction machines”[23]. Despite of excellent advantages of LS-PMSM, its application could not be found in the industries because of its high price. Advances in technology of permanent magnet materials that offer synthesis of high-energy permanent magnet materials with affordable prices has recently paved the path for commercialization of the high efficiency LS-PMSMs. As a result, the biggest electrical machine manufacturer (WEG Company) launched in 2015, and the number of LS-PMSM motors employed in different fields is about to increase.

2.2.1 Structure

As mentioned, Stator of LS-PMSM is similar to induction machines, while its rotor is different. Its hybrid rotor involves electricity conducting squirrel cage and pairs of permanent magnet poles. The structure and configuration of the LS-PMSM is depicted in Figure 2.2.

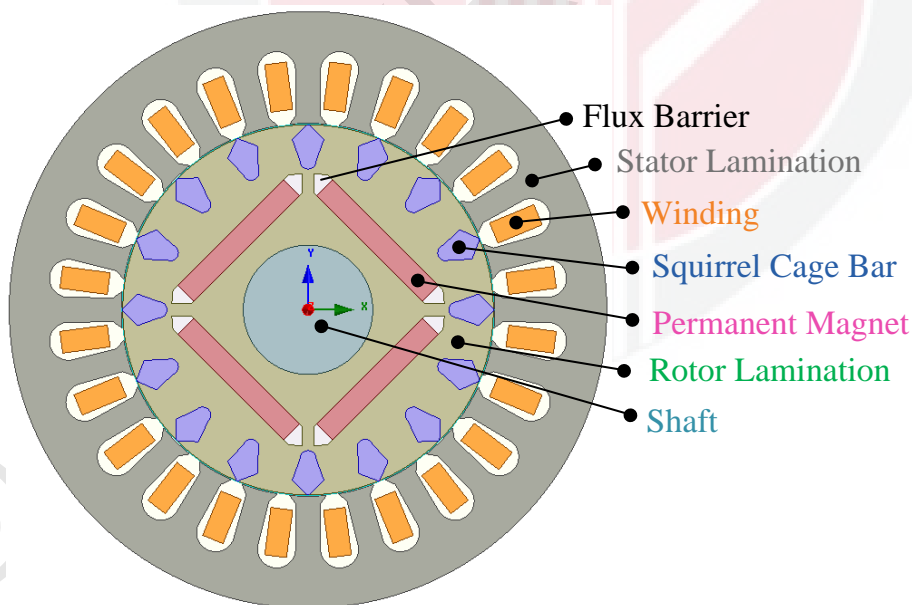


Figure 2.2: The structure and configuration of the LS-PMSM (Four Pole)

2.2.1.1 Stator Parts

The stator is made up of three parts: windings, lamination core and frame. Windings consist of three coils, which are connected to the three-phase power supply and equally distributed along the stator lamination core. Frame mechanically supports both stator and shaft bearings of rotor. Bearings, located on both sides of the end shield, allow the rotor to spin freely inside the stator.

2.2.1.2 Rotor Parts

The rotor is made up of four parts: lamination core, squirrel cage bars, permanent magnet and shaft. The lamination core that mechanically supports other parts of motor consists of laminated sheets made of iron alloy. Another function of lamination core is to concentrate the magnetic flux. The rotor bars, that are short-circuited on both sides by the end rings, circulate electric current from one side to other side of the rotor cage. The outer diameter of the end-rings is equal to the rotor core and both end-rings and rotor bars are made of the same material. The bars, enveloped by a lamination core, bring the rotor speed up to the synchronous speed at startup. Besides, bars moderate any speed fluctuations that may occur as a result of sudden load changes. During steady-state operation, if the load changes abruptly, an oscillatory movement is placed over the normal synchronous rotation of the shaft and the rotor bars minimize these oscillations. The squirrel cage bars can also protect the magnets from demagnetization during the transients associated with the start-up. Permanent magnets are used for the generation of synchronous torque at steady state.

2.2.2 Operation

In synchronous machines, torque is produced if the rotor turns at its synchronous speed (speed of the stator field), where the rotating field of stator is synchronized with the field of rotor. At start-up, field of stator first attracts and then repels the rotor field. Therefore, sufficient torque to start the machine cannot be produced. To overcome this obstacle, rotor bars are placed near the surface of the pole faces of a synchronous motor to bring a motor near to the synchronous speed.

Function of LS-PMSM at start-up is similar to induction machine that is accelerated by a cage torque. However, the running up of the LS-PMSM is quasi-static because of its hybrid structure and hence its speed–torque characteristic is composed of both squirrel-cage IM and the PMSM parts. The transient state of an LS-PMSM is rather complex, compared to induction machine, because different torques, as illustrated in Figure 2.3, affects its behavior. In general, the process of rotor pulling of the LS-PMSM into synchronism is complex and depends on the balance of four components, which form the total torque acting on the motor shaft: (a) synchronous torque T_{Sync} , (b) cage torque T_{Cage} , (c) dynamic braking torque $T_{Break}(s)$ and (d) load torque T_{Load} [24].

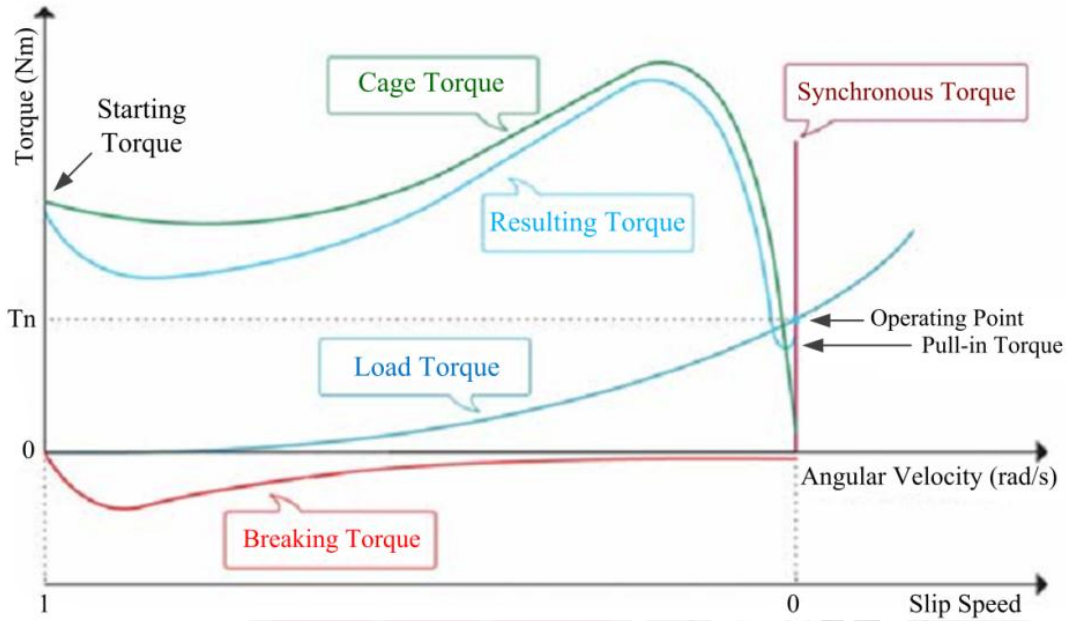


Figure 2.3: Torque components of an LS-PMSM [24]

In the startup, when three phase supply is applied to the stator winding, a rotating magnetic field is created. As the rotating field moves past the bar, a current is induced in rotor bars. The interaction between this current and the rotating air-gap field produces sufficient torque to start the motor. This torque accelerates the motor that overcomes the lag in its speed. Two different types of torque come into the process of starting, cage torque and dynamic braking torque [25].

The dynamic braking torque is resulted from the permanent magnet flux in the rotor. During running up, the permanent magnet rotor field induces a symmetric voltage system of frequency $f_m = p \cdot n$ into the stator winding. This voltage system is not at line frequency; hence the power supply and its impedance represent a short circuit. The resulting phase currents lead to active power expenditure in the stator winding and the power grid impedance. It has to be mechanically covered by the dynamic braking torque [26]. The magnets in the rotor create not only braking torque but also oscillatory torque at all non-synchronous speed.

The cage torque is directly linked and produced by the squirrel cage and accounts for the successful starting the LS-PMSM to near synchronous speed. The cage torque must overcome not only the applied load torque but also the generated dynamic braking torques, which is due to the presence of the permanent magnet during run-up. However the cage must be designed to provide optimum startup torque and a breakdown slip point close enough to synchronize.

When the motor approaches synchronous speed, the level of accelerating torque is lowered and the magnet torque reverses its role and becomes the sole source of accelerating torque. In this situation, no eddy current excluding harmonics field currents flows into the bars. This synchronizing torque from the permanent magnet

must be big enough so as to pull the machine into synchronism. The mechanical equation of LS-PMSM that is called “equation of motion” is given by [24]:

$$-\frac{J\omega_s^2}{p} \cdot s \frac{ds}{d\delta} = T_{\text{Sync}}(\delta) + T_a(s) - T_{\text{Load}}(s) \quad 2.1$$

$$T_a(s) = T_{\text{Break}}(s) + T_{\text{Cage}}(s) \quad 2.2$$

where J is the total moment of inertia of the considered system, ω_s is the Electrical synchronous speed, s is the slip, δ is a Load angle (rad), and p is a Pole pairs and T_a is the average torque. The equation for cage torque is [24]:

$$T_{\text{Cage}}(s) = \frac{mp}{2\pi f} \cdot \frac{sR_2'V_{ph}^2}{(sR_1 + c_1R_2')^2 + s^2(X_1 + c_1X_2')^2} \quad 2.3$$

where m is Stator phases, V_{ph} is rms phase voltage, c_1 is T_{Cage} correction factor, R_1 is Stator resistance, R_2' is Rotor resistance referred, X_1 is Stator leakage reactance and X_2' is Rotor leakage reactance referred. Based on the Equation (2.3), the starting torque of the machine is directly related to the cage resistance (R_2').

2.3 Motor Faults

As electrical machines are usually operated in undesirable situations, like corrosive and dusty environments, and exposed to miss operations, various failures, depending on the structure of machine, may be generated in different parts of them. The failures are generally progressive and result in unserviceable condition for electrical machines [13,27-28]. Despite of diversity in failures happened in electrical machine, the statistical studies of EPRI and IEEE classified these faults into four main categories as rotor faults, stator faults, bearing faults and other faults [29]. As this research concentrates on broken rotor bar, which is a kind of rotor fault, the following paragraphs will only focus on describing of rotor failure in electrical machines. Rotor faults in electrical machines can be mechanical and/or electrical. The most frequently encountered rotor faults for electrical machines are briefly classified in Figure 2.4. These defects come from various stresses, which are summarized in Table 2.1 [30].

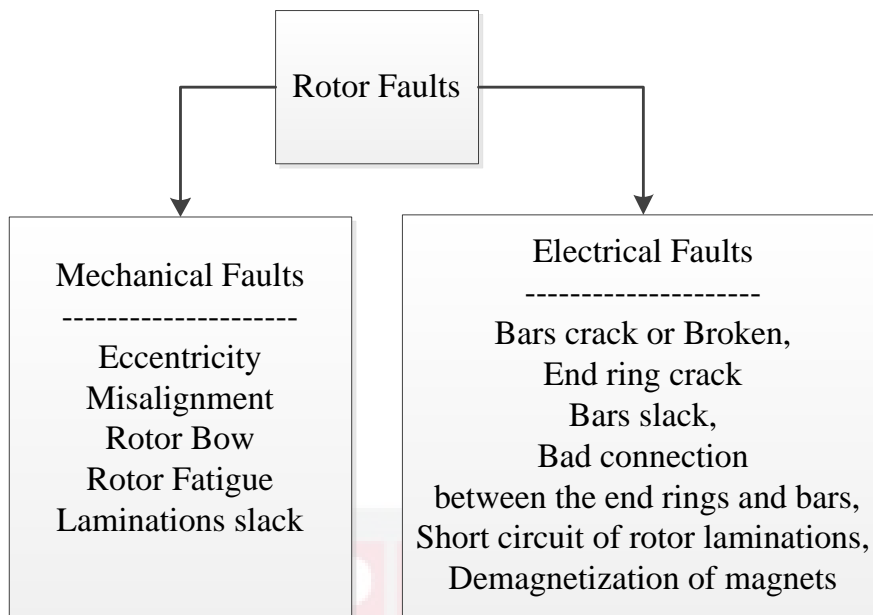


Figure 2.4: Rotor Faults in Electrical Machines

Table 2.1: Rotor Assembly Stresses [30]

Thermal	Environmental
Thermal Overload	Contamination
Thermal Unbalance	Abrasion
Excessive Rotor Losses	Foreign Particles
Hot Spots	Restricted Ventilation
Sparking	Excessive Ambient Temperature
Magnetic	Mechanical
Rotor Pullover	Casting Variations
Noise	Loose Laminations
Vibration	Incorrect Shaft/Core Fit
Off Magnetic Center	Fatigue or Part Breakage
Saturation of Lamination	Poor Rotor to stator Geometry
Circulating Currents	Material Deviations
Residual	Other
Stress Concentrations	Misapplication
Uneven Bar Stress	Poor Design Practices
Dynamic	Manufacturing Variation
Vibration	Loose Bars, Core
Rotor Rub	Transient Torque
Over-speeding	Wrong Direction of Rotation
Cyclic Stresses	
Centrifugal Force	

2.3.1 Rotor fault

The squirrel cage rotor is the inner part of the motors and it is rotated by electromagnetic field, which is induced in its coils by stator field. The rotor then applies the rotational force to the external equipment. Squirrel cage rotor, depending on the construction of the cage, is divided into cast and fabricated rotor. The material used for cast cage is aluminum and the cast cage rotors are generally used in small size motors. Whereas, the material used for fabricated cage is copper and fabricated cage rotors are used for high-power motors. Although the squirrel cage rotor is rugged, rotor defects, such as broken rotor bar, cracked end-ring and bent shaft, do occur. The percentage of motor failures attributed to rotor problems is not too large, but they can cause extensive damage to the motor if left undetected [31].

Broken bar faults may happen due to a variety of reasons, such as mechanical, thermal or magnetic stresses; environmental stresses during motor operation; defects in design of motor structure and its manufacturing [13,28]. Among different types of rotor fault, broken bar and end ring are mainly caused because of manufacturing defects and excessive start-stop cycles or frequent speed changes. Motors of low and medium power generally involve casting rotor bars. Small defects that may occur during casting process cause important failures in the bar and the other reasons mentioned in [10]. In the rotor of high power motor, copper bars are generally connected to the end rings through welding and if this procedures are not performed carefully; some defects are generated [32]. Rotor design plays a key role in the severity of rotor irregularity. If the rotor has a closed bar design, the fault severity is expected to be low because of iron acting of rotor that holds asymmetrical bar in place. Nevertheless, if the rotor has an open bar design, the asymmetrical severity enhances, significantly [31].

The electromagnetic behavior of synchronous machines with a squirrel cage (LS-PMSM) during startup is similar to induction machines. During transient times, when the synchronous machines accelerate from zero speed to synchronous speed, current flows in the rotor bars drastically [33]. Excessive start/stop cycles and/or speed changes cause breakage in damper bars. When a bar breaks, almost no current can flow in this bar and thus will flow in the two adjacent bars. This phenomena, itself, also leads to generating breakage in other bars [34].

2.3.2 Secondary failures caused by broken rotor bar

Rotor bar failures bring about secondary failures in other parts of electrical machine. These secondary failures cause severe malfunctions of the motor and reduce the motor efficiency that increases the operational costs. For example, current in bars adjacent to the broken one increases up to 50% of rated current [6] and thus causes unbalanced currents and torque pulsation, which decrease the average torque [4]. When distribution of rotor current is changed, adjacent bars to broken one are overheated that cause other irregularities [5] and breakage of several other bars [34]. Variation of heating around the bars can also make a bow in rotor and then generates

eccentricity. Rotor eccentricity causes basic rotor unbalance and a greater unbalanced magnetic pull [7]. Moreover, if a broken rotor bar rises out of the slot due to the centrifugal force, the bar will contact the stator winding and damage it. The small pieces come from a broken rotor bar also damage the stator windings and laminations during operation [10]. In addition to the secondary failures from broken rotor bar, mentioned above, this failure leads to a shaft vibration and thus air gap eccentricity [8]. Besides vibration, broken rotor bar also causes sparking and noise during the motor start-up and its normal operation [10,11], which threatens the operation safety. It is evident that during start-up, more excessive vibration, more destructive sparking and louder noise are generated.

According to the explanation above, the effects of broken bar significantly lessen the efficiency and performance of electrical machines and early detection of this failure is essential [35]. Detection of broken rotor bar in its early ages not only secures the motor performance but also reduces risk of other types of failures. When the failure is at its early stage, symptoms of the faults are small and the motor apparently operates normally, therefore, the fault cannot be detected [35]. A relatively large number of studies have been performed on early detection of rotor faults, especially broken rotor bar, in squirrel cage induction machines [13]. However, no study has been reported for broken rotor bars detection in LS-PMSM yet as this type of motor has only been applied recently in different fields. However, due to similarity between LS-PMSM and induction machine, some principles used for broken rotor detection can be taken into account, nevertheless, differences in their structure necessitates a detailed observation.

2.4 Condition Monitoring Techniques

The key for successful fault detection in electrical machines relies on availability of accurate information from them that allows understanding of machine condition. Thus, the basis of any fault detection system is a precise condition monitoring. It can easily be realized from the words that condition monitoring is an act to observe the performance of a device, including electric machines, with the purpose of maintenance strategy. The reliability of condition monitoring techniques depends upon the best understanding of motor characteristics, including electrical and mechanical characteristics, in both healthy and faulty conditions. In this respect, condition monitoring techniques have continuously been developed over the years resulting in a range of available methods for failure diagnosis in electrical devices. Condition monitoring techniques presented for broken rotor bar detection in induction machines, which is the interest of this research, can be classified into the following categories [13]:

- Acoustic Emission,
- Air Gap Torque,
- Stator Current,
- Electromagnetic Field Monitoring,
 - Search coils,
 - Stray Flux,
- Instantaneous Angular Speed,

- Instantaneous Power,
- Motor Circuit Analysis,
- Vibration,
- Voltage.

The output of any condition monitoring technique is a signal indicating fluctuation of a specific parameter, like current, voltage, vibration, torque, etc. of the device. Different signals have been used for fault diagnosing of induction machine [35]. According to the nature of the signals, being invasive and non-invasive, condition monitoring techniques are classified into two main categories [36]. Invasive techniques require disassembly of the machine to introduce specific transducers or to conduct a visual inspection. These techniques utilize special sensors and devices installed on the body of desired motor for measuring some consequences as fault indices. Condition monitoring of an electrical machine based on signals (like acoustic waves, magnetic flux density, speed, temperature, torque and vibration) requires an appropriate sensor (or sensors) installed on the motor. Non-invasive techniques use consequences of the motor terminal current or voltage as indices and thus no need to install any equipment on the body of motor. These techniques allow the health of the motor to be monitored whilst the machine is still in normal operation. Condition monitoring of an electrical machine based on signals like current, instantaneous torque, magnetic flux density (stray flux sensor) and voltage does not require the sensor to be installed inside the machine. Other excellent characteristics of non-invasive techniques that make them trustworthy are as follows [37,38]:

- possibility to be installed outside the machine body,
- no need of any precaution for the installation,
- no interruption in normal operation of motor for measurement because no sensor or special equipment is required,
- using only instrument with reasonable price,
- simplicity of remote measurement of motor parameter from supply and control section,
- no interfere from other measuring devices that present in the practical environment with the measuring system of motor under consideration, and
- feasibility of developing an on-line fault detection system.

Invasive techniques were broadly used for fault diagnosis purposes in the past. However, nowadays these techniques are out of date and not popular. Among various un-invasive techniques for fault diagnosis of electrical machines (namely power, current and voltage signals), measurement of current provides particular advantages. For instance, in the case of applying unbalanced voltages to the motor, diagnosis of other faults and their discrimination from the voltage unbalanced features is difficult. Several other criteria, like sensitivity of the motor current to any failure in the motor and accessibility of appropriate sensors with reasonable price that offer high quality measurement, also suggests measuring stator current signal is the prior for fault diagnosing [35,37].

Condition monitoring techniques of electrical machines can be performed on-line or off-line [39]. On-line monitoring techniques offer inspecting and monitoring of the machine condition while it is under normal operating. On-line monitoring could have attracted a great attention for fault detection in electrical machines because of its advantages addressed as follows [13,39]:

- possibility of acquiring data without disruption of its application,
- ability of direct detection of different faults in electric machines,
- fast response to the fault development,
- proper warning of the crucial failure,
- specifying necessary maintenance,
- planning for optimum maintenance schedules,
- minimum downtime, and
- allowing the users to have necessary spare parts before machine is stripped down.

The important weakness of off-line methods compared to the on-line methods is interruption of the motor operation or its shutdown for measurement. However, there are some circumstances that off-line monitoring offer some advantageous, like reduction in noise contamination, and load and speed repeatability [40].

2.4.1 Acoustic Noise Monitoring

Acoustic emission is the generation of transient elastic wave due to a rapid release of strain energy caused by structural alteration in a solid under stresses [41]. Analysis of acoustic spectrum measured during operation of electrical machine is one of the conventional methods for condition monitoring of electrical machines. Acoustic noise monitoring has widely been applied for detection of bearing faults. However, in [42], Li and Mechefske used this method for detection of rotor faults. They, in a comparative study, demonstrated that the acoustic signatures contain information related to the broken rotor bar in induction machines. Authors finally proposed that the acoustic analysis can be used as a supplementary method for broken rotor bar detection in induction machines.

In 2014, Germen and their co-researchers [43] proposed a special method for detection of both mechanical and electrical failures by microphones. They noted that the failures can be classified based on analysis of the acoustic data recorded by using several microphones simultaneously. The true nature of sound propagation around the running motor provides specific clues about the types of the fault [43]. However, acoustic emission has some disadvantages that influence the reliability of this technique [42,44-46]. First, the acoustic spectrum depends on the motor design and its geometry and thus the noise from one induction machine is different from another motor with different size or geometry. It requires a noise-free environment and a noisy background reduces the accuracy of fault detection using acoustic measurement. The important obstacle is the spectrum obtained by the sensor depends on the position of sensor.

2.4.2 Air Gap Torque Monitoring

In electrical machines, Torque is produced by the tendency of the two component “rotor and stator magnetic fields” to line up their magnetic axes [47]. Currents in the motor windings generate magnetic flux in the air gap between the rotor and stator, and hence the flux linkage produces air gap torque. Almost all failures in electrical machine create harmonics with the special frequencies in the air gap torque. The shape of the air-gap torque indicated whether the unbalance is caused by the cracked rotor bars or by unbalanced stator windings [48]. Due to inherent asymmetry in the machine structure caused by broken rotor bar, the low frequency backward field is strengthen and thus the air gap flux density is distorted [49]. Hsu et al. show that if any rotor defect exists, the torque has one constant component and one fluctuating component. This fluctuating component, which is related to the rotor defect, generates a double-slip frequency in the airgap torque spectrum, as [48]:

$$f_{fbrb} = 2ksf \quad 2.4$$

Where $k = 1, 2, 3, \dots$ is the integer; s : the slip and f : the stator supply frequency or fundamental frequency.

Airgap torque can be determined using two different methods. One is using torque sensor that measures the real value of the air gap torques from machine shaft. The second method is using voltage and current sensors. In this method, current and voltage signals are used to calculate the torque based on mathematical model. Both methods can successfully be applied to find the fault signatures. In the first method, the harmonic index of the electromagnetic torque spectrum for a healthy electrical machine is described by [50]:

$$f_{T\pm} = [\pm v \pm lN_R \left(\frac{1-s}{p}\right) \pm 2k' \pm \mu]f \quad 2.5$$

Where, v : the stator harmonic rank number; μ : the rotor harmonic rank number; $l = 1, 2, 3, \dots$: the rotor slot related harmonic rank number; $k' = 1$ or 0 : when exists or not effect of saturation, respectively; N_R : the number of rotor slot; p : the Number of pole pairs; s : the slip; f : the fundamental frequency.

If broken rotor bar presents, position of the fault's signatures is in the area between f_{T-} and f_{T+} . This harmonic, which is related to the fault, are mutually amplified and can be found through [50]:

$$f_{Tbrb} = f_{T\pm} \pm f_{fbrb} \quad 2.6$$

This method has an important drawback that the diagnosis is sensitive to speed oscillations, because the model used to compute the torque does not consider speed or resistant torque. Another imperative obstacle for this technique is measurement of airgap torque cannot be performed directly and accurately. Practically, the measured pulsating torques of an electrical machine obtained by using torque sensors coupled to the machine shaft are different from the real value of the air gap torques. The

reason is the rotor; shaft and frame in the motors as well as the mechanical load constitute an individual torsional spring system that has their own natural frequency. Most mechanical torque sensors have also their specific natural frequencies and bandwidths [48].

The second method was first proposed for the rotor fault detection based on torque monitoring by [51]. They calculated torque from the line currents and the *emf* across flux sensors placed in the stator windings. In this method, the flux sensors are not essential to determine the electromagnetic torque [52]. In [48] proposed measuring voltages and currents for reconstruction of the airgap torque. They define calculation of airgap torque using measurable motor terminal quantities as:

$$T = \frac{p}{\sqrt{3}} \{ (i_A - i_B) \cdot \int [v_{CA} - R(i_C - i_A)] dt - (i_C - i_A) \cdot \int [v_{AB} - R(i_A - i_B)] dt \} \quad 2.7$$

where i_A , i_B , and i_C are three-phase line currents of an induction machine, v_{CA} and v_{AB} are line-to-line voltages, R is half of the line-to-line resistance, and p is the number of pole pairs.

To derive Equation (2.7), the magnetic paths of three phases were assumed identical. It is known that only interaction between stator currents and fluxes produced by rotor currents yields torque. Although the interactions between stator currents and fluxes produced by the stator currents do not produce torque, these currents can affect the saturation of magnetic paths. Once the leakage reactance and magnetic paths of the three phases become asymmetrical, errors are induced and calculation of air gap torque using Equation (2.7) is not precise [53]. In [52] proposed reconstruction of the airgap torque using voltages and currents measurement based on d-q model. They used the results of their model for detection of end-ring fault at steady state condition under no-load. The harmonic index of the electromagnetic torque spectrum for asymmetric rotor can be described by [52]:

$$f_{T_{brb_1}} = f \cdot \left(\frac{N_R}{p} (1 - s) \pm n' \right) \quad 2.8$$

$$f_{T_{brb_2}} = f \cdot \left(\frac{N_R}{p} (1 - s) \pm n' \right) \pm 4sf \quad 2.9$$

where N_R is the number of rotor slots; p is the number of pole pairs; s is the slip; f is the fundamental frequency and n' is a sum or difference of any two integers $n' = -2, -1, 0, 1, 2, \dots$

In 1998, Wieser and co-researchers developed a special method, called Vienna monitoring [54]. This method uses the output of the current model and voltage model to estimate the electromagnetic torque of an inverter-fed induction machines for on-line monitoring of rotor cage [54-56]. Vienna monitoring method compares the outputs of a reference model (an ideal motor) with a measurement model. For a symmetrical motor, the torque values obtained from these two models should be equal. Any rotor failure, however, leads to different values for torque. Consequently, evaluating the ripple component in the torque difference at the double slip frequency

provides broken bar detection. The difference between the estimated torques obtained from those two models gives an indication of the existence of broken bars.

However, this method is not reliable for light load conditions. Analogous to the method of model reference estimation, Vienna monitoring cannot provide accurate estimation for motor parameters. The reason is to achieve accurate models, it requires various machine parameters, like including stator resistance, rotor reactance and rotor time constant [57]. Vienna monitoring method is not much attractive, because it needs two different sensors (current and voltage), and hence it demands excess costs.

In [58], Thomas et al. proved that the electromagnetic torque calculated for symmetrical healthy motor using measured motor variable scan be used for diagnosis of asymmetric conditions. These results were taken through modeling and simulation of an electrical machine and were justified with practical observation. They compared the result of estimated the air-gap torque by using the detailed machine model and the d-q model [58].

In [59], Da Silva et al. presented a method for condition monitoring of induction machine using data analysis of air gap torque profile in conjunction with a Bayesian classifier. Their method was trained off-line with data sets and provided effective monitoring of induction machines. Since torque oscillations extremely depends on the *rms* value of the supply voltage, it is crucial to find a reliable index, which is less sensitive to the factors other than broken bars fault [60].

2.4.3 Stator Current Monitoring

The current drawn by a healthy electrical machine has a single component at the supply. Any mechanical or magnetic asymmetric generates frequency components in the stator current spectrum of the motor. The value of these induced frequency components correspond to the specific fault presented in the motor. Accordingly, sensing the stator current and extraction of the induced frequencies in the current spectrum can reveal the presence of any failure in electrical machines. It is worth mentioning that the stator current may be monitored during the normal operation of electrical machine or during its start-up. The important role of the frequency components induced in stator current spectrum for fault detection in electrical machine is well documented in [13,28,61]. Motor current signature analysis (MCSA), as a condition monitoring technique, utilizes the results of current spectrum analysis to pinpoint an existing or incipient failure in the electrical machines [62]. Since the objective of this research is early detection of broken rotor bar in LS-PMSMs based on MCSA, following sections will focus on the effects of this failure on the spectrum of stator current.

2.4.3.1 Effect of Broken Rotor Bar Fault on Rotor Magneto-Motive Force

In this section, the effect of broken rotor bar on the rotor magneto-motive force (MMF) and consequently its impact on the stator current waveform will be discussed. The MMF of the rotor can be resolved into the forward component corresponding to the healthy case, which is rotating at synchronous speed, ω_{syn} , with respect to the stator (or $s\omega_{syn}$ with respect to the rotor). However, when a rotor bar cracks, no current can flow through the bar and hence no magnetic flux is generated around that bar (Figure 2.5). In case, there is no magnetic flux around a bar, a non-zero backward rotating field and thus an asymmetry in the rotor MMF is produced. It has to be noted that for a symmetrical rotor with no broken bar the resultant of backward rotating field is zero. The non-zero backward rotating component, which is generated due to the virtual presence of a bar carrying an equal opposite current to the original bar, subject to breakage in the healthy rotor.

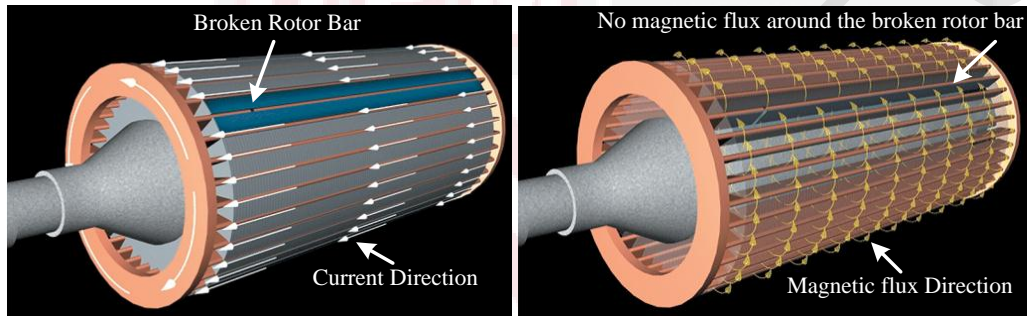


Figure 2.5: Illustration of rotor bar current and magnetic flux in the existence of a broken rotor bar [63]

This non-zero backward MMF due to broken bar rotates at slip frequency corresponding to the slip speed, $s\omega_{syn}$, with respect to the rotor and induces harmonic currents in the stator windings, which are superimposed on the stator winding currents. Accordingly, the speed of the non-zero backward MMF with respect to the stator can be calculated as follow:

$$\omega_{bMMF} = -s\omega_{syn} + \omega_m = -s\omega_{syn} + (1 - s)\omega_{syn} = (1 - 2s)\omega_{syn} \quad 2.10$$

These superimposed features are used as signatures for detection of broken rotor bar in MCSA techniques [64]. Figure 2.6 shows the effect of broken rotor bar faults in MMF of rotor for cage with 16 bars per pair of poles.

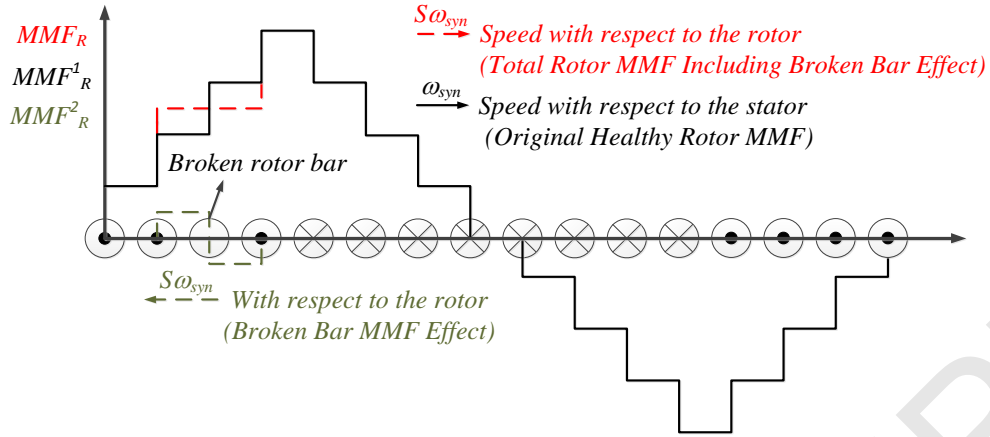


Figure 2.6: Effect of broken rotor bar in MMF of rotor [65]

2.4.3.2 Effect of Broken Rotor Bar in Frequency Domain

The non-zero backward MMF induces an electro motive forces (EMFs) in the stator windings at a frequency equals to $(1 - 2ks)f$ where f is the fundamental frequency, s is slip and $k = 1, 2, 3, \dots$. The fundamental frequency is defined as $= (p/4\pi)\omega_{syn}$, where p is the number of poles and ω_{syn} is synchronous speed. This sideband component appears in the frequency spectrum of the stator around the fundamental frequency in the presence of the cracked or broken rotor bar. It has been indicated that the amplitude of this sideband frequency component is proportional to the number of broken rotor bar that presents in electrical machine [66]. Another parameter that can affect the magnitude of these sidebands is motor-load inertia [28]. Besides, some factors like the mode of supply, the level of load and the motor speed affect the fault detection directly [60].

In fact, the current component with $(1 - 2s)f$ frequency produces a torque pulsation with a frequency equals to $2sf$. Consequently, a speed ripple with the same frequency is generated if the inertia of the rotating mass is not too large. This speed variation then generates another component in the stator current at a frequency equal to $(1 + 2s)f$, which is the right sideband component at a frequency $(1 + 2s)f$. Broken rotor bar indirectly produces the right sideband component at a frequency $(1 + 2s)f$ in the stator current and a speed ripple (or torque pulsation) is created by the right sideband component at twice of slip frequency, $2sf$. The amplitude of the right sideband component at $(1 + 2s)f$ is diminished by an increase in the inertia of the motor-load system. The second component at a frequency $(1 + 2s)f$ in the stator currents induces a current at triple the slip frequency, $3sf$, in the rotor. The later, owing to rotor asymmetry, causes a stator component at frequency $(1 + 4s)f$ as well. If further torque pulsation and speed ripple harmonics are considered, the frequency chain, $((1 - s) \pm ks)f$, with k being equal to odd numbers, appears in the current spectra [67]. Generally, the value of broken rotor bar frequency is taken in to account as $f_{brb} = (1 \pm 2ks)f$. The left sideband component, $f_{brb-} = f_{LSH} = (1 - 2ks)f$, is specifically due to the broken bar while the right sideband component $(1 + 2ks)f_s$ is due to the consequent speed oscillation and saturation phenomena [49,67]. Accordingly, the right sideband component, $f_{brb+} = (1 + 2s)f$, may be used in

monitoring of broken rotor bar and its severity [68]. However, if an external device sets the motor speed, the right-sideband components disappear [49]. In this respects, other spectral components values in the stator line current relevant to the broken rotor bar frequencies were proposed. For example, in [34,69-70] presented broken rotor bar frequencies as:

$$f_{brb} = \left(\frac{k}{p}(1-s) \pm s\right)f \quad 2.11$$

where $k/p = 1,2,3, \dots$

Thomson et al. have shown that the slot harmonic frequencies for a rotor with asymmetry (broken bar, end-ring fault or eccentricity) become:

$$f_{sh} = f \cdot \left(\frac{N_R}{p}(1-s) \pm k\right) \pm 2sf \quad 2.12$$

where N_R is the number of rotor slots; p is the pole pairs; s is the slip; f is the fundamental frequency and $k = 1,2,3, \dots$. They claim that the slot harmonic components frequencies of the stator currents caused by the rotor slotting harmonic can be used for a rotor fault diagnostic [71].

2.4.3.3 Influence of Broken Rotor Bar locations in detection

Rastko and Ferkolj (1998) are the first researchers who used finite element method to study the effects of broken rotor bar asymmetry on the magnetic field of motor [72]. Using finite element method, the induced currents in rotor cage can be determined. Besides that, the steady-state and transient characteristics of electrical machine in the case of any rotor bars asymmetry can be calculated considering the numbers of broken bars and their position. They show the magnetic field is symmetrically distributed with regard to pole-pair division in the case of symmetrical stator and rotor winding. Broken rotor bar produces asymmetrical magnetic field due to the lack of induced currents in faulty rotor bars and leads to a local saturation in the stator and rotor teeth near the broken bars. As a consequence, unproportional distribution of magnetic field is generated in the air-gap that leads to several electromagnetic phenomena like increase of higher harmonic components, development of inverse magnetic field, torque pulsation, unbalanced magnetic pull etc. [73]. Rastko and Ferkolj (1998) indicated both the number of broken bars and their position in the rotor cage play role in the resulting undesired phenomena in the machine. For instance, the same number of broken bars situated under different poles brings about less asymmetry in other parts of machine compare to the faulty bars that concentrated close together. Based on their results, the worst case of asymmetry is generated if the faulty bars are concentrated close together one by one under the same magnetic pole. These researchers also provide another research based on the location of the broken rotor bars in different pole pitch [5]. They also prove that the same percentage of broken bars does not mean the same degradation of operation performance of the induction motor.

In [74], was Modeled very precisely and with minimum simplifying assumptions of broken bars fault in different location or distributed over poles of the motor using Time stepping finite element method. They are shown that the location of the broken rotor bars is the third factor which affects the diagnosis of its. In their research, they consider stator current and torque frequency spectrum as two different condition monitoring and shown that the broken rotor bar location influences the amplitudes of harmonic components. Similar to Rastko and Ferkolj (1998), they proved the location of broken bars significantly influence the motor performance. They also indicated that allocation of broken rotor bars over different poles of motor decreases the amplitude of harmonic components and concentration of the broken bars on one pole of the motor increases the motor oscillation.

In 2010, Riera-Guasp and coresearchers carried out a comprehensive study including both theoretical analysis, simulation and experimental activities to investigate the effects of location and numbers of broken bars on the fault diagnosis using MCSA [75]. They presented a physical interpretation of the left sideband appearance under different broken rotor bar conditions. It was indicated that the amplitude of sideband decreases as the second broken bar moves away from the first and it gets to a minimum when approximately half the pole pitch separates both bars. The amplitude then increases until to reach a maximum when a pole pitch separates the bars. At this case, the sideband amplitude practically doubles the amplitude corresponding the a single breakage.

In a similar study, Ying (2010) investigated the influences of broken rotor bars located at different relative positions in an induction motor using both experimental and mathematical modeling of motor by finite-element method for both thermal and electromagnetic condition [76]. They studied the effects of equal numbers of broken with different positions on the motor's performance and found the stator current and starting torque are greatly influenced from the position of broken rotor bars.

Later on, Faiz and coresearcher (2012), used both modeling with winding function method and experimental activity to investigate the effects of four broken rotor bars with different positions on the competency of the amplitude of the sideband components at frequencies $(1 \pm 2ks)f_s$ with influence of control techniques via the open- loop constant voltage/frequency and closed-loop direct torque control techniques [49]. It was shown that at constant load and reference speed, the amplitude of the fault index is reduced by distributing the broken bars over different poles. This change may cause errors in the accurate diagnosis of the fault degree; however they mentioned that the locations of the broken bars are diagnosable with reasonable accuracy.

2.4.3.4 Left Sideband Component Values and Number of Broken Rotor Bar

Some general empirical conclusion based on the values of the left sideband component in the motor current spectrum proposed threshold values of the left sideband component for motor fault classification under a nominal load. For

instance, in [77], Faiz et al. proposed the magnitude greater than -54 dB correspond to a faulty motor. In [78,79], Hirvonen and Benbouzid et al. proposed smaller threshold values of the left sideband component for a faulty motor as they said the magnitude of the left sideband component greater than -50 dB is an indication of broken rotor bars. In [80,81], Thomson and Fenger and Siau et al. even believe a smaller threshold and they said the magnitude of the left sideband component greater than -45 dB could be corresponded to the faulty motor.

In [66] indicated that the current flowing in a completely broken bar versus the length of the rotor (l_x) can be estimated by:

$$\frac{I_{(1-2s)f}}{I_f} = 1 - \frac{1}{\cosh(\lambda l_x)} \quad 2.113$$

where $\lambda = \sqrt{3 \left| \frac{Z_b}{R_c} \right|}$, Z_b is the bar impedance and R_c is the contact resistance between the bar and the rotor core.

Besides broken rotor bar detection, some researchers moved forward and elaborated to find a specific criterion to determine the number of broken rotor bar or severity of the fault from stator current spectrum [66,78,82-84]. Table 2.2 summarizes the correlations proposed for estimation of the rotor fault severity.

Table 2.2: The correlations proposed for estimation of rotor fault severity

Ref.	Current Component	Estimation of number of broken rotor bar	Definition
[66]	$(1 - 2s)f$	$\frac{I_{(1-2s)f}}{I} = \frac{\sin \alpha}{2p(2\pi - \alpha)}$	$\alpha = \frac{2\pi p N_{BRB}}{N_R}$
[78]	$(1 - 2s)f$	$\frac{N_{BRB}}{N_R} = \frac{2 I_{(1-2s)f}}{I + 2p \cdot I_{(1-2s)f}}$	
[82]	$(1 \pm 2s)f$	$\frac{I_{(1\pm 2s)f}}{I} = \frac{N_{BRB}}{2N_R - N_{BRB}p}$	
[83]	$(1 \pm 2s)f$	$\frac{I_{(1\pm 2s)f}}{I} = \frac{N_{BRB}}{N_R}$	
[84]	$(1 - 2s^{(v)})\omega^{(v)}$	$\frac{2 \Gamma^{(v)}}{p} = \frac{N_{BRB}}{N_R}$	$\Gamma^{(v)}(s, \omega) = \frac{I_{(1-2s^{(v)})\omega^{(v)}}}{I_{(\omega^{(v)})}}$ $v=5,7,9,\dots$

2.4.4 Electromagnetic Field Monitoring

The air gap flux during normal condition of the motor ideally varies sinusoidally both in space and time. Any failure in stator and/or rotor causes deviations of such sinusoidal variation [85]. If any rotor bar is broken, its current re-distributes in the surrounding rotor bars. In [86] studied the field distribution of induction machines by

finite element analysis and indicated that the broken bar causes an anomalously high air gap local field that rotates at rotor speed. This field pulsates at slip frequency and modulates coil-induced voltage at a characteristic frequency f_{brb} , modified from the presented equation to be as follow:

$$f_{brb} = \left(\frac{2f_s}{p}\right)(1 - s) \pm sf \quad 2.14$$

Monitoring of magnetic field can be measured through both internal search coil and external search coil. The former one used searches coil mounted on the internal stator tooth tip and the induced voltage waveform is used to detect the presence of faults. Different types of internal search coil have been designed and used by [87-90]. However, the insertion of the search coils in the stator slots represents a highly invasive monitoring technique.

The external search coil or stray flux is installed outside of the motor and studied via its axial, radial and combination of this two fields [91]. Different types of external search coil have been designed and used by other researchers for detecting rotor faults [37,91-93]. In [94] investigated the broken bar diagnosis via the external search coil measurement after supply disconnection.

In [95] compared induced voltages in search coils located both internally and externally for broken rotor bar detection. They well justified that the analysis of induced voltage in an external search coil is adequate to detect the presence of the broken bars. They believe external search coil offers some priorities, as they are non-invasive and can easily be interfaced to the equipment. An external search coil is fixed on the motor frame to observe electromagnetic force. Using search in the industries coil is useful because the there is no need of motor modification or its temporarily taking in out the service. Nevertheless, monitoring of electromagnetic field via search coil is not being widely applied in the industry due to some practical limitations [37,96]. The important obstacle is the impact of sensor position on the magnitude of the output signal. Moreover, it is not often possible to install the coil in the correct position to ensure a reliable signal. Dimension of stray flux sensor is somewhat related to the size of induction machine and importantly, analysis of the air gap and axial flux signals cannot be quantified as a function of the fault severity.

2.4.5 Instantaneous Angular Speed Measurement

In practice, electrical machines rotate with changeable speed. Instantaneous angular speed is variation of motor speed that occurs within a single shaft revolution. Accordingly, measuring and analysis of the instantaneous angular speed of the rotor can give information about the motor dynamics. This information then can be used for fault diagnosis in electrical machines. Measurement of angular speed is based on two basic principles, which are counting the pulse numbers in certain time duration and measuring of elapsed time for a single cycle of encoder signal. Laser-based techniques and shaft encoders are the commonly used methods of instantaneous angular speed measurement.

Since the pulsating torque due to the rotor faults alters rotor speed, measuring and analysis of the instantaneous angular speed can reveal the size and location of the damage in a rotor [69,97]. Despite of its capability in fault detection, monitoring of instantaneous angular speed is less popular compared to the other existing conventional methods. An important obstacle in analysis of instantaneous angular speed is the uncertainties in the speed estimation of the underlying system that makes it not to be precise for fault diagnosis. For example, instantaneous angular speed measurement is inevitably influenced by random fluctuations in load and electric supply. In [40], Sasi et al. presented a complete explanation of the advantages and drawbacks of this method. In [98] investigated the effects of noise on measurement of the instantaneous angular speed.

2.4.6 Power Analysis

Stator voltages and currents in electrical machines are measured and employed for computation of the input power. Waveforms of the instantaneous power are subsequently analyzed using signal processing method to extract interested features and characteristic spectral components. Different types of power monitoring have been presented and applied for fault detection in electrical machines. For instance, instantaneous power was used for detection of stator winding faults like inter turn short circuits in squirrel cage induction machine [99]. The instantaneous power was also proposed as a medium to detect the presence of a variable load and torsional vibrations of the motors shaft in induction machine [100,101]. The power spectrum was also applied for detection of fault in rotor cage as defects produce harmonic torques with frequencies at even multiples of the slip frequency [102]. This method is proposed based on the fact that, in the power spectrum, frequency components representing the fault are not present anymore as sidebands of the fundamental frequency [100]. Instantaneous power was used for broken rotor bar detection and its severity [103,104]. The severity was determined through defining a severity factor, which is the ratio of the amplitudes corresponding to $2sf$ component and dc term for the total instantaneous power. In [104], Cruz and Cardoso mentioned that this evaluation is almost independent of parameters like motor rating, magnetizing current or motor-load inertia. In [105] compared partial powers and total power for broken rotor bar detection, and they indicated the partial power is more reliable than other method. Since load anomalies can also have affects on the instantaneous power spectrum, Drif et al. compared the effect of different load anomalies with other machine anomalies, such as broken bar [106]. In [107], Liu et al. used the instantaneous power spectrum for detection of mixed fault (broken rotor bar and eccentricity). The two different features of $(2sf)$ and $(2f \pm 2ksf)$ were used for broken rotor bar detection. They indicated theoretical and experimental ability of $2sf$ for broken rotor bar detection. Drif and Cardoso tried to improve and develop different types of the instantaneous power monitoring like, instantaneous power phase angle [108], instantaneous non-active power [109], instantaneous power factor approach [110], instantaneous active and reactive power [111], instantaneous reactive power [112,113] for broken rotor bar detection. Later on, they used the signatures obtained from analysis of instantaneous active and re-active power and their resulting signals (namely, instantaneous phase angle and power factor) for

discriminating motor failures, like broken bars and airgap eccentricity, from irregular mechanical load and/or any oscillation in induction machines [114].

Spectra analysis of both instantaneous active and reactive powers, Angelo et al. proposed a technique to discriminate the broken bars and oscillations caused from low-frequency load [115]. They also proposed a fault severity factor independent of the motor load that makes quantification of the broken rotor bar fault practical. In [116], Maouche et al. introduced high order rotor slot harmonic components from instantaneous phase power induced by broken rotor bar as a fault signature under low slip. They indicated there is great dependence between the load level and the $2ksf$ harmonic components in the partial and total instantaneous power spectrums. They also mentioned that in the case using variable speed drives, $2ksf$ close to dc component depends greatly on the load level and oscillation load. The frequency of components related to the failure has strongly been spread in large bandwidths and it is proportional to the load variation. Accordingly, the values of instantaneous slip cannot be defined accurately and thus it is difficult to identify their amplitude and location in the spectrum precisely. To resolve this obstacle, Yahia et al. proposed a method based on discrete wavelet transform of the instantaneous reactive power signal [117]. The results of this analysis were used for diagnoses of broken bars in IMs that operate under time-varying load condition. In [118], Kim et al. proposed a new feature $(6 - 8s)f$ in instantaneous power spectrum for broken rotor bar detection. They believed the conventional feature $(2sf)$ is not reliable for broken bar detection as it produces some false features in the power spectrum due to influence of rotor axial air ducts, rotor anisotropy or load oscillations. They also mentioned that $(2sf)$ in the power spectrum might be because of space harmonics of stator winding.

2.4.7 Motor Circuit Analysis

A method based on measuring the electromagnetic properties of the induction machines, well-known as motor circuit analysis, was also proposed for identification of IMs defects. Motor circuit analysis may include simple tests of resistance (milli-Ohms) impedance, and inductance and phase angle, or may include more complex tests like proprietary testing, which is taken on the de-energized rotating equipment. To the best of our knowledge, Penrose and co-workers are the only research group who has utilized motor circuit analysis hitherto. They found a simple measurement of just resistance or inductance alone are extremely anomalous for fault detection and a complete combination of standard engineering measurements of resistance, impedance, phase angle, and inductance provide a highly accurate view of the IM condition. Furthermore, they annotated that the accurate motor circuit analysis of the induction machine requires study of AC electrical basics (inductance, impedance, phase angle and milli-Ohms of DC resistance). As the circuit of three-phase induction machines is expected to have three sets of equivalent windings separated by 120° electrical, detection and analysis will include the balance between each circuit. They also alluded that as a low amount of energy with amplified responses is applied in motor circuit analysis method, the responses help in evaluating the condition of both windings and rotor through the comparative readings [119,120].

2.4.8 Vibration Monitoring

An ideal induction machine generates minor vibration during its operation and any malfunction in internal parts of the motor causes this vibration intensive. The flux density produces radial magnetic forces between surfaces of stator and rotor when it rotates and any incipient failure will increase the levels of mechanical vibration [121]. Accordingly, vibration signal is measured and analyzed for diagnosing a faulty condition in electrical machine. Vibration monitoring is generally used to detect the mechanical failures like rotor misalignment, bearing problems, gear mesh defects and mass unbalance [122]. Vibration of stator frame could be a function of an inter-turn winding fault, single phasing or supply-voltage unbalance [123]. To detect rotor faults in [124], Kang and Kim measured vibration signal using three accelerometers, which were located on the stator frame in axial, horizontal, and vertical directions.

In [125], McCully and Landy demonstrated that a broken rotor bar excites the field disturbance electromagnetically and thus intensifies the torque modulations and vibrations of the housing. Later on, these authors quantified the frequencies of the radial vibrations caused by the increased inter-bar currents due to a rotor fault, and presented a new method to detect broken rotor bars based on the presence of inter-bar currents [126]. In [42], Li and Mechevske elaborated a research to compare the capability of the vibration monitoring with two other methods, MCSA and acoustic noise measurement, for detection of broken rotor bar and bearing failure under different speed and load conditions. They elucidated that MCSA is more sensitive than the two others for broken rotor bar detection. It was also indicated that, in contrast to stator current monitoring, the sideband amplitudes in the vibration signal depend on the motor speed more than external load. In [122] also emphasized that vibration monitoring is an important and reliable technique to detect bearing and other strictly mechanical failures.

Vibration analysis is sensitive to both rotor and stator faults. Nevertheless, the main weakness of this technique is the need of detailed information about design characteristics of motor. For instance, response functions of frequency must be known for quantification of the fault because mechanical and electrical responses depend on position of accelerometer [127].

2.4.9 Voltage Monitoring

Different types of condition monitoring based on voltage measurement have been developed for fault detection in electrical machine. These methods differ depends on the type of voltage, i.e. the line-neutral voltage (the voltage between the supply and the stator neutrals), shaft voltages or voltage induced in the stator winding after electrical machine disconnection, is measured. The condition monitoring based on measurement of shaft voltage is only used for fault detection in generator, which is not the focus of this research. The other two voltages have considerably been used for fault detection in induction machine and so they are discussed as below.

In [95], Elkasabgy et al. introduced a condition monitoring method based on measurement of the voltage induced in the stator after induction machine disconnection for broken rotor bar detection. When the motor is disconnected from the supply, the stator currents rapidly come down to zero, and thus the rotor current is the only source of induced voltages in the stator windings. If any bar is cracked, it will then directly influence the induced voltages in the stator windings after induction machine disconnection. In a healthy condition of induction machine, when the stator phases are disconnected, the magneto-motive force generated by the current of rotor bar is predominantly sinusoidal. Accordingly, induced voltage in the stator due to this magneto-motive force should not have any significant harmonic content other than the fundamental because of the stepped rotor current distribution. However, if any bar is broken or cracked, the wave-shape of the magneto-motive force will deviate from its sinusoidal nature and so the induced stator voltage will contain harmonic contents other than the fundamental. Differences in voltage spectra when the motor is healthy with the time it has no ideality in the rotor bar can be used for detection of broken rotor bar. It was declared that voltage monitoring is a reliable method even for an unloaded machine as the effects of source non-idealities (such as unbalance, presence of time harmonics, etc.) and nonlinearity of the machine magnetizing characteristics due to the saturation could be removed [128]. Despite of its capability, voltage monitoring however has some limitations when applied to the practical systems. For instance, it requires tests to be carried out with the motor in the healthy state to develop a baseline response. It is also sensitive to the load variation, system inertia, rotor temperature and supply voltage [129]. An important drawback for voltage monitoring is the magnitude of harmonic components is not sensitive to the number of broken bars and thus the fault cannot be qualified. Another problem with voltage monitoring is inter-bar currents, dependence of the spectral amplitude on the instance of disconnection, and short length of data adversely influence the detection accuracy [128]. Nevertheless, further studies have been directed to use an advanced signal processing technique to improve the broken bar detection by monitoring of induced voltage [129,130].

In [131], Razik and Didier studied spectral analysis of line-neutral voltage for broken bar detection in induction machine operating under several loads. The basis of using line-neutral voltage for broken rotor bar relies on rising of harmonic components as diagnosis signatures in its spectrum. These components are generated from asymmetries induced in the mutual inductance of induction machine because of broken rotor bar [132]. Simulation and experimental studies proved the effectiveness of using line-neutral voltage for detection of even partial broken rotor bar [132-135]. Analysis of line-neutral voltage not only preserves the advantage and simplicity of MCSA, but also it is more sensitive to motor failures. For instance, if any broken rotor bar exists, extra harmonic frequencies with more significant amplitude appeared in the voltage spectrum compared to current spectrum [131]. In addition, due to both space distribution of rotor bars and variation of the air-gap permeance, the line-neutral voltage spectrum shows other high harmonics, known as rotor slot harmonics. Nonetheless, analysis of line-neutral voltage signatures still requires some improvements to make it an appropriate parameter for overall fault diagnosis of induction machines.

2.5 Signal Processing Techniques

Basically, the raw signal acquired by the sensor is complex and needs to be converted to a more understandable signal. Signal processing encompasses the processing, analysis and transforming the raw signal to a meaningful representation of the information contained in the raw signal. Computer algorithms, based on mathematical transformer, are applied to a raw signal to extract the important information on the specific issue for decision-making. Signal processing can be carried out either in time domain, frequency domain or time-frequency domain [136]. Selection of processing domain and characteristic features depends on the nature of signal and required information. Signal processing and data analysis accompanied with condition monitoring are the key parts of the fault detection scheme in electrical machine. Signal processing techniques help to interpret the information obtained from the motor and extract the fault signature. Accordingly, to complete the discussion on fault diagnoses of induction machine, the various signal processing techniques will be presented in this section.

2.5.1 Time domain analysis

Time domain graphs show how a signal changes over time and the analysis of mathematical functions or physical signals is performed with respect to time. Time domain analysis has a significant advantage that provides a great deal of detailed information and almost no information is lost. Common statistical analyses are applied to describe the probability density function of a time-varying signal. In time-domain analysis, the fault features may be extracted from the signals through calculation of various statistical parameters, such as means, standard deviation, variances, covariance, root mean square, skewness, kurtosis, crest factor, Shape factor, entropy error, entropy estimation, upper and lower bound of histogram, and envelop [88,137-138].

The other type of time domain signal used for fault detection is envelope signal, which is extracted from original signal. When the broken rotor bar occurs in the squirrel cage electrical machine, frequency components of $2sf$ is induced in stator current signal. Based on the backward field theory, Bellini et al. explained the flux density in electrical machines in two states; the motor is healthy or faulty [6]. In case of rotor asymmetry caused by broken rotor, the stator current can be written as [139,140]:

$$i(t) = I_f \cos(2\pi ft - \varphi) + \sum_k I_{(1-2ks)f}^K \cos(2\pi(f - 2ksf)t - \varphi_{(1-2ks)f}^k) + \sum_k I_{(1+2ks)f}^K \cos(2\pi(f + 2ksf)t - \varphi_{(1+2ks)f}^k) \quad 2.15$$

where φ : Main phase shift angle of stator current; $I_{(1-2ks)f}^K$: Amplitude for harmonic component $f_{(1-2ks)f}$; $I_{(1+2ks)f}^K$: Amplitude for harmonic component $f_{(1+2ks)f}$; $\varphi_{(1-2ks)f}^k$: Phase shift angle of harmonic component $f_{(1-2ks)f}$; $\varphi_{(1+2ks)f}^k$: Phase shift angle of harmonic component $f_{(1+2ks)f}$.

Equation (2.15) can be rephrased as:

$$i(t) = A(t) \cos(2\pi ft) + B(t) \sin(2\pi ft) \quad 2.16$$

$$A(t) = I_f \cos(\varphi) + \sum_k ((I_{(1-2ks)f}^K \cos \varphi_{(1-2ks)f}^k + I_{(1+2ks)f}^K \cos \varphi_{(1+2ks)f}^k) \cos(2\pi(2ksf)t + (I_{(1+2ks)f}^K \sin \varphi_{(1+2ks)f}^k - I_{(1-2ks)f}^K \sin \varphi_{(1-2ks)f}^k) \sin(2\pi(2ksf)t)) \quad 2.17$$

$$B(t) = I_f \sin(\varphi) + \sum_k ((I_{(1-2ks)f}^K \sin \varphi_{(1-2ks)f}^k + I_{(1+2ks)f}^K \sin \varphi_{(1+2ks)f}^k) \cos(2\pi(2ksf)t + (I_{(1-2ks)f}^K \cos \varphi_{(1-2ks)f}^k - I_{(1+2ks)f}^K \cos \varphi_{(1+2ks)f}^k) \sin(2\pi(2ksf)t)) \quad 2.18$$

The Equation (2.16) can be rewritten as follows:

$$i(t) = I_m(t) \sin(2\pi ft + \theta(t)) \quad 2.19$$

with:

$$I_m(t) = \sqrt{A(t)^2 + B(t)^2} \quad 2.20$$

$$\theta(t) = \arctan\left(\frac{A(t)}{B(t)}\right) \quad 2.21$$

From Equation (2.19), the current envelope and its phase shift that depend on broken rotor bar can be extracted [67]. As shown in correlations of $A(t)$ and $B(t)$, the broken rotor bar in squirrel cage electrical machine induces amplitude at frequency components of $2ksf$ in the stator current. The amplitude of these frequency components can be used as indication of fault, named fault-related feature [141,142]. In [83], Filippetti et al. proved the feature amplitude increases when the number of broken bars increases and on the other hand, the $2ksf$ term rises due to increase of the slip [143]. The modulation index (β) for this fault frequency, and the estimated frequency amplitude ($I_{(1-2ks)f}^K$) can be thus referred as [66,83,144]:

$$\beta \approx \frac{I_{(1-2ks)f}^K}{I_f} = \frac{N_{BRB}}{N_R} \quad 2.22$$

In this purpose, Hilbert transform is suitable for extraction of faults with low frequency, like features corresponds to " $2ksf$ ", which are used for broken rotor bars diagnosis in squirrel cage electrical machine. Hilbert transform is an ideal phase shifting tool in signal processing techniques to extract the instantaneous magnitude (envelope) of current signal. The important advantage of Hilbert transform is increasing of resolution, both in amplitude and frequency regions [141]. The complete explanation on application of Hilbert transform for current analysis of electrical machines, both in faulty and healthy conditions, is discussed in [143]. Some researchers used Hilbert transform to extract the envelope signal, and the

statistical features obtained from the envelope were used to detect broken rotor bar in squirrel cage electrical machine [138,145-147].

2.5.2 Frequency domain analysis

A raw signal, which is in time domain, is transformed to the frequency domain using different spectral estimation techniques. These techniques can be based on nonparametric, parametric or high-resolution spectrum analysis methods [6,148,149]. Nonparametric methods basically apply conventional Fourier transform and generally values, such as amplitudes, powers, intensities, or phases are calculated. Variation of the calculated parameter is then presented versus frequency and this spectra indicates signatures related to the failure under observation. Other statistical features, like frequency centre, root mean square frequency and root variance frequency also can be extracted from frequency domain [150,151]. Power spectral density (PSD) analysis is another technique used for electrical machines fault detection [152-155]. Besides Fourier transform analysis, there are other nonparametric methods, like periodogram [156] and Welch analysis [157]. Similar to Fourier transform, these analysis methods only provide the value of different frequencies and their amplitudes in a signal. There are several methods that provide higher order spectra, defined in terms of higher order statistics. These higher order spectra bring insights into non-linear coupling between frequencies (as it involves both amplitudes and phases) of a signal [158]. An example for such analysis is Bispectrum, called third-order spectrum, which is defined in terms of the 2-dimensional Fourier transform [159]. Another example is Cepstrum [160], which is the inverse Fourier transform of the logarithmic spectrum.

Nonparametric methods estimate the statistical parameters from the available data directly. Parametric methods, as expected, use a different approach for spectral estimation. In this method, the data is first modeled as the output of a linear system driven by white noise, and then the parameters of that linear system are estimated. Autoregressive, such as Yule-Walker, Burg, covariance, or modified covariance, is generally used to establish a model fitted with time series of the signal. The model parameters are then used to compute the frequency spectrum. One more practical signal analysis in frequency domain is Prony's method, considered as a high resolution parametric method. Prony's method first extracts valuable information from a raw signal and then creates a series of damped complex exponentials or sinusoids. Prony's method allows estimation of frequency, amplitude, phase and damping components of a signal. Several researchers used Prony's method for broken rotor bar detection [161-163]. High-resolution spectrum methods, such as multiple signal classification (MUSIC), Root-MUSIC and Zoom-MUSIC, compute the autocorrelation matrix of the time series signal, and its eigenvalues can be separated into signal and noise spaces. Another type of high resolution technique recently introduced for induction machine fault detection is fast orthogonal search algorithm [164,165]. There are also other types of frequency estimation algorithm based on FFT with resolution improvement, such as, the zoom- FFT and the chirp Z-transform methods [166]. Another useful transform, Hilbert transform, has also been used for machine fault detection and diagnostics. In [167], Aydin et al. presented a brief review on using Hilbert transform for broken rotor bar detection.

Although Fast Fourier Transform (FFT) analysis is traditionally used in fault detection of electrical machine, transforming a signal from time-domain to the frequency-domain leads to information loss. This problem is considered to be one of the main disadvantages of the frequency-domain transition [168]. In industrial environment, there are some practical limitations for application of MCSA method based on FFT analysis to detect rotor failure at low slip. This inability of method is related to the effects of time-varying load and confusing mechanical frequencies on the spectrum spectral leakage due to finite-time window and need of high frequency resolution for Fourier- based analysis [143,146].

2.5.3 Time-Frequency domain analysis

In order to overcome the problem of non-stationary signals, time-frequency analysis, consists of the 3-D time, frequency, and amplitude representation of a signal, has been proposed. The most popular time-frequency analysis methods are short-time Fourier transform (STFT), wavelet transform and Wigner-Ville distribution. Short-time Fourier transform divides the whole waveform signal into segments with short-time window and then apply Fourier transform to each segment. Consequently, the STFT can extract the frequency information of a signal while keeping its time information. Accordingly, this technique allows observation of the frequency content of the signal in any time interval. On the other hand, the STFT reduces the frequency resolution of the signal because the signal is divided into smaller sub-blocks which represent less observation time. In other words, the frequency resolution is limited by the size of the segments. Therefore, the frequency and time resolution of the STFT technique depend on the length of the window. A longer window means higher frequency resolution but lower time resolution while a shorter window means lower frequency resolution but higher time resolution. Accordingly, the window has to be selected as a tradeoff between time and frequency resolutions. In summary, STFT method reduces the computational cost as well as time period of data acquisition. Therefore, better time resolution is achieved and the condition is close to the assumption of being stationary. However, since the frequency resolution in STFT is poor, it is not an attractive analysis method for diagnosis purposes [94].

Another time-varying spectral representation is Spectrogram that can be estimated by computing the squared magnitude of the STFT of the raw signal. Wigner-Ville distribution is the basic transform of bilinear transforms that, unlike STFT, does not segment the data. It is based on the instantaneous frequency, which is the derivative of the phase of the signal. The Wigner-Ville distribution is often smoothed by filtering functions in order to reduce the interference called Smoothed Pseudo-Wigner-Ville distribution [42,169,170].

Another transform for time–frequency analysis is wavelet transform that is a time-scale representation of a signal [171]. Wavelet analysis was introduced to overcome the resolution problems of STFT. In recent years, wavelet analysis has attracted the researchers' attention in areas where signal processing is required. Wavelet analysis

of a waveform signal expresses the signal in a series of oscillatory functions with different frequencies at different time. Wavelet transform can provides both the frequency information and the time information of a signal by using a variable length window. It divides the signal into time-scale space and the size of the window at time and frequency (scale) is not rigid [172]. The way wavelet analysis localizes signal's information in the time–frequency plane makes it especially appropriate for analysis of non-stationary signals. It is, therefore, a good alternative to traditional STFT analysis. In [173], Mallat introduced a practical version of wavelet transform, called wavelet multi-resolution analysis, for the first time. Basically it is based on the fact that, one signal is decomposed into a series of small waves belonging to a wavelet family. There are different types of Wavelet transform techniques widely used in electrical machine condition monitoring [19,174].

2.6 Broken Rotor Bar Fault Detection in Induction Machine

The various types of techniques were used to detect broken rotor bar fault in IM. Table 2.3 presents the type of techniques used for broken rotor bar detection in the cited papers. The importance of broken rotor bar fault is its subsequent disastrous failures. This fact in addition to increasing the application of LS-PMSM in various fields as well as lack of information about detection of broken rotor bar fault in LS-PMSM is the major motivation to commence a research based on detection of broken rotor bar fault in LS-PMSM which is presented in the subsequent chapters.

Table 2.3: Summary of published paper with the aim of broken rotor bar detection in IM (continued)

Ref	Data Monitoring	Signal Processing	Decision Making	Purpose	Achievement and Limitation
[37]	Stray Flux, MCSA	Spectrum analysis	ANN	To compare the performances of current and flux monitoring for voltage unbalance and BRB detections.	A simple external stray flux sensor is more efficient than the classical stator current sensor to detect BRB and voltage unbalance using data processing at low-frequency resolution especially in the case of unloaded machine.
[56]	Air gap Torque	Fourier Analysis	-	To develop Vienna monitoring method for BRB detection.	Developed Vienna monitoring works without the need of a position or speed sensor. <i>Limitation: Partly cracked rotor bars could not be detected.</i>
[64]	MCSA	-	-	To present a model for predictive diagnosis of BRB and breakage in end-ring connector segments.	The effects and implications of BRB on core loss distributions were quantified and described. The proposed model has great potential in future applications to generate data bases for use in overall non-invasive diagnostics of faults.
[67]	Air-Gap Torque, MCSA,IP	Fast Fourier transform	-	To evaluate the performance of different monitoring techniques for detection and quantification of BRB.	MCSA provides more accurate information to diagnose and quantify the BRB.
[68]	Current (Start-up)	Discrete Wavelet Transform	-	To improve the start-up current monitoring procedure for BRB detection using a filter that actively tracks the changing amplitude, phase and frequency to extract the fundamental from the transient.	This method does not require parameters such as speed or number of rotor bars. It is not load dependent and can be applied to IMs that operate continuously in the transient mode.
[92]	MCSA, Stray Flux	Zoom Fast Fourier transform	-	To investigate MCSA and stray flux MTs for BRB detection.	The Zoom Fast Fourier transform improved the frequency resolution in a narrow frequency bandwidth by using a small number of samples. The procedure can be applied whatever the load is, even when the shaft of the machine is free of mechanical load or even in the manufacturing process.
[94]	IP	Discrete Wavelet Transform	-	To improve IP monitoring for BRB detection under various load levels.	Wavelet approach applied to IP showed superior ability for BRB detection compared to the frequency domain analysis.
[98]	Instantaneous angular speed	Fast Fourier Transforms	-	To investigate the effects of measurement noise in the use of IAS for BRB and shaft misalignment detection	The measurement noise of IAS could be controlled by the IAS measurement parameters: the resolution of the encoder and the length of the data stream. IAS measurement is better than that of conventional vibration in diagnosing incipient faults in the motor driving system.
[105]	MCSA, Torque	IP, Fast Fourier transform	-	To evaluate the performance of different monitoring techniques for BRB detection under various load levels.	The IP monitoring showed the best ability for fault detection.

Table 2.3: Summary of published paper with the aim of broken rotor bar detection in IM (continued)

Ref	Data Monitoring	Signal Processing	Decision Making	Purpose	Achievement and Limitation
[107]	IP	Frequency Domain	-	To present a diagnosis method for detection and quantification of the BRB and air-gap eccentricity.	The spectrum of the instantaneous power is clear from any component at the fundamental supply frequency, and the fault characteristics can be highlighted, which is effective toward the separation of mixed faults and the quantification of the fault extent.
[115]	IP	Frequency Domain	-	To propose a new strategy for discrimination of broken rotor bar and oscillating load.	A broken bar fault can be detected and diagnosed, even in the presence of load oscillations. A fault severity factor was proposed for broken rotor bar fault quantification.
[126]	Vibration	Fast Fourier Transforms	-	To develop a vibration monitoring for BRB detection.	Interbar currents which produce an axial force can be used in vibration monitoring for BRB detection
[128]	Induced Voltage	Fast Fourier Transform	-	To proposes a novel monitoring technique for BRB detection.	This technique is reliable enough for BRB detection even for an unloaded machine. <i>Limitation: Interbar currents, dependence of the spectral amplitude on the instance of disconnection, and short length of data adversely affect the detection technique. The number of broken bars can not be identified.</i>
[129]	Induced Voltage	Fast transform and Wavelet	Fourier and -	To investigate the limitations and harmonics of the induced voltage after supply disconnection harmonics for BRB detection.	Fourier transform did not provide information about fault severity and load variations. A method based on wavelet analysis of induced voltage spectrum was developed for BRB detection <i>Limitation: Tests need to be carried out for healthy motor to develop a baseline response. It is sensitive to changes in load, system inertia, rotor temperature and supply voltage.</i>
[130]	Induced Voltage	MUSIC & STMUSIC	-	To develop induced voltage monitoring for BRB detection	The proposed approach is effective regardless the load condition of the machine, source characteristics and iron saturation.
[134]	Neutral Voltage	Hilbert Transform	-	To investigate neutral voltage monitoring for BRB detection.	The harmonic frequency related to BRB appears as clear jumps in the Hilbert phase.
[137]	Current (Start-up)	Discrete wavelet transform	Principle Component Analysis, Kernel PCA, Support vector machine	To develop transient current monitoring procedure using intelligent system for detection and classification of various faults including BRB .	Feature reduction and extraction using component analysis via PCA and KPCA are highlighted. The performance of WSVM is validated by applying it to faults detection and classification of induction motor based on start-up transient current signal. <i>Limitation: A proper preprocessing for the transient current signal is needed to improve emerging the salient differences between conditions in induction motors.</i>

Table 2.3: Summary of published paper with the aim of broken rotor bar detection in IM (continued)

Ref	Data Monitoring	Signal Processing	Decision Making	Purpose	Achievement and Limitation
[139]	Current (Envelopes)	Discrete wavelet transform	-	To propose a new technique, slip independent, for BRB detection under different load levels.	The proposed method gives the same reliable results for BRB detection under different loads levels when applying to the stator-current space-vector magnitude and the instantaneous magnitude of the stator-current signal.
[142]	Current (Envelopes)	Time domain	Gaussian Mixture Models and the Bayesian Maximum	To develop MCSA monitoring procedure using envelope extraction of current spectrum for BRB and stator short-circuit detection.	It diagnoses the fault severity, i.e. number of interturn short circuits in stator windings or the number of BRBs.
[152]	MCSA	Short-time Fourier transform, Wavelet Transform	-	To improve MCSA monitoring procedure for BRB and stator shorted turns detection.	Wavelet decomposition is superior to STFT. Power spectral density for wavelet details was introduced as a merit factor for fault diagnosis. The proposed method can diagnose shorted turns and BRB in nonconstant-load-torque IM applications.
[153]	MCSA	Fast Fourier, Wavelet transform	-	To proposes a new method for early fault detection.	The approach has been proved to be effective to detect the failure in its very early stages.
[157]	Current (zero crossing times)	Fast Fourier Transforms	-	To investigate zero crossing times analysis of current spectrum for BRB detection.	The 2sf frequency component is independent of inertia, load, and harmonics, and thus it is suitable as an index for broken rotor bar. <i>Limitation: Accurate prediction of rotor faults depends on the ability of precise reading of motor slip in order to extract the right frequencies from the spectrum.</i>
[162]	MCSA	Discrete Fourier transform & Prony Analysis	-	To propose a BRB diagnostics method based on Prony analysis.	The method is able to detect the BRB sideband frequency components in light and time-varying load conditions.
[167]	MCSA	Sliding windows based on Hilbert transform.	-	To propose a new method for early fault detection at no load condition.	The method determines the number of BRBs at absolute no-load condition. One and two broken rotor bars were detected under no-load conditions. <i>Limitation: the effect of load needs to be considered.</i>
[175]	Acoustic MCSA Vibration	, smoothed pseudo Wigner-Ville distribution	-	To evaluate the performance of different monitoring techniques for BRB and bearing fault detection under different speed and load conditions.	The stator current is the most sensitive method for the BRB detection. Sidebands are independent of load and speed.
[176]	Air gap Torque	Fourier Analysis	-	To propose a new approach for on-line monitoring of IM drives.	Vienna Monitoring Method was proposed using output of the current and voltage model to estimate electromagnetic torque.
[177]	MCSA & Extended Park's Vector	Fourier Analysis	-	To develop on-line current monitoring system for BRB and stator short circuit detection.	A knowledge-based system was constructed in order to carry out the diagnosis task from estimated data obtained from experimental observations and the knowledge of the IM.

Table 2.3: Summary of published paper with the aim of broken rotor bar detection in IM (continued)

Ref	Data Monitoring	Signal Processing	Decision Making	Purpose	Achievement and Limitation
[178]	MCSA	Discrete Fourier transform & Hilbert Transform.	Statistical-based Algorithm	To improve MCSA procedure for BRB detection.	A partially BRB for a load level equals to 25% was detected. The method does not require a healthy motor reference.
[179]	MCSA	Wavelet Packet Decomposition	Adaptive Neuro-Fuzzy	To present a novel on-line diagnostic algorithm for BRB and air-gap eccentricity detection in variable speed drive systems.	Although the algorithm is able to detect the fault with high accuracy, the number of training iterations and the CPU processing time were reduced.
[180]	MCSA	Fast Fourier transform & Filter	Fuzzy	To improve MCSA monitoring procedure for BRB and air-gap eccentricity detection.	The system was able to detect different IM faults, though very precise information about the motor slip is not needed. The amount of data, computation and cost were reduced.
[181]	MCSA	PSD estimation using Welch's periodogram	Multiple Discriminate Analysis and ANN	To compare ANN and linear discriminate analysis using single or multiple signature processing for BRB detection.	The multiple signature processing provides a better accuracy performance when compared to the single signature processing. The accuracy performance of the ANN is higher than the Linear Discriminate Analysis.
[182]	MCSA	Fast Fourier transform	ANN	To improve MCSA monitoring procedure for detection of various faults including BRB.	The method does not require any information about the IM or load characteristics.
[183]	MCSA	Maximum covariance frequency tracking, Zoom FFT	-	To improve MCSA monitoring procedure for BRB detection.	The constraints of limited time or frequency resolutions of traditional Fourier based method were overcome.
[184]	MCAS	Statistical Time domain Analysis	Bayesian, Gaussian Mixture Model, Fisher's linear Discriminate Analysis	To improve MCSA monitoring procedure for BRB and air-gap eccentricity detection.	Developed system is able to indicate the load level and the type of a fault in multi-dimensional feature space representation.
[185]	MCSA	Time Domain	Principle Component Analysis	To propose an on-line diagnosis method using a fully automatic algorithm, based on the eigenvector/eigenvalue analysis of the motor line current.	The proposed method quantitatively identifies two distinct faults, stator winding faults and BRBs.

Table 2.3: Summary of published paper with the aim of broken rotor bar detection in IM (continued)

Ref	Data Monitoring	Signal Processing	Decision Making	Purpose	Achievement and Limitation	
[186]	MCSA	DFT , Maximum covariance frequency tracking	-	To improve MCSA monitoring procedure for BRB detection.	The MCMFT allowed achieving high frequency resolution in the tracking of supply and rotor slotting frequency for IM. High accuracy could be achieved even with low sampling frequency and low acquisition period. The procedure is more sensitive to changes in frequency than Fourier Transform methods.	
[187]	MCSA, Voltage, Speed	Wavelet packet decomposition	ANN	To develop a model-based diagnosis system for detection of various faults including BRB.	The proposed system was shown effective in detecting early stages of different IM faults.	
[188]	MCSA	Wavelet packet decomposition	ANN	To improve MCSA monitoring procedure for BRB and air-gap eccentricity detection.	It provides feature representations of multiple frequency resolutions for faulty modes.	
[189]	MCSA	Fourier Analysis, Wavelet packets decomposition	-	To improve MCSA monitoring procedure for detection of various faults including BRB.	The features of BRB and static eccentricity yield similar results in the wavelet analysis, but were different in Fourier analysis. Therefore the use of both types of analysis together can distinguish the faults.	
[190]	MCSA	Fast Fourier transform	-	To improve MCSA monitoring procedure for detection of various faults including BRB.	Advanced signal and data processing algorithms composed of an optimal slip estimation algorithm, a proper sample selection algorithm, and a frequency auto search algorithm for were proposed.	
[191]	MCSA	Fourier Analysis, wavelet packets	Fuzzy ANN	Entropy-ANN	To improve MCSA monitoring procedure for detection of various faults including BRB.	An approach was proposed based on Fourier and Wavelet transformations and neural network system to classify the faults.
[192]	MCSA	Wavelet packet decomposition	ANN	To propose a novel on-line diagnosis algorithm for BRB detection.	The diagnosis can be performed with reduced load condition. An accurate measurement of the slip speed is not necessary.	
[193]	MCSA	Fast Fourier Transforms combine with amplitude recovery method	-	To improve MCSA monitoring procedure for BRB detection.	The ARM algorithm can filter out the fundamental component in stator currents of tested induction motor . <i>Limitation: the ARM must be applied in three phases of currents in induction machines.</i>	
[194]	MCSA	WT,PSD	-	To develop BRB detection methods based on MCSA	The method has the ability to detect BRB for both constant torque and for variable load torque	
[195]	Current (Start-up)	Complex wavelet	-	To develop start-up current monitoring procedure for BRB detection.	The information contained in the start-up transient signal can be effectively separated and detected using a complex vector wavelet transform.	

Table 2.3: Summary of published paper with the aim of broken rotor bar detection in IM (continued)

Ref	Data Monitoring	Signal Processing	Decision Making	Purpose	Achievement and Limitation
[196]	Current (Start-up)	Wavelet Ridge	-	To develop start-up current monitoring procedure for BRB detection.	The influence of power frequency was effectively eliminated. Detection scheme was sensitive enough even for the case of only one BRB.
[197]	Current (Start-up)	Discrete wavelet transform	-	To develop start-up current monitoring procedure for BRB detection.	The method is not load dependent and can be effective on small lightly loaded machines.
[198]	Current (Start-up)	Discrete wavelet transform	-	To develop start-up current monitoring procedure for BRB detection. To compare the influence of the Discrete wavelet transform parameters (type of mother wavelet, order of the mother wavelet, sampling rate, or number of levels of the decomposition) over the diagnosis.	The tests show that if the start-up transient is not very short, the reliability of the proposed method for BRB detection is similar to that of the classical approach, based on the Fourier transform, in the case of loaded motors, but, in addition, the method can detect faults in an unloaded condition, and it allows a correct diagnosis of a healthy machine in some particular cases where Fourier analysis leads to an incorrect fault diagnosis..
[199]	Current (Start-up)	Discrete wavelet transform	-	To develop start-up current monitoring procedure for distinguishing various faults including BRB and other phenomena, such as load torque oscillations.	The proposed methodology showed promising ability for the reliable discrimination of simultaneous electromechanical faults and the diagnosis of faults combined with other phenomena.
[200]	Current (Park's Vector)	Frequency Domain	-	To introduce a new approach based on spectral analysis of the current Park's vector modulus for BRB detection.	Even for the case of only one BRB, this characteristic component is clearly visible.
[201]	Current	Park's transformation	Bayes Minimum Error	To develop a pattern recognition technique for BRB detection.	This algorithm can be revised to include other faults such as eccentricity and phase unbalance. It also, can be applied for fault classification in other electric machines.
[202]	Current (Park's Vector)	Hilbert Transform	-	To improve MCSA monitoring procedure for detection of various faults including BRB.	Hilbert Modulus showed the same BRB detection ability as the Extended Park's Vector Approach. The vital advantage of the former is the smaller hardware and software.
[203]	Current (Envelope Start-up)	Continuous wavelet transform	-	To develop start-up current monitoring procedure using envelope extraction of current spectrum for BRB detection.	The procedure is not affected by various other factors, such as initial rotor position, phase of the supply, and supply imbalance. It is able to classify the different degrees of BRB. <i>Limitation : A partial BRB could not be indicated.</i>

Table 2.3: Summary of published paper with the aim of broken rotor bar detection in IM (continued)

Ref	Data Monitoring	Signal Processing	Decision Making	Purpose	Achievement and Limitation
[204]	Neutral Voltage	Fast Fourier Transforms	-	To investigate neutral voltage monitoring for BRB detection under supply unbalance and speed ripples.	Besides BRB detection, a conclusion on the level of vibration in the motor as well as the level of unbalance in the voltage supply could be drawn.
[205]	MCSA Vibration	Time and Frequency Domain	ANN Dempster-Shafer theory	To develop a procedure based on vibration and current monitoring for detection of various fault including BRB.	The fusion of classification results from vibration and current classifiers increases the diagnostic accuracy. It is essential to develop feature extraction and selection techniques to determine the state of machine condition to achieve reliable classifiers.
[206]	MCSA Vibration	Time and Frequency Domain	Independent Components (ICs) , Principal Components (PCs) , Support Vector Machines (SVMs)	To develop a procedure based on vibration and current monitoring for detection of various fault including BRB.	Selecting the proper parameters values through cross-validation, a classification model with high performance and accuracy was achieved. The combination of ICs (Classifier) and SVMs (training) can serve as a promising alternative for intelligent faults diagnosis in the future.
[207]	MCSA Vibration	Time and Frequency Domain	kernel PCA, kernel ICA , SVMs	To develop a procedure based on vibration and current monitoring for detection of various fault including BRB.	The kernel ICA outperforms kernel PCA in clustering based on the investigation of average of Euclidean distance. The nonlinear feature extraction can improve the performance of classifier with respect to reduce the number of support vector. The application of nonlinear feature extraction and SVMs can serve as a promising alternative for intelligent faults diagnosis in the future.
[208]	MCSA Vibration	Time and Frequency Domain	-	To develop a procedure based on vibration and current monitoring for detection of various fault including BRB.	A decision fusion system for fault diagnosis, which integrates data sources from different types of sensors and decisions of multiple classifiers were proposed.
[209]	MCSA Vibration	Time and Frequency Domain	ANNs , Fuzzy , CART	To develop a procedure based on vibration and current monitoring for detection of various fault including BRB.	The proposed model is able to classify and diagnose IM faults.
[210]	Vibration	WPD,EMD	ANN	To integrate the fine resolution advantage of WPD with the self-adaptive filtering characteristics of empirical mode decomposition (EMD) to early fault diagnosis	Ability to extract weak signals and early fault detection of rotating machinery

Table 2.3: Summary of published paper with the aim of broken rotor bar detection in IM

Ref	Data Monitoring	Signal Processing	Decision Making	Purpose	Achievement and Limitation
[211]	MCSA	Stationary WPD	Multiclass SVMs	BRB feature extraction by SWPT under lower-sampling rate	Lower computation and cost without any effect on the performance of SWPT to detect BRB
[212]	MCSA	DWT	-	To investigate the ability of different types of wavelet functions for early BRB detection	The reliability of the fault detection depends on the type of wavelet function applied for decomposition of the signal

2.7 Research Trends in LS-PMSM

Detection of broken rotor bar, as an important fault in various types of squirrel cage electrical motors, can absorb great attentions. Hitherto, several researches have been conducted for broken rotor bar detection in induction machines. However, it is fair to declare that no work has been presented to detect broken rotor bar in LS-PMSM as it is new in industry.

The role of rotor bars in LS-PMSMs is to speed up the rotor to the synchronous speed at startup. The rotor bars also moderate any speed fluctuations that may occur because of sudden load changes. During steady-state operation, if the load abruptly changes, an oscillatory movement will be superimposed on the normal synchronous rotation of the shaft and rotor bars damp out these oscillations. Consequently, indication of broken bar can only be found during transient part of motor running. Transient MCSA has proven as a valuable source of information in some real situations.

In the case of broken rotor bar fault, it is difficult to find the exact fault feature like $f_{brb} = (1 \pm 2ks)f$ or $f_{brb} = (\frac{k}{p}(1 - s) \pm s)f$ because of the slip “s” change. As the slip changes, the frequency value related to the broken rotor bar varies and then it cannot be determined accurately. Accordingly, in the case of slip change it is useless to use frequency domain analysis and using time, and time-frequency domain analysis can be a solution for this situation. A graphical interpretation for the propagation mechanism of the rotor fault harmonics is depicted in Figure 2.7. The periods of the fault harmonics are illustrated on the x-axis, ordered according to the propagation mechanism, whereas the y-axis shows the corresponding frequencies. This illustration may help to understand the effect of rotor faults in three different signal processing analysis.

The importance of rotor fault in addition to increasing the application of LS-PMSM in various fields and lack of information about rotor fault detection in this type of motor are the major motivation to commence a research on rotor fault detection in LS-PMSM.

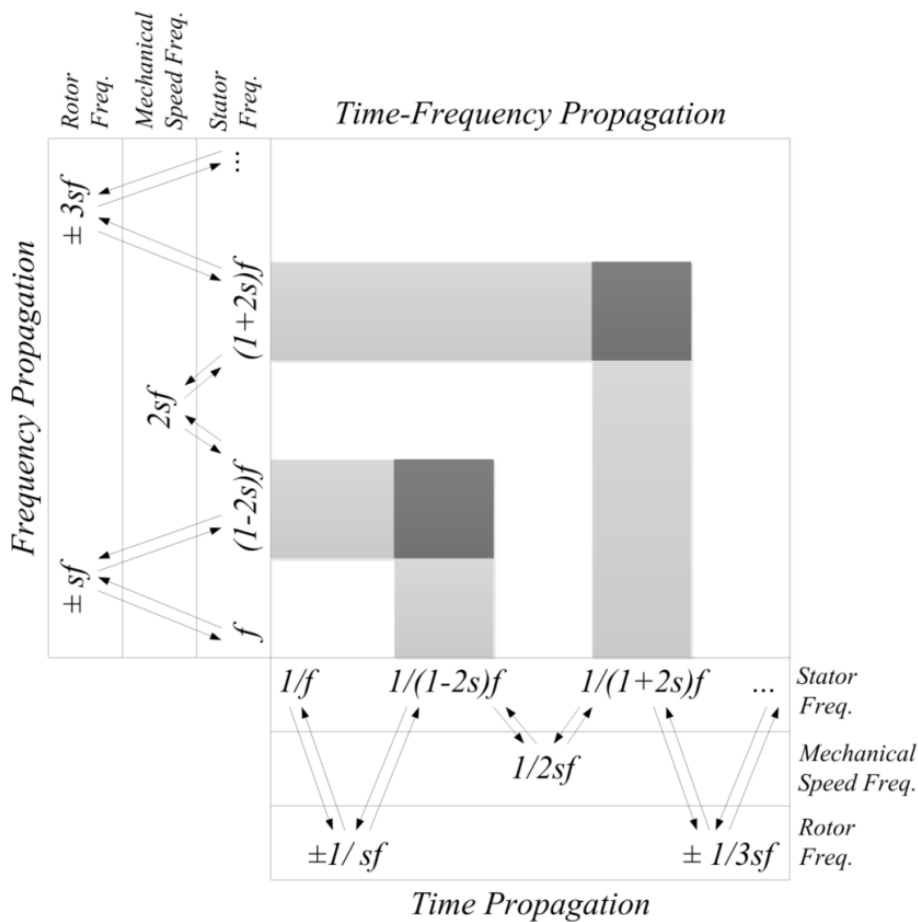


Fig. 2.7: Time–frequency propagation of the rotor fault components [20].

2.7 Summary

This chapter presented an overview on the trends in the detection of broken rotor bars fault in squirrel cage electrical machines. The advantages of LS-PMSM illustrated as new development of squirrel cage electrical machines in industry. Although the squirrel-cage rotors are rugged, broken rotor bar does occur due to various stresses that machine is subjected to. Broken rotor bar is of importance, as it brings about secondary faults that cause the machine fails to work. To prevent such a cumulative destructive process, the problem should be detected early. The growth of employing LS-PMSM in the industry is started and this type of fault has not been investigated for this motor, because of that this fact is introduced as the main motivation of this research work.

Condition monitoring techniques used in electrical machines were introduced. The characteristic fault components in the spectrum obtained from various sensors, such as stator current signals, leakage flux signals, and motor vibration signals were also reviewed. There is a consensus in scientific literature that motor current signature analysis is the most constructive technique for broken rotor bar detection because it is a noninvasive monitoring technique. However, without an effective signal processing method, the fault detection fails. Signal processing can be carried out either in time domain, frequency domain or time-frequency domain. The

characteristics of signal processing methods described in order to analyze the reference signal of motor for the purpose of feature extraction.

Accordingly, a research activity based on motor current signature analysis was designed for broken rotor bar detection in LS-PMSM. The fault under observation, here, was broken rotor bar. Time domain analysis as well as time-frequency analysis of signal were investigated to diagnose the failure at its early stage (when just one bar has been broken) under various levels of load. A detail description of experimental activity and results will be presented in the following chapters.



CHAPTER 3

METHODOLOGY

3.1 Introduction

This chapter presents the methodology employed in the research design for detection of broken rotor bar in LS-PMSM. The methodology contains four main stages in this study and each stage includes various aspects. A brief overview of the methodology employed in this research is depicted in Figure 3.1. The first stage includes modeling of LS-PMSM using finite element method (FEM) in healthy and faulty conditions. In this stage, a 2-D model is developed for three-phase 4-pole LSPMSM. The model is obtained by Ansoft[®] Maxwell 2D software based on the real dimensions of motor, which is used in the work. The approach used here provides an advanced tool for simulation of motor that yields accurate results. The output of this stage is first-hand information on the motor parameters that can be used for fault detection analysis. In the second stage, experimental activities are conducted to monitor motor performance in the cases there is no broken bar and one broken bar. Full explanation on the instruments or devices used for testing and data acquisition is provided in Section 3.3. In the fourth stage, the feature extraction methods based on time and time-frequency domain analyses are applied in order to determine the features that can be related to the fault under observation. In the final stage, to identify which features are reliably attributed to the broken bar, statistical methods like boxplots and analysis of variance (ANOVA) are used to analyze the features determined in stage 3. Both experimental and simulation data are considered.

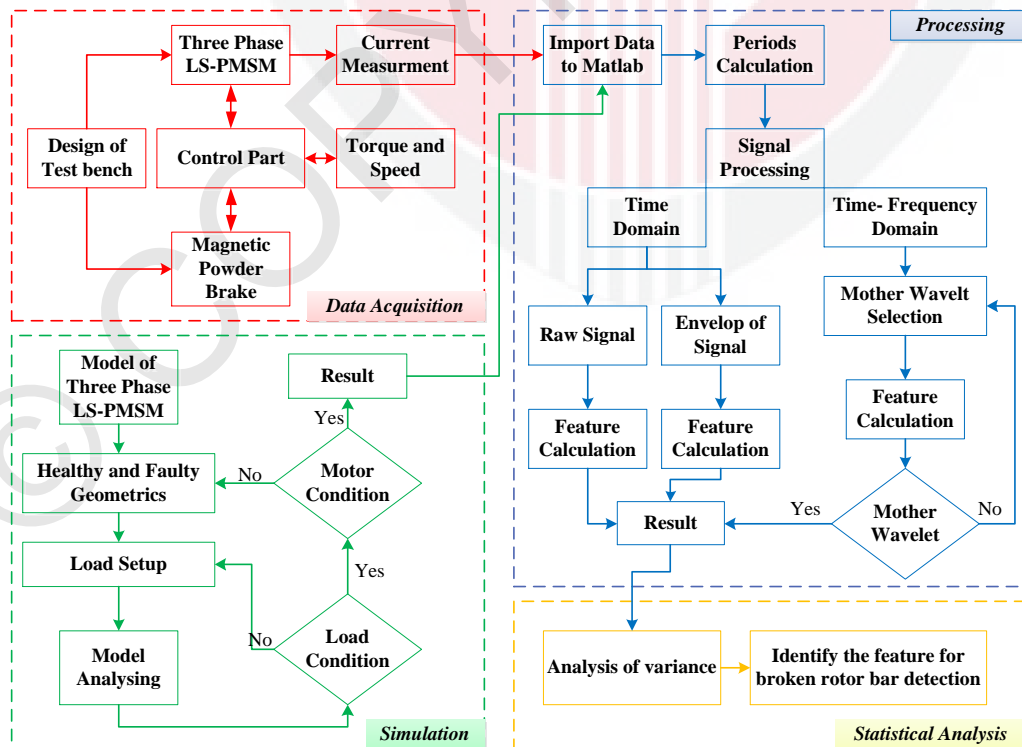


Figure 3.1: Methodology Employed in Research Design

3.2 Simulation of Electrical Motor with Finite Element Method (FEM)

Numerical methods, like boundary element method, finite difference method and FEM, are commonly used to analyze the electromagnetic field problems in electrical machines. Each of these methods has several advantages and some drawbacks. For example, finite difference method is not easily applicable to the field involving rapid changes of the gradient or complex geometries. Nodal distribution can be very inefficient. Equally, boundary element method is not efficient at handling non-linear materials [213]. However, FEM includes nearly all of the advantages of the other two methods exclusive of their significant drawbacks. Especially, finite element method is a powerful method to analysis electric machines; where many aspects (like induced currents, complex geometries, magnetic and electric materials, coupling of thermal and mechanical effects, etc.) need to be considered.

The FEM was first introduced for the computation of magnetic field in nonlinear electromagnetic devices by [214]. It was mainly for solving nonlinear magneto static problems. In [215] pioneered the numerical calculation of transient phenomenon during the operation of electric machines. They used time stepping techniques and nodal method to predict the transient behavior of electric machines. The use of time-stepping finite element method for analyzing nonlinear transient electromagnetic field problems in electrical machines was presented by [216].

The FEM can use topology of magnetic circuit and winding layouts of machine to model the effects of magnetic nonlinearities and space harmonics. In this approach, the geometric model of the machine is divided into a mesh of elements, which means triangle or rectangular finite elements. In each finite element, the partial differential equations that model the motor are replaced by linear interpolation functions, which are solved together with the boundary conditions. To build up a model using FEM, some parameters, like general motor specification, design diameter, material and winding layouts, are required. The FEM is gaining in popularity as computers increase in power and software techniques are implemented that reduce the computational time required to find a solution [217].

In recent years, more attention has been taken to study the electromagnetic performance of permanent magnet synchronous motors using FEM [218]. In reality, different circuits, like stator windings, rotor cage bars and permanent magnets, are directly coupled with the electromagnetic field of the electric machines. The electrical machine has a very complicated geometry and magnetic circuit and it gets further complicated by using rotor cage bars for self-starting. Accordingly, such configuration forces a different modeling which considers the role of rotor as a self-starting component too. This study looks into the dynamics of LS-PMSM using a two-dimensional time-stepping FEM method. The major advantage of using two-dimensional model is to reduce the computation time. In this research, Ansoft® Maxwell 2D software version 16 is used to simulate healthy and faulty condition of LS-PMSMs.

At the first stage, a three-phase LS-PMSM (750 W, 415 V, four-pole) is designed using Ansoft® RMxprt software. Rotational Machine Expert (RMxprt™) is an interactive software package used to design and analyze rotating electrical machines. The design diameters of the motor obtained using the real motor measurement. The design parameters include power, voltage, frequency, poles, material of stator, rotor and shaft, number of stator slots and rotor bar, stator winding layout find in data sheet of motor and some from measure of real motor. Figure 3.2 and 3.3 illustrates the Maxwell 2D model for a LS-PMSM and the meshed region of simulated LS-PMSM, respectively. The specifications and dimensions of the machine are shown in Appendix A. The RMxprt creates some outputs like rotor and/or stator resistance, leakage reactance and/or magnetic reactance, and different type of curves.

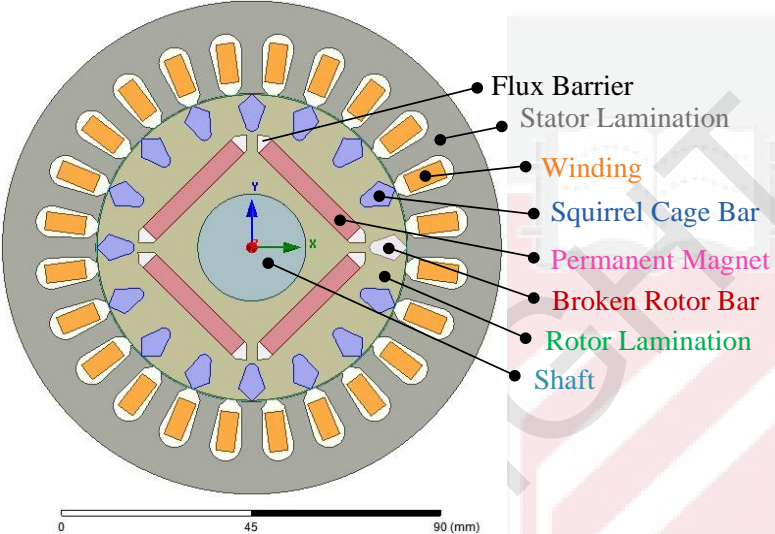


Figure 3.2: The geometry of the LS-PMSM with one Broken Rotor Bar

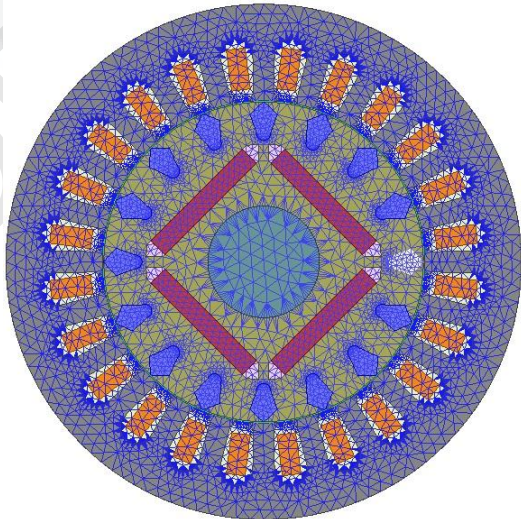


Figure 3.3: Cross-Section of LS-PMSM with Mesh Plotting

Once the motor is designed and a corresponding FEM model is created, the FEM can be conducted in Maxwell 2D. The detailed process of solving a model in Maxwell 2-D is described in Figure 3.4 (ANSYS® Maxwell,15.0). The solution type includes

the transient solver for modeling of motor as it allows analyzing the solutions at each time step of a specified period. Hence, transient solver with time integration method based on backward Euler is employed to compute the stator current of LSPMSM.

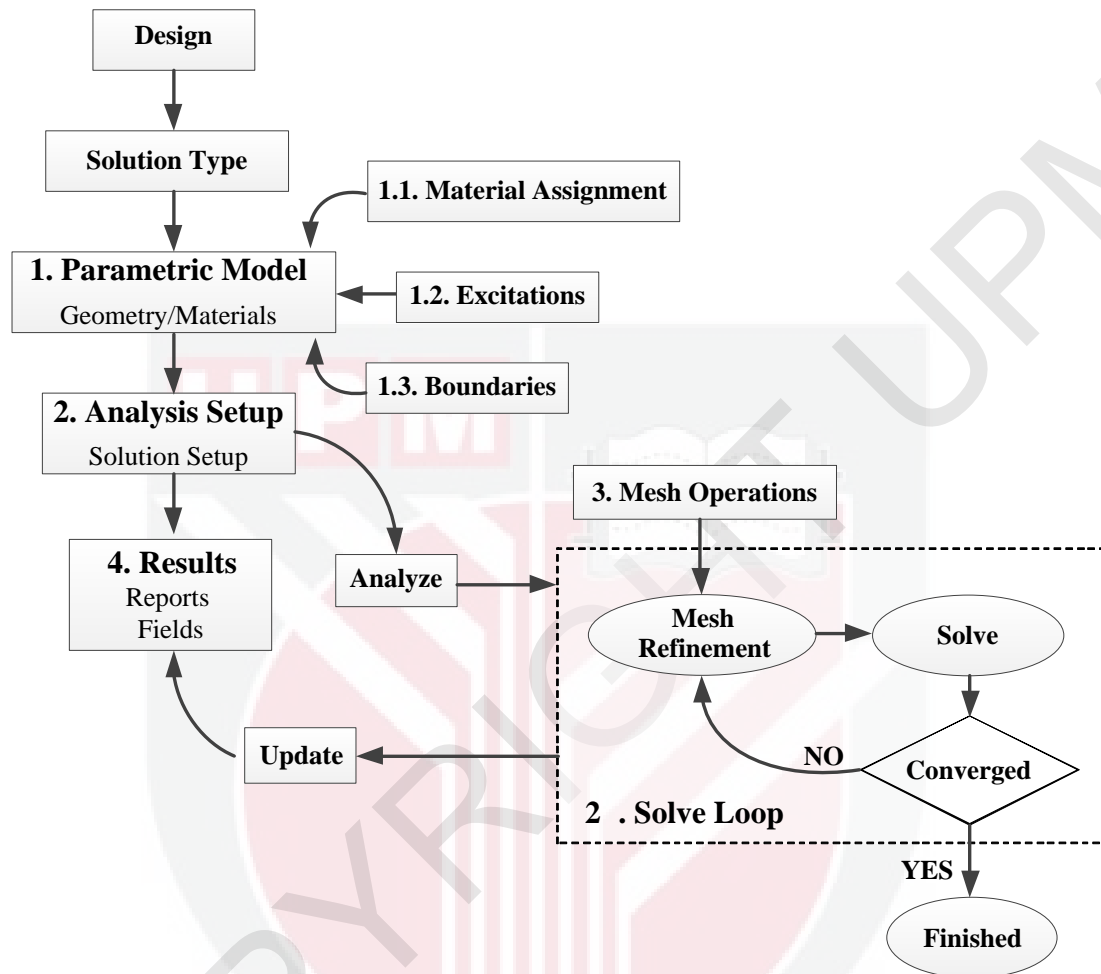


Figure 3.4: The detail process of model solving in Maxwell 2-D

The finite element solution program requires input material characteristics for all magnetic materials in the part of pre-processing. The stator and rotor lamination materials are DR510-50 and the saturation magnetic flux density is 1.85 T, relative permeability of 7000. The B-H curve and Iron loss curve for stator and rotor lamination are shown in Appendix B. The NdFeB permanent magnet (N38SH) is modeled with a straight line B-H curve in the second quadrant. The residual flux density B_r is 1.235 Tesla and the relative permeability μ_r is 1.05. The details are shown in Appendix C.

The excitation sources comprise of phase windings distribution that should be specified. Three-phase sinusoidal voltages are applied to the three stator phase windings as excitation. The voltages for the three stator phase windings can be

represented by Equation (3.1), where $V_{p(L-N)}$ is peak phase voltage, φ_0 is initial phase angle and θ_0 is phase angle shift.

$$V_p = V_{p(L-N)} \sin(2\pi t f + \varphi_0 + \theta_0) \quad 3.1$$

For this study: $V_{rms(L-L)} = 415V$, $f = 50Hz$ and $\varphi_0 = 0$

$$V_{rms(L-N)} = \frac{V_{rms(L-L)}}{\sqrt{3}} = \frac{V_{p(L-N)}}{\sqrt{2}} \quad 3.2$$

$$V_{p(L-N)} = \frac{\sqrt{2}V_{rms(L-L)}}{\sqrt{3}} \quad 3.3$$

$$V_{p(L-N)} = \frac{\sqrt{2} \times 415}{\sqrt{3}} = 338.84 V \quad 3.4$$

$$V_1 = 338.84 \sin(2\pi t \times 50) \quad 3.5$$

$$V_2 = 338.84 \sin(2\pi t \times 50 - 2\pi/3) \quad 3.6$$

$$V_3 = 338.84 \sin(2\pi t \times 50 - 4\pi/3) \quad 3.7$$

3.3 Experimental Design

This section provides a full understanding of the experimental design used in this work. A diagram of the complete experimental test setup is depicted in Figure 3.5. To analyze the effects of broken rotor bar in LS-PMSM on the stator current, an experimental setup has been designed and built in the electrical power laboratory, UPM. Experimental results are used to explain the tests phenomena. The setup consists of an electrical power panel, machine test stand which includes the test machines and load, and data acquisition system. A power panel including motor protection, switch, electromagnetic breaker and contactor are employed for distribution of three-phase electrical power. The LS-PMSM is coupled to the torque and speed sensors through a mechanical coupling in order to measure the torque and speed values in different operation condition. On the other side, a mechanical variable load has been provided by electromagnetic power brake which is coupled to torque sensor using a mechanical coupling. Experimental data including current, torque and speed was acquired from the healthy and faulty motor in identical condition under different loads. The data acquisition system samples the current and speed, and then stores the collected data on a PC for later analysis. Different load and running speed conditions were considered during the motor experiment. Features from current signals were extracted to diagnose the broken rotor bar.

There are a number of factors, which influence accuracy of measurement because of the nature of parameters measured (high bandwidth, low magnitude). These factors are the foundation of the motor and the alignment. The motor must have a firm and rigid foundation to eliminate the vibration and noise. Besides that, the misalignment reduces efficiency of the motor setup. Thus, all the equipment such as motor, torque sensor and electromagnetic power brake are fully fixed on a particular stand follow by proper alignment. Figure 3.6 shows a general overview of the experimental test

rig which includes line start permanent magnet motor, powder break, and torque and speed sensor used in this research.

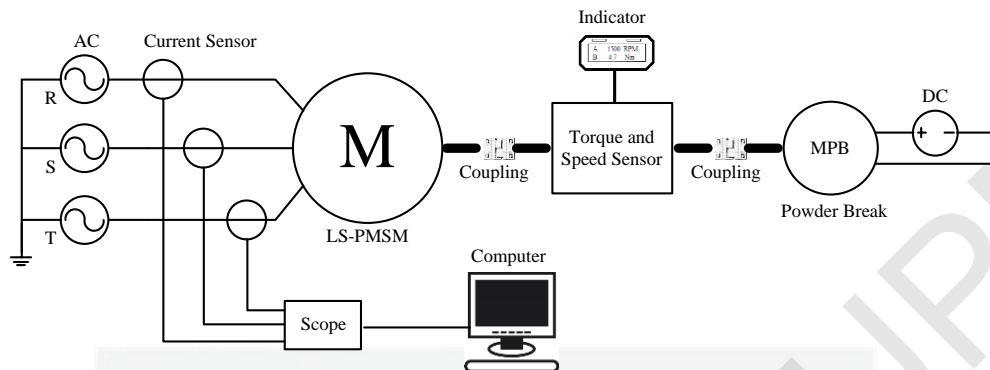


Figure 3.5: Illustration of experimental set up

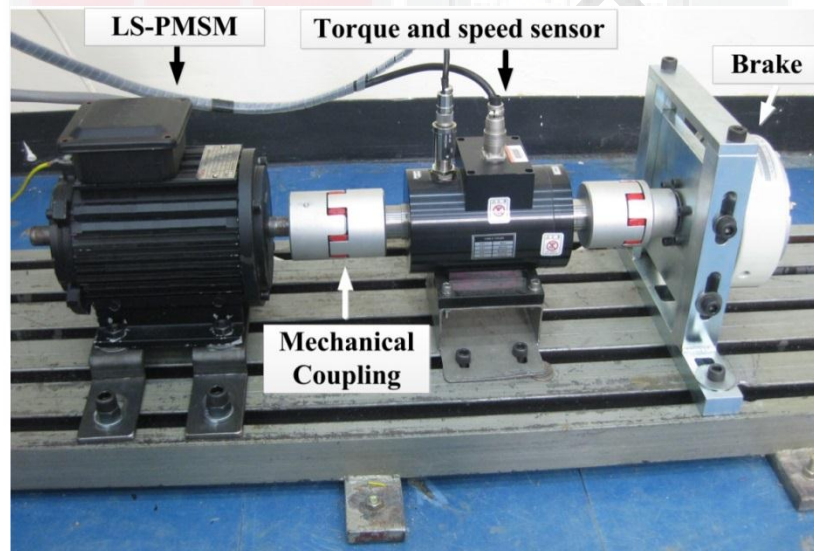


Figure 3.6: Experimental test rig

3.3.1 Experimental Devices

The machine test stand consists of a three-phase power supply, test machines and an electromagnetic power brake used as a load in this research. This section provides a full understanding and complete detailed descriptions of the devices used in current work.

3.3.1.1 Electrical Panel

The LS-PMSM is supplied through the three phase electrical panel. In the electrical panel, motor protection is used for over current protection and earth fault instrument is used for human protection. The electrical circuit for start and stop of motor is also designed and assembled.

3.3.1.2 LS-PMSMs

The main characteristics of the tested motors are: Rated voltage: 415 V, Rated power: 750 W, 4 poles, primary Rated current: 1.2 A, Rated speed: 1500 rpm, Star connection, the number of stator slots: 24, the number of rotor bars: 16. The LS-PMSM used in this research and its nameplate are shown in Figure 3.7.



Figure 3.7: (a) LS-PMSM used in this research and (b) its nameplate

The test motors include healthy motor and motor with one broken rotor bar. The broken rotor was simulated in this study by opening the motor and by drilling a hole in the bar as a common practice [219,220]. The drilled hole is 7 mm in Diameter with a depth of 9.4 mm which can separate the bar completely from end ring. Figure 3.8 is a demonstration of a broken rotor bars made artificially in the laboratory using drill.

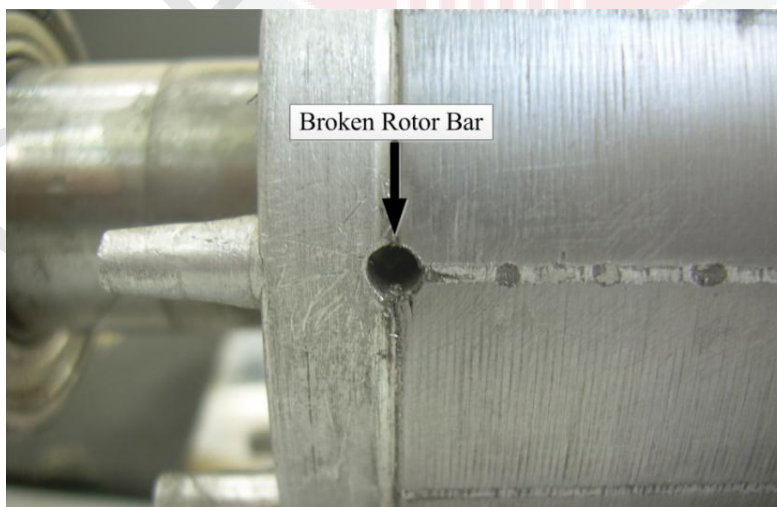


Figure 3.8: Demonstration of the rotor with one broken bar

3.3.1.3 Electromagnetic Power Brake

A mechanical load is set for experimental tests using an electromagnetic power brake. The electromagnetic power brake has three main components: stator, rotor and coil. When the brake is connected to the electricity supply, the magnetic field induced in the coil starts to fluctuate that depends on the ratio of current intensity. These fluctuations in magnetic field change the viscosity of magnetic powder between rotor and stator. The coil in brake, when receives electrical power, causes the particles line up along the force lines of the magnetic field, which bind the rotor and stator together, and produce friction that ensues braking. However, when the connection to electricity supply is ceased, a centrifugal force presses the powder against the stator and consequently the rotor is released that can rotate freely once more. There are some advantages of using electromagnetic power brake instead of conventional mechanical load such as generator for experimental test, such as:

- Excellent slip capacity: operate in a constant slip mode
- Fast response: voltage to torque is almost linear, so quick-response tension is extremely fast.
- Accurate control: controllability of electromagnetic power brake is very accurate.
- Stable torque: Torque does not depend on speed, but it is proportional to the voltage/current applied to the field

The electromagnetic power brake depicted in Figure 3.9 is used in this research. The specification of electromagnetic power brake is described in Table 3.1. Model YSB-2.5 is manufactured by Dongguan Weizheng Electromechanical Technology Co., Ltd.

Table 3.1: Specification of YSB-2.5

Parameters	Value
Model	YSB-2.5
Rated Torque (N.m)	25
Power (W)	30
Voltage (V-DC)	24
Current (A)	1.24
Moment of Inertia	3.8×10^{-3}
Weight (Kg)	9
Maximum Speed (rpm)	1800

No load condition is established via electromagnetic power brake at no-excitation and also different load levels are furnished upon adjusting the DC voltage at electromagnetic power brake terminals up to full load rate, which is 4.8 N.m. A special adjustable stand is designed for MPB in order to connect it properly with the object.



Figure 3.9: Electromagnetic Power Brake Model YSB-1.2

3.3.1.5 Coupling

The connections between electromagnetic power brake, tachometer and motor are made by a flexible Lovejoy coupling shown in Figure 3.10. The flexible shaft coupling compensates for shaft misalignment and damping of critical vibrations. It has other advantageous such as being variable, selectable damping, easy, plug-type assembly.

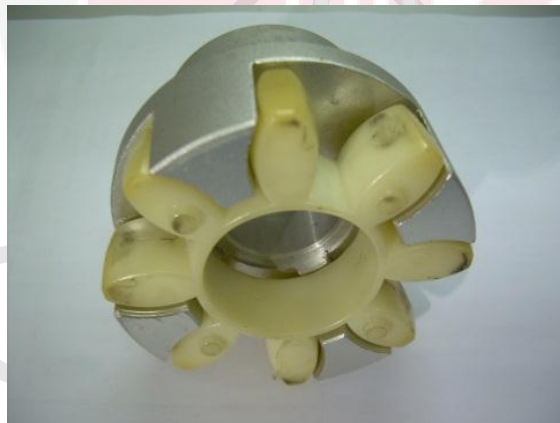


Figure 310: Lovejoy coupling

3.3.1.6 Measurement instruments

This section provides a full understanding of the instruments used in current work. These include complete detailed descriptions of the measurement instruments and digital data acquisition system utilized here.

3.3.1.7 Current transducer

The DAQ system used in this research allows for voltage measurements. For the case of current measurements, the LEM current transducer (LTS 25-NP) was chosen for these purposes. The LTS 25-NP current transducer is specially used for electronic measurement of AC and DC type currents, with a galvanic isolation between the primary circuit (high power) and the secondary circuit (electronic circuit), in applications such as adjustable speed drives, power converters, uninterruptible power supplies, and switched mode power supplies. This current transducer possesses the characteristics of excellent accuracy ($\pm 0.7\%$) and very good linearity ($< 0.1\%$). The LTS 25-NP series have ability of measuring currents up to 80 A for a maximum nominal current of 25 A, precisely. The output of this transducer is an analog output voltage signal that can be calculated from following formula:

$$V_{out} = 2.5 \pm (0.625 \times \frac{I_p}{I_{pn}}) \quad 3.8$$

where I_{pn} : Primary nominal RMS current 6/15/25 At and I_p : Primary current, measuring range.

In this research, three sets of LEM current transducer (LTS 25-NP) were used for measuring the three phases of current. At each test condition the currents were sampled simultaneously through three channels of a scope and stored directly on a personal computer. Figure 3.11 illustrates the board consisting of three sets of LEM current transducer (LTS 25-NP). The specifications of current transducer are shown in Appendix D.

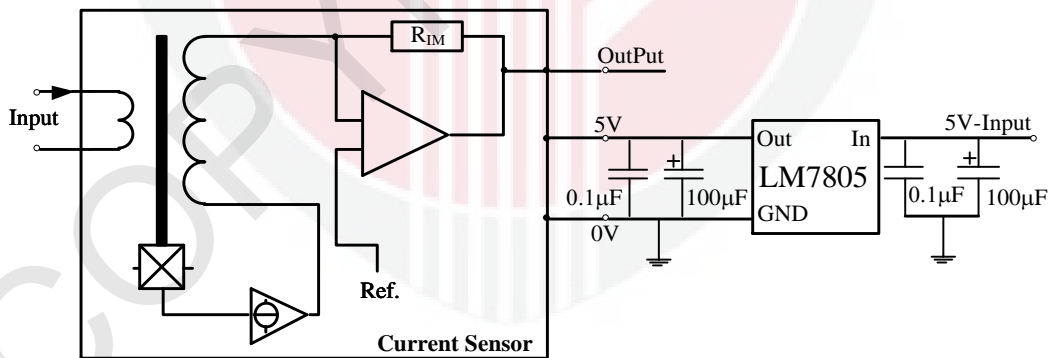


Figure 3.11: Demonstration of the current measurement circuit

3.3.1.8 Torque sensor

The model allows measuring the torque of continuous rotating object. The rated capacity of TRB-10K torque sensor, which the maximum axial load that can be measured by this model, is 10kgf-m (98.07N-m). The TRB-10K possess the characteristics of excellent accuracy, i.e., nonlinearity (0.3 % Rated Output) and hysteresis (0.2 % Rated Output). Rated output is the algebraic difference between the outputs at no-load and at rated load. Besides that, the ability of the TRB-10K to

reproduce output readings when the same load is applied to it consecutively, under the same conditions, and in the same direction is 0.3 % rated output. Figure 3.12 shows the appearance of the torque sensor, Model TRB-10K and its indicator DN-100.



Figure 3.12: Torque sensor and its indicator

3.3.1.9 Speed sensor

A speed sensor, MODEL MP-981, measures speed of the motor. According to the catalogue provided by the manufacturer, this model is a magneto-type detector using a hall element, which is suitable for rpm measurement from ultra-low speed to high speeds. This type of detector uses an internal hall element, a permanent magnet, DC amplifier, and voltage regulator and respond to flux (i.e., the resistance value changes in respond to flux changes), then a rectangle waveform is derived from ultra-low speed all way through high speeds. Figure 3.13 shows the speed sensor, MODEL MP-981, used in this research.



Figure 3.13: Demonstration of the magneto-type detector (MODEL MP-981)

3.3.1.10 The Data Acquisition System

The high sampling rate and high resolution of the system allow the user to get precise and accurate data structures, which are extremely important especially in the areas of motor fault diagnostics. These features are very important because any extraneous information in the motor signals arising due to situations such as noises may yield a false indication of fault. Therefore, such a high quality system is recommended for fault diagnostic applications. The high accuracy and precision of the PC Oscilloscopes provided by Pico technology is used in this work. The PicoScope 4000 Series of PC Oscilloscopes is a range of compact, high-resolution scope units designed to replace traditional bench-top oscilloscopes and it is a very attractive and reliable data collection tool. The current waveforms of three-phase LSPMSM at both healthy and faulty conditions are captured via a high resolution computer-based acquisition system model PicoScope 4424. The configuration of PicoScope 4424 is represented in Figure 3.14. This system is well suited for measuring various input range from small signals as well as higher range signals for general, scientific and field-service usages. The aforementioned system is USB-connected including an industry-leading signal acquisition path that provides 80 MS/s ADC on each channel with 1% accuracy. The PicoScope 4000 Series have input ranges from ± 50 mV to ± 100 V full-scale (± 50 mV to ± 20 V for the PicoScope 4224 IEPE). Accordingly, it offers measuring of small signals from sensors as well as higher voltages from power supply circuits and motor drives. Having a 12-bit resolution (adjustable up to 16 bits in enhanced resolution mode) and accuracy of about 1% make them an excellent option for analysis of noise, vibration and mechanical.



Figure 3.14: PicoScope 4424

3.3.1.11 Voltage Probe

A voltage differential probe is used to measure the voltage difference between two test points, where neither is at ground. Due to their rejection capability, this probe is the best option for making non-ground referenced, floating or isolated measurements in large part. Voltage differential probe extends the functionality of standard single-ended input oscilloscopes and allows a safe and accurate method of measurements for voltage difference. In this research, the stator current of LS-PMSM is measured utilizing current probe model TA041 manufactured by Pico Technology which is displayed in Figure 3.15.



Figure 3.15: Voltage differential probe model TA041

3.3.2 PicoScope and MATLAB Software

PicoScope 6 is the oscilloscope software supplied with all PicoScope® oscilloscopes. PicoScope 6 has a screen to display the signal properly and the most commonly used functions are available by just clicking a button. The best traditional way to control a bench-top oscilloscope was with knobs and dials. Pico Technology created PC-based oscilloscopes, in which there are no hardware to control the device itself and everything is controlled by the software instead. The software environment of PicoScope 6 is depicted in Figure 3.16. Since mouse or keyboard or touchscreen are the means of control and capture in a PC environment, the interface had undergone an evolutionary change.

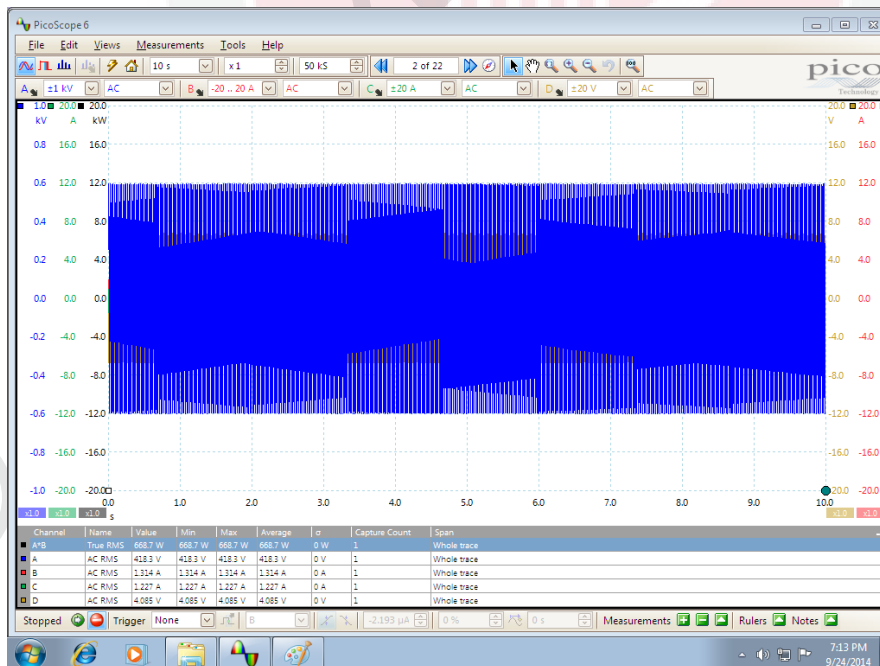


Figure 3.16: PicoScope 6 environment

Nowadays, MATLAB® environment is the fundamental tool for analyzing the simulated and measured data in almost all research. This software provides a flexible mode of introducing the data to be analyzed. It has a set of powerful functions that allow the signal analysis in the time, frequency and time-frequency domain. In this research work, MATLAB workspace has extensively been applied for signal analysis. The MATLAB® command line is used for analysis of the original signal in Time domain and Time-Frequency domain. Therefore, the M-file was written in MATLAB® workspace appended in Appendix E.

3.4 Sampled Signals Procedure

The signals can be divided into two types; stationary and non-stationary. In this study, the start-up signal of LS-PMSM is considered for feature extraction and this signal is non-stationary. In this study, four different levels of load have been applied to the electromagnetic power brake as: (0, 0.5, 1, and 1.5) Nm for both healthy and faulty conditions to study the effects of loads in fault identification procedure. To work on transient signal, a pre-processing is necessary in order to highlight the differences of signals obtained from healthy and faulty electrical motors. Accordingly, after signal measurement and before the analysis of signal a pre-processing is necessary. The pre-processing step is the key factors for accurate signal analysis and to data measurement.

Zero crossing and selecting an equal number of periods in the signal are important pre-processing techniques that should apply to transient signals before any analysis. If signal processing is implemented for the fault detection of electrical machine, the current signal is required to be synchronized first. Therefore, the acquired signal is first preprocessed by synchronizing the starting origin with phase 0. In order to have the same condition for data analysing, 40 periods in transient current signal, from zero starting point to steady state condition, are selected and then around 4000 samples are given for each data set. Transient stator current signals are measured experimentally under four different load conditions. The waveforms of the signal that selected for processing are shown in Figure 3.17 for No-load condition.

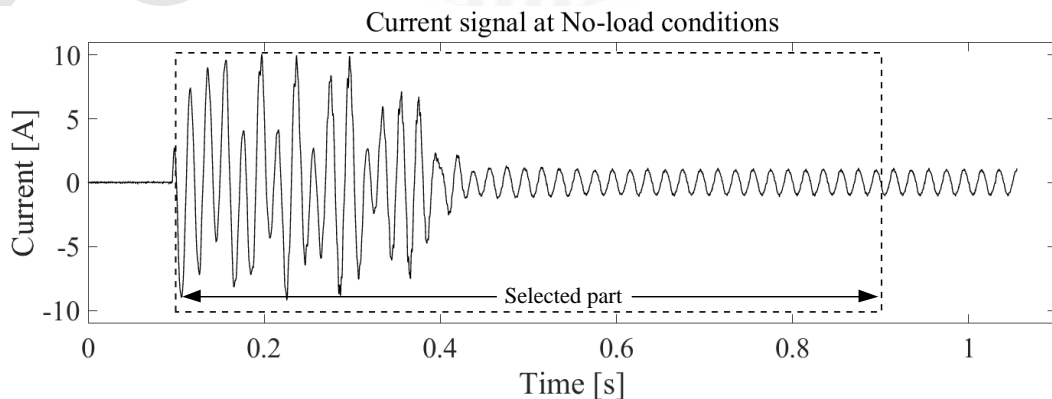


Figure 3.17: The transient stator current signals that selected for processing

3.5 Signal Processing Procedure

Raw signals acquired from measuring instruments and sensors, which measure a physical parameter over a period, always contain noises. Therefore, it is generally impractical to obtain meaningful information from a raw signal by just looking at it. A technique that suppresses the effects of noise and transforms the raw signal to a meaningful representation using computer algorithms is called signal processing. In this respects, a signal acquired from condition monitoring of an electrical motor needs to be analyzed using a signal processing method to extract fault-related features necessary to make decision. The synchronized signal is analyzed to extract the features related to broken rotor bar fault. Following sections present the procedure for time domain and time- frequency domain analysis of current signal for broken rotor bar detection.

3.5.1 Time Domain Analysis

Time-domain analysis helps to extract characteristic features from time waveform signals as descriptive statistics. In any fault diagnosis algorithm, extraction of characteristic feature from a signal is the key step, since the critical information for decision-making is obtained from this step and thus its accuracy directly influences the final monitoring results [221]. Han et al. compared the features obtained from time domain analysis of the steady state current signal and indicated the ability and efficiency of these features for detection of different faults [221].

Statistic features can be used to characterize the behavior alteration of a signal when any failure occurs in a device. The simplicity of features extraction from time waveform signals and their implementation accompanied with a low computational time make time domain analysis attractive for detection of failure in electrical devices [222]. In this research, time domain signal processing is used to analyze the signals acquired during start-up operation of motor. Analysis of a raw signal, time domain signal, can be used for extraction of features related to broken rotor bar. Statistical parameters use as a quick test for changes in the pattern of signals. Accordingly, a detector was developed based on statistic features of the acquired line current. In the following, two different algorithms for time domain analysis are discussed.

3.5.1.1 Statistical feature in time domain

The broken bars cause harmonic components $f_{LSH} = (1 - 2s)f$ in the stator current as explained in chapter 2. During the startup, the slip of motor changes from a value to be equal to one at the beginning to a value to be equal to zero in steady state. Hence, the frequency of left sideband harmonic (f_{LSH}) changes from the fundamental frequency to zero and again to the fundamental frequency. This left sideband harmonic is directly added to the signal. The measured signals obtained from the experiment were calculated to obtain the most significant features by feature calculation. The accuracy of feature calculation is of substantial importance since it directly affects the final diagnosis results.

Using different statistical features related to the fault increases the reliability of fault detection in the equipment. As the goal of this research was to find a suitable fault-related feature for broken rotor bar detection through a statistical analysis, for each specified condition, 40 tests were executed. Measurement was performed for two healthy and faulty motors at 4 levels of load condition, and hence 320 data sets were obtained for each statistical features. In total, 4160 data are obtained from these 13 features for two healthy and faulty motors.

Characteristic features or feature parameters extracted from a raw signal in time domain include both dimensional and the non-dimensional statistical parameters. Examples of dimensional parameters are Mean, Root Mean Square (RMS), Root-sum-of-squares level (RSS), Peak-Peak value, Energy, variance, standard deviation. Non-dimensional parameters are pulse index, waveform index (Shape Factor), impulsion index, peak index (Crest factor), tolerance index (Margin factor), skewness index, kurtosis index. These feature parameters are listed as below:

A. Dimensional Parameters:

1. Mean

$$X_{Mean} = \frac{1}{N} \sum_{i=1}^N X_i \quad 3.9$$

2. RMS

$$X_{RMS} = \sqrt{\frac{1}{N} \sum_{i=1}^N X_i^2} \quad 3.10$$

3. RSS

$$X_{RSS} = \sqrt{\sum_{i=1}^N |X_i^2|} \quad 3.11$$

4. Peak to peak value

$$X_{PP} = \max(X) - \min(X) \quad 3.12$$

5. Energy

$$X_{Energy} = \sum_{i=1}^N X_i^2 \quad 3.13$$

B. Non-dimensional Parameters:

1. Waveform index (Shape Factor)

$$X_{Wi} = \frac{X_{RMS}}{\frac{1}{N} \sum_{i=1}^N |X_i|} \quad 3.14$$

2. Impulsion index

$$X_{Ii} = \frac{\max|X|}{\frac{1}{N} \sum_{i=1}^N |X_i|} \quad 3.15$$

3. Peak index (Crest factor)

$$X_{Pi} = \frac{\max|X|}{X_{RMS}} \quad 3.16$$

4. Tolerance index (Margin factor)

$$X_{Ti} = \frac{\max|X|}{\left(\frac{1}{N} \sum_{i=1}^N |X_i|^{1/2}\right)^2} \quad 3.17$$

5. Peak-to-average power ratio

$$X_{PA} = \frac{(\max(X))^2}{(X_{RMS})^2} \quad 3.18$$

6. Variance

$$X_{Va} = \frac{1}{N-1} \sum_{i=1}^N |X_i - X_{Mean}|^2 \quad 3.19$$

7. Skewness index

$$X_{Si} = \frac{1}{N} \sum_{i=1}^N \frac{(X - X_{Mean})^3}{\sigma^3} \quad 3.20$$

8. Kurtosis index

$$X_{Ki} = \frac{1}{N} \sum_{i=1}^N \frac{(X - X_{Mean})^4}{\sigma^4} \quad 3.21$$

Where X is a signal, N is number of sampled data points of signal, and σ is standard deviation that is calculated from

$$\sigma = \sqrt{\frac{1}{N} \sum_{i=1}^N (X - X_{Mean})^2} \quad 3.22$$

3.5.1.2 Statistical feature in envelop time domain

The instantaneous magnitude of the stator current (or current modulation) can be used as indication of fault in electrical machine [142]. Due to fault occurrence, like broken bar, the modulation of the stator current, called envelope, is generated in amplitude of the stator currents. The envelope is cyclically repeated at a frequency equals to twice the slip frequency $2sf$ [223,224].

The nature of rotating magnetic field in a healthy motor is an ideal periodical profile over a two-pole pitch that leads to a circular sketch of the space vector for magnetic field. When a bar in the rotor breaks, no induced current can flow in it and thus the ideal periodical profile is missed over the two pole pitches of the rotor [225]. As a result, the neutral plane orientation of magnetic field in faulty rotor deviates from its position in a healthy motor, and thus an angular shifting is generated in the waveform of magneto motive force for rotor. This angular shifting changes in a cyclical manner depending upon the number of broken bars and its geometric distribution around the rotor [225]. Alteration in orientation of the magnetic field, which results local saturation in the rotor laminations around the broken bars, leads the space vector of magnetic field becomes quasi-elliptical and modulate the stator current in sequence [142].

In this part, envelope is used as a feature (or fault characteristic) for diagnosis of broken rotor bar in LS-PMSM. The first step of the proposed approach is to extract the analytic signal from one phase current signal by applying the Hilbert transform to the current signal. The Hilbert transform is defined as a convolution between the original signal and the function $1/\pi t$. Considering a real time current signal $i(t)$, Hilbert transform for this signal, $H(i(t))$, is expressed as [145]:

$$H(i(t)) = i(t) * \frac{1}{\pi t} = \frac{1}{\pi} \int_{-\infty}^{\infty} \frac{x(\tau)}{t-\tau} d\tau \quad 3.23$$

The Fourier Transform of the function $(1/\pi t)$ is defined as:

$$F\left(\frac{1}{\pi t}\right) = \begin{cases} -j & \text{if } f > 0 \\ j & \text{if } f < 0 \end{cases} \quad 3.24$$

Where f is the frequency in Hertz.

Equation (3, 24) relies on positive frequencies in the $i(t)$ spectrum that are shifted by -90° and the negative frequencies shifted by 90° . Depending on the frequency sign of input signal, Hilbert transform can then be applied as a filter of amplitude unity and phase $\pm 90^\circ$. A new complex signal, called analytic signal, $Z(t)$, is created using adding a real signal $i(t)$ and its Hilbert transform defined as Equation (3.25):

If $y(t) = H(i(t))$

$$Z(t) = i(t) + jy(t) \quad 3.25$$

The signal $Z(t)$ filters all the negative frequencies of $i(t)$. The analytic signal $Z(t)$ also can be defined as

$$Z(t) = a(t)e^{j\theta(t)} \quad 3.26$$

Where $a(t)$ and $\theta(t)$ are the instantaneous amplitude and the phase of $Z(t)$, respectively. These parameters can be computed as follows.

$$a(t) = \sqrt{i^2(t) + y^2(t)} \quad 3.27$$

$$\theta(t) = \arctan(y(t)/i(t)) \quad 3.28$$

When the analytic signal is obtained using Equation (3.25) or (3.26), the envelope of this complex, defined as the absolute value of the signal, is comprised using Equation (3.29).

$$E(t) = |Z(t)| = |i(t) + jy(t)| = a(t) \quad 3.29$$

Due to the above explanation, the same procedure was followed for extracting the envelopes of measured signals. The envelopes of startup current signals were extracted by the Hilbert transform using MATLAB software. Figure 3.18 shows the current signal and envelope on it in no load condition for both healthy and faulty machine.

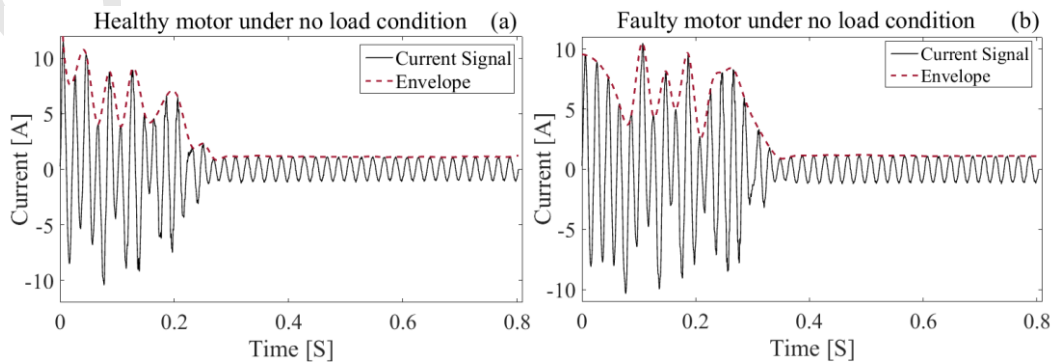


**Figure 3.18: The transient current signal and its envelope
a) healthy motor, b) faulty motor**

The next step includes analyzing the envelop signal to extract the statistical feature from it. These parameters used are described in section 3.5.1.1. Using different statistical features related to the fault increases the reliability of fault detection in the equipment. As the goal of this part was to find a suitable fault-related feature for broken rotor bar detection through a statistical analysis using transient envelop signal. For each specified condition, 40 tests were executed. Measurement was performed for two motors (healthy and faulty) at 4 levels of load condition, and hence 320 data sets were obtained for each statistical features. In total, 4160 data are obtained from these 13 features for two motors (healthy and faulty).

3.5.2 Time-Frequency Analysis

In order to overcome the problem of non-stationary signals, time-frequency analysis, consists of the time, frequency, and amplitude representation of a signal, has been proposed. There are many time-frequency tools that have satisfactorily been applied for the diagnosis of different motor faults. In qualitative terms, time-frequency transforms can be divided into two main types: discrete and continuous. Each of these groups has its own characteristics and advantages for the diagnosis [226].

Continuous like: Short Time Fourier Transform (STFT) or the Continuous Wavelet Transform (CWT) and Wigner-Ville Distribution (WVD)

- more complete representation of the fault components evolutions,
- enable the diagnostic based on more harmonic: higher reliability,
- enable the discrimination among failures and between failures and other phenomena, and
- suitable for off-line diagnosis.

Discrete like: Discrete Wavelet Transform (DWT)

- simple,
- usually with lower computational burden,
- facilitate the quantification of the fault severity, and
- suitable for on-line diagnostic systems

In this study, Discrete Wavelet Transform is used as a time-frequency domain analysis.

Wavelet Transform is an effective signal processing which has been found to be successfully useful in area of analysing non-stationary signal to describe aperiodic, intermittent, noisy, and transient and so on. Wavelet Transform is the transform of a signal from time domain to time-frequency domain and has the ability to look at the signal simultaneously in time and frequency domain in a distinctly different from other traditional time-frequency domain transform. The resolution problem of the STFT is also solved by using Wavelet Transform.

Wavelet analysis of a waveform signal expresses the signal in a series of oscillatory functions with different frequencies at different time. It divides the signal into time-scale space and the size of the window at time and frequency (scale) is not rigid

[172]. Figure 3.19 illustrate the principle of Time–Frequency resolution for wavelet transform and STFT approach.

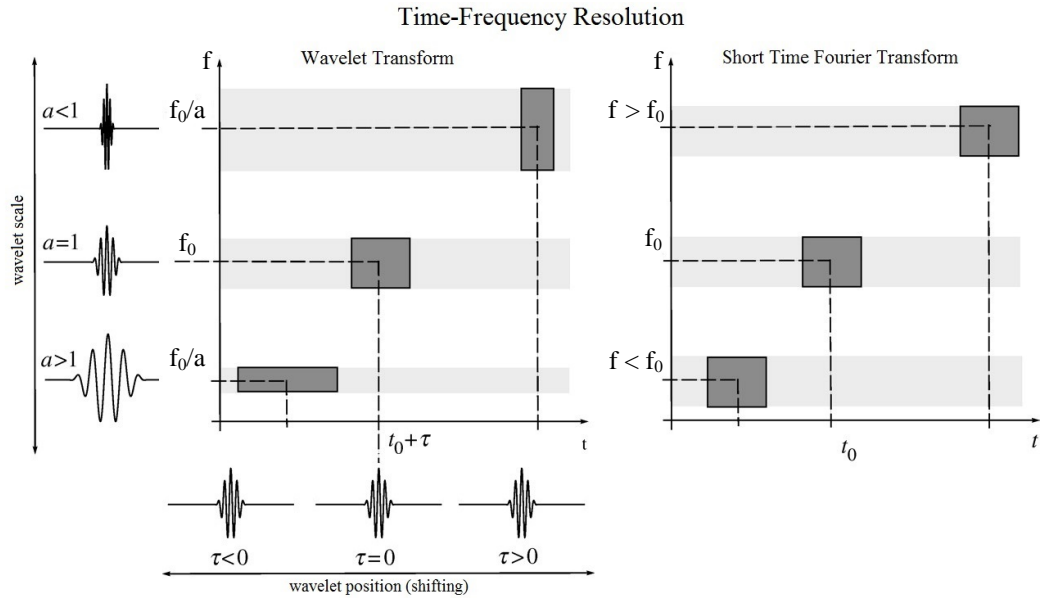


Figure 3.19: Illustration of the principle of Time–Frequency resolution for wavelet transform and STFT approach

A wavelet is a waveform of effectively limited duration that has an average value of zero. Wavelet transform refers to a mathematical processing to transform a raw signal $f(t)$ to a signal in term of shifted and dilated version of singular function, called mother wavelet $\Psi(t)$ (analyzing wavelet). A function called family wavelet is defined as [173] :

$$\Psi_{a,\tau}(t) = \frac{1}{\sqrt{a}} \Psi\left(\frac{t-\tau}{a}\right) \quad 3.30$$

where a is wavelet scale, τ is the wavelet position (time parameter, shifting). Scaling and a wavelet means compressing or stretching the wavelet, while shifting a wavelet means hastening or delaying its onset. Delaying a function $f(t)$ by τ is mathematically represented by $f(t - \tau)$. Figure 3.17 also illustrates the principle of wavelet transform, scaling and shifting of a signal.

In Discrete Wavelet Transform, the scale a and the time τ are described as follow: $a = a_0^m$ and $\tau = na_0^m \tau_0$, where m and n are integers. Accordingly, discretized family wavelet is defined as:

$$\Psi_{m,n}(t) = a_0^{-m/2} \Psi(a_0^{-m} t - n\tau_0) \quad 3.31$$

The discrete wavelet transform of the signal $f(t)$ is defined by

$$DWT_{\psi} f(m, n) = \int_{-\infty}^{\infty} f(t) \Psi_{m,n}^*(t) \quad 3.32$$

The resolution of the signal, which is a measure of the amount of detailed information in the signal, is changed by the filtering operations, and the scale is changed by down sampling operations. The procedure starts with passing the signal $f(t)$ with the length N through a half-band digital low pass filter with impulse response $g[n]$ and a half band digital high pass filter with impulse response $h[n]$. The low-pass filter is called scaling filter, while high-pass filter is referred as wavelet filters. The output of these filters consists of N wavelet coefficients. The outputs from the low-pass filter are the approximation coefficients at the first level of resolution. The outputs from the high-pass filter are the detail coefficients at the first level of resolution. The coefficients produced from wavelet analysis however are different depending on the wavelet family selected. This constitutes first level of decomposition, and can mathematically be expressed as:

$$A_n^1 = \sum_{k=0}^{N-1} g[k]f[t - k] \quad 3.33$$

$$D_n^1 = \sum_{k=0}^{N-1} h[k]f[t - k] \quad 3.34$$

The approximation coefficients at the first level of resolution are used as inputs for another pair of wavelet filters (identical with the first pair). Therefore, sets of approximations and detail coefficients of length $N/2$ are generated at the second level of resolution [227]. For second level of decomposition, the approximation and detail coefficients can mathematically be expressed as:

$$A_n^2 = \sum_{k=0}^{N/2-1} g[k]A_n^1[2t - k] \quad 3.35$$

$$D_n^2 = \sum_{k=0}^{N/2-1} h[k]D_n^1[2t - k] \quad 3.36$$

In [173], Mallat introduced a practical version of discrete wavelet transform, called wavelet multi-resolution analysis. This algorithm is based on the fact that, one signal is decomposed into a series of small waves belonging to a wavelet family. The multi-resolution analysis commonly uses discrete dyadic wavelet, in which scales and positions are based on powers of two. The multi-resolution analysis extracts approximations and details of the original signal at different levels of resolution. An approximation is a low resolution representation of the original signal. The detail represents the high frequency contents of the signal. The approximations and details can be determined using low and high pass filters. In the multi-resolution analysis, the approximations are split successively, while the details are never analysed further. A discrete signal $f[t]$ could be decomposed as:

$$f[t] = \sum_k A_{m_0,n} \phi_{m_0,n}[t] + \sum_{m=m_0}^{m-1} \sum_n D_{m,n} \psi_{m,n}[t] \quad 3.37$$

where ϕ is the scaling functions, deduced by father wavelet and ψ is the wavelet functions, deduced by mother wavelet, A is approximate coefficients and D is detail coefficients. In this approach, the scaling function is represented by the following mathematical expression:

$$\phi_{m_0,n}[t] = 2^{m_0/2} \phi(2^{m_0}t - n) \quad 3.38$$

i.e. $\phi_{m_0,n}$ is the scaling function at a scale of 2^{m_0} shifted by n . Wavelet function is also defined as

$$\psi_{m,n}[t] = 2^{m/2}\psi(2^m t - n) \quad 3.39$$

i.e. $\psi_{m,n}$ is the mother wavelet at a scale of 2^m shifted by n .

Generally, approximate coefficients $A_{m_0,n}$ are obtained through the inner product of the original signal and the scaling function.

$$A_{m_0,n} = \int_{-\infty}^{\infty} f(t) \phi_{m_0,n}(t) dt \quad 3.40$$

The approximate coefficients decomposed from a discretized signal can be expressed as

$$A_{(m+1),n} = \sum_{n=0}^N A_{m,n} \int \phi_{m,n}(t) \phi_{m+1,n}(t) dt = \sum A_{m,n} \cdot g[n] \quad 3.41$$

In dyadic approach, the approximation coefficients $A_{m_0,n}$ are at a scale of 2^{m_0} . The filter $g[n]$ is a low-pass filter. Similarly, the detail coefficients $D_{m,n}$ can generally be obtained through the inner product of the signal and the complex conjugate of the wavelet function.

$$D_{m,n} = \int_{-\infty}^{\infty} f(t) \cdot \psi_{m,n}^*(t) dt \quad 3.42$$

The detail coefficients decomposed from a discretized signal can be expressed as

$$D_{(m+1),n} = \sum_{n=0}^N A_{m,n} \int \phi_{m,n}(t) \cdot \psi_{m+1,n}(t) dt = \sum A_{m,n} \cdot h[n] \quad 3.43$$

In dyadic approach, $D_{m,n}$ are the detail coefficients at a scale of 2^{m_0} . The filter $h[n]$ is a high-pass filter. It is significant to note that the wavelet coefficients are directly dependent on the shape of the wavelet function.

The decomposition process can be iterated, with successive approximations being decomposed in turn, hence one signal is broken down into many lower resolution components. This process is called the wavelet decomposition tree. Figure 3.20 illustrates the dyadic wavelet decomposition algorithm regarding the coefficients of the transform at the different levels.

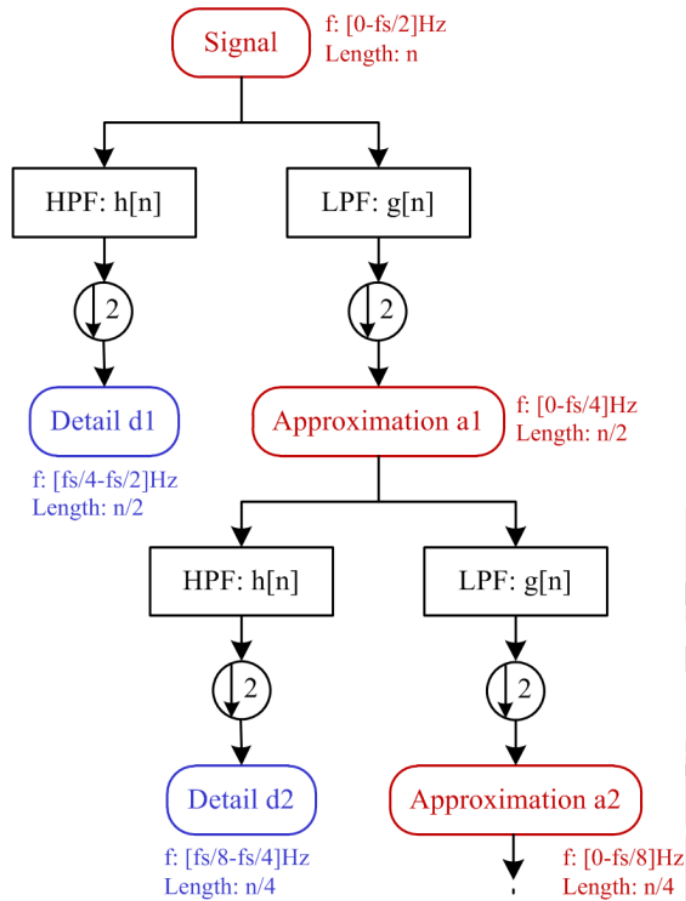


Figure 3.20: Dyadic Wavelet Decomposition Algorithm

In wavelet analysis, an appropriate wavelet function has to be selected to perform the best signal decomposition. However, the results produced are unique to the selected wavelet function, because their ability at encoding, de-noising, compressing, decomposing and reconstructing of the signal is different. The types of wavelet function for fault diagnosis purpose have been chosen by user's decision so far. It is therefore desirable to select a wavelet function that produces the best results for the signal being analyzed and prevent to misleading diagnosis. Accordingly, the selections of best wavelet functions with different order are essential. In this research, 102 wavelet functions have been chosen for examination of incipient broken rotor bar detection to find the best wavelet functions. Table 3.2 shows the wavelet functions that are used in this research.

Wavelet transform provides a set of decomposed signals in independent frequency bands, which depends on level of decomposition. In other words, each level of decomposition provides a signal of a certain frequency band and the levels of resolution determine the resolution of a signal in terms of its time and frequency. Therefore, to obtain a signal that encompasses frequencies of interest, the level of decomposition should be determined first.

Table 3.2: Wavelet functions

Wavelet Functions	Wavelet order
Haar	'haar'
Daubechies	'db1', 'db2', ... , 'db10', ... , 'db45'
Coiflets	'coif1', ... , 'coif5'
Symlets	'sym2', ... , 'sym8', ... , 'sym20'
Discrete Meyer	'dmey'
Biorthogonal	'bior1.1', ..., 'bior6.8'
Reverse Biorthogonal	'rbio1.1', ..., 'rbio6.8'

Depends on the type of application, a signal may contain high frequency with low time resolution or low frequency with high time resolution. The optimum number for levels of resolution is the minimum number of levels that the decomposed signal can be reconstructed to the original form without any loss of information. If the f_s is the sampling frequency used to capture the signal, then the interval frequency for the detail space D_m and approximation space A_m are extracted from these equations:

$$f(D_m) \in [2^{-(m+1)} f_s, 2^{-m} f_s] Hz \quad 3.44$$

$$f(A_m) \in [0, 2^{-(m+1)} f_s] Hz \quad 3.45$$

Therefore, discrete wavelet transform carries out the filtering process like shown in Figure 3.21.

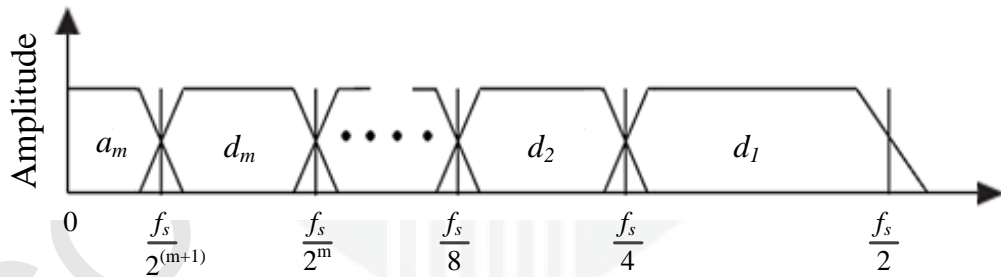


Figure 3.21: Filtering Process

The sampling frequency used for capturing the data in this research is 5000 samples/second. To determine the appropriate level of decomposition, the original signal of motor current was first decomposed into 7 levels. Each level has its own range of frequencies. Tables 3.3 present the frequency ranges corresponding to each level. It is clear that the fundamental frequency is located in the frequency range corresponding to detail 6.

Table 3.3: Frequency ranges for wavelet decomposition of signal

Decomposition Level	Frequency ranges (Hz)	
	Detail	Approximation
level 1	2500-1250	1250-0
level 2	1250-625	625-0
level 3	625-312.5	312.5-0
level 4	312,5-156,2	156,2-0
level 5	156.25-78.12	78.12-0
level 6	78.12-39.06	39.06-0
level 7	39.06-19.53	19.53-0

As explained in chapter 2, broken bars cause harmonic components $(1 - 2ks)f$ in the stator current. Among these components, the main one corresponds to the frequency that has k to be equal to 2, called left sideband harmonic and defined as:

$$f_{LSH} = (1 - 2s)f \quad 3.46$$

During the startup, the slip of motor changes from a value to be equal to one at the beginning to a value to be equal to zero in steady state. Hence, the frequency of left sideband harmonic (f_{LSH}) changes from the fundamental frequency to zero and again to the fundamental frequency. The appearance of this harmonic and its particular evolution was also explained in [36]. The behavior of left sideband harmonic frequency during the start-up transient is shown in Figure 3.22.

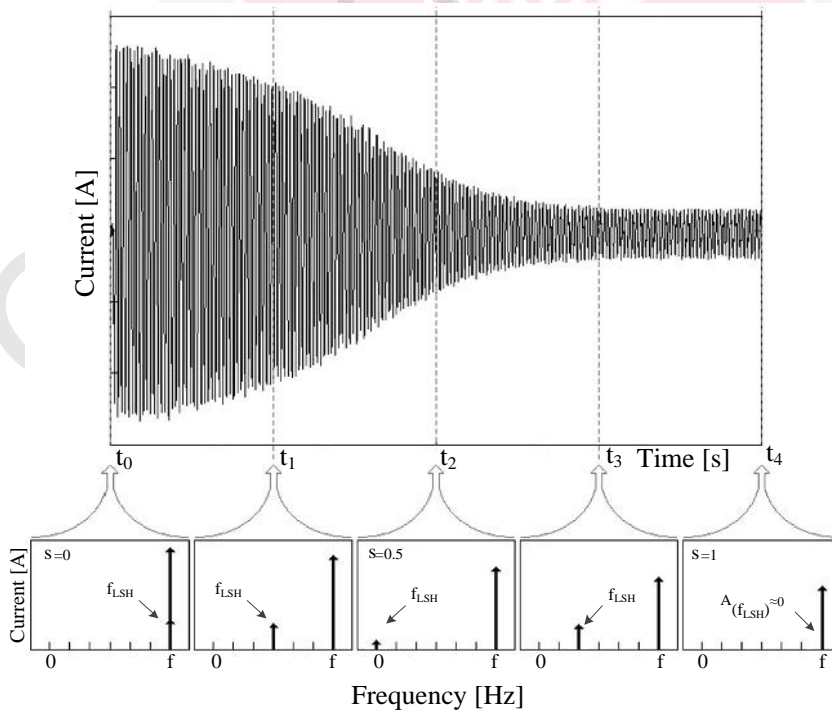


Figure 3.22: Behavior f_{LSH} during the start-up

Ideally, the frequency of the left sideband harmonic (f_{LSH}) varies from the frequency of stator supply to zero and it returns near the frequency of supply again (Figure 3.20). The main idea underlying this alternative methodology is tracking the characteristics transient evolution of the fault related feature to the left side harmonic frequency comes from [228]. A qualitative pattern rising in high decomposition level of the signals shows a good indicator for the fault detection as shown in Figure 3.23. Hence, the reconstructed signal that comes from the detail and approximation of level 7 and also approximation of level 6 are used as an input signal for calculating the fault related feature. The relevant frequency bands of D7, A7 and A6 are shown in Table 3.3.

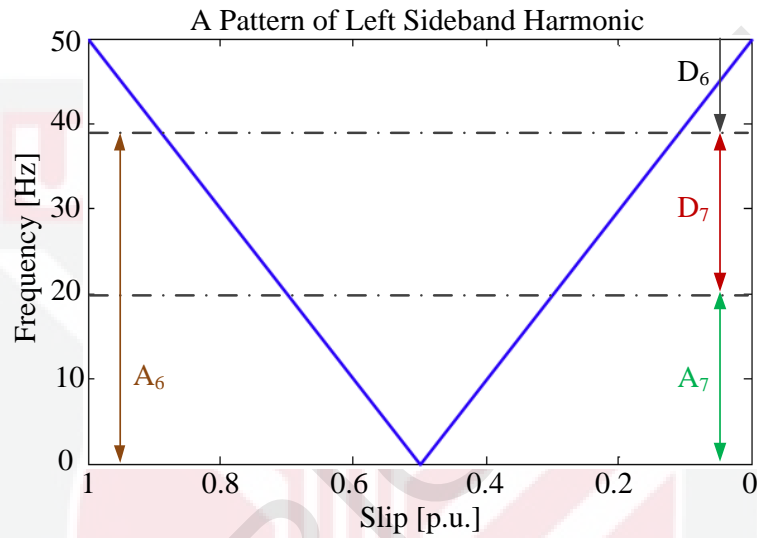


Figure 3.23: Theoretical behavior of f_{LSH} as a function of slip.

The applicability of using wavelet transform analysis for electrical motor health monitoring and fault diagnosis is based on the existence of some sensitive bands in the monitored signals which reflects the machine's healthy or faulty status. Accordingly, the features are evaluated in this research for monitoring of broken rotor bar fault in LS-PMSM. The features used in this research are Log energy Entropy and Shannon Entropy. These features are common concept in many fields, mainly in wavelet transform signal processing and listed as bellow:

1. Entropy "Shannon"

$$X_{EShannon} = - \sum_i X_n^2 \log X_n^2 \quad 3.47$$

with the convention ($0 \log(0) = 0$)

2. Entropy "Log energy"

$$X_{ELog \text{ energy}} = \sum_i \log(X_n^2) \quad 3.48$$

with the convention ($\log(0) = 0$)

where, X_n is the reconstructed signal from level n .

Wavelet analysis of the current signal was performed using Wavelet Toolbox™ in MATLAB environment and the M-file was written in MATLAB® workspace appended in Appendix E.

3.6 Statistical Analysis

General analysis used statistical methods like boxplots and analysis of variance (ANOVA) to analyse the data obtained from experimental study. After calculation of features, the methods should be used for exploratory data analysis. Various methods used for visualizing the distribution shape in exploratory data analysis for better understanding of general characteristics of the data. The evaluation of statistical significance of differences was tested with two-way ANOVA, and Tukey's honest significant differences method was also used for multiple comparisons after ANOVA.

Checking the assumption of normality, can be used by boxplot for a visual check of normality for multi-level experiments by listing all data with a multiplier. Boxplot (box-and-whisker diagrams) is one of the popular methods used [229]. Boxplots are an excellent and useful visual tool to visualize the summary statistics, which is used to compare means and variability between different data distributed and to supplement multivariate displays with univariate information. Boxplots are used in this research to analyse and compare different features of parameter. The boxplots for this study visualize two different motor situations as healthy and faulty and in each situation four different levels of starting load are considered. As above-mentioned, the motor was tested in all starting load conditions, from no load to full load, in each group of tests.

In statistics, analysis of variance (ANOVA) involves a collection of statistical models to test differences between two or more means and their associated procedures. The difference in a particular variable is then partitioned into components attributable to different sources of variation. ANOVA, in the simplest form, provides a statistical test of whether or not the means of several groups are all equal [230]. ANOVA tests the hypothesis that explains as Null hypothesis: the mean of groups for all condition is equal and Alternative hypothesis: at least the mean of one group is different from the others. The purpose of two-way ANOVA is to find out whether data from several groups have a common mean. The significance level is performed as 0.05. Here, for decision making survey a platform is designed, that means which features can be used for detection of fault in LS-PMSM. In this analysis, the statistical features are taken as continuous response variables (dependent variable) and “machine condition (healthy and faulty)” and “load condition” as categorical explanatory variables (independent variables).

When more than one variable is compared across groups, two-way ANOVA followed by post-hoc, Tukey's honest significant differences method is used. In this procedure, the significant differences detected by ANOVA are further investigated using a Tukey's honest significant differences post-hoc test. Tukey's honest

significant differences method provides a multiple testing by comparing the mean values [231]. In this study, Tukey's method was implemented as post-hoc testing procedure to perform a statistical comparison for the mean values of each feature at four different load conditions. The mean values were compared using Tukey's honest significant differences test at $P \leq 0.05$.

ANOVA analyses of the results were performed using Statistical Toolbox™ in MATLAB environment and the M-file was written in MATLAB® workspace appended in Appendix E.

3.7 Summary

This chapter presents simulation and an experimental setup to evaluate the broken rotor bar fault in three-phase LS-PMSM. An experimental setup is designed and implemented for both healthy motor and faulty motor in identical condition under different levels of load. The experimental procedure and configuration are presented subsequently. The rotor bar breakage was forced in the laboratory by opening the motors and drilling the bar artificially. Condition monitoring and data collection setup for sampling the stator current of motor is presented. Experimental data including current, torque and speed were acquired in equal condition. Torque and speed were also measured that are used for checking the motor condition to be identical in each test. Additionally, the case study motor is modeled based on FEM using Maxwell 2-D software for evaluation of the related parameters. The modeling study is introduced for both healthy and broken rotor bar fault conditions. Finally, the signal processing methods are used for identification of fault features in this type of electrical motors and were implemented using MATLAB software. Experimental and simulation results are used to explain tests phenomena and to support the effectiveness of proposed scheme which are presented in the following chapter.

CHAPTER 4

RESULTS AND DISCUSSION

4.1 Introduction

This chapter presents two aims of this research; first the effects of broken rotor bar fault on the motor performance under different levels of load and second extracting the fault related features for broken rotor bar detection in LS-PMSM. The results are studied both in experimental and simulation (motor modeling) with the effect of starting load.

4.2 Performance of LS-PMSM with presence of faults

In this section, the effects of broken rotor bar on the performance of motor during starting time are investigated. In the first step, the simulation result was used to analyze the performance of a healthy motor and also a motor with one broken bar under different levels of load. In the second step, the experimental result was used to confirm the effect of fault on machine performance.

4.2.1 Simulation Result

In this part, FEM is applied to investigate the performance of LS-PMSM when any broken rotor bar exists. The waveform of magnetic field contains comprehensive information about the stator and mechanical parts of the motor. Figure 4.1(a) shows the symmetrical distribution of magnetic flux in the healthy motor and Figure 4.1(b) presents the asymmetrical distribution of magnetic flux in a motor with one broken rotor bar under 1.5Nm starting torque. Furthermore, distribution of the flux lines around the broken bars differs from healthy bars. Comparing the Figures 4.1(a) and 4.1(b) shows density increasing of magnetic flux in the rotor core around broken bar, stator core, and the air gap. The concentration of magnetic flux observed around the broken bar creates asymmetric distribution of magnetic flux in this area. When a bar breaks, its current is distributed in the adjacent bars that mean more current flows in them. The excess current makes saturation and generates more heat in adjacent bars that result in asymmetrical distribution of magnetic flux. The generated heat makes the situation of adjacent bars worse and then makes a problem for permanent magnet because of the proximity of the cages to the magnets. Both the residual flux density and coercivity of permanent magnets reduce as a function of temperature.

According to Faraday's law, an electromagnetic field will be induced in the cage because of magnetic field fluctuating. The electromagnetic field will then generate a current through the cage and the situation becomes as a current carrying loop is situated in a magnetic field. According to Lorentz law, a magnetic force is produced

in the cage that causes the cage starts to rotate. Figure 4.2 shows the simple procedure of this function.

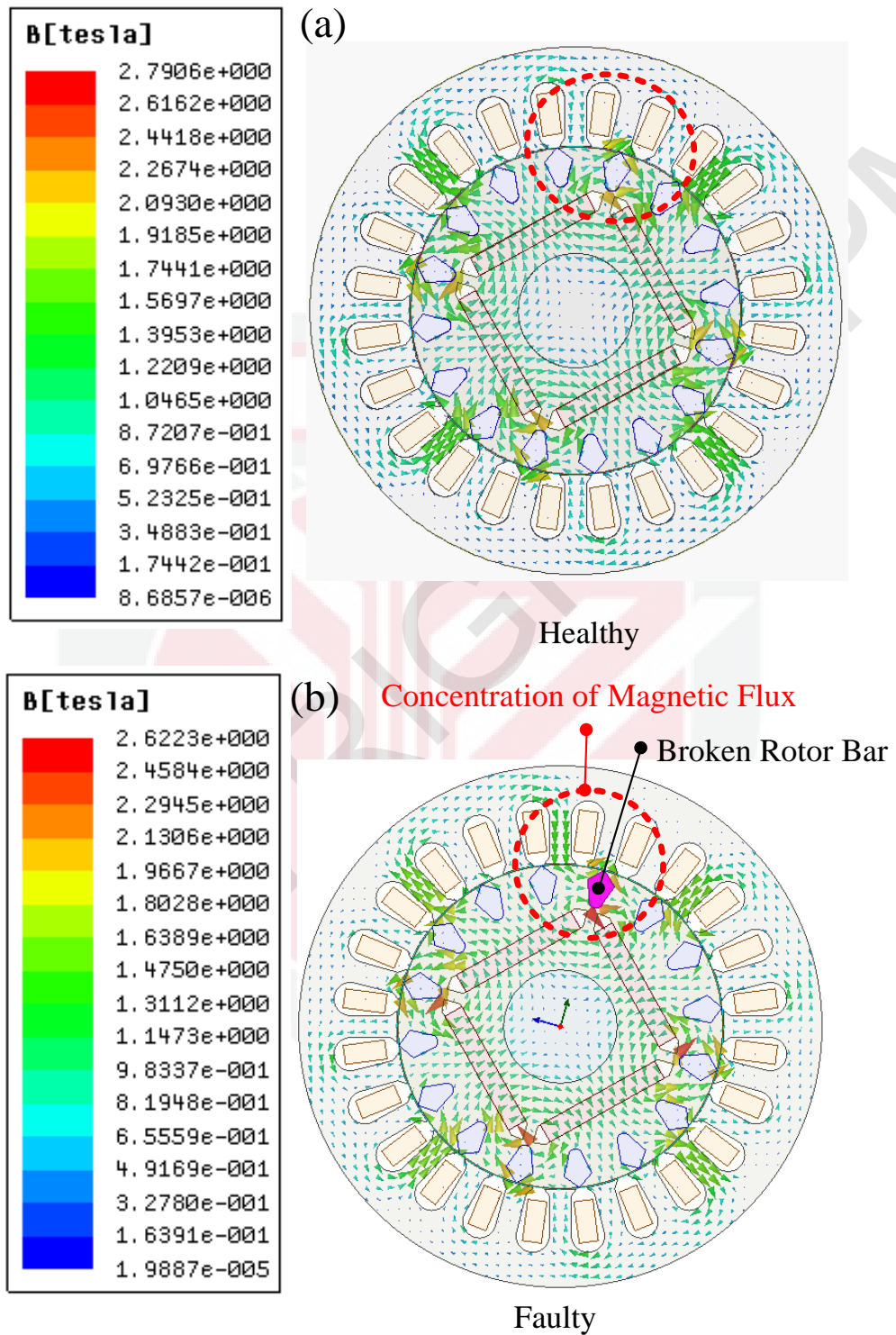


Figure 4.1: (a) The magnetic flux line in healthy motor, (b) the magnetic flux line in the motor with broken rotor bar.

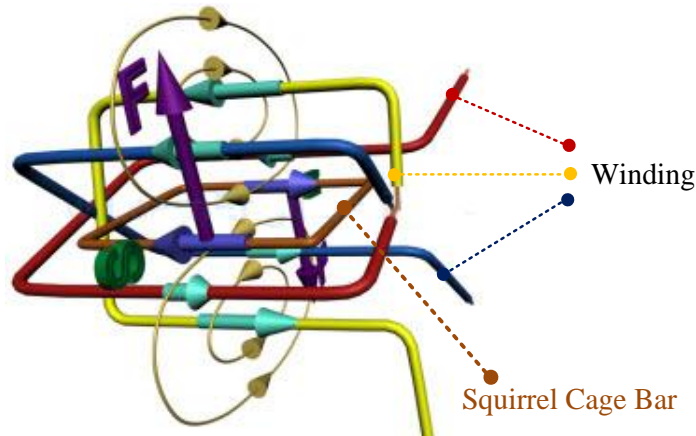


Figure 4.2: Rotating Magnetic Field produces a Force on Squirrel Cage Rotor

Magnetic force in a healthy rotor is symmetrically distributed around the rotor. A magnetic asymmetry due to the broken rotor bar introduces an unbalanced magnetic force. For both healthy motor and motor with broken rotor bar, the magnetic force distributions on the rotor bar at start-up (0 Nm) are computed by the FEM method. The results shown in the Figure 4.3 reveals that the amplitude of magnetic force for faulty motor is higher than for healthy motor. Such non-uniform distribution of the force inevitably leads to excessive mechanical stress in the bars, and the bars would become more susceptible to additional wearing and eventual breaking.

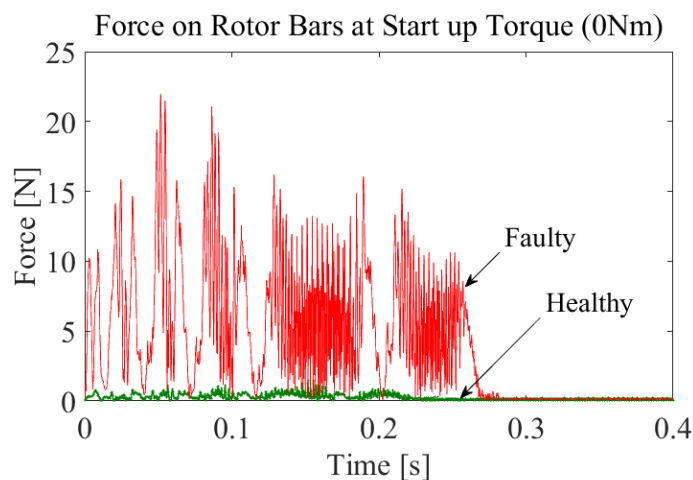


Figure 4.3: Magnetic Force in Starting Torque (a) Healthy and (b) Faulty Motor

The squirrel cage bars in the rotor can provide the accelerating torque that drives the machine to near synchronous speed. The accelerating torque must overcome not only the applied load torque but also the generated magnet braking torques, which is due to the presence of the permanent magnet. When broken rotor bar happens, the torque characteristics of the motor also change. Figure 4.4 shows the comparison of healthy and faulty motor under maximum starting torque. As it is clear, the motor with one broken rotor bar cannot run at starting torque value of “2.3Nm”, which the motor design is for it and the starting torque value decreases to near 1.75Nm. Accordingly, the value of starting torque is decreased whenever there is a broken rotor bar in LS-PMSM, while this phenomenon has not been reported for induction machine. As

presence of broken rotor bar change the torque characteristic of the LS-PMSM, early detection of this fault is very important.

Based on the Equation 2.3, the starting torque of the machine is also directly related to the cage resistance (R'_2). In the presence of BRB fault, the value of cage resistance is increases. This value affects by reducing the value of cage torque. Thus, detection of BRB in early stage is important to keep the startup torque of the machine in the design value as well as to prevent the machine from secondary failure.

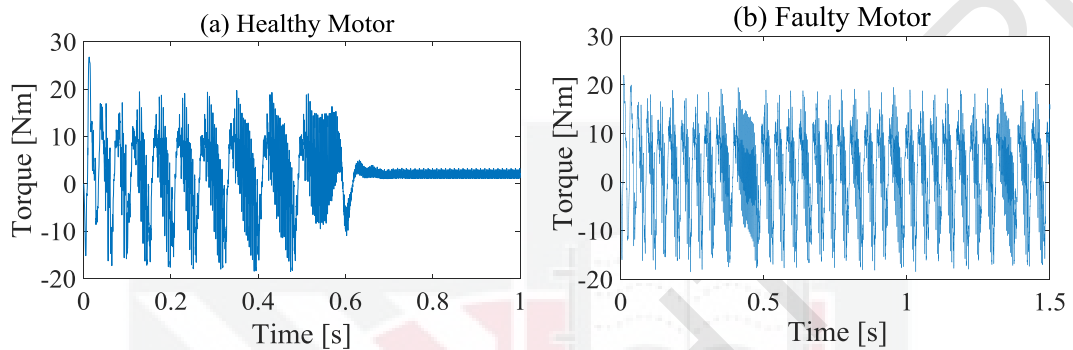


Figure 4.4: The Comparison of Maximum Starting Torque [2.3 Nm] for (a) Healthy and (b) Faulty Motor.

Another issue found during the simulation analysis is increasing of time duration for transient section when any bar is broken. Figure 4.5 shows the current signal in different load condition for both healthy and faulty motors. As it is clear in this Figure 4.5, with the presence of fault in the motor, starting time is increased. Figure 4.6 illustrates the starting time for both healthy and faulty motor under different levels of the load. As it is clear, the starting time trend is also increased based on increasing the load. A recent research conducted on induction machine revealed that the load condition of motor is not important when approaches based on the transient analysis are used [232]. Other researchers also did not consider the effects of load for fault detection in induction machine based on analysis of current in transient state [233,234]. However, this research indicates that the load effect in the starting time should be carefully taken into account for fault detection in LS-PMSM.

For LS-PMSM that start with squirrel cage, the application of the technique is even more justified, because these elements only carry significant currents during those transients. This is the fact that makes the application of conventional diagnosis based on steady-state impractical. Presence of broken rotor bars in the LS-PMSM causes changes in the air gap flux and the current distribution among the rotor bars during acceleration from standstill to rated speed. This part indicated that the broken rotor bars slightly change the performance of motor during startup. This situation is critical for broken rotor bars fault detection in this motor during transient time.

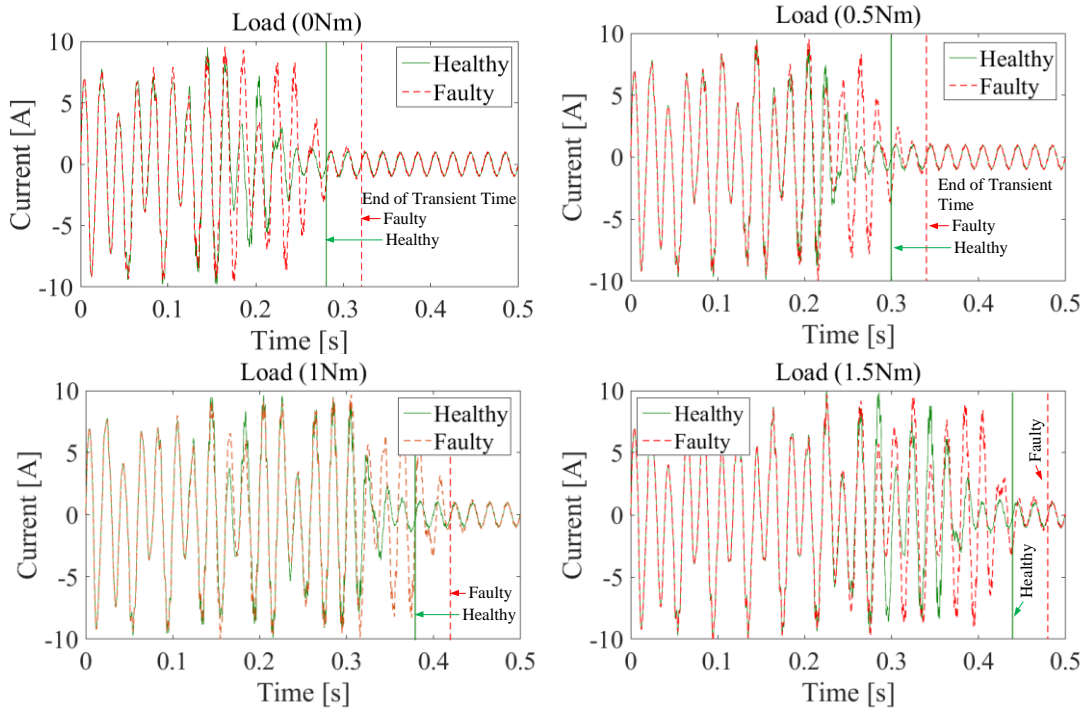


Figure 4.5: Simulation current signal in four-load condition for healthy and faulty motor

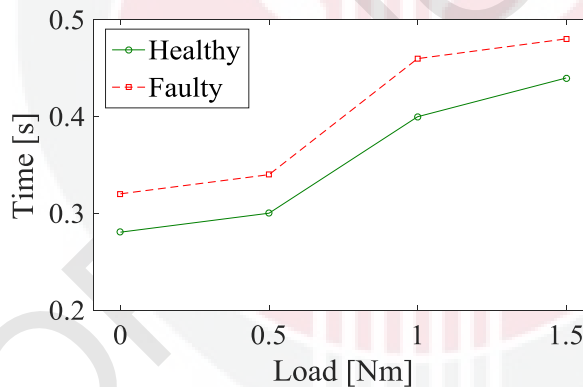


Figure 4.6: Comparison the result of starting time for different loads

4.2.2 Experimental Result

The effect of broken rotor bar in starting torque is also observed experimentally. It is found that, the motor with one broken rotor bar cannot run at starting torque value of “2.3Nm”, which the motor design is for it and the starting torque value decreases to near 1.70Nm. The rate of torque variations for the faulty motor is higher than for the healthy one, so higher noise accompanied with lower performance are expected from the faulty motor.

The time duration for transient section is also determined through experimental work. Figure 4.7 shows the current signal in different load condition for both healthy and faulty motors. As it is clear in this figure, with the presence of broken rotor bar, the duration of starting time is increased. Figure 4.8 provides comparison between

starting time for both healthy and faulty motors in different level of the load. The results presented in Figure 4.8 are based on mean of 40 samples for each condition.

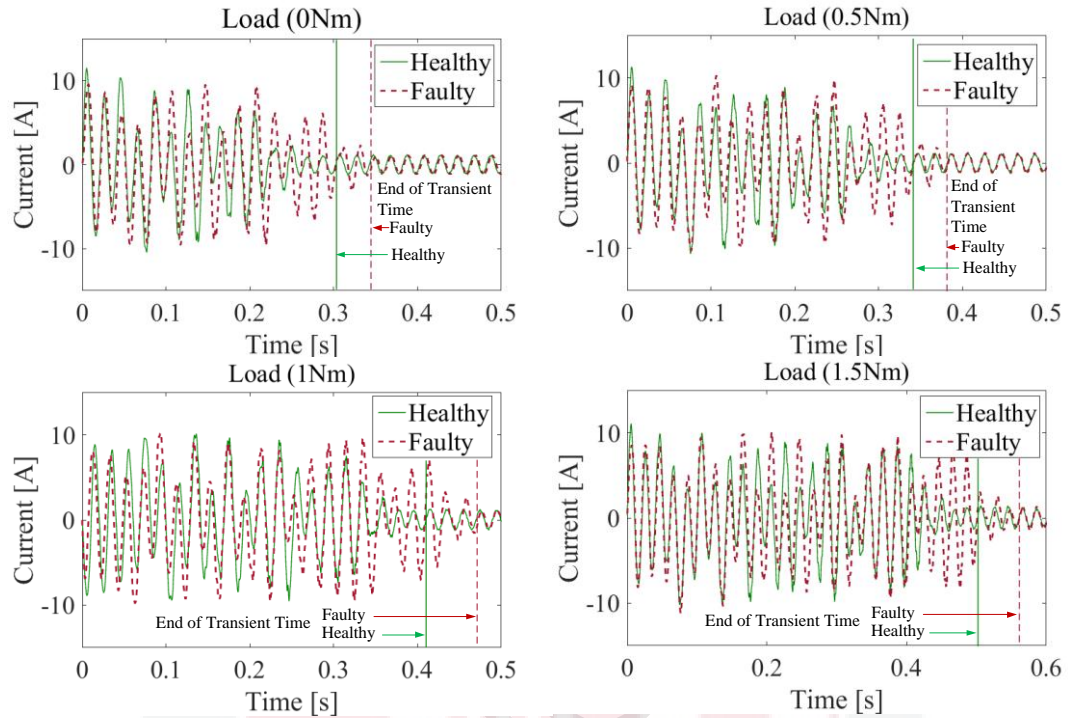


Figure 4.7: Experimental current signal in four-load condition for Healthy and Faulty motor

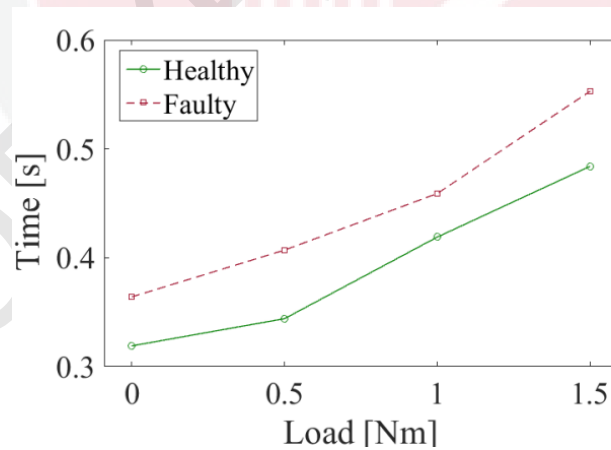


Figure 4.8: Comparison the result of starting time in different load based on the mean value of 40 Samples for each load

4.3 Data Processing for Fault Detection

The signals can be divided into two types; stationary and non-stationary. In this study, the start-up signal of LS-PMSM is considered for feature extraction and this signal is non-stationary. Transient stator current signals are measured experimentally

under four different load conditions. Two different type of signal processing method used in this study (Time domain and Time-frequency domain analysis).

4.3.1 Time Domain Analysis

After pre-processing, a time domain analysis is applied to the acquired signal in order to extract the features related to the fault. Two different methods are used to identify the features related to the fault under observation, broken rotor bar. The first one is analysis of raw time domain signal and the second one is analysis of the envelope of the raw signal in time domain.

4.3.1.1 Time Domain Analysis based on Raw Signal

In this section, 13 statistical parameters are calculated and used to extract the features in time domain signal for broken rotor bar detection as mentioned in the section 3.5.1.1. In total, 4160 data are obtained from these 13 parameters for two motors (healthy and faulty) that run at four different levels of load and 40 measurements are performed for each condition.

Traditional statistical features can characterize the behavior change of signals when any fault occurs or load condition is changed. Different researchers have used different types and numbers of statistical features to extract the faults in electrical machines. Therefore, to testify which features are more accurate and reliable for fault detection, this study surveys the trend of these features in different load conditions. The distances between different conditions can indicate the efficiency of the features. If the trend of a feature for healthy and faulty motor does not overlap with each other, this feature is appropriate for fault detection. In this respect, trend of different features and their boxplots are used to compare the values of any feature for healthy and faulty motors in different load conditions. In trend and boxplots graphs, the x-axis legend is based on the starting load. Figure 4.9 and Figure 4.10 show the trend and boxplot graphs for dimensional parameters and non-dimensional parameters, used as fault feature, respectively. Analysis of these figures will lead to several interesting conclusions. The most obvious one is the results are not similar for all cases and each case should be studied and analyzed separately.

The trend graphs for dimensional parameters show no overlap exists between the healthy and faulty situation at any levels of starting load. However, when a boxplot for these features are considered, there is some antithesis. As Figure 4.9 (d) shows, where the Peak to Peak feature is used, there is an overlapping between boxes corresponding to the condition that cannot be understandable from the trend graph. In Figure 4.9 (b,c and e), where RMS, RSSQ and energy features are considered, an overlapping between boxes in low level of load condition can be detected too.

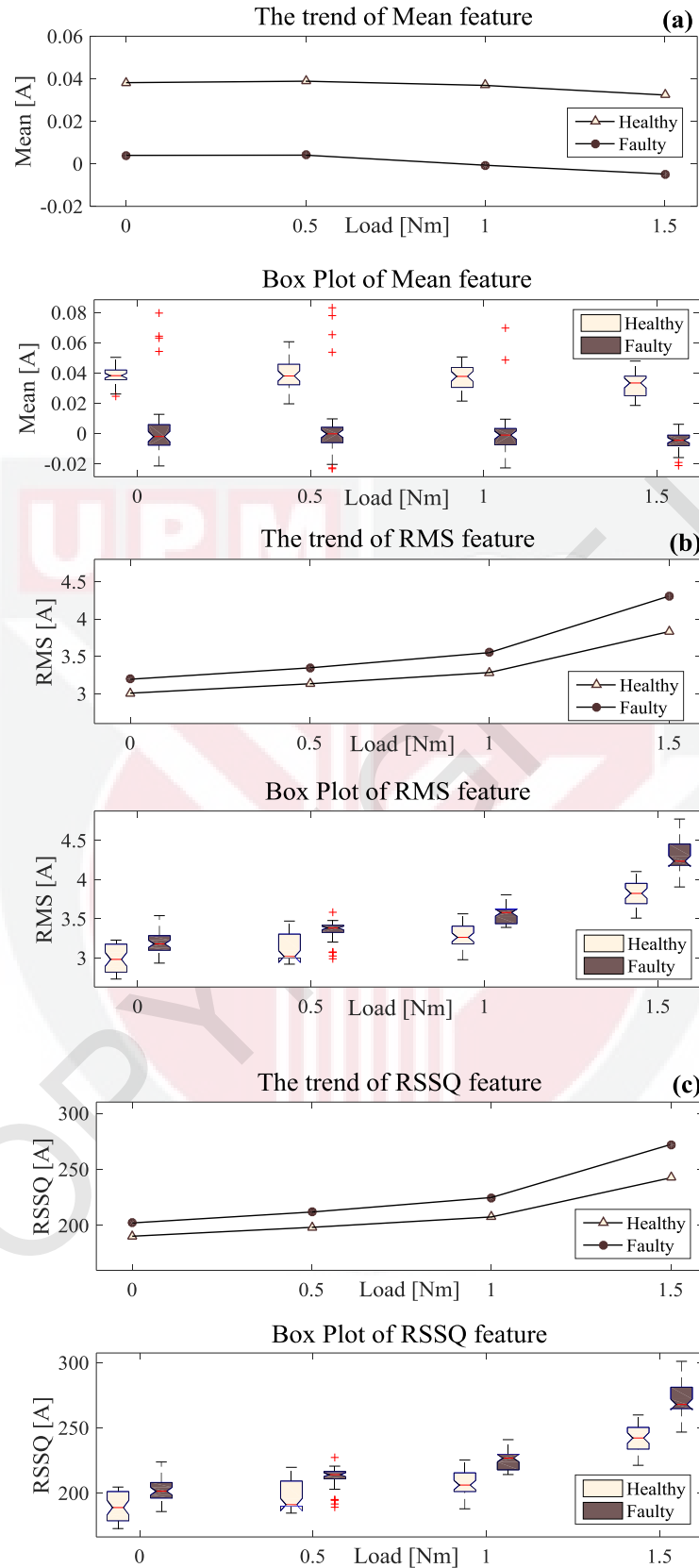


Figure 4.9: Trend and Boxplot for dimensional features in time domain analysis
 (a) Mean, (b) RMS, (c) RSSQ, (d) Peak to Peak and (e) Energy (*Continued*)

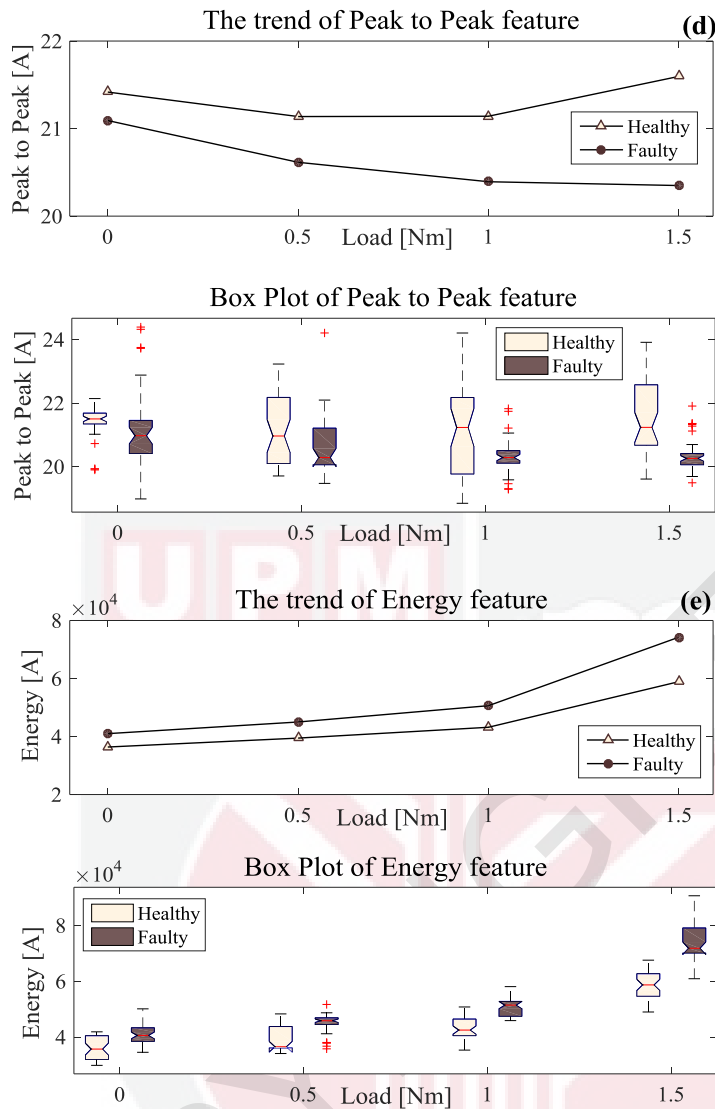


Figure 4.9: Trend and Boxplot for dimensional features in time domain analysis (a) Mean, (b) RMS, (c) RSSQ, (d) Peak to Peak and (e) Energy

ANOVA analysis can complete the graphic information given by the boxplots. Table 4.1 presents the result of ANOVA models for this five dimensional parameters adjusted based on motor condition; starting load condition and their interaction. In Table 4.1, the p-value for the Mean feature is more than 0.05 for interaction condition states that can check with post-hoc test. The performed ANOVA (Table 4.1) for the rest of the features reveals a significant impact in the distinction among different test conditions. To perform a statistical comparison among the means for the features at different conditions, Tukey's honest significant differences method was applied as post-hoc testing procedure. Table 4.2 presents the results of post-hoc testing procedure for dimensional parameters. The results indicate the p-value for the Peak to Peak feature is not significant in this test for the low load condition, the same result is also observed in the boxplots of Figure 4.9 (d), where there is an overlapping between the conditions. However, the remaining features have a significant p-value.

Table 4.1. Analysis of variance for dimensional parameter features in time domain analysis

Feature	Source	Sum of Squares	df	Mean Square	F	P value
Mean	Motor Condition	1.03E-01	1	1.03E-01	508.694	1.71E-67
	Load	3.03E-03	3	1.01E-03	4.976	2.19E-03
	Interaction	1.70E-04	3	5.68E-05	0.28	0.84
	Error	6.33E-02	312	2.03E-04		
	Total	1.70E-01	319			
RMS	Motor Condition	6.526	1	6.526	274.615	1.10E-44
	Load	44.0642	3	14.6881	618.074	6.80E-131
	Interaction	1.0238	3	0.3413	14.361	8.68E-09
	Error	7.4144	312	0.0238		
	Total	59.0285	319			
RSSQ	Motor Condition	2.63E+04	1	2.63E+04	275.309	9.17E-45
	Load	1.75E+05	3	5.83E+04	610.481	3.60E-130
	Interaction	3.87E+03	3	1.29E+03	13.527	2.55E-08
	Error	2.98E+04	312	95.449		
	Total	2.35E+05	319			
Peak to Peak	Motor Condition	40.404	1	40.404	39.504	1.10E-09
	Load	10.477	3	3.492	3.414	1.70E-02
	Interaction	9.451	3	3.15	3.08	2.70E-02
	Error	319.106	312	1.023		
	Total	379.437	319			
Energy	Motor Condition	5.42E+09	1	5.42E+09	285.842	5.67E-46
	Load	3.72E+10	3	1.24E+10	653.36	4.00E-134
	Interaction	1.42E+09	3	4.75E+08	25.017	1.57E-14
	Error	5.92E+09	312	1.90E+07		
	Total	4.99E+10	319			

Table 4.2: P-value calculation from post- hoc test procedure for dimensional parameter features in time domain analysis

Load (Nm)	Mean	RMS	RSSQ	Peak to Peak	Energy
0	6.0E-08	1.7E-06	1.6E-06	0.840	5.9E-05
0.5	6.0E-08	7.6E-08	7.1E-08	0.287	3.8E-07
1	6.0E-08	6.0E-08	6.0E-08	2.10E-02	6.0E-08
1.5	6.0E-08	6.0E-08	6.0E-08	1.03E-06	6.0E-08

Figure 4.10 shows the trend and boxplot graph for non-dimensional parameters. The comparison of the trend graph for non-dimensional parameter indicates there is an overlapping between the healthy situation and faulty one at different levels of starting load for some features like Shape Factor, Impulse Factor and Skewness (Figure 4.10 (a,b and g)). The remaining features do not have any overlapping between the healthy and faulty conditions (Figure 4.10 (c,d,e,f and h)). However, when the boxplot for these features are considered, a proof is obtained for this antithesis. In the case of Shape Factor and Impulse Factor (Figure 4.10 (a and b)), an overlapping can be seen between boxes corresponding to the conditions. The same overlapping is also observed in the trend graph. In Figure 4.10(g), where the Skewness feature is used, an overlapping between boxes in high level of load condition is also observed. It can be concluded that Shape Factor and Impulse Factor

feature are not appropriate parameter for fault detection. The Skewness feature, also, can be only used when the level of load is low.

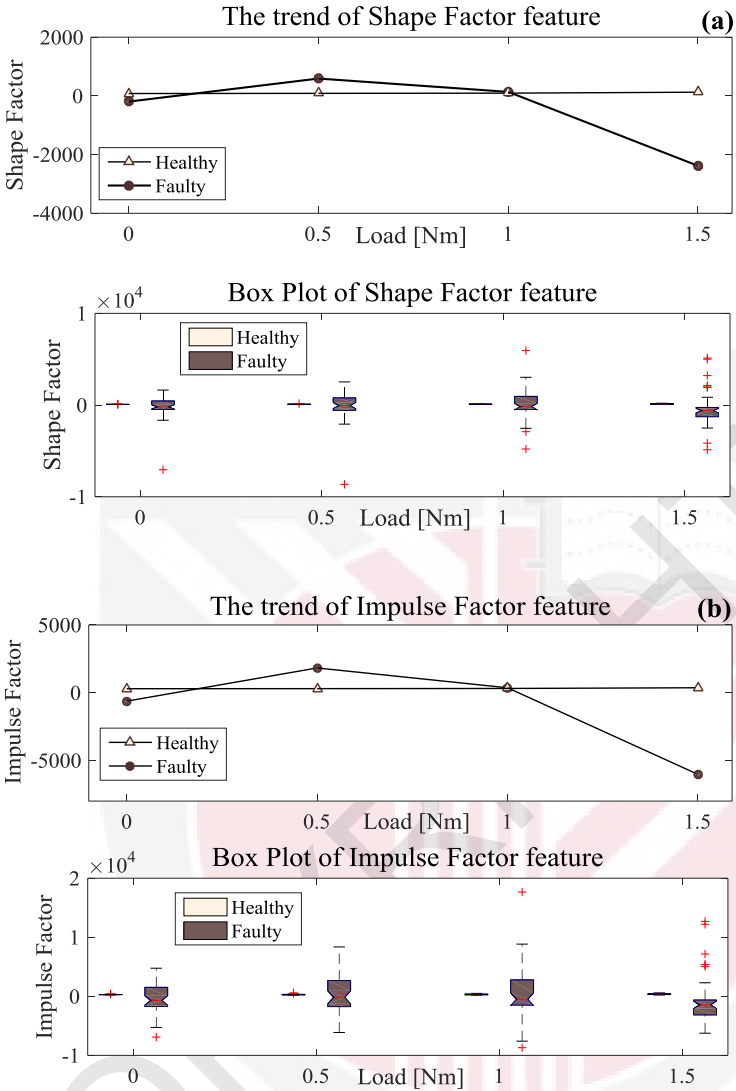


Figure 4.10: Trend and Boxplot for non-dimensional features in time domain analysis a) Shape Factor, b) Impulse Factor, c) Crest Factor, d) Margin Factor, e) Peak-to-average power ratio, f) Variance, g) Skewness and h) Kurtosis (Continued)

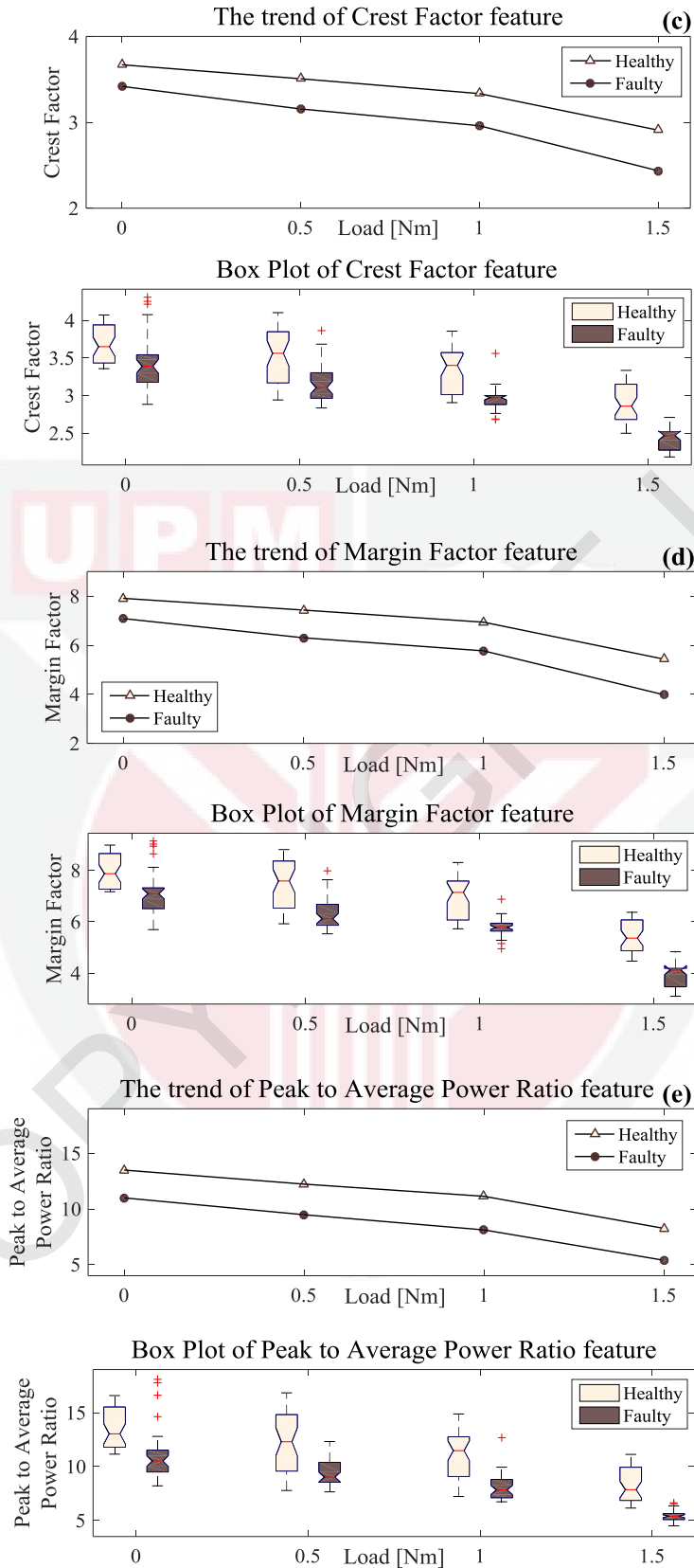


Figure 4.10: Trend and Boxplot for non-dimensional features in time domain analysis a) Shape Factor, b) Impulse Factor, c) Crest Factor, d) Margin Factor, e) Peak-to-average power ratio, f) Variance, g) Skewness and h) Kurtosis (Continued)

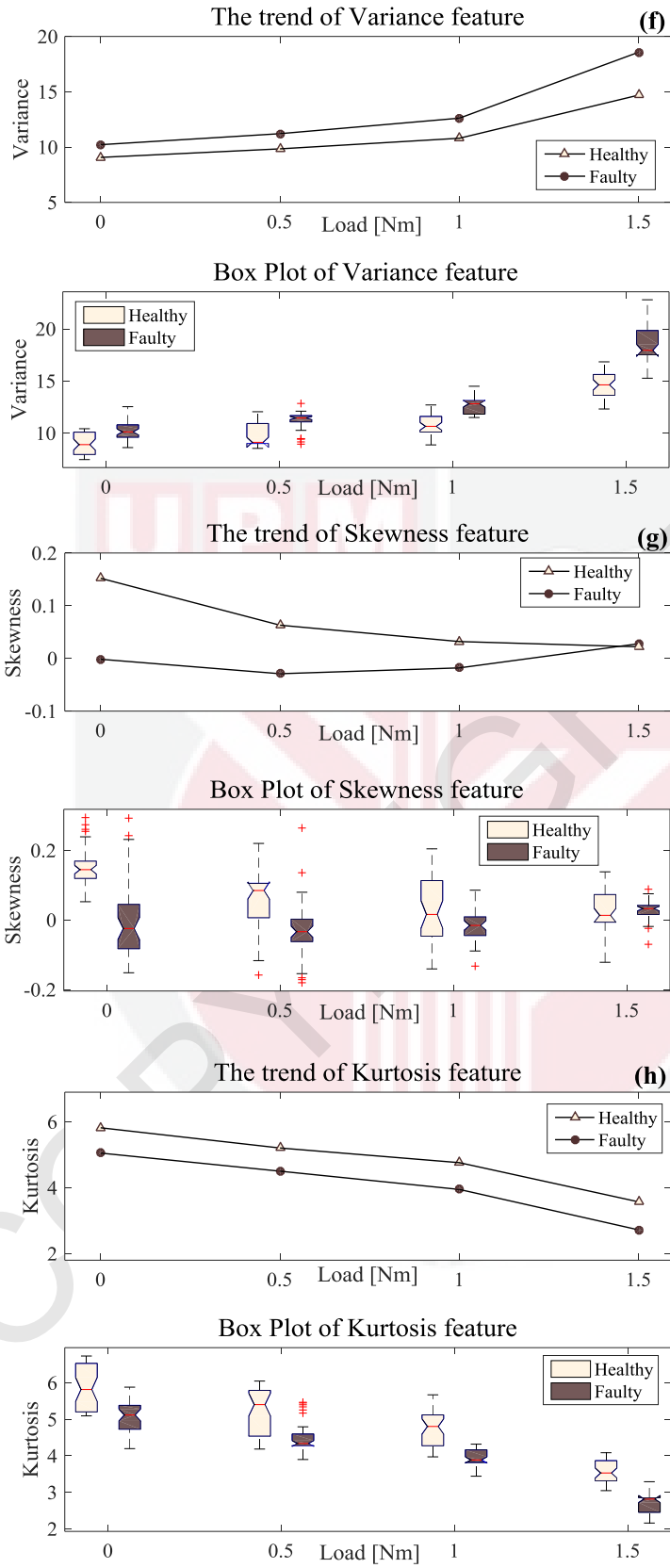


Figure 4.10: Trend and Boxplot for non-dimensional features in time domain analysis a) Shape Factor, b) Impulse Factor, c) Crest Factor, d) Margin Factor, e) Peak-to-average power ratio, f) Variance, g) Skewness and h) Kurtosis

Table 4.3 presents the results of ANOVA models for eight non-dimensional parameters adjusted based on motor condition; starting load condition and their interaction. In Table 4.3, the p-value for the Shape Factor and Impulse Factor have values more than 0.05 for each motor condition, load and interaction condition states. This overlapping can be also observed in the boxplots of (Figure4.10-a,b), where there is an overlapping between the conditions. Hence, there is no significant evidence for interaction among the load conditions. In the Crest Factor, Peak-to-average power ratio and Skewness features also have an insignificant impact in interaction part that can check with post-hoc test. The performed ANOVA (Table 4.3) for the rest of features show a significant impact in the difference among conditions. Table 4.4 presents the results of post-hoc testing procedure for non-dimensional parameters. The results show that at all load levels, the p-value for the Shape Factor and Impulse Factor feature are not significant. The p-value for the Skewness feature is not significant for high level of load condition too. The remaining features have significant p-values.

This paragraph sums up the results obtained from time domain analysis of the signal. Three features, namely peak to peak, shape factor and impulse factor could not distinguish faulty state of motor from faulty-free state based on upward or downward trend. Skewness also failed to detect broken bar when the starting torque is high. This result also indicated the importance and significance of load value in starting torque on the fault diagnosis. The simulation results are presented in Appendix F. These results also concur with the experimental result in term of trend condition. Based on simulation results, four features, namely peak to peak, shape factor, impulse factor and Skewness had overlapping between load conditions and thus could not distinguish healthy state from faulty state based on upward or downward trend.

Table 4.3: Analysis of variance for non-dimensional parameter features in time domain analysis

Feature	Source	Sum of Squares	df	Mean Square	F	P value
Shape Factor	Motor Condition	2.50E+07	1	2.50E+07	1.0331	0.310
	Load	1.02E+08	3	3.39E+07	1.4015	0.242
	Interaction	1.07E+08	3	3.58E+07	1.4823	0.219
	Error	7.54E+09	312	2.42E+07		
	Total	7.77E+09	319			
Impulse Factor	Motor Condition	1.64E+08	1	1.64E+08	0.984	0.322
	Load	6.91E+08	3	2.30E+08	1.383	0.248
	Interaction	7.16E+08	3	2.39E+08	1.433	0.233
	Error	5.20E+10	312	1.67E+08		
	Total	5.35E+10	319			
Crest Factor	Motor Condition	10.512	1	10.512	143.140	2.09E-27
	Load	33.128	3	11.043	150.366	2.77E-60
	Interaction	0.496	3	0.165	2.250	0.083
	Error	22.913	312	0.073		
	Total	67.048	319			
Margin Factor	Motor Condition	104.619	1	104.619	222.211	2.56E-38
	Load	342.719	3	114.240	242.644	3.22E-81
	Interaction	3.958	3	1.319	2.803	0.040
	Error	146.893	312	0.471		
	Total	598.189	319			
Peak-to-average power ratio	Motor Condition	6.20E+02	1	620.019	181.270	6.86E-33
	Load	1.28E+03	3	425.582	124.424	5.16E-53
	Interaction	2.90E+00	3	0.968	0.283	0.838
	Error	1.07E+03	312	3.420		
	Total	2.97E+03	319			
Variance	Motor Condition	337.406	1	337.406	285.559	6.11E-46
	Load	2341.225	3	780.408	660.489	9.3E-135
	Interaction	93.396	3	31.132	26.348	3.23E-15
	Error	368.647	312	1.182		
	Total	3140.674	319			
Skewness	Motor Condition	0.420	1	0.420	71.791	8.7E-41
	Load	0.221	3	0.074	12.597	6.4E-103
	Interaction	0.272	3	0.091	15.526	0.7589
	Error	1.825	312	0.006		
	Total	2.739	319			
kurtosis	Motor Condition	49.144	1	49.1436	241.923	9.60E-16
	Load	227.714	3	75.9047	373.662	8.54E-08
	Interaction	0.239	3	0.0796	0.392	1.94E-09
	Error	63.379	312	0.2031		
	Total	340.476	319			

Table 4.4: P-value calculation from post-hoc test procedure for non-dimensional parameter features in time domain analysis

Load (Nm)	Shape Factor	Impulse Factor	Crest Factor	Margin Factor	Peak-to-average power ratio	Variance	Skewness	kurtosis
0	1.00	1.00	8.7E-04	2.2E-06	1.0E-07	6.2E-05	6.0E-08	6.0E-08
0.5	1.00	1.00	2.4E-07	6.0E-08	6.1E-08	5.1E-07	2.0E-06	6.0E-08
1	1.00	1.00	7.8E-08	6.0E-08	6.0E-08	6.0E-08	0.068	6.0E-08
1.5	0.304	0.304	6.0E-08	6.0E-08	6.0E-08	6.0E-08	1.000	6.0E-08

4.3.1.2 Time Domain Analysis based on Envelope Signal

The broken rotor bar in squirrel cage induction machine induces the stator current amplitude (envelope) [37]. The amplitude of these frequency components can be used as indication of fault related feature. A new approach based on feature extraction from the envelope of the start-up current signal is investigated in this research. After pre-processing, the envelopes of startup current signals are extracted by using MATLAB software. Similar to the time domain analysis of raw signal, thirteenth statistical parameters are calculated and used to extract the features in time domain for broken rotor bar detection. Here also, 4160 data are obtained from these 13 parameters for two motors (healthy and faulty) that run at four different levels of load and 40 measurements were performed for each condition.

Figure 4.11 and Figure 4.12 show the trend and boxplot graph for different features, dimensional parameter and non-dimensional parameter, respectively. Analysis of these figures calculated from analysis of envelope will lead to several interesting conclusions. The overall conclusion is similar to the time analysis of raw signal, which is the results are not a like for all cases, each case should be studied and analysed separately. Results also indicate that for some features, it could be difficult to distinguish healthy and the faulty state, however these features are not exactly the one determined through time analysis of raw signal. The trend graphs for dimensional parameters obtained from time domain analysis of envelope show no overlap exists between the healthy and faulty situation at any levels of starting load. However, when a boxplot for these features are considered, there is some antithesis. In Figure 4.11(a,b,c and e), where Mean, RMS, RSSQ and Energy features are considered, there is an overlapping between boxes in low level of load condition. As Figure 4.11(d) shows, a few samples have overlapping between motor conditions in each level of load, while this overlapping cannot be observed in the trend graph.

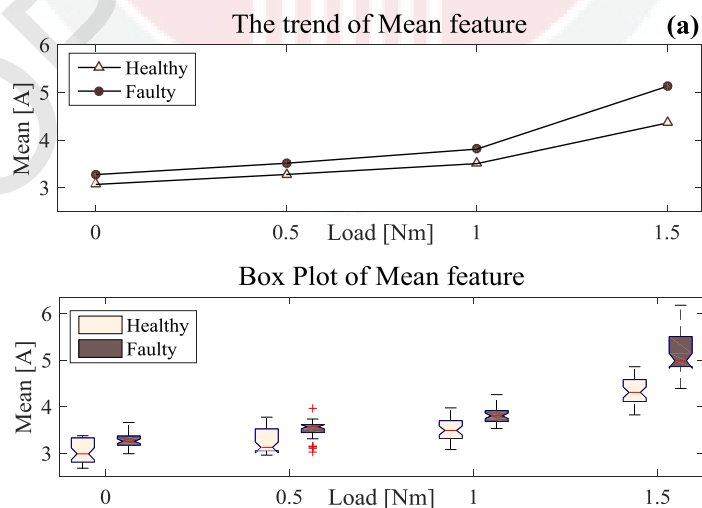


Figure 4.11: Trend and Boxplot for dimensional features in envelope analysis a) Mean, b) Root Mean Square (RMS), c) RSSQ, d) Peak to Peak and e) Energy (Continued)

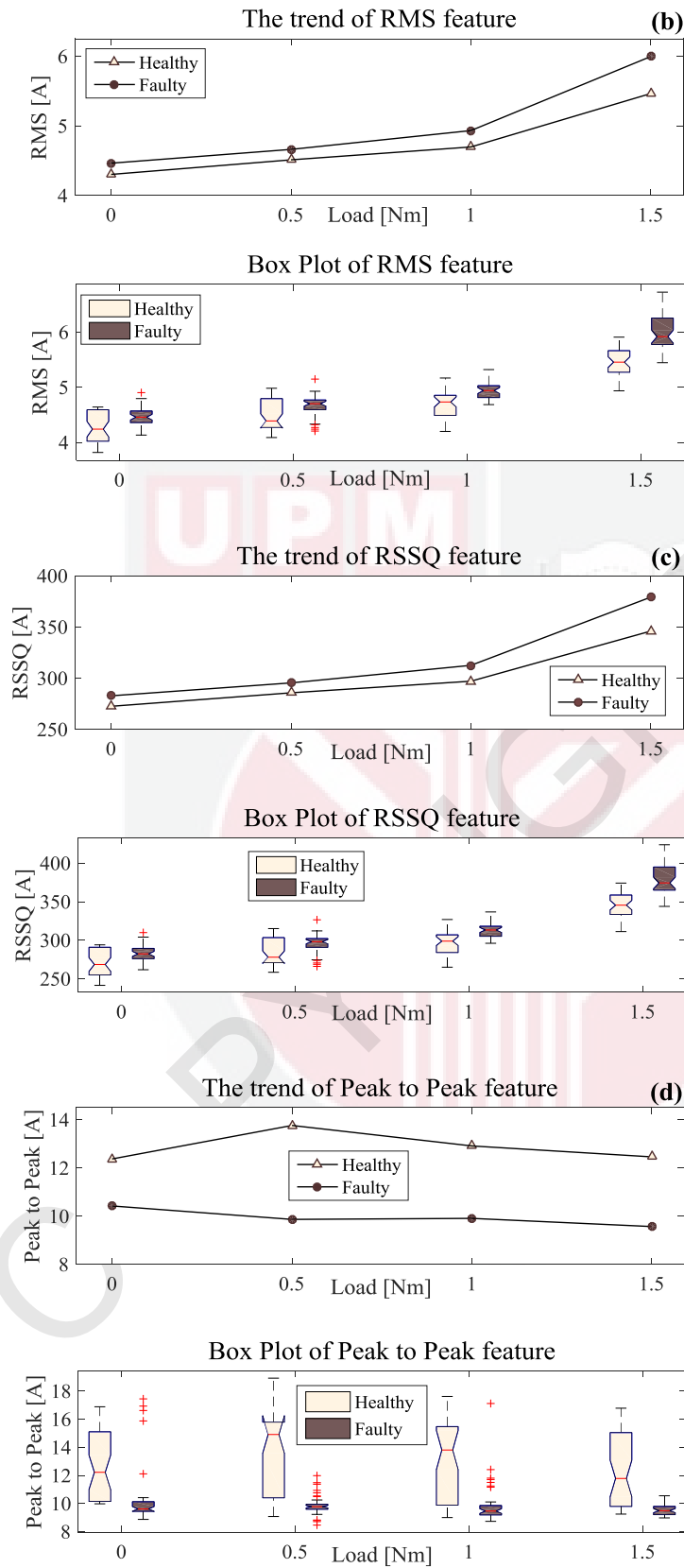


Figure 4.11: Trend and Boxplot for dimensional features in envelope analysis a) Mean, b) Root Mean Square (RMS), c) RSSQ, d) Peak to Peak and e) Energy (Continued)

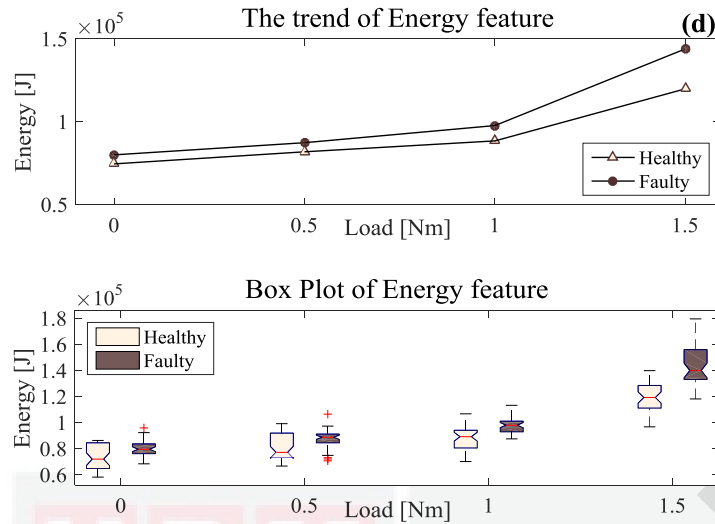


Figure 4.11: Trend and Boxplot for dimensional features in envelope analysis a) Mean, b) Root Mean Square (RMS), c) RSSQ, d) Peak to Peak and e) Energy

Table 4.5 presents the results of ANOVA models for this five dimensional parameters adjusted based on motor condition; starting load condition and their interaction. In Table 4.5, the p-value for the Peak to Peak feature is more than 0.05 for load and interaction condition states. The same result is observed in the boxplots of Figure 4.11(d), where there is an overlapping between the conditions. Hence, there is no significant evidence of interaction between the load condition states. The performed ANOVA (Table 4.5) for the rest of the features shows a significant impact in the distinction among different test conditions. To perform a statistical comparison among the means for the selected features at different conditions, Tukey's honest significant differences method is applied as post-hoc testing procedure. Table 4.6 presents the results of post-hoc testing procedure for dimensional parameters. The results indicate the p-value for the RMS, RSSQ and Energy features are not significant in the low level of load; however, the remaining features have a significant p-value.

Table 4.5: Analysis of variance for dimensional parameter features in envelope analysis

Feature	Source	Sum of Squares	df	Mean Square	F	P value
Mean	Motor Condition	1.15E+01	1	1.15E+01	177.952	1.98E-32
	Load	1.16E+02	3	3.88E+01	600.846	2.95E-129
	Interaction	4.15E+00	3	1.38E+00	21.435	1.193E-12
	Error	2.01E+01	312	6.45E-02		
	Total	1.52E+02	319			
RMS	Motor Condition	5.81480	1	5.815	101.878	6.47E-21
	Load	84.82857	3	28.276	495.412	2.76E-118
	Interaction	1.91975	3	0.640	11.212	5.25E-07
	Error	17.80776	312	0.057		
	Total	110.37089	319			
RSSQ	Motor Condition	2.35E+04	1	2.35E+04	102.560	4.99E-21
	Load	3.37E+05	3	1.12E+05	490.257	1.06E-117
	Interaction	7.23E+03	3	2.41E+03	10.535	1.28E-06
	Error	7.14E+04	312	228.799		
	Total	4.39E+05	319			
Peak to Peak	Motor Condition	689.523	1	689.523	142.563	2.55E-27
	Load	25.641	3	8.547	1.767	0.1534
	Interaction	38.008	3	12.669	2.619	0.0509
	Error	1509.023	312	4.837		
	Total	2262.196	319			
Energy	Motor Condition	9.81E+09	1	9.81E+09	108.422	5.47E-22
	Load	1.42E+11	3	4.74E+10	523.681	2.09E-121
	Interaction	4.71E+09	3	1.57E+09	17.367	1.88E-10
	Error	2.82E+10	312	9.04E+07		
	Total	1.85E+11	319			

Table 4.6: P-value calculation from post- hoc test procedure for dimensional parameter features in envelope analysis

Load (Nm)	Mean	RMS	RSSQ	Peak to Peak	Energy
0	6.70E-03	0.052	0.05	1.87E-03	0.170
0.5	8.79E-04	0.093	0.08	5.99E-08	0.163
1	2.28E-06	2.82E-04	1.30E-04	8.64E-08	3.58E-04
1.5	5.99E-08	5.99E-08	5.99E-08	1.72E-07	5.99E-08

Figure 4.12 shows the trend and boxplot graph for non-dimensional parameters obtained from time domain analysis of envelope. The comparison of the trend graph for non-dimensional parameter indicates there is an overlapping between the healthy situation and faulty one at different levels of starting load for the Variance features (Figure 4.12(f)). The remaining features do not have any overlap between the healthy and faulty conditions (Figure 4.12(a-e,g,h)). When the boxplot for these features are considered, the same results are concluded for these features too.

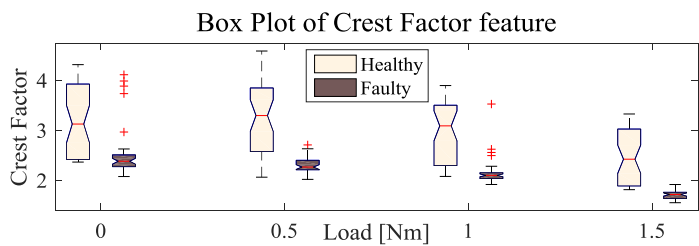
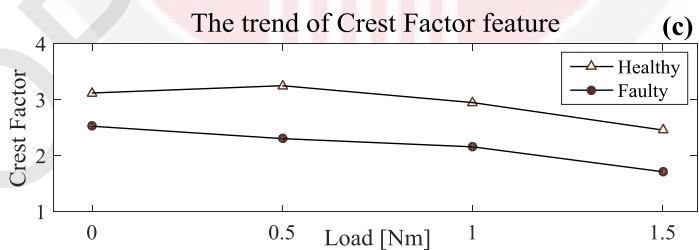
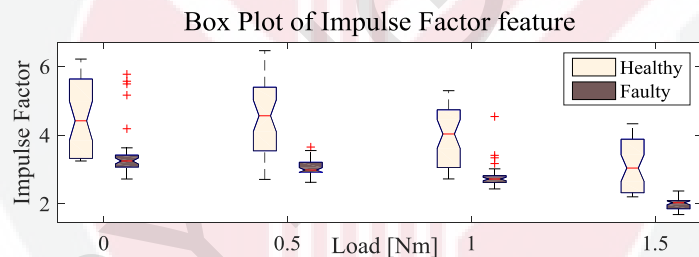
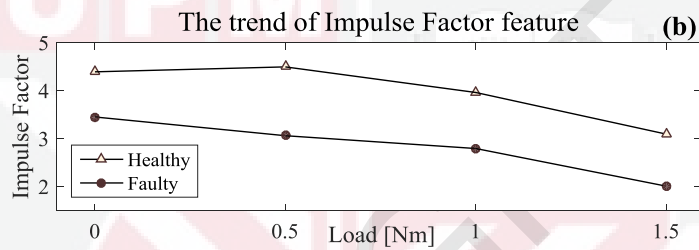
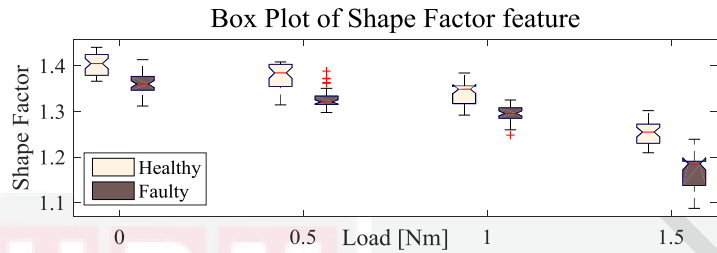
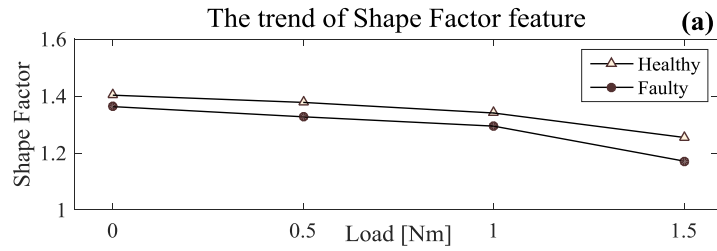


Figure 4.12: Trend and Boxplot for non-dimensional features in envelope analysis a) Shape Factor, b) Impulse Factor, c) Crest Factor, d) Margin Factor, e) Peak-to-average power ratio, f) Variance, g) Skewness and h) Kurtosis (Continued)

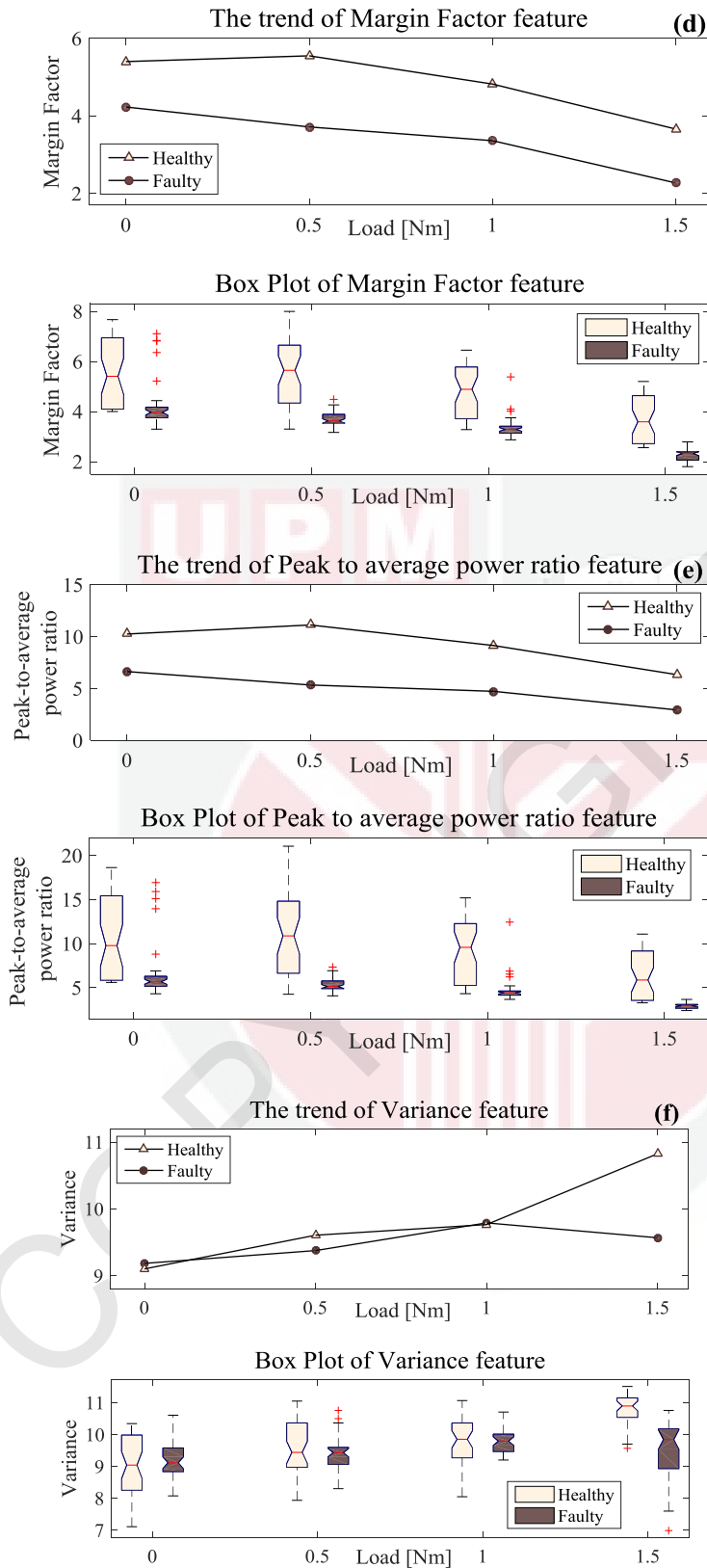


Figure 4.12: Trend and Boxplot for non-dimensional features in envelope analysis a) Shape Factor, b) Impulse Factor, c) Crest Factor, d) Margin Factor, e) Peak-to-average power ratio, f) Variance, g) Skewness and h) Kurtosis (Continued)

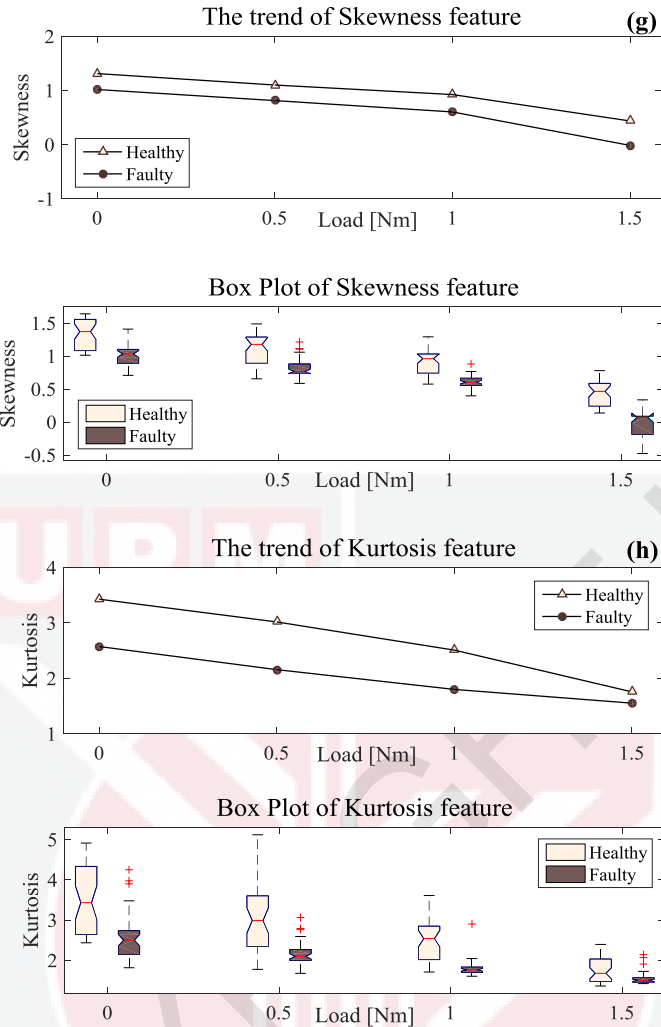


Figure 4.12: Trend and Boxplot for non-dimensional features in envelope analysis a) Shape Factor, b) Impulse Factor, c) Crest Factor, d) Margin Factor, e) Peak-to-average power ratio, f) Variance, g) Skewness and h) Kurtosis.

Table 4.7 presents the results of ANOVA models for eight non-dimensional parameters adjusted based on motor condition; starting load condition and their interaction. In Table 4.7, the p-value for the Impulse Factor, Crest Factor, Margin Factor and Peak-to-average power ratio have values more than 0.05 for each interaction condition states. Hence, there is no significant evidence for interaction among the motor condition and load conditions. The performed ANOVA (Table 4.7) for the rest of the features show a significant impact in the difference among conditions. Table 4.8 presents the results of post-hoc testing procedure for non-dimensional parameters. The results show that the p-value for the Variance feature is not significant in this test for all levels of load except full load condition. The p-value for the Kurtosis feature is also not significant for high level of load condition and the remaining features have a significant p-value.

Table 4.7: Analysis of variance for non-dimensional parameter features in envelope analysis

Feature	Source	Sum of Squares	df	Mean Square	F	P value
Shape Factor	Motor Condition	2.41E-01	1	2.41E-01	384.324	2.47E-56
	Load	1.31E+00	3	4.37E-01	695.986	7.88E-138
	Interaction	2.22E-02	3	7.40E-03	11.776	2.50E-07
	Error	1.96E-01	312	6.28E-04		
	Total	1.77E+00	319			
Impulse Factor	Motor Condition	1.07E+02	1	1.07E+02	187.471	9.67E-34
	Load	9.09E+01	3	3.03E+01	52.980	1.05E-27
	Interaction	2.58E+00	3	8.61E-01	1.505	0.213
	Error	1.78E+02	312	5.72E-01		
	Total	3.79E+02	319			
Crest Factor	Motor Condition	47.294	1	47.294	173.386	8.59E-32
	Load	27.367	3	9.122	33.444	9.06E-19
	Interaction	1.258	3	0.419	1.537	0.205
	Error	85.104	312	0.273		
	Total	161.023	319			
Margin Factor	Motor Condition	171.370	1	171.370	196.200	6.39E-35
	Load	166.255	3	55.418	63.448	4.72E-32
	Interaction	4.555	3	1.518	1.738	0.159
	Error	272.516	312	0.873		
	Total	614.696	319			
Peak-to-average power ratio	Motor Condition	1.48E+03	1	1481.137	148.549	3.27E-28
	Load	7.33E+02	3	244.292	24.501	2.91E-14
	Interaction	6.99E+01	3	23.294	2.336	0.074
	Error	3.11E+03	312	9.971		
	Total	5.39E+03	319			
Variance	Motor Condition	9.513	1	9.513	19.233	1.58E-05
	Load	47.739	3	15.913	32.173	3.81E-18
	Interaction	23.297	3	7.766	15.701	1.56E-09
	Error	154.320	312	0.495		
	Total	234.869	319			
Skewness	Motor Condition	9.167	1	9.167	269.610	4.22E-44
	Load	40.236	3	13.412	394.469	8.42E-106
	Interaction	0.352	3	0.117	3.449	1.70E-02
	Error	10.608	312	0.034		
	Total	60.363	319			
kurtosis	Motor Condition	34.497	1	34.497	122.507	3.07E-24
	Load	80.151	3	26.717	94.878	1.17E-43
	Interaction	5.764	3	1.921	6.823	1.82E-04
	Error	87.857	312	0.282		
	Total	208.269	319			

Table 4.8: P-value calculation from post-hoc test procedure for non-dimensional parameter features in envelope analysis

Load (Nm)	Shape Factor	Impulse Factor	Crest Factor	Margin Factor	Peak-to-average power ratio	Variance	Skewness	kurtosis
0	5.9E-08	7.6E-07	1.0E-05	6.2E-07	8.3E-06	1.00	5.9E-08	5.9E-08
0.5	5.9E-08	5.9E-08	5.9E-08	5.9E-08	5.9E-08	0.83	6.0E-08	5.9E-08
1	5.9E-08	6.0E-08	6.0E-08	5.9E-08	7.0E-08	1.00	5.9E-08	1.2E-07
1.5	5.9E-08	6.3E-08	6.4E-08	6.0E-08	4.1E-05	5.9E-08	5.9E-08	0.68

This paragraph sums up the results obtained from time domain analysis based on Envelope Signal. Four features, namely RMS, RSSQ, Energy and Variance could not distinguish faulty state of motor from faulty-free state in low level of load. The variance feature is also failed to detect the fault based on upward or downward trend. Kurtosis feature is also failed to detect broken rotor bar when the starting torque was high. The mentioned results also proved the importance and significance of load value in starting torque on the fault diagnosis. The simulation results presented in Appendix G. is also following the experimental result in term of trend condition. Two features, namely peak to peak and Variance had overlapping between load conditions and hence could not distinguish faulty-free state from faulty state based on upward or downward trend.

4.3.2 Time-Frequency Domain Analysis

In order to examine wavelet analysis for broken rotor bar detection, stator current of healthy motor and faulty motor with one broken bar were monitored under different levels of starting load (0, 0.5, 1 and 1.5Nm). The motor under observation was sampled 40 times at each case, hence 320 samples were obtained. Wavelet analysis of the current signal was performed using Wavelet Toolbox™ in MATLAB environment and the M-file was written in MATLAB® workspace appended in Appendix E. The types of wavelet function for fault diagnosis purpose have been chosen by user's decision so far. It is therefore desirable to select a wavelet function that produces the best results for the signal being analyzed and prevent to misleading diagnosis. Several types of wavelet function, which have been applied in previous research, were investigated for providing features that can be associated to the existing fault, broken rotor bar, in a motor under different levels of load. It is important to realize the complexity of wavelet function selection for fault-related feature extraction. Accordingly, the selections of best wavelet functions with different order are essential. In this research, 102 wavelet functions have been chosen for examination of broken rotor bar detection to find the best wavelet functions as describe in Table 3.2. In this part, the selected decomposition level was verified such that the number of appropriate features was compared in the levels six and seven using the proposed algorithm. The reconstructed signal that come from the detail and approximation of level 7 and also approximation of level 6 are used as an input signal for calculating the fault related feature. The features that used in this research are Log energy Entropy and Shannon Entropy. After analysing the data and compute the features, the ANOVA analysis can compare the result based on motor condition; starting load condition and their interaction. Accordingly, the objective of this part is

to examine different wavelet functions for broken rotor bar detection based on three features that mentioned.

Table 4.9 presents the results of ANOVA models for one type of mother wavelet named “dmey” for Log energy Entropy and Shannon Entropy features based on motor condition; starting load condition and their interaction features in Detail of level 7. The p-values for the two features are less than 0.05 for each condition, load and interaction states that means, the performed ANOVA (Table 4.9) indicates a significant impact in the difference among conditions. Table 4.10 presents the results of post-hoc testing procedure for Entropy features using “dmey” mother wavelet. The results show that the p-value for the Shannon Entropy feature is not significant in this test in low levels of load except full load condition. The p-value for the Log Energy Entropy feature is also significant for all levels of load condition.

From the results of Table 4.9 and Table 4.10 it can be concluded that with using “dmey” mother wavelet and Log Energy Entropy feature, broken rotor bar fault can be detected in LS-PMSM. The 102 different mother wavelets were tested with this method to determine the ability of the features and mother wavelet to detect broken rotor bar fault and the results are shown in Table 4.11, Table 4.12 and Table 4.13.

Table 4.9: Analysis of variance for Entropy features using “dmey” mother wavelet in Detail of level 7.

Feature	Source	Sum of Squares	df	Mean Square	F	P value
Shannon Entropy	Motor Condition	2.29E+08	1	2.29E+08	72.073	8.54E-16
	Load	1.70E+09	3	5.66E+08	178.433	2.32E-67
	Interaction	5.49E+07	3	1.83E+07	5.767	7.54E-04
	Error	9.90E+08	312	3.17E+06		
	Total	2.97E+09	319			
Log Energy Entropy	Motor Condition	6.57E+08	1	6.57E+08	255.206	2.14E-42
	Load	4.43E+09	3	1.48E+09	573.843	1.3E-126
	Interaction	6.19E+07	3	2.06E+07	8.021	3.64E-05
	Error	8.03E+08	312	2.57E+06		
	Total	5.95E+09	319			

Table 4.10: P-value calculation from post-hoc test procedure for Entropy features using “dmey” mother wavelet in Detail of level 7.

Load (Nm)	Shannon Entropy	Log Energy Entropy
0	0.764	1.2E-04
0.5	0.082	6.0E-08
1	6.6E-08	6.0E-08
1.5	7.3E-08	6.0E-08

Table 4.11, Table 4.12 and Table 4.13 present the results of ANOVA and post-hoc testing procedure for two different features in 102 different mother wavelets. The mean values were compared using Tukey's honest significant differences test at $P \leq 0.05$ and in the tables, it put "Y" if the values are significant for all P-value. In Table 4.11 used the Frequency band ranges of [39.06-0]Hz that is belong to the approximation of level 6. As it is clear in this table the Shannon Entropy feature is not significant for broken rotor bar detection in different type of mother wavelet. However, Log Energy Entropy is highly significant to detection of broken rotor bar. In Table 4.12 used the Frequency band ranges of [39.06-19.53]Hz that is belong to decomposition of original signal in detail of level 7. The result in this table present that Shannon Entropy is not significant for broken rotor bar detection, and the only feature can used is Log Energy Entropy. Table 4.13 used the Frequency band ranges of [19.53-0]Hz that is belong to decomposition of original signal of the approximation of level 7. As it is clear also in this table, Shannon Entropy is not significant for broken rotor bar detection, and the only feature can used is Log Energy Entropy for using a few type of mother wavelet. The simulation results using time-frequency domain method (Wavelet Transform) are presented in Appendix H. The result of simulation also shows that the Log Energy Entropy feature is highly significant to detection of broken rotor bar.

In summary the result are as follow:

- among a wide variety of mother wavelets, Log Energy Entropy has satisfactory performances for broken rotor bar fault detection compare to Shannon Entropy.
- the results are not the same with different approximation and detail coefficient in same decomposition level. The results also present that the most effective part is the Detail of level 7 that include the Frequency band ranges of [39.06-19.53]Hz. This is also observed in the simulation result.

4.4 Summary

In summary, the results and the corresponding discussions are presented in this chapter. The outcomes are derived based on the application of the methodology introduced in the previous chapter. The simulation work considering the detailed real-world parameters conforms to the experimental work to validate the accuracy of results. Different signal processing techniques based on Time domain and time-frequency domain in current spectrum of 4-pole LSPMSM are analyzed. The effective features related to broken rotor bar are identified for further detection process and maintenance strategies. The capabilities of relevant features versus load variation are investigated.

Table 4.11: P-value signification from post-hoc test procedure for features in approximation of level 6

Mother Wavelet	Features		Mother Wavelet	Features	
	Shannon Entropy	Log Energy Entropy		Shannon Entropy	Log Energy Entropy
'dmey'	-	-	'sym5'	-	Y
'haar'	-	-	'sym6'	-	Y
'db1'	-	-	'sym7'	-	Y
'db2'	-	Y	'sym8'	-	Y
'db3'	-	Y	'sym9'	-	Y
'db4'	-	Y	'sym10'	-	Y
'db5'	-	Y	'sym11'	-	Y
'db6'	-	Y	'sym12'	-	Y
'db7'	-	Y	'sym13'	-	Y
'db8'	-	Y	'sym14'	-	Y
'db9'	-	Y	'sym15'	-	Y
'db10'	-	Y	'sym16'	-	Y
'db11'	-	Y	'sym17'	-	Y
'db12'	-	Y	'sym18'	-	Y
'db13'	-	Y	'sym19'	-	Y
'db14'	-	Y	'sym20'	-	Y
'db15'	-	Y	'coif1'	-	Y
'db16'	-	Y	'coif2'	-	Y
'db17'	-	Y	'coif3'	-	Y
'db18'	-	Y	'coif4'	-	Y
'db19'	-	Y	'coif5'	-	Y
'db20'	-	Y	'bior1.1'	-	-
'db21'	-	Y	'bior1.3'	-	-
'db22'	-	-	'bior1.5'	-	Y
'db23'	-	Y	'bior2.2'	-	Y
'db24'	-	Y	'bior2.4'	-	Y
'db25'	-	-	'bior2.6'	-	Y
'db26'	-	-	'bior2.8'	-	Y
'db27'	-	-	'bior3.1'	-	Y
'db28'	-	-	'bior3.3'	-	Y
'db29'	-	-	'bior3.5'	-	-
'db30'	-	-	'bior3.7'	-	Y
'db31'	-	-	'bior3.9'	-	Y
'db32'	-	-	'bior4.4'	-	Y
'db33'	-	-	'bior5.5'	-	Y
'db34'	-	-	'bior6.8'	-	Y
'db35'	-	-	'rbio1.1'	-	-
'db36'	-	-	'rbio1.3'	-	-
'db37'	-	-	'rbio1.5'	-	-
'db38'	-	-	'rbio2.2'	-	Y
'db39'	-	-	'rbio2.4'	-	Y
'db40'	-	-	'rbio2.6'	-	Y
'db41'	-	-	'rbio2.8'	-	Y
'db42'	-	-	'rbio3.1'	-	Y
'db43'	-	-	'rbio3.3'	-	Y
'db44'	-	-	'rbio3.5'	-	Y
'db45'	-	-	'rbio3.7'	-	Y
'sym1'	-	-	'rbio3.9'	-	Y
'sym2'	-	Y	'rbio4.4'	-	Y
'sym3'	-	Y	'rbio5.5'	-	Y
'sym4'	-	Y	'rbio6.8'	-	Y

Table 4.12: P-value signification from post-hoc test procedure for features in Detail of level 7

Mother Wavelet	Features		Mother Wavelet	Features	
	Shannon Entropy	Log Energy Entropy		Shannon Entropy	Log Energy Entropy
'dmey'	-	Y	'sym5'	-	Y
'haar'	-	-	'sym6'	-	Y
'db1'	-	-	'sym7'	-	Y
'db2'	-	Y	'sym8'	-	Y
'db3'	-	Y	'sym9'	-	Y
'db4'	-	Y	'sym10'	-	Y
'db5'	-	Y	'sym11'	-	Y
'db6'	-	Y	'sym12'	-	Y
'db7'	-	Y	'sym13'	-	Y
'db8'	-	Y	'sym14'	-	Y
'db9'	-	Y	'sym15'	-	Y
'db10'	-	Y	'sym16'	-	Y
'db11'	-	Y	'sym17'	-	-
'db12'	-	Y	'sym18'	-	Y
'db13'	-	Y	'sym19'	-	Y
'db14'	-	-	'sym20'	-	Y
'db15'	-	Y	'coif1'	-	Y
'db16'	-	Y	'coif2'	-	Y
'db17'	-	Y	'coif3'	-	Y
'db18'	-	-	'coif4'	-	Y
'db19'	-	Y	'coif5'	-	Y
'db20'	-	Y	'bior1.1'	-	-
'db21'	-	Y	'bior1.3'	-	Y
'db22'	-	-	'bior1.5'	-	Y
'db23'	-	Y	'bior2.2'	-	Y
'db24'	-	Y	'bior2.4'	-	Y
'db25'	-	Y	'bior2.6'	-	Y
'db26'	-	Y	'bior2.8'	-	Y
'db27'	-	Y	'bior3.1'	-	Y
'db28'	-	Y	'bior3.3'	-	Y
'db29'	-	Y	'bior3.5'	-	Y
'db30'	-	Y	'bior3.7'	-	Y
'db31'	-	Y	'bior3.9'	-	Y
'db32'	-	Y	'bior4.4'	-	Y
'db33'	-	-	'bior5.5'	-	Y
'db34'	-	-	'bior6.8'	-	Y
'db35'	-	Y	'rbio1.1'	-	-
'db36'	-	Y	'rbio1.3'	-	-
'db37'	-	Y	'rbio1.5'	-	-
'db38'	-	Y	'rbio2.2'	-	Y
'db39'	-	Y	'rbio2.4'	-	Y
'db40'	-	Y	'rbio2.6'	-	Y
'db41'	-	Y	'rbio2.8'	-	Y
'db42'	-	Y	'rbio3.1'	-	Y
'db43'	-	Y	'rbio3.3'	-	Y
'db44'	-	Y	'rbio3.5'	-	Y
'db45'	-	Y	'rbio3.7'	-	Y
'sym1'	-	-	'rbio3.9'	-	Y
'sym2'	-	Y	'rbio4.4'	-	Y
'sym3'	-	Y	'rbio5.5'	-	Y
'sym4'	-	Y	'rbio6.8'	-	Y

Table 4.13: P-value signification from post-hoc test procedure for features in approximation of level 7

Mother Wavelet	Features		Mother Wavelet	Features	
	Shannon Entropy	Log Energy Entropy		Shannon Entropy	Log Energy Entropy
'dmey'	-	-	'sym5'	-	Y
'haar'	-	-	'sym6'	-	-
'db1'	-	-	'sym7'	-	-
'db2'	-	Y	'sym8'	-	-
'db3'	-	Y	'sym9'	-	-
'db4'	-	-	'sym10'	-	-
'db5'	-	-	'sym11'	-	-
'db6'	-	-	'sym12'	-	-
'db7'	-	-	'sym13'	-	-
'db8'	-	-	'sym14'	-	-
'db9'	-	-	'sym15'	-	-
'db10'	-	-	'sym16'	-	-
'db11'	-	-	'sym17'	-	-
'db12'	-	-	'sym18'	-	-
'db13'	-	-	'sym19'	-	-
'db14'	-	-	'sym20'	-	-
'db15'	-	-	'coif1'	-	Y
'db16'	-	-	'coif2'	-	Y
'db17'	-	-	'coif3'	-	-
'db18'	-	-	'coif4'	-	-
'db19'	-	-	'coif5'	-	-
'db20'	-	-	'bior1.1'	-	-
'db21'	-	-	'bior1.3'	-	-
'db22'	-	-	'bior1.5'	-	-
'db23'	-	-	'bior2.2'	-	Y
'db24'	-	-	'bior2.4'	-	Y
'db25'	-	-	'bior2.6'	-	Y
'db26'	-	-	'bior2.8'	-	-
'db27'	-	-	'bior3.1'	-	Y
'db28'	-	-	'bior3.3'	-	Y
'db29'	-	-	'bior3.5'	-	-
'db30'	-	-	'bior3.7'	-	-
'db31'	-	-	'bior3.9'	-	-
'db32'	-	-	'bior4.4'	-	Y
'db33'	-	-	'bior5.5'	-	Y
'db34'	-	-	'bior6.8'	-	-
'db35'	-	-	'rbio1.1'	-	-
'db36'	-	-	'rbio1.3'	-	-
'db37'	-	-	'rbio1.5'	-	-
'db38'	-	-	'rbio2.2'	-	-
'db39'	-	-	'rbio2.4'	-	Y
'db40'	-	-	'rbio2.6'	-	Y
'db41'	-	-	'rbio2.8'	-	Y
'db42'	-	-	'rbio3.1'	-	-
'db43'	-	-	'rbio3.3'	-	-
'db44'	-	-	'rbio3.5'	-	-
'db45'	-	-	'rbio3.7'	-	-
'sym1'	-	-	'rbio3.9'	-	-
'sym2'	-	Y	'rbio4.4'	-	-
'sym3'	-	Y	'rbio5.5'	-	-
'sym4'	-	Y	'rbio6.8'	-	-

CHAPTER 5

CONCLUSION AND FUTURE RECOMMENDATIONS

This chapter presents a summary of the accomplishments and reviews the observations and achievements of the current research. It also addresses suggestions regarding possible directions of future research topics.

5.1 Conclusions

Electrical machine is one of the most important equipment in industrial processes. However, failures in different parts of electrical machine do occur because it is generally under different stresses. Fault diagnosis of electrical machine is an on-going research topic. The new electrical machine namely, LS-PMSM has been recently introduced and launched to be operated in industrial sectors. This motor is a suitable choice because of its high efficiency and high power factor. Application of LS-PMSM is growing gradually while the industry is still lacking an accurate fault detection criterion for maintenance policy of the motor. The main objective of this research is to study and investigate broken rotor bar fault detection in a LS-PMSM. The proposed method can be applied in the fault detection devices and also in the online monitoring systems. Moreover, the proposed method can be helpful for the manufacture to set the preventive maintenance programs based on signal analysis of input current duration of motor operation.

As LS-PMSM is new, no research has been performed on its fault detection. The importance of broken bar detection has been addressed comprehensively based on squirrel cage induction machine in Chapter 2. Different types of signal can be collected from electrical machine to discover the condition or situation of machine, however, for reliable fault detection the best signal should be selected and captured correctly. In the second part of Chapter 2, different types of signals that can be collected from electrical machine and employed for broken rotor bar detection in squirrel-cage induction machine was extensively described. Signal capturing is a significant step involved in fault detection procedures and can be performed by on-line or off-line techniques with invasive or non-invasive characteristics. Non-invasive methods provide useful information for fault detection without installation of extra sensor or changing of the machine structure. A non-invasive technique known as Motor Current Signature Analysis (MCSA) has been considered as the most promising technique for broken rotor bar detection and thus is selected for this research. The stator current signal of LS-PMSM during its start-up is sampled for signature analysis and extraction of fault-related features. Current signal at transient condition (start-up condition) of LS-PMSM is analysed because the squirrel cage of LS-PMSM is only working during transient condition.

In the third part of Chapter 2, Different types of signal processing methods for extracting of features related to broken bar in squirrel cage induction machine was

extensively described. Among different methods of signal processing, time domain analysis and Wavelet transform (a time-frequency domain analysis) are applied based on the nature of the signal used in this study. Thirteen statistical features in time domain and two features in time-frequency domain are appraised to find the reliable features related to broken rotor bar. In the last part of Chapter 3, the statistical analysis was introduced to evaluate the features used in this study for broken bar detection. Investigation of behavior of these features is critical for decision making step. Trend and box plot graphs are used to evaluate the effects of load on tendency of feature with increasing and decreasing of incline. Analysis of Variance (ANOVA) is also used to evaluate the features characteristic in each condition and load.

Finite Element Method (FEM) is a precise technique to analyse the electrical machines in different conditions. An investigation based on FEM is performed using Maxwell 2-D software according to real detailed parameters and the condition of experiment in order to validate with experimental result. In this research, broken rotor bar detection is also experimentally investigated. A three-phase, 4-pole LS-PMSM model (TA80-4) is utilized to investigate the effects of broken rotor bar on motor performance. Laboratory test rig is developed using the relevant equipment to carry out the experimental study.

This research indicates the importance of load effects on broken bar detection. The current signal is collected in different load levels of starting torque within four steps, which increases from 0% to 65%. The experimental and simulation result substantiate that increasing the load, will also increase the starting time duration. The time duration of machine with one broken rotor bar also increases compared to healthy condition. The broken rotor bar also affects the value of starting torque. The experimental and simulation results both proved that starting torque for motor with one broken rotor bar drops to near 1.7(Nm), where starting torque for healthy motor is 2.3(Nm).

In the time domain analysis, three features, namely peak to peak, shape factor and impulse factor cannot distinguish faulty state of motor from faulty-free state based on upward or downward trend. Skewness also fails to detect broken bar when the starting torque is high. In time domain analysis using of envelop signal, four features, namely RMS, RSSQ, Energy and Variance cannot distinguish faulty state of motor from healthy state in low level of load. The variance feature also fails to detect the fault based on upward or downward trend. When the starting torque is high, Kurtosis feature is not a suitable feature to detect broken rotor bar. Experimental and simulation results corroborate each other and validate the overall work.

In the time-frequency domain analysis, Log Energy Entropy feature has satisfactory performances for broken rotor bar detection compare to Shannon Entropy feature. The result also presents that the most effective sub-band frequency is Detail of level 7 that includes the frequency band ranges of [39.06-19.53]Hz.

The significant contribution of this research is investigation of broken rotor bar in three-phase LS-PMSM under different operation conditions. Since the current research is the first work on broken rotor bar detection in LS-PMSM, the simulation and experimental results are compared to identify the efficient features extracted from start-up current signal for reliable and cost-effective detection. Experimental and simulation results corroborate each other and validate the overall work.

5.2 Future works and Recommendations

Since the study of faults in LS-PMSM has just started, it is of interest to propose further overall works according to the results achieved. The following researches are suggested:

- 1) to extend the detection method for diagnosis of broken rotor bar in LS-PMSM that use drive system, and
- 2) applying of intelligent techniques to increase the ability and accuracy of fault detection in the decision making part, and
- 3) to extend the detection method for diagnosis of other electrical and mechanical faults in LS-PMSM.

REFERENCES

- [1] H. A. Toliyat and G. B. Kliman, *Handbook of Electric Motors*. 2004.
- [2] WEG, *WQuattro-Super Premium Efficiency Motor*. 2015.
- [3] J. Pyrhonen, T. Jokinen, and V. Hrabovcova, *Design of Rotating Electrical Machines*. Wiley, 2009.
- [4] J. Ilonen, J.-K. Kamarainen, T. Lindh, J. Ahola, H. Kalviainen, and J. Partanen, "Diagnosis Tool for Motor Condition Monitoring," *IEEE Transactions on Industry Applications*, vol. 41, no. 4, pp. 963–971, Jul. 2005.
- [5] R. Fiser and S. Ferkolj, "Application of a finite element method to predict damaged induction motor performance," *IEEE Transactions on Magnetics*, vol. 37, no. 5, pp. 3635–3639, 2001.
- [6] A. Bellini, F. Filippetti, C. Tassoni, and G.-A. Capolino, "Advances in Diagnostic Techniques for Induction Machines," *IEEE Transactions on Industrial Electronics*, vol. 55, no. 12, pp. 4109–4126, Dec. 2008.
- [7] W. R. Finley, M. M. Hodowanec, and W. G. Holter, "An Analytical Approach to Solving Motor Vibration Problems," in *IEEE 46th Annual Industry Applications Society*, 1999, pp. 217–232.
- [8] P. Zhang, Y. Du, T. G. Habetler, and B. Lu, "A Survey of Condition Monitoring and Protection Methods for Medium-Voltage Induction Motors," *IEEE Transactions on Industry Applications*, vol. 47, no. 1, pp. 34–46, Jan. 2011.
- [9] H. M. Zubayer, "Design Analysis of Line-start Interior Permanent Magnet Synchronous Motor," Memorial University of Newfoundland, 2011.
- [10] I. Culbert and W. Rhodes, "Using Current Signature Analysis Technology to Reliably Detect Cage Winding Defects in Squirrel Cage Induction Motors," *IEEE Transactions on Industry Applications*, vol. 43, no. 2, pp. 95–101, 2007.
- [11] A. H. Bonnett and G. C. Soukup, "Rotor Failures in Squirrel Cage Induction Motors," *IEEE Transactions on Industry Applications*, vol. IA-22, no. 6, pp. 1165–1173, Nov. 1986.
- [12] J. Faiz, B. M. Ebrahimi, and M. B. B. Sharifian, "Time Stepping Finite Element Analysis of Broken Bars Fault in a Three-Phase Squirrel-Cage Induction Motor," *Progress In Electromagnetics Research*, vol. 68, pp. 53–70, 2007.
- [13] M. R. Mehrjou, N. Mariun, M. Hamiruce Marhaban, and N. Misron, "Rotor fault condition monitoring techniques for squirrel-cage induction machine—A review," *Mechanical Systems and Signal Processing*, vol. 25, no. 8, pp. 2827–2848, Nov. 2011.
- [14] International Energy Agency, "Energy Efficiency Roadmap for Electric Motors and Motor Systems," 2015.
- [15] I. Ahmed, R. Supangat, J. Grieger, N. Ertugrul, and W. Soong, "A Baseline Study for On-Line Condition Monitoring of Induction Machines," in *Australasian Universities Power Engineering Conference*, 2004.
- [16] P. Walde and C. Brunner, "Energy-efficiency policy opportunities for electric motor-driven systems," 2011.
- [17] A. Hassanpour Isfahani and S. Vaez-Zadeh, "Line start permanent magnet synchronous motors: Challenges and opportunities," *Energy*, vol. 34, no. 11. Elsevier Ltd, pp. 1755–1763, 2009.
- [18] O. Arabacı, Hayri and Bilgin, "Analysis of Rotor Faults Effects on Submersible Induction Motor Efficiency," in *Proceedings of The World*

- Congress on Engineering and Computer Science*, 2013.
- [19] C. da Costa, M. Kashiwagi, and M. H. Mathias, "Rotor failure detection of induction motors by wavelet transform and Fourier transform in non-stationary condition," *Case Studies in Mechanical Systems and Signal Processing*, vol. 1, pp. 15–26, 2015.
- [20] Y. Gritli, S. Bin Lee, F. Filippetti, and L. Zarri, "Advanced Diagnosis of Outer Cage Damage in Double-Squirrel-Cage Induction Motors Under Time-Varying Conditions Based on Wavelet Analysis," *IEEE Transactions on Industry Applications*, vol. 50, no. 3, pp. 1791–1800, May 2014.
- [21] Ž. Kanovi, D. Mati, Z. Jeli, M. Rapai, B. Jakovljevi, and M. Kapetina, "Induction Motor Broken Rotor Bar Detection Using Vibration Analysis – A Case Study," in *9th IEEE International Symposium on Diagnostics for Electric Machines, Power Electronics and Drives*, 2013, pp. 64–68.
- [22] F. W. Merrill, "Permanent magnet excited synchronous motors," *Electrical Engineering*, vol. 74, no. 2, pp. 143–143, Feb. 1955.
- [23] T. J. E. Miller, "Synchronization of Line-Start Permanent-Magnet AC Motors," *IEEE Transactions on Power Apparatus and Systems*, vol. PAS-103, no. 7, pp. 1822–1828, 1984.
- [24] A. Chama, A. J. Sorgdrager, and R. Wang, "Analytical synchronization analysis of line-start permanent magnet synchronous motors," *Progress In Electromagnetics Research M*, vol. 48, no. May, pp. 183–193, 2016.
- [25] T. J. E. Miller, M. Popescu, C. Cossar, M. McGilp, G. Strappazon, N. Trivillin, and R. Santarossa, "Line-Start Permanent-Magnet Motor Single-Phase Steady-State Performance Analysis," *IEEE Transactions on Industry Applications*, vol. 40, no. 2, pp. 516–525, Mar. 2004.
- [26] G. Huth and R. Fischer, "Running up and pulling into step of PM line-start motors with surface-mounted magnets," *Electrical Engineering*, vol. 97, no. 1, pp. 13–24, 2014.
- [27] J. Faiz, B. M. Ebrahimi, and M. B. B. Sharifian, "Different Faults and Their Diagnosis Techniques in Three-Phase Squirrel-Cage Induction Motors—A Review," *Electromagnetics*, vol. 26, no. 7, pp. 543–569, 2006.
- [28] S. Nandi, H. A. Toliyat, and X. Li, "Condition monitoring and fault diagnosis of electrical motors-A review," *IEEE Transactions on Energy Conversion*, vol. 20, no. 4, pp. 719–729, Dec. 2005.
- [29] G. . Singh and S. Ahmed Saleh Al Kazzaz, "Induction machine drive condition monitoring and diagnostic research—a survey," *Electric Power Systems Research*, vol. 64, no. 2. pp. 145–158, 2003.
- [30] A. H. Bonnett and G. C. Soukup, "Cause and analysis of stator and rotor failures in three-phase squirrel-cage induction motors," *IEEE Transactions on Industry Applications*, vol. 28, no. 4, pp. 921–937, 1992.
- [31] N. Bethel, "Motor Efficiency and Fault Zone Analysis," *PdMA® Corporation*, 2013. [Online]. Available: http://www.pdma.com/pdfs/Articles/WhitePapers/Motor_Efficiency_and_Fault_Zone_Analysis.pdf. [Accessed: 07-Feb-2016].
- [32] H. Arabaci, O. Bilgin, and Á. Squirrel, "Efficiency Analysis of Submersible Induction Motor with Broken Rotor Bar," in *Transactions on Engineering Technologies*, H. K. Kim, S.-I. Ao, and M. A. Amouzegar, Eds. Dordrecht: Springer Netherlands, 2014, pp. 27–40.
- [33] M. M. Rahimian, "Broken Bar Detection in Synchronous Machines Based Wind Energy Conversion System," Texas A&M University, 2011.

- [34] G. B. Kliman, R. A. Koegl, J. Stein, R. D. Endicott, and M. W. Madden, "Noninvasive Detection of Broken Rotor Bars in Operating Induction Motors," *IEEE Transactions on Energy Conversion*, vol. 3, no. 4, pp. 873–879, 1988.
- [35] B. M. Ebrahimi, J. Faiz, S. Lotfi-fard, and P. Pillay, "Novel Indices for Broken Rotor Bars Fault Diagnosis in Induction Motors Using Wavelet Transform," *Mechanical Systems and Signal Processing*, vol. 30, pp. 131–145, Jul. 2012.
- [36] R. Burnett, J. F. Watson, and S. Elder, "The Application of Modern Signal Processing Techniques for Use in Rotor Fault Detection and Location within Three-Phase Induction Motors," *Signal Processing*, vol. 49, no. 1, pp. 57–70, Feb. 1996.
- [37] K. Bacha, H. Henao, M. Gossa, and G.-A. Capolino, "Induction Machine Fault Detection Using Stray Flux EMF Measurement and Neural Network-Based Decision," *Electric Power Systems Research*, vol. 78, no. 7, pp. 1247–1255, Jul. 2008.
- [38] J. Faiz and M. Ojaghi, "Different indexes for eccentricity faults diagnosis in three-phase squirrel-cage induction motors: A review," *Mechatronics*, vol. 19, no. 1, pp. 2–13, Feb. 2009.
- [39] K. F. Martin, "A review by discussion of condition monitoring and fault diagnosis in machine tools," *International Journal of Machine Tools and Manufacture*, vol. 34, no. 4, pp. 527–551, May 1994.
- [40] A. Y. Ben Sasi, F. Gu, B. Payne, and A. Ball, "Instantaneous Angular Speed Monitoring of Electric Motors," *Journal of Quality in Maintenance Engineering*, vol. 10, no. 2, pp. 123–135, 2004.
- [41] N. Tandon and A. Choudhury, "A review of vibration and acoustic measurement methods for the detection of defects in rolling element bearings," *Tribology International*, vol. 32, no. 8, pp. 469–480, Aug. 1999.
- [42] W. Li and C. Mechefske, "Detection of Induction Motor Faults A Comparison of Stator Current, Vibration and Acoustic Methods," *Journal of vibration and Control*, vol. 12, no. 2, pp. 165–188, Feb. 2006.
- [43] E. Germen, M. Başaran, and M. Fidan, "Sound Based Induction Motor Fault Diagnosis using Kohonen Self-Organizing Map," *Mechanical Systems and Signal Processing*, vol. 46, no. 1, pp. 45–58, May 2014.
- [44] A. Gaylard, A. Meyer, and C. Landy, "Acoustic evaluation of faults in electrical machines," *Electrical Machines and Drives conference*, no. 412, pp. 147–150, 1995.
- [45] S. P. Verma, "Noise and vibrations of electrical machines and drives; their production and means of reduction," in *Proceedings of International Conference on Power Electronics, Drives and Energy Systems for Industrial Growth*, 1996, vol. 2, pp. 1031–1037.
- [46] S. P. Verma and W. Li, "Measurement of Vibrations and Radiated Acoustic Noise of Electrical Machines," *Electrical Machines and Systems, 2003. ICEMS 2003. Sixth International Conference on*, vol. 2, pp. 861–866 vol.2, 2003.
- [47] S. Umans, A. Fitzgerald, and C. Kingsley, *Fitzgerald and Kingsley's electric machinery*. McGraw-Hill Higher Education, 2013.
- [48] J. S. Hsu, "Monitoring of Defects in Induction Motors Through Air-gap Torque Observation," *IEEE Transactions on Industry Applications*, vol. 31, no. 5, pp. 1016–1021, 1995.

- [49] J. Faiz, V. Ghorbanian, and B. M. Ebrahimi, "Locating Broken Bars in Line-Start and Inverter-Fed Induction Motors Using Modified Winding Function Method," *Electromagnetics*, vol. 32, no. 3, pp. 173–192, Mar. 2012.
- [50] K. N. Gyftakis, D. V. Spyropoulos, J. C. Kappatou, and E. D. Mitronikas, "A Novel Approach for Broken Bar Fault Diagnosis in Induction Motors Through Torque Monitoring," *IEEE Transactions on Energy Conversion*, vol. 28, no. 2, pp. 267–277, Jun. 2013.
- [51] F. Thollon, G. Grellet, and A. Jammal, "Asynchronous motor cage fault detection through electromagnetic torque measurement," *European Transactions on Electrical Power*, vol. 3, no. 5, pp. 375–378, Sep. 2007.
- [52] H. Yahoui and G. Grellet, "Detection of an End-Ring Fault in Asynchronous Machines by Spectrum Analysis of the Observed Electromagnetic Torque," *Journal de Physique III*, vol. 6, no. 4, pp. 443–448, 1996.
- [53] X. Huang, "Diagnostics of Air Gap Eccentricity IN Closed-Loop Drive-Connected Induction Motors," Georgia Institute of Technology, 2005.
- [54] R. S. Wieser, M. Schagginger, C. Kral, and F. Pirker, "The integration of machine fault detection into an indirect field oriented induction machine drive control scheme-the Vienna Monitoring Method," in *Conference Record of 1998 IEEE Industry Applications Conference. Thirty-Third IAS Annual Meeting (Cat. No.98CH36242)*, 1998, vol. 1, pp. 278–285.
- [55] C. Kral, F. Pirker, and G. Pascoli, "Detection of Rotor Faults in Squirrel-Cage Induction Machines at Standstill for Batch Tests by Means of the Vienna Monitoring Method," *IEEE Transactions on Industry Applications*, vol. 38, no. 3, pp. 618–624, May 2002.
- [56] C. Kral, F. Pirker, and G. Pascoli, "Model-Based Detection of Rotor Faults Without Rotor Position Sensor—The Sensorless Vienna Monitoring Method," *IEEE Transactions on Industry Applications*, vol. 41, no. 3, pp. 784–789, May 2005.
- [57] L. Wu, "Separating Load Torque Oscillation and Rotor Faults in Stator Current Based-Induction Motor Condition Monitoring," Georgia Institute of Technology, 2007.
- [58] V. V. Thomas, K. Vasudevan, and V. J. Kumar, "Online cage rotor fault detection using air-gap torque spectra," *IEEE Transactions on Energy Conversion*, vol. 18, no. 2, pp. 265–270, 2003.
- [59] A. M. da Silva, "Rotor Bar Fault Monitoring Method Based on Analysis of Air-Gap Torques of Induction Motors," *IEEE Transactions on Industrial Informatics*, vol. 9, no. 4, pp. 2274–2283, Nov. 2013.
- [60] V. Ghorbanian and J. Faiz, "A survey on time and frequency characteristics of induction motors with broken rotor bars in line-start and inverter-fed modes," *Mechanical Systems and Signal Processing*, vol. 54–55, pp. 427–456, Mar. 2015.
- [61] M. El Hachemi Benbouzid, "A review of induction motors signature analysis as a medium for faults detection," *IEEE Transactions on Industrial Electronics*, vol. 47, no. 5, pp. 984–993, 2000.
- [62] A. Siddique, G. S. Yadava, and B. Singh, "A Review of Stator Fault Monitoring Techniques of Induction Motors," *IEEE Transactions on Energy Conversion*, vol. 20, no. 1, pp. 106–114, Mar. 2005.
- [63] O. Article, "MachineLibrary™ – Broken Rotor Bar and Motor Malfunctions," 1999. [Online]. Available: http://www.ge-mcs.com/download/orbit-archives/2001-2005/2nd_quarter_2001/2q01machinelib.pdf. [Accessed: 08-

- Feb-2016].
- [64] J. F. Bangura and N. a. Demerdash, "Diagnosis and Characterization of Effects of Broken Bars and Connectors in Squirrel-Cage Induction Motors by a Time-Stepping Coupled Finite Element-State Space Modeling Approach," *IEEE Transactions on Energy Conversion*, vol. 14, no. 4, pp. 1167–1176, 1999.
 - [65] B. Mirafzal, "Incipient Fault Diagnosis in Squirrel-Cage Induction Motors," Marquette University, 2005.
 - [66] C. Hargis, B. Gaydon, and Kamash, K, "The detection of rotor defects in induction motors," in *IEE Int. Conf. Electrical Machines, Design and Application*, 1989, pp. 216–220.
 - [67] A. Bellini, F. Filippetti, G. Franceschini, C. Tassoni, and G. B. Kliman, "Quantitative Evaluation of Induction Motor Broken Bars by Means of Electrical Signature Analysis," *IEEE Transactions on Industry Applications*, vol. 37, no. 5, pp. 1248–1255, 2001.
 - [68] H. Douglas, P. Pillay, and A. K. Ziarani, "A New Algorithm for Transient Motor Current Signature Analysis Using Wavelets," *IEEE Transactions on Industry Applications*, vol. 40, no. 5, pp. 1361–1368, Sep. 2004.
 - [69] B. G. Gaydon, "An Instrument to Detect Induction Motor Rotor Circuit Defects by Speed Fluctuation Measurements," in *InProc. Electr. Test Meas. Instrum.–Testmex*, 1979, pp. 5–8.
 - [70] W. Deleroi, "Squirrel cage motor with broken bar in the rotor-physical phenomena and their experimental," in *In Proc. of Int. Conf. On Electrical Machines*, 1982, pp. 767–770.
 - [71] W. Thomson, N. Deans, R. Leonard, and A. Milne, "Monitoring strategy for discriminating between different types of rotor defects in induction motors.," in *InProceedings of the Universities Power Engineering Conference*, 1983, pp. 241–246.
 - [72] R. Fiser and S. Ferkolj, "Calculation of Magnetic Field Asymmetry of Induction Motor with Rotor Faults," in *9th Mediterranean Electrotechnical Conference. Proceedings , (MELECON 98).*, 1998, vol. 2, pp. 1175–1179.
 - [73] T. Vaimann and A. Kallaste, "Detection of Broken Rotor Bars in Three-Phase Squirrel-Cage Induction Motor using Fast Fourier Transform," in *10th International Symposium "Topical Problems in the Field of Electrical and Power Engineering,"* 2011, pp. 52–56.
 - [74] J. Faiz and B. M. Ebrahimi, "Locating Rotor Broken Bars in Induction Motors Using Finite Element Method," *Energy Conversion and Management*, vol. 50, no. 1, pp. 125–131, Jan. 2009.
 - [75] M. Riera-Guasp, M. F. Cabanas, J. A. Antonino-Daviu, M. Pineda-Sanchez, and C. H. R. Garcia, "Influence of Nonconsecutive Bar Breakages in Motor Current Signature Analysis for the Diagnosis of Rotor Faults in Induction Motors," *IEEE Transactions on Energy Conversion*, vol. 25, no. 1, pp. 80–89, Mar. 2010.
 - [76] X. Ying, "Performance Evaluation and Thermal Fields Analysis of Induction Motor With Broken Rotor Bars Located at Different Relative Positions," *IEEE Transactions on Magnetics*, vol. 46, no. 5, pp. 1243–1250, May 2010.
 - [77] J. Faiz, B. M. Ebrahimi, and H. A. Toliyat, "Signature Analysis of Electrical and Mechanical Signals for Diagnosis of Broken Rotor Bars in an Induction Motor," *Electromagnetics*, vol. 27, no. 8, pp. 507–526, Nov. 2007.
 - [78] R. Hirvonen, "On-line condition monitoring of defects in squirrel cage

- motors,” in *In Proc. Int. Conf. Electrical Machines*, 1994, pp. 267–272.
- [79] M. Benbouzid, M. Vieira, and C. Theys, “Induction motors’ faults detection and localization using stator current advanced signal processing techniques,” *IEEE Transactions on Power Electronics*, vol. 14, no. 1, pp. 14–22, 1999.
- [80] W. T. Thomson and M. Fenger, “Current Signature Analysis to Detect Induction Motor Faults,” *IEEE Industry Applications Magazine*, vol. 7, no. 4, pp. 26–34, 2001.
- [81] J. M. B. Siau, A. L. Graff, W. L. Soong, and N. Ertugrul, “Broken bar detection in induction motors using current and flux spectral analysis,” *Australian Journal of Electrical and Electronics Engineering*, vol. 1, no. 3, pp. 171–177, 2004.
- [82] W. Thomson, “On-Line Fault Diagnosis in Induction Motor Drives via MCSA,” *EM Diagnostics Ltd., Scotland*, 2001.
- [83] F. Filippetti, M. Martelli, G. Franceschini, and C. Tassoni, “Development of expert system knowledge base to on-line diagnosis of rotor electrical faults of induction motors,” in *Conference Record of the 1992 IEEE Industry Applications Society Annual Meeting*, 1992, pp. 92–99.
- [84] C. Bruzzese, O. Honorati, E. Santini, and D. Sciunnache, “New Rotor Fault Indicators for Squirrel Cage Induction Motors,” in *Conference Record of the 2006 IEEE Industry Applications Conference Forty-First IAS Annual Meeting*, 2006, vol. 3, no. c, pp. 1541–1548.
- [85] O. V. Thorsen and M. Dalva, “Failure identification and analysis for high-voltage induction motors in the petrochemical industry,” *IEEE Transactions on Industry Applications*, vol. 35, no. 4, pp. 810–818, 1999.
- [86] N. M. Elkasabgy, A. R. Eastham, and G. E. Dawson, “The detection of broken bars in the cage rotor of an induction machine,” in *Conference Record of the 1988 IEEE Industry Applications Society Annual Meeting*, 1992, vol. 28, no. 1, pp. 181–187.
- [87] D. H. Hwang, S. B. Han, B. C. Woo, J. H. Sun, D. S. Kang, B. K. Kim, and Y. H. Cho, “Detection of air-gap eccentricity and broken-rotor bar conditions in a squirrel-cage induction motor using the radial flux sensor,” in *Journal of Applied Physics*, 2008, vol. 103, no. 7, pp. 129–132.
- [88] G. Niu, J.-D. Son, A. Widodo, B.-S. Yang, D.-H. Hwang, and D.-S. Kang, “A Comparison of Classifier Performance for Fault Diagnosis of Induction Motor using Multi-type Signals,” *Structural Health Monitoring*, vol. 6, no. 3, pp. 215–229, Sep. 2007.
- [89] Y.-W. Youn, D.-H. Hwang, J.-H. Sun, and D.-S. Kang, “A Method for Identifying Broken Rotor Bar and Stator Winding Fault in a Low-voltage Squirrel-cage Induction Motor Using Radial Flux Sensor,” *Journal of Electrical Engineering and Technology*, vol. 6, no. 5, pp. 666–670, Sep. 2011.
- [90] Y. Xie, “Investigation of Broken Rotor Bar Faults in Three-Phase Squirrel-Cage Induction Motors,” in *Finite Element Analysis - From Biomedical Applications to Industrial Developments*, InTech, 2012, pp. 477–496.
- [91] R. Pusca, R. Romary, V. Fireteanu, and A. Ceban, “Finite Element Analysis and Experimental Study of the Near-Magnetic field for Detection of Rotor Faults in Induction Motors,” *Progress In Electromagnetics Research B*, vol. 50, no. February, pp. 37–59, 2013.
- [92] A. Yazidi, H. Henao, G. A. Capolino, M. Artioli, and F. Filippetti, “Improvement of frequency resolution for three-phase induction machine fault diagnosis,” in *Fourtieth IAS Annual Meeting. Conference Record of the 2005*

- Industry Applications Conference, 2005.*, 2005, vol. 1, no. 1, pp. 20–25.
- [93] C. Concari, G. Franceschini, and C. Tassoni, “Differential Diagnosis Based on Multivariable Monitoring to Assess Induction Machine Rotor Conditions,” *IEEE Transactions on Industrial Electronics*, vol. 55, no. 12, pp. 4156–4166, 2008.
- [94] S. H. Kia, A. M. Mabwe, H. Henao, and G.-A. Capolino, “Wavelet Based Instantaneous Power Analysis for Induction Machine Fault Diagnosis,” in *IECON 2006 - 32nd Annual Conference on IEEE Industrial Electronics*, 2006, pp. 1229–1234.
- [95] N. Elkasabgy, A. R. Eastham, and G. E. Dawson, “Detection of Broken Bars in the Cage Rotor on an Induction Machine,” *IEEE Transactions on Industry Applications*, vol. 28, no. 1, pp. 165–171, 1992.
- [96] W. T. Thomson, D. Rankin, and D. G. Dorrell, “On-line current monitoring to diagnose airgap eccentricity in large three-phase induction motors-industrial case histories verify the predictions,” *IEEE Transactions on Energy Conversion*, vol. 14, no. 4, pp. 1372–1378, 1999.
- [97] M. Feldman and S. Seibold, “Damage Diagnosis of Rotors: Application of Hilbert Transform and Multihypothesis Testing,” *Journal of Vibration and Control*, vol. 5, no. 3, pp. 421–442, May 1999.
- [98] F. Gu, I. Yesilyurt, Y. Li, G. Harris, and A. Ball, “An Investigation of The Effects of Measurement Noise in The Use of Instantaneous Angular Speed for Machine Diagnosis,” *Mechanical Systems and Signal Processing*, vol. 20, no. 6, pp. 1444–1460, Aug. 2006.
- [99] R. Maier, “Protection of Squirrel-Cage Induction Motor Utilizing Instantaneous Power and Phase Information,” *IEEE Transactions on Industry Applications*, vol. 28, no. 2, pp. 376–380, 1992.
- [100] S. F. Legowski, A. H. M. Sadrul Ula, and A. M. Trzynadlowski, “Instantaneous Power as a Medium for the Signature Analysis of Induction Motors,” *IEEE Transactions on Industry Applications*, vol. 32, no. 4, pp. 904–909, 1996.
- [101] A. M. Trzynadlowski, M. Ghassemzadeh, and S. F. Legowski, “Diagnostics of Mechanical Abnormalities in Induction Motors Using Instantaneous Electric Power,” *IEEE Transactions on Energy Conversion*, vol. 14, no. 4, pp. 1417–1423, 1999.
- [102] P. Tavner and J. Penman, *Condition Monitoring of Electrical Machines*. Research Studies Press and John Wiley & Sons, 1987.
- [103] M. Drif, N. Benouzza, and J. A. Dente, “Rotor Cage Faults Detection in 3-Phase Induction Motors Using Instantaneous Power Spectrum,” in *Modelling and Simulation of Electric Machines Converters and Systems (IMACS)*, 1999, pp. 287–292.
- [104] S. M. a. Cruz and A. J. M. Cardoso, “Rotor Cage Fault Diagnosis in Three-Phase Induction Motors By The Total Instantaneous Power Spectral Analysis,” *Conference Record of the 1999 IEEE Industry Applications Conference. Thirty-Forth IAS Annual Meeting (Cat. No.99CH36370)*, vol. 3, pp. 1929–1934, 1999.
- [105] a. M. Trzynadlowski and E. Ritchie, “Comparative Investigation of Diagnostic Media for Induction Motors A Case of Rotor Cage Faults,” *IEEE Transactions on Industrial Electronics*, vol. 47, no. 5, pp. 1092–1099, 2000.
- [106] M. Drif, N. Benouzza, A. Bendiabdelah, and J. A. Dente, “Induction motor load effect diagnostic utilizing instantaneous power spectrum,” in *In Proc. of*

- EPE*, 2001.
- [107] Z. Liu, X. Yin, Z. Zhang, D. Chen, and W. Chen, "Online Rotor Mixed Fault Diagnosis Way Based on Spectrum Analysis of Instantaneous Power in Squirrel Cage Induction Motors," *IEEE Transactions on Energy Conversion*, vol. 19, no. 3, pp. 485–490, Sep. 2004.
 - [108] M. Drif and a J. M. Cardoso, "Rotor Cage Fault Diagnostics in Three-Phase Induction Motors, by the Instantaneous Phase-Angle Signature Analysis," in *Proceedings of IEEE International Electric Machines and Drives Conference, IEMDC 2007*, 2007, vol. 2, pp. 1440–1445.
 - [109] M. Drif and A. J. M. Cardoso, "Rotor Cage Fault Diagnostics in Three-Phase Induction Motors, by the Instantaneous Non-Active Power Signature Analysis," in *IEEE International Symposium on Industrial Electronics*, 2007, vol. 3, pp. 1050–1055.
 - [110] M. Drif and A. J. Marques Cardoso, "The Instantaneous Power Factor Approach for Rotor Cage Faults Diagnosis in Three-Phase Induction Motors," in *2008 International Symposium on Power Electronics, Electrical Drives, Automation and Motion*, 2008, pp. 173–178.
 - [111] M. Drif and A. J. Marques Cardoso, "On-line fault diagnostics in operating three-phase induction motors by the active and reactive power media," in *2008 18th International Conference on Electrical Machines*, 2008, pp. 1–6.
 - [112] M. Drif and A. J. M. Cardoso, "The Instantaneous Reactive Power Approach for Rotor Cage Fault Diagnosis in Induction Motor Drives," in *2008 IEEE Power Electronics Specialists Conference*, 2008, pp. 1548–1552.
 - [113] M. Drif and A. J. M. Cardoso, "The Use of the Instantaneous-Reactive-Power Signature Analysis for Rotor-Cage-Fault Diagnostics in Three-Phase Induction Motors," *IEEE Transactions on Industrial Electronics*, vol. 56, no. 11, pp. 4606–4614, Nov. 2009.
 - [114] M. Drif and A. J. Marques Cardoso, "Discriminating the Simultaneous Occurrence of Three-Phase Induction Motor Rotor Faults and Mechanical Load Oscillations by the Instantaneous Active and Reactive Power Media Signature Analyses," *IEEE Transactions on Industrial Electronics*, vol. 59, no. 3, pp. 1630–1639, Mar. 2012.
 - [115] C. H. De Angelo, G. R. Bossio, and G. O. García, "Discriminating Broken Rotor Bar from Oscillating Load Effects Using the Instantaneous Active and Reactive Powers," *IET Electric Power Applications*, vol. 4, no. 4, p. 281, 2010.
 - [116] Y. Maouche, M. El Kamel Oumaamar, M. Boucherma, and A. Khezzar, "A New Approach for Broken Bar Fault Detection in Three-Phase Induction Motor Using Instantaneous Power Monitoring under Low Slip Range," *International Journal of Electrical and Computer Engineering (IJECE)*, vol. 4, no. 1, pp. 52–63, Feb. 2014.
 - [117] K. Yahia, A. J. Marques Cardoso, A. Ghoggal, and S.-E. Zouzou, "Induction Motors Broken Rotor Bars Diagnosis Through the Discrete Wavelet Transform of the Instantaneous Reactive Power Signal under Time-varying Load Conditions," *Electric Power Components and Systems*, vol. 42, no. 7, pp. 682–692, Apr. 2014.
 - [118] J. Kim, S. Shin, S. Bin Lee, K. N. Gyftakis, M. Drif, and A. J. M. Cardoso, "Power Spectrum-Based Detection of Induction Motor Rotor Faults for Immunity to False Alarms," *IEEE Transactions on Energy Conversion*, pp. 1–10, 2015.

- [119] H. W. Penrose and J. Jette, "Static Motor Circuit Analysis: an Introduction to Theory and Application," *IEEE Electrical Insulation Magazine*, vol. 16, no. 4, pp. 6–10, Jul. 2000.
- [120] H. W. Penrose, "Estimating motor life using motor circuit analysis predictive measurements. Part II," in *Conference Record of the 2004 IEEE International Symposium on Electrical Insulation*, 2004, no. September, pp. 15–17.
- [121] V. Climente-Alarcon, J. A. Antonino-Daviu, F. Vedreno-Santos, and R. Puche-Panadero, "Vibration Transient Detection of Broken Rotor Bars by PSH Sidebands," *IEEE Transactions on Industry Applications*, vol. 49, no. 6, pp. 2576–2582, Nov. 2013.
- [122] C. Kral, T. G. Habetler, R. G. Harley, F. Pirker, G. Pascoli, H. Oberguggenberger, and C. J. M. Fenz, "A comparison of rotor fault detection techniques with respect to the assessment of fault severity," in *4th IEEE International Symposium on Diagnostics for Electric Machines, Power Electronics and Drives, 2003. SDEMPED 2003.*, 2003, no. August, pp. 265–270.
- [123] P. J. Tavner, B. G. Gaydon, and D. M. Ward, "Monitoring generators and large motors," *IEE Proceedings B Electric Power Applications*, vol. 133, no. 3, p. 169, 1986.
- [124] M. Kang and J. Kim, "Reliable Fault Diagnosis of Multiple Induction Motor Defects Using a 2-D Representation of Shannon Wavelets," *IEEE Transactions on Magnetics*, vol. 50, no. 10, pp. 1–13, Oct. 2014.
- [125] P. J. McCully, "Evaluation of current and vibration signals for squirrel cage induction motor condition monitoring," in *Eighth International Conference on Electrical Machines and Drives*, 1997, vol. 1997, no. 444, pp. 331–335.
- [126] G. Muller and C. Landy, "A Novel Method to Detect Broken Rotor Bars in Squirrel Cage Induction Motors When Interbar Currents are Present," *IEEE Transactions on Energy Conversion*, vol. 18, no. 1, pp. 71–79, Mar. 2003.
- [127] B. Liang, S. D. Iwnicki, and A. D. Ball, "Asymmetrical Stator and Rotor Faulty Detection Using Vibration, Phase Current and Transient Speed Analysis," *Mechanical Systems and Signal Processing*, vol. 17, no. 4, pp. 857–869, Jul. 2003.
- [128] J. Milimonfared, H. Kelk, S. Nandi, A. D. Minassians, and H. A. Toliyat, "A Novel Approach for Broken-Rotor-Bar Detection in Cage Induction Motors," *IEEE Transactions on Industry Applications*, vol. 35, no. 5, pp. 1000–1006, 1999.
- [129] R. Supangat, J. Grieger, N. Ertugrul, W. L. Soong, D. A. Gray, and C. Hansen, "Detection of Broken Rotor Bar Faults and Effects of Loading in Induction Motors during Rundown," in *2007 IEEE International Electric Machines & Drives Conference*, 2007, pp. 196–201.
- [130] F. Cupertino, E. DeVanna, L. Salvatore, and S. Stasi, "Analysis Techniques for Detection of IM Broken Rotor Bars After Supply Disconnection," *IEEE Transactions on Industry Applications*, vol. 40, no. 2, pp. 526–533, Mar. 2004.
- [131] H. Razik and G. Didier, "A novel method of induction motor diagnosis using the line-neutral voltage," in *Proc. EPE-PEMC, Riga, Latvia*, 2004.
- [132] M. E. K. Oumaamar, F. Babaa, A. Khezzer, and M. Boucherma, "Diagnostics of Broken Rotor Bars in Induction Machines Using the Neutral Voltage," in *International Conference on Electrical Machines*, 2006, no. 679, pp. 1–6.
- [133] F. Babaa, M. E. K. Oumaamar, A. Khezzer, and M. Boucherma, "Multiple Coupled Circuit Modeling of squirrel- cage Induction Motors Including Space

- Harmonics and Line Neutral Voltage,” in *proceedings of the International Conference on Electrical Machines*, 2006, no. 680.
- [134] M. E. K. Oumaamar, A. Khezzar, M. Boucherma, H. Razik, R. N. Andriamalala, and L. Baghli, “Neutral Voltage Analysis for Broken Rotor Bars Detection in Induction Motors Using Hilbert Transform Phase,” in *2007 IEEE Industry Applications Annual Meeting*, 2007, pp. 1940–1947.
- [135] A. Khezzar, M. El Kamel Oumaamar, M. Hadjami, M. Boucherma, and H. Razik, “Induction Motor Diagnosis Using Line Neutral Voltage Signatures,” *IEEE Transactions on Industrial Electronics*, vol. 56, no. 11, pp. 4581–4591, Nov. 2009.
- [136] P. Jayaswal, A. K. Wadhvani, and K. B. Mulchandani, “Machine Fault Signature Analysis,” *International Journal of Rotating Machinery*, vol. 2008, pp. 1–10, 2008.
- [137] A. WIDODO and B. S. YANG, “Wavelet Support Vector Machine for Induction Machine Fault Diagnosis based on Transient Current Signal,” *Expert Systems with Applications*, vol. 35, no. 1–2, pp. 307–316, Jul. 2008.
- [138] J. Wang, S. Liu, R. X. Gao, and R. Yan, “Current Envelope Analysis for Defect Identification and Diagnosis in Induction Motors,” *Journal of Manufacturing Systems*, vol. 31, no. 4, pp. 380–387, 2012.
- [139] S. H. Kia, H. Henao, and G. -a. Capolino, “Diagnosis of Broken-Bar Fault in Induction Machines Using Discrete Wavelet Transform Without Slip Estimation,” *IEEE Transactions on Industry Applications*, vol. 45, no. 4, pp. 1395–1404, Jul. 2009.
- [140] W. Laala, S.-E. Zouzou, and S. Guedidi, “Induction motor broken rotor bars detection using fuzzy logic: experimental research,” *International Journal of System Assurance Engineering and Management*, vol. 5, no. 3, pp. 329–336, 2014.
- [141] I. Jaksch, “Faults diagnosis of three-phase induction motors using envelope analysis,” in *4th IEEE International Symposium on Diagnostics for Electric Machines, Power Electronics and Drives, 2003. SDEMPED 2003.*, 2003, pp. 289–293.
- [142] A. M. da Silva, R. J. Povinelli, and N. A. O. Demerdash, “Induction Machine Broken Bar and Stator Short-Circuit Fault Diagnostics Based on Three-Phase Stator Current Envelopes,” *IEEE Transactions on Industrial Electronics*, vol. 55, no. 3, pp. 1310–1318, Mar. 2008.
- [143] R. Puche-Panadero, M. Pineda-Sanchez, M. Riera-Guasp, J. Roger-Folch, E. Hurtado-Perez, and J. Perez-Cruz, “Improved Resolution of the MCSA Method Via Hilbert Transform, Enabling the Diagnosis of Rotor Asymmetries at Very Low Slip,” *IEEE Transactions on Energy Conversion*, vol. 24, no. 1, pp. 52–59, Mar. 2009.
- [144] W. T. Thomson and D. Rankin, “Case Histories of On-Line Rotor Cage Fault Diagnosis,” in *in Proc. Int. Conf: Condition Monitoring*, 1987, pp. 798–819.
- [145] G. a. Jiménez, A. O. Muñoz, and M. a. Duarte-Mermoud, “Fault Detection in Induction Motors Using Hilbert and Wavelet Transforms,” *Electrical Engineering*, vol. 89, no. 3, pp. 205–220, Feb. 2006.
- [146] D. Matić, F. Kulić, M. Pineda-Sánchez, and I. Kamenko, “Support Vector Machine Classifier for Diagnosis in Electrical Machines: Application to Broken Bar,” *Expert Systems with Applications*, vol. 39, no. 10, pp. 8681–8689, Aug. 2012.
- [147] D. Matic, Z. Kanovic, D. Reljic, F. Kulic, D. Oros, and V. Vasic, “Broken bar

- detection using current analysis-A case study,” in *2013 9th IEEE International Symposium on Diagnostics for Electric Machines, Power Electronics and Drives (SDEMPED)*, 2013, pp. 407–411.
- [148] T. W. S. Chow and H.-Z. Tan, “HOS-Based Nonparametric and Parametric Methodologies for Machine Fault Detection,” *IEEE Transactions on Industrial Electronics*, vol. 47, no. 5, pp. 1051–1059, 2000.
- [149] B. Ayhan and H. J. Trussell, “On the Use of a Lower Sampling Rate for Broken Rotor Bar Detection With DTFT and AR-Based Spectrum Methods,” *IEEE Transactions on Industrial Electronics*, vol. 55, no. 3, pp. 1421–1434, Mar. 2008.
- [150] A. Widodo, B. S. Yang, D. S. Gu, and B. K. Choi, “Intelligent fault diagnosis system of induction motor based on transient current signal,” *Mechatronics*, vol. 19, no. 5, pp. 680–689, Aug. 2009.
- [151] V. T. Tran and B.-S. Yang, “Machine Fault Diagnosis and Condition Prognosis Using Classification and Regression Trees and Neuro-Fuzzy Inference Systems,” *Control and Cybernetics*, vol. 39, no. 1, pp. 25–54, 2010.
- [152] J. Cusido, L. Romeral, J. A. Ortega, J. A. Rosero, and A. Garcia Espinosa, “Fault Detection in Induction Machines Using Power Spectral Density in Wavelet Decomposition,” *IEEE Transactions on Industrial Electronics*, vol. 55, no. 2, pp. 633–643, 2008.
- [153] L. A. García-Escudero, O. Duque-Perez, D. Morinigo-Sotelo, and M. Perez-Alonso, “Robust Condition Monitoring for Early Detection of Broken Rotor Bars in Induction Motors,” *Expert Systems with Applications*, vol. 38, no. 3, pp. 2653–2660, Mar. 2011.
- [154] B. M. Ebrahimi, J. Faiz, and B. Akin, “Pattern Recognition for Broken Bars Fault Diagnosis in Induction Motors Under Various Supply Conditions,” *European Transactions on Electrical Power*, vol. 22, no. 8, pp. 1176–1190, Nov. 2012.
- [155] M. Seera, C. P. Lim, D. Ishak, and H. Singh, “Offline and Online Fault Detection and Diagnosis of Induction Motors using a Hybrid Soft Computing Model,” *Applied Soft Computing*, vol. 13, no. 12, pp. 4493–4507, Dec. 2013.
- [156] E. H. El Bouchikhi, V. Choqueuse, and M. Benbouzid, “Induction Machine Faults Detection Using Stator Current Parametric Spectral Estimation,” *Mechanical Systems and Signal Processing*, vol. 52–53, pp. 447–464, Feb. 2015.
- [157] H. Çalış and A. Çakır, “Experimental Study for Sensorless Broken Bar Detection in Induction Motors,” *Energy Conversion and Management*, vol. 49, no. 4, pp. 854–862, Apr. 2008.
- [158] W. B. Collis, P. R. White, and J. K. Hammond, “Higher-Order Spectra: The Bispectrum and Trispectrum,” *Mechanical Systems and Signal Processing*, vol. 12, no. 3, pp. 375–394, May 1998.
- [159] M. E. H. Benbouzid and G. B. Kliman, “What stator current processing-based technique to use for induction motor rotor faults diagnosis?,” *IEEE Transactions on Energy Conversion*, vol. 18, no. 2, pp. 238–244, 2003.
- [160] B. Liang, S. D. Iwnicki, and Y. Zhao, “Application of power spectrum, cepstrum, higher order spectrum and neural network analyses for induction motor fault diagnosis,” *Mechanical Systems and Signal Processing*, vol. 39, no. 1–2, pp. 342–360, 2013.
- [161] S. Chen, “Induction Machine Broken Rotor Bar Diagnostics Using Prony Analysis,” 2008.

- [162] S. Chen and R. Živanović, “Estimation of Frequency Components in Stator Current for the Detection of Broken Rotor Bars in Induction Machines,” *Measurement*, vol. 43, no. 7, pp. 887–900, Aug. 2010.
- [163] M. Sahraoui, A. J. M. Cardoso, and A. Ghoggal, “The Use of a Modified Prony Method to Track the Broken Rotor Bar Characteristic Frequencies and Amplitudes in Three-Phase Induction Motors,” *IEEE Transactions on Industry Applications*, vol. 51, no. 3, pp. 2136–2147, May 2015.
- [164] D. McGaughey, G. King, and M. Tarbouchi, “Current signature analysis of induction machine rotor faults using the fast orthogonal search algorithm,” in *5th IET International Conference on Power Electronics, Machines and Drives (PEMD 2010)*, 2010, vol. 2010, pp. 215–215.
- [165] G. King, M. Tarbouchi, and D. McGaughey, “Rotor fault detection in induction motors using the fast orthogonal search algorithm,” in *2010 IEEE International Symposium on Industrial Electronics*, 2010, pp. 2621–2625.
- [166] S. Kia, H. Henao, and G. Capolino, “A High-Resolution Frequency Estimation Method for Three-Phase Induction Machine Fault Detection,” *IEEE Transactions on Industrial Electronics*, vol. 54, no. 4, pp. 2305–2314, Aug. 2007.
- [167] I. Aydin, M. Karakose, and E. Akin, “A New Method for Early Fault Detection and Diagnosis of Broken Rotor Bars,” *Energy Conversion and Management*, vol. 52, no. 4, pp. 1790–1799, Apr. 2011.
- [168] S. V. Vaseghi, *Advanced Digital Signal Processing and Noise Reduction*. John Wiley & Sons, 2008.
- [169] V. Climente-Alarcon, J. a. Antonino-Daviu, M. Riera-Guasp, R. Puche-Panadero, and L. Escobar, “Application of The Wigner–Ville Distribution for The Detection of Rotor Asymmetries and Eccentricity Through High-Order Harmonics,” *Electric Power Systems Research*, vol. 91, pp. 28–36, Oct. 2012.
- [170] V. Climente-Alarcon, J. A. Antonino-Daviu, M. Riera-Guasp, and M. Vlcek, “Induction Motor Diagnosis by Advanced Notch FIR Filters and the Wigner–Ville Distribution,” *IEEE Transactions on Industrial Electronics*, vol. 61, no. 8, pp. 4217–4227, Aug. 2014.
- [171] a. K. S. Jardine, D. Lin, and D. Banjevic, “A review on machinery diagnostics and prognostics implementing condition-based maintenance,” *Mechanical Systems and Signal Processing*, vol. 20, no. 7, pp. 1483–1510, 2006.
- [172] I. Daubechies, “The wavelet transform, time-frequency localization and signal analysis,” *IEEE Transactions on Information Theory*, vol. 36, no. 5, pp. 961–1005, 1990.
- [173] S. G. Mallat, “A Theory for Multiresolution Signal Decomposition: the Wavelet Representation,” *IEEE Transactions on Pattern Analysis and Machine Intelligence*, vol. 11, no. 7, pp. 674–693, Jul. 1989.
- [174] H. Keskes and A. Braham, “Recursive Undecimated Wavelet Packet Transform and DAG SVM for Induction Motor Diagnosis,” *IEEE Transactions on Industrial Informatics*, vol. 11, no. 5, pp. 1059–1066, Oct. 2015.
- [175] A. J. Ellison and S. J. Yang, “Effects of Rotor Eccentricity on Acoustic Noise from Induction Machines,” in *Proceedings of the Institution of Electrical Engineers*, 1971, vol. 118, no. 1, p. 174.
- [176] R. Wieser, C. Kral, F. Pirker, and M. Schagginger, “On-line rotor cage monitoring of inverter-fed induction machines by means of an improved method,” *IEEE Transactions on Power Electronics*, vol. 14, no. 5, pp. 858–

- 865, 1999.
- [177] G. G. Acosta, C. J. Verucchi, and E. R. Gelso, "A Current Monitoring System for Diagnosing Electrical Failures in Induction Motors," *Mechanical Systems and Signal Processing*, vol. 20, no. 4, pp. 953–965, May 2006.
- [178] G. Didier, E. Ternisien, O. Caspary, and H. Razik, "A New Approach to Detect Broken Rotor Bars in Induction Machines by Current Spectrum Analysis," *Mechanical Systems and Signal Processing*, vol. 21, no. 2, pp. 1127–1142, Feb. 2007.
- [179] Z. Ye, A. Sadeghian, and B. Wu, "Mechanical Fault Diagnostics for Induction Motor with Variable Speed Drives using Adaptive Neuro-Fuzzy Inference System," *Electric Power Systems Research*, vol. 76, no. 9–10, pp. 742–752, Jun. 2006.
- [180] P. V. J. Rodríguez, M. Negrea, and A. Arkkio, "A Simplified Scheme for Induction Motor Condition Monitoring," *Mechanical Systems and Signal Processing*, vol. 22, no. 5, pp. 1216–1236, Jul. 2008.
- [181] B. Ayhan, M.-Y. Chow, and M.-H. Song, "Multiple Discriminant Analysis and Neural-Network-Based Monolith and Partition Fault-Detection Schemes for Broken Rotor Bar in Induction Motors," *IEEE Transactions on Industrial Electronics*, vol. 53, no. 4, pp. 1298–1308, Jun. 2006.
- [182] R. R. Schoen, B. K. Lin, T. G. Habetler, J. H. Schlag, and S. Farag, "An Unsupervised, On-Line System for Induction Motor Fault Detection Using Stator Current Monitoring," *IEEE Transactions on Industry Applications*, vol. 31, no. 6, pp. 1280–1286, 1995.
- [183] A. Bellini, A. Yazidi, F. Filippetti, C. Rossi, and G.-A. Capolino, "High Frequency Resolution Techniques for Rotor Fault Detection of Induction Machines," *IEEE Transactions on Industrial Electronics*, vol. 55, no. 12, pp. 4200–4209, Dec. 2008.
- [184] S. Günel, D. Gökhan Ece, and Ö. Nezih Gerek, "Induction Machine Condition Monitoring Using Notch-Filtered Motor Current," *Mechanical Systems and Signal Processing*, vol. 23, no. 8, pp. 2658–2670, Nov. 2009.
- [185] V. F. Pires, J. F. Martins, and A. J. Pires, "Eigenvector/Eigenvalue Analysis of a 3D Current Referential Fault Detection and Diagnosis of an Induction Motor," *Energy Conversion and Management*, vol. 51, no. 5, pp. 901–907, May 2010.
- [186] A. Bellini, G. Franceschini, and C. Tassoni, "Monitoring of Induction Machines by Maximum Covariance Method for Frequency Tracking," *IEEE Transactions on Industry Applications*, vol. 42, no. 1, pp. 69–78, Jan. 2006.
- [187] Kyusung Kim and A. Parlos, "Induction motor fault diagnosis based on neuropredictors and wavelet signal processing," *IEEE/ASME Transactions on Mechatronics*, vol. 7, no. 2, pp. 201–219, Jun. 2002.
- [188] Z. Ye, B. Wu, and A. Sadeghian, "Current Signature Analysis of Induction Motor Mechanical Faults by Wavelet Packet Decomposition," *IEEE Transactions on Industrial Electronics*, vol. 50, no. 6, pp. 1217–1228, Dec. 2003.
- [189] H. Bae, S. Kim, Y. T. Kim, and S. Lee, "Application of Time-Series Data Mining for Fault Diagnosis of Induction Motors," in *Computational Science and Its Applications*, 2005, pp. 1085–1094.
- [190] J.-H. Jung, J.-J. Lee, and B.-H. Kwon, "Online Diagnosis of Induction Motors Using MCSA," *IEEE Transactions on Industrial Electronics*, vol. 53, no. 6,

- pp. 1842–1852, Dec. 2006.
- [191] S. Lee, S.-P. Cheon, Y. Kim, and S. Kim, “Fourier and Wavelet Transformations for the Fault Detection of Induction Motor with Stator Current,” in *International Conference on Intelligent Computing*, 2006, pp. 557–569.
- [192] A. Sadeghian, Y. Zhongming, and B. Wu, “Online Detection of Broken Rotor Bars in Induction Motors by Wavelet Packet Decomposition and Artificial Neural Networks,” *IEEE Transactions on Instrumentation and Measurement*, vol. 58, no. 7, pp. 2253–2263, Jul. 2009.
- [193] Y. Liu, L. Guo, Q. Wang, G. An, M. Guo, and H. Lian, “Application to Induction Motor Faults Diagnosis of The Amplitude Recovery Method Combined With FFT,” *Mechanical Systems and Signal Processing*, vol. 24, no. 8, pp. 2961–2971, Nov. 2010.
- [194] J. Cusidó, L. Romeral, J. a. Ortega, A. Garcia, and J. R. Riba, “Wavelet and PDD as fault detection techniques,” *Electric Power Systems Research*, vol. 80, no. 8, pp. 915–924, Aug. 2010.
- [195] F. Briz, M. W. Degner, P. Garcia, and D. Bragado, “Broken Rotor Bar Detection in Line-Fed Induction Machines Using Complex Wavelet Analysis of Startup Transients,” *IEEE Transactions on Industry Applications*, vol. 44, no. 3, pp. 760–768, 2008.
- [196] Z. Zhang, Z. Ren, and W. Huang, “A Novel Detection Method of Motor Broken Rotor Bars Based on Wavelet Ridge,” *IEEE Transactions on Energy Conversion*, vol. 18, no. 3, pp. 417–423, Sep. 2003.
- [197] H. Douglas, P. Pillay, and A. K. Ziarani, “Broken Rotor Bar Detection in Induction Machines With Transient Operating Speeds,” *IEEE Transactions on Energy Conversion*, vol. 20, no. 1, pp. 135–141, Mar. 2005.
- [198] J. A. Antonino-Daviu, M. Riera-Guasp, J. R. Folch, and M. P. M. Palomares, “Validation of a New Method for the Diagnosis of Rotor Bar Failures via Wavelet Transform in Industrial Induction Machines,” *IEEE Transactions on Industry Applications*, vol. 42, no. 4, pp. 990–996, Jul. 2006.
- [199] J. A. Antonino-Daviu, P. Jover Rodriguez, M. Riera-Guasp, M. Pineda-Sánchez, and A. Arkkio, “Detection of Combined Faults in Induction Machines With Stator Parallel Branches Through the DWT of the Startup Current,” *Mechanical Systems and Signal Processing*, vol. 23, no. 7, pp. 2336–2351, Oct. 2009.
- [200] S. M. A. Cruz, A. J. Marques Cardoso, “Rotor Cage Fault Diagnosis in Three-Phase Induction Motors by Extended Park’s Vector Approach,” *Electric Machines & Power Systems*, vol. 28, no. 4, pp. 289–299, Apr. 2000.
- [201] M. Haji and H. Toliyat, “Pattern Recognition-A Technique for Induction Machines Rotor Broken Bar Detection,” *IEEE Transactions on Energy Conversion*, vol. 16, no. 4, pp. 312–317, 2001.
- [202] Zhenxing Liu, Xiaolong Zhang, Xianggen Yin, and Zhe Zhang, “Rotor Cage Fault Diagnosis in Induction Motors Based on Spectral Analysis of Current Hilbert Modulus,” in *IEEE Power Engineering Society General Meeting, 2004.*, 2004, vol. 2, pp. 1500–1503.
- [203] R. Supangat, N. Ertugrul, W. L. Soong, D. A. Gray, C. Hansen, and J. Grieger, “Broken Rotor Bar Fault Detection in Induction Motors Using Starting Current Analysis,” in *European Conference on Power Electronics and Applications*, 2005, p. 10 pp.-pp.P.10.
- [204] A. Khezzar, M. El Kamel Oumaamar, M. Hadjami, M. Boucherma, and H.

- Razik, "Induction Motor Diagnosis Using Line Neutral Voltage Signatures," *IEEE Transactions on Industrial Electronics*, vol. 56, no. 11, pp. 4581–4591, Nov. 2009.
- [205] B.-S. Yang and K. J. Kim, "Application of Dempster–Shafer Theory in Fault Diagnosis of Induction Motors Using Vibration and Current Signals," *Mechanical Systems and Signal Processing*, vol. 20, no. 2, pp. 403–420, Feb. 2006.
- [206] A. Widodo, B. S. Yang, and T. Han, "Combination of Independent Component Analysis and Support Vector Machines for Intelligent Faults Diagnosis of Induction Motors," *Expert Systems with Applications*, vol. 32, no. 2, pp. 299–312, Feb. 2007.
- [207] A. Widodo and B. S. Yang, "Application of Nonlinear Feature Extraction and Support Vector Machines for Fault Diagnosis of Induction Motors," *Expert Systems with Applications*, vol. 33, no. 1, pp. 241–250, Jul. 2007.
- [208] G. Niu, T. Han, B.-S. Yang, and A. C. C. Tan, "Multi-Agent Decision Fusion for Motor Fault Diagnosis," *Mechanical Systems and Signal Processing*, vol. 21, no. 3, pp. 1285–1299, Apr. 2007.
- [209] V. T. Tran, B.-S. Yang, M.-S. Oh, and A. C. C. Tan, "Fault Diagnosis of Induction Motor Based on Decision Trees and Adaptive Neuro-fuzzy Inference," *Expert Systems with Applications*, vol. 36, no. 2, pp. 1840–1849, Mar. 2009.
- [210] G. F. Bin, J. J. Gao, X. J. Li, and B. S. Dhillon, "Early fault diagnosis of rotating machinery based on wavelet packets—Empirical mode decomposition feature extraction and neural network," *Mechanical Systems and Signal Processing*, vol. 27, pp. 696–711, 2012.
- [211] H. Keskes, A. Braham, and Z. Lachiri, "Broken rotor bar diagnosis in induction machines through Stationary Wavelet Packet Transform under lower sampling rate," in *2012 First International Conference on Renewable Energies and Vehicular Technology*, 2012, vol. 97, pp. 452–459.
- [212] M. R. Mehrjou, N. Mariun, M. Karami, N. Misron, S. Toosi, and M. R. Zare, "Evaluation of Wavelet-Functions for Broken Rotor Bar Detection of Induction Machine Using Coefficient-Related Features," *International Journal of Applied Electronics in Physics & Robotics*, vol. 1, no. 1, pp. 18–23, 2013.
- [213] A. Reece and T. Preston, *Finite Element Methods in Electrical Power Engineering*. Courier Corporation, 2000.
- [214] M. K. Chari and P. Silvester, "Analysis of Turboalternator Magnetic Fields by Finite Elements," *IEEE Transactions on Power Apparatus and Systems*, vol. PAS-90, no. 2, pp. 454–464, Mar. 1971.
- [215] A. Y. Hannalla and D. C. MacDonald, "Numerical Analysis of Transient Field Problems in Electric Machines," in *IEE Proceedings*, 1976, pp. 893–898.
- [216] S. Tandon, A. Armor, and M. V. K. Chari, "Nonlinear Transient Finite Element Field Computation for Electrical Machines and Devices," *IEEE Transactions on Power Apparatus and Systems*, vol. PAS-102, no. 5, pp. 1089–1096, May 1983.
- [217] S. Ho, W. Fu, and H. Wong, "Application of Automatic Choice of Step Size for Time Stepping Finite Element Method to Induction Motors," *IEEE Transactions on Magnetics*, vol. 33, no. 2, pp. 1370–1373, Mar. 1997.
- [218] M. a. Jabbar, Zhejie Liu, and Jing Dong, "Time-Stepping Finite-Element Analysis for the Dynamic Performance of a Permanent Magnet Synchronous Motor," *IEEE Transactions on Magnetics*, vol. 39, no. 5, pp. 2621–2623, Sep.

- 2003.
- [219] T. Göktaş, M. Arkan, and Ö. F. Özgüven, "Detection of rotor fault in three-phase induction motor in case of low-frequency load oscillation," *Electrical Engineering*, vol. 97, no. 4, pp. 337–345, 2015.
 - [220] H. Akcay and E. Germen, "Subspace-Based Identification of Acoustic Noise Spectra in Induction Motors," *IEEE Transactions on Energy Conversion*, vol. 30, no. 1, pp. 32–40, Mar. 2015.
 - [221] T. Han, B.-S. Yang, W.-H. Choi, and J.-S. Kim, "Fault Diagnosis System of Induction Motors Based on Neural Network and Genetic Algorithm Using Stator Current Signals," *International Journal of Rotating Machinery*, vol. 2006, pp. 1–13, 2006.
 - [222] J. Ben Ali, N. Fnaiech, L. Saidi, B. Chebel-Morello, and F. Fnaiech, "Application of empirical mode decomposition and artificial neural network for automatic bearing fault diagnosis based on vibration signals," *Applied Acoustics*, vol. 89, no. 2015, pp. 16–27, Mar. 2015.
 - [223] A. Sapena-Bano, M. Pineda-Sanchez, R. Puche-Panadero, J. Martinez-Roman, and Z. Kanovic, "Low-Cost Diagnosis of Rotor Asymmetries in Induction Machines Working at a Very Low Slip Using the Reduced Envelope of the Stator Current," *IEEE Transactions on Energy Conversion*, pp. 1–11, 2015.
 - [224] J. Zhang, N. Zhu, L. Yang, Q. Yao, and Q. Lu, "A Fault Diagnosis Approach for Broken Rotor Bars Based on EMD and Envelope Analysis," *Journal of China University of Mining and Technology*, vol. 17, no. 2, pp. 205–209, Jun. 2007.
 - [225] B. Mirafzal and N. a O. Demerdash, "Effects of Load Magnitude on Diagnosing Broken Bar Faults in Induction Motors Using the Pendulous Oscillation of the Rotor Magnetic Field Orientation," *IEEE Transactions on Industry Applications*, vol. 41, no. 3, pp. 771–783, 2005.
 - [226] J. Pons-Llinares, J. A. Antonino-Daviu, M. Riera-Guasp, S. Bin Lee, T. J. Kang, and C. Yang, "Advanced Induction Motor Rotor Fault Diagnosis Via Continuous and Discrete Time–Frequency Tools," *IEEE Transactions on Industrial Electronics*, vol. 62, no. 3, pp. 1791–1802, 2015.
 - [227] E. Y. Hamid and Z.-I. Kawasaki, "Wavelet-based data compression of power system disturbances using the minimum description length criterion," *IEEE Transactions on Power Delivery*, vol. 17, no. 2, pp. 460–466, Apr. 2002.
 - [228] M. Pineda-Sanchez, M. Riera-Guasp, J. A. Antonino-Daviu, J. Roger-Folch, J. Perez-Cruz, and R. Puche-Panadero, "Instantaneous Frequency of the Left Sideband Harmonic During the Start-Up Transient: A New Method for Diagnosis of Broken Bars," *IEEE Transactions on Industrial Electronics*, vol. 56, no. 11, pp. 4557–4570, Nov. 2009.
 - [229] J. Tukey, *Exploratory data analysis*. Addison-Wesley, 1977.
 - [230] M. R. Spiegel, J. Schiller, and A. Srinivasan, *Theory And Problems Of Probability And Statistics*. McGraw-Hill Education, 2003.
 - [231] R. Christensen, "Analysis of Variance, Design, and Regression: Applied Statistical Methods," Chapman and Hall/CRC, 1996.
 - [232] M. Riera-Guasp, J. A. Antonino-Daviu, J. Rusek, and J. Roger-Folch, "Diagnosis of Rotor Asymmetries in Induction Motors Based on the Transient Extraction of Fault Components Using Filtering Techniques," *Electric Power Systems Research*, vol. 79, no. 8, pp. 1181–1191, Aug. 2009.
 - [233] V. T. Tran, F. AlThobiani, A. Ball, and B.-K. Choi, "An Application to Transient Current Signal Based Induction Motor Fault diagnosis of Fourier–

Bessel expansion and Simplified Fuzzy ARTMAP,” *Expert Systems with Applications*, vol. 40, no. 13, pp. 5372–5384, Oct. 2013.

- [234] E. Cabal-Yepez, R. J. Romero-Troncoso, A. Garcia-Perez, and R. a. Osornio-Rios, “Single-Parameter Fault Identification Through Information Entropy Analysis at the Startup-Transient Current in Induction Motors,” *Electric Power Systems Research*, vol. 89, pp. 64–69, Aug. 2012.



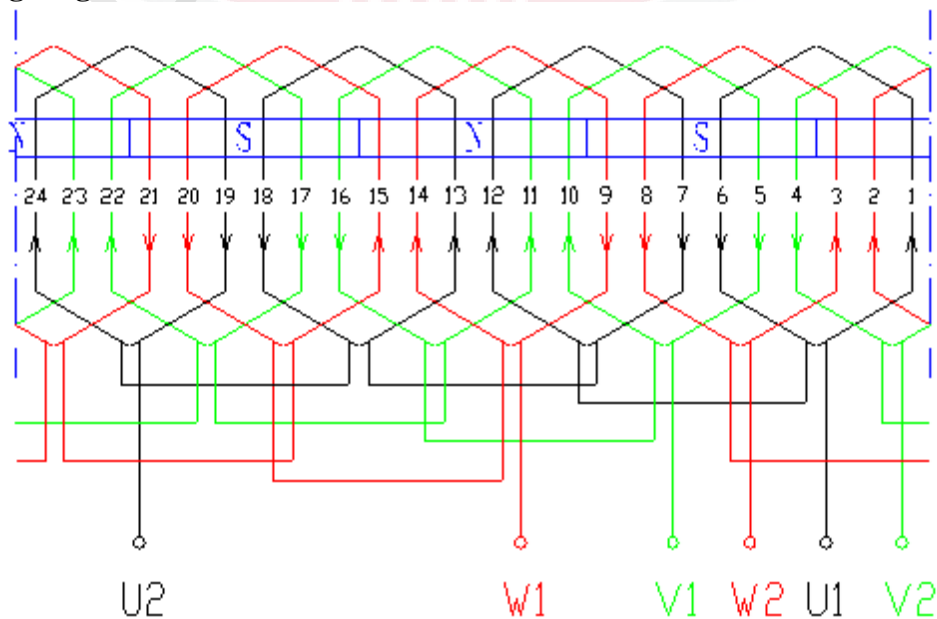
APPENDICES

APPENDIX A

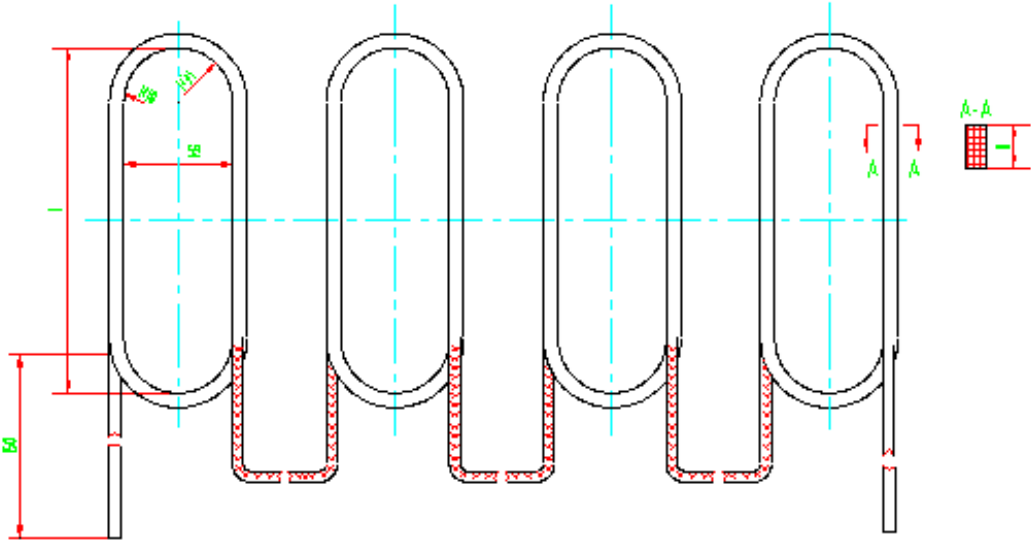
The specifications and dimensions of the machine

Three-phase permanent magnet synchronous motor electromagnetic design single								
Model	TA80MB-4	Power	0.75 kW		Reference frequency	50 Hz	Number of poles	4
Voltage	415V	Electric current	1.28 A		Torque	4.8 N.m	定额	S1
Stator			Stator punching through Y80-4 Stator oblique one stator slot 9.8mm Rotor punching RP075026216-TA Permanent magnet NdFeB N38SH25×30×4.5, 12bar			Rotor		
Outer diameter	120	Outer diameter				74.4		
Inner diameter	75	Inner diameter				26		
Total length	75	Total length				75		
The number of slots	24	The number of slots				16		
Air gap	0.30	-----				-----		
Wire	QZ-2/155	Leads				Aluminum AL99.7		
AWG	Φ0.53	Line regulation				Cast aluminum		
The number of lines per slot	139	The size of the end of the circle				60 mm ²		
Number of lines per lap	139	Main Performance						
Winding way	Monolayer chain	Performance indicators	Standard	Design	Test			
Parallel ones	1	Each part of the loss	Design value	Experimental values	Performance%	83.50	85.04	
Wiring	Y	The stator copper consumption W	90		Power Factor	0.98	0.980	
Pitch	1-6	The rotor copper consumption W	---		Out torque	2.00	2.11	
Slot insulation thickness	0.25	Iron loss W	23		Minimum torque	---	---	
Slot fill factor	74.7 %	Mechanical losses W	12		Stall current	---	---	
Insulation class	F	Stray loss W	7		Stall torque	---	---	
Phase resistor	19.154Ω	Total loss W	132		Noise LW	---	---	
Thermal load	1006	EMF V	195.4		Vibration mm / s	---	---	
General								
Silicon steel sheet	DR510-50	8.26 kg						
Stator wire	QZ-2/155 Φ0.53	1.15 kg						
Rotor conductors	Aluminum ingots for remeltingAL99.7	0.12 kg						
Cited wiring	Rubber sheathed cable 0.50	3×150 mm						

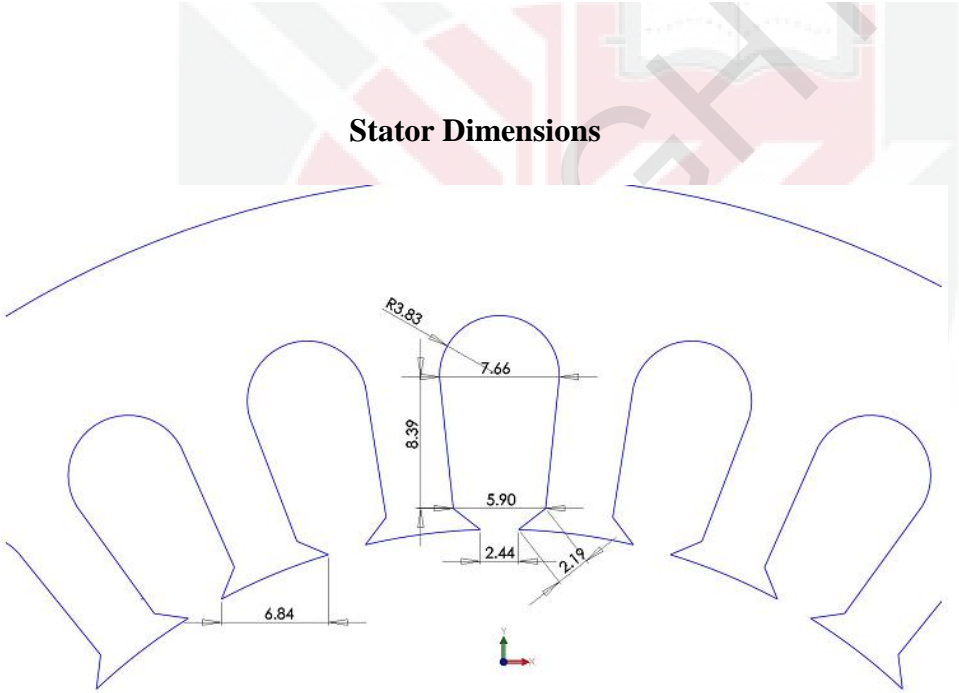
Winding diagram



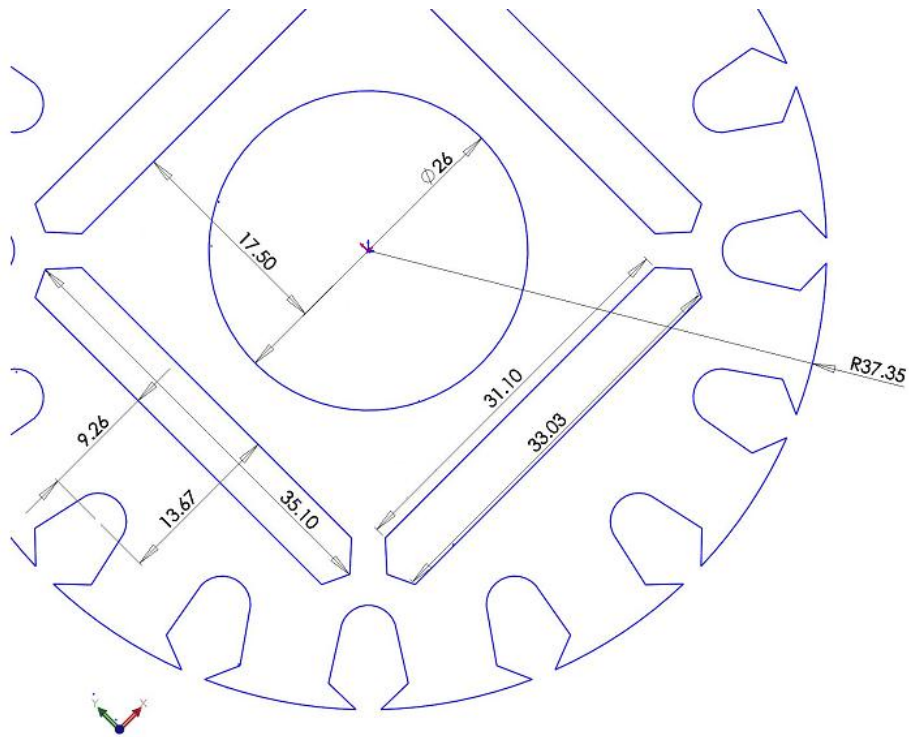
Coil Diagram



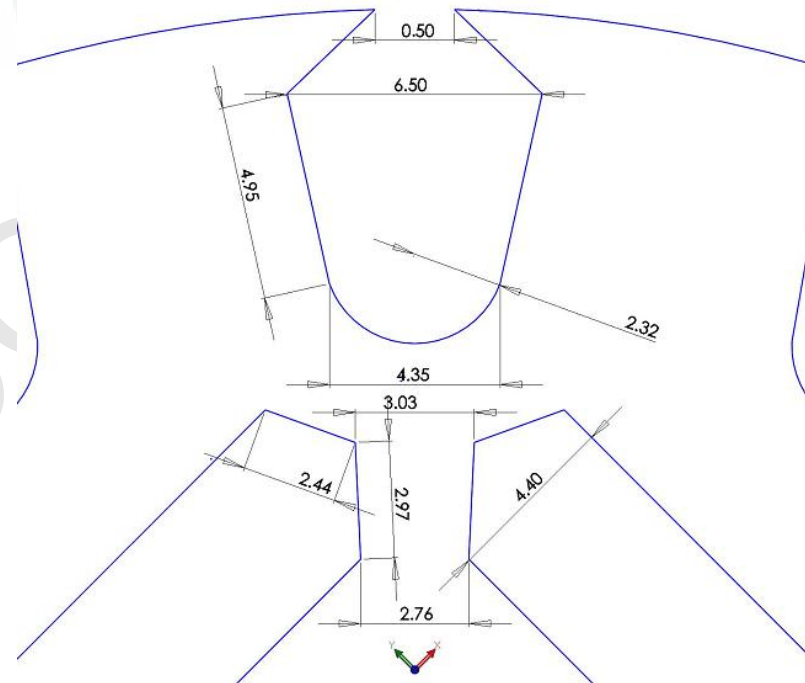
Stator Dimensions



Rotor Dimensions



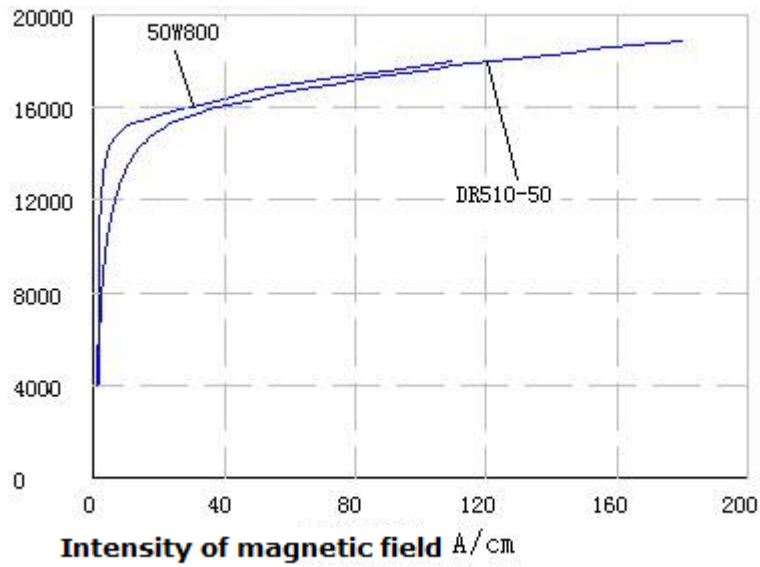
Rotor Dimensions



APPENDIX B

The B-H curve and Iron loss curve for stator and rotor lamination.

Intensity of magnetization(Gs)



50W800 and DR510-50 B-H Curve

Intensity of magnetization, Gs

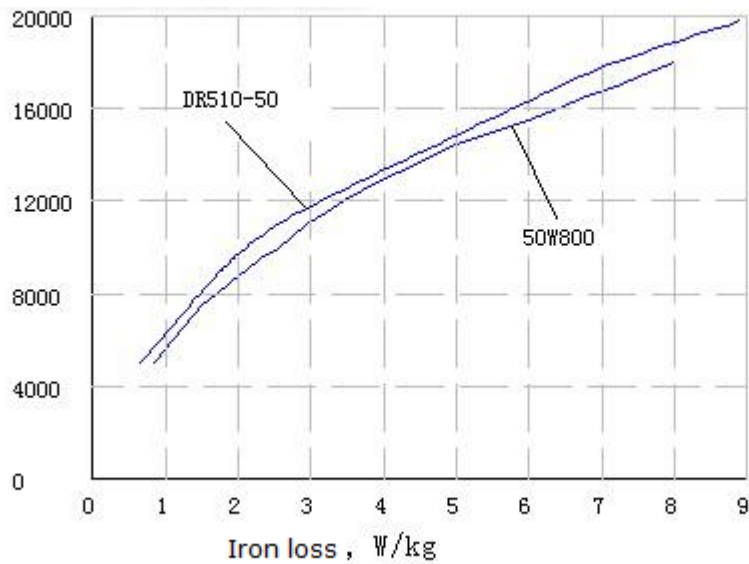


图4 50W800和DR510-50 Iron loss curve

APPENDIX C

The details of permanent magnet



N38SH

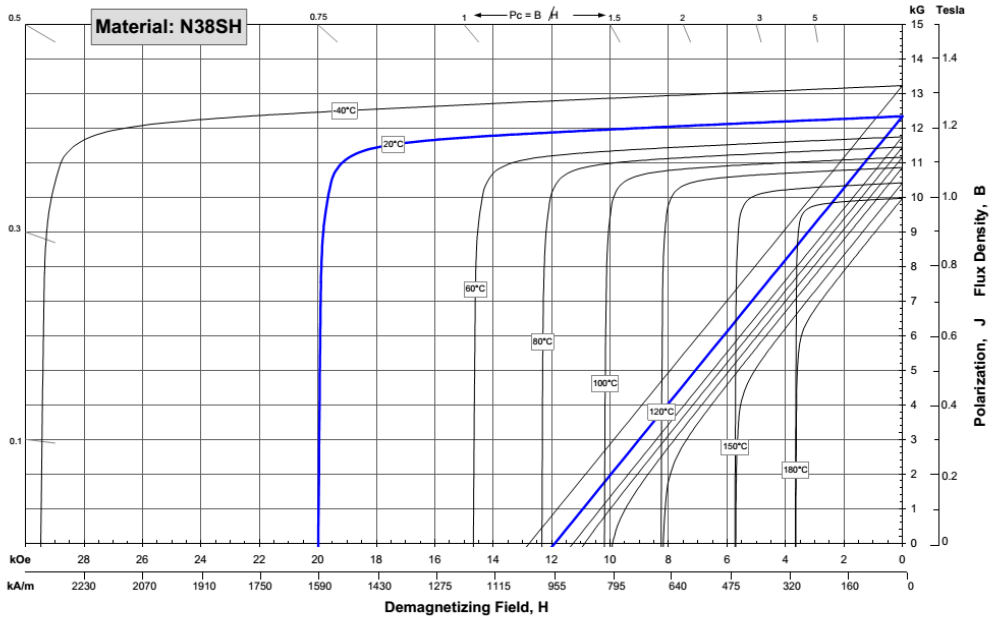
Sintered Neodymium-Iron-Boron Magnets

These are also referred to as "Neo" or NdFeB magnets. They offer a combination of high magnetic output at moderate cost. Please contact Arnold for additional grade information and recommendations for protective coating. Assemblies using these magnets can also be provided.

Characteristic	Units	Units		
		min.	nominal	max.
Br , Residual Induction	Gauss	12,200	12,350	12,500
	mT	1220	1235	1250
H_{cb} , Coercivity	Oersteds	11,400	11,700	12,000
	kA/m	907	931	955
H_{cj} , Intrinsic Coercivity	Oersteds	20,000		
	kA/m	1,592		
BH_{max} , Maximum Energy Product	MGOe	36	38	39
	kJ/m ³	287	299	310

Characteristic	Units	C //	C. I.
Reversible Temperature Coefficients ⁽¹⁾			
of Induction, α(Br)	%/°C		-0.12
of Coercivity, α(H _{cj})	%/°C		-0.55
Coefficient of Thermal Expansion ⁽²⁾	ΔL/L per °C×10 ⁻⁶	7.5	-0.1
Thermal Conductivity	kcal/mhr°C	5.3	5.8
Specific Heat ⁽³⁾	cal/g°C		0.11
Curie Temperature, T _c	°C		340
Other Properties	Flexural Strength	psi	41,300
		MPa	285
	Density	g/cm ³	7.5
	Hardness, Vickers	Hv	620
Electrical Resistivity, ρ	μΩ • cm		180

Notes: (1) Coefficients measured between 20 and 150 °C
(2) Between 20 and 200 °C
(3) Between 20 and 140 °C



Notes The material data and demagnetization curves shown above represent typical properties that may vary due to product shape and size. Demagnetization curves show nominal Br and minimum Hci. Magnets can be supplied thermally stabilized or magnetically calibrated to customer specifications. Additional grades are available. Please contact the factory for information.



Rev. 100924b

© Arnold Magnetic Technologies Corp.
770 Linden Avenue, Rochester, NY 14625
Ph: (+1) 585-385-9010

E-mail: info@arnoldmagnetics.com
www.arnoldmagnetics.com

APPENDIX D

The specifications of current transducer.



Current Transducer LTS 25-NP

$I_{PN} = 25 \text{ At}$

For the electronic measurement of currents : DC, AC, pulsed, mixed, with a galvanic isolation between the primary circuit (high power) and the secondary circuit (electronic circuit).



Electrical data

I_{PN}	Primary nominal current rms	25	At
I_{PN}	Primary current, measuring range	0 .. ± 80	At
V_{OUT}	Output voltage (Analog) @ $I_p = 0$	$2.5 \pm (0.625 \cdot I_p / I_{PN})$	V
		2.5 ¹⁾	V
G	Sensitivity	25	mV/A
N_s	Number of secondary turns ($\pm 0.1\%$)	2000	
R_L	Load resistance	≥ 2	k Ω
R_{IM}	Internal measuring resistance ($\pm 0.5\%$)	50	Ω
TCR_{IM}	Temperature coefficient of R_{IM}	< 50	ppm/K
V_C	Supply voltage ($\pm 5\%$)	5	V
I_C	Current consumption @ $V_C = 5 \text{ V}$	Typ $28 + I_S^2 \cdot (V_{OUT} / R_L)$	mA

Accuracy - Dynamic performance data

X	Accuracy @ $I_{PN}, T_A = 25^\circ\text{C}$	± 0.2	%
	Accuracy with R_{IM} @ $I_{PN}, T_A = 25^\circ\text{C}$	± 0.7	%
ϵ_L	Linearity error	< 0.1	%
TCV_{OUT}	Temperature coefficient of V_{OUT} @ $I_p = 0$	Typ 50 Maxi 100	ppm/K
		150	ppm/K
TCG	Temperature coefficient of G	50 ³⁾	ppm/K
V_{OM}	Magnetic offset voltage @ $I_p = 0$, after an overload of	$3 \times I_{PN}$ $5 \times I_{PN}$ $10 \times I_{PN}$	± 0.5 ± 2.0 ± 2.0 mV
t_{ra}	Reaction time @ 10% of I_{PN}	< 100	ns
t_r	Response time to 90% of I_{PN} step	< 400	ns
di/dt	di/dt accurately followed	> 60	A/ μs
BW	Frequency bandwidth (0 .. -0.5 dB) (-0.5 .. 1 dB)	DC .. 100 DC .. 200	kHz

General data

T_A	Ambient operating temperature	-40 .. +85	$^\circ\text{C}$
T_S	Ambient storage temperature	-40 .. +100	$^\circ\text{C}$
	Insulating material group	III a	
m	Mass	10	g
	Standards ⁴⁾	EN 50178: 1997 IEC 60950-1: 2001	

Notes: ¹⁾ Absolute value @ $T_A = 25^\circ\text{C}$, $2.475 < V_{OUT} < 2.525$

²⁾ $I_S = I_p / N_s$

³⁾ Only due to TCR_{IM}

⁴⁾ Specification according to IEC 61000-4-3 are not guaranteed between 180 and 220 MHz.

Features

- Closed loop (compensated) multi-range current transducer using the Hall effect
- Unipolar voltage supply
- Isolated plastic case recognized according to UL 94-V0
- Compact design for PCB mounting
- Incorporated measuring resistance
- Extended measuring range.

Advantages

- Excellent accuracy
- Very good linearity
- Very low temperature drift
- Optimized response time
- Wide frequency bandwidth
- No insertion losses
- High immunity to external interference
- Current overload capability.

Applications

- AC variable speed drives and servo motor drives
- Static converters for DC motor drives
- Battery supplied applications
- Uninterruptible Power Supplies (UPS)
- Switched Mode Power Supplies (SMPS)
- Power supplies for welding applications.

Application domain

- Industrial

Copyright protected.

APPENDIX E

The M-file was written in MATLAB® workspace for signal processing.

Time Domain Analysis

```
load('Healthy.mat')
a=1;

for i=1:4; % Loop for different Load

    for j = 1:40; Loop for different sample

        % open the file
        file_name=Healthy{i,j};
        data = load(file_name);
        A = struct2cell(data);
        B= cell2mat(A);

        % ----- Calculation of Statistical Feature based on Time domain ----- %
        X=B(:,2);
        RMS = rms(X);
        RSSQ = rssq(X); % Root-sum-of-squares level
        KURTOSIS = kurtosis(X);
        SKEWNESS = skewness(X);
        Mean = mean(X); % mean
        Variance = moment(X,2); % variance
        PtoP = peak2peak(X); % Peak-to-Peak
        PtoRMS = peak2rms(X); % CrestFactor
        PAPR = ((max(X))^2)/((rms(X))^2); % Peak-to-average power ratio(dB)
        ShapeFactor = rms(X)/mean(X);
        ImpulseFactor = max(abs(X))/mean(X);
        RootX= abs((X.^0.5));
        MarginFactor = max(abs(X))/(sum(RootX)/N)^2; %N:lenght X
        Energy = sum(X.^2);

        ResultRMS(j,a) = RMS; % 1
        ResultRSSQ(j,a) = RSSQ; % 2
        ResultKurtosis(j,a) = KURTOSIS; % 3
        ResultSkewness(j,a) = SKEWNESS; % 4
        ResultMean(j,a) = Mean; % 5
        ResultVariance(j,a) = Variance; % 6
        ResultPtoP(j,a) = PtoP; % 7
        ResultPtoRMS(j,a) = PtoRMS; % 8
        ResultPAPR(j,a) = PAPR; % 9
        ResultShapeFactor(j,a) = ShapeFactor; % 10
        ResultImpulseFactor(j,a) = ImpulseFactor; % 11
        ResultMarginFactor(j,a) = MarginFactor; % 12
        ResultEnergy(j,a) = Energy; % 13

        clear RMS RSSQ KURTOSIS SKEWNESS Mean MOMENT2
        clear PtoP PtoRMS PAPR ShapeFactor ImpulseFactor MarginFactor HistogramLower
        clear HistogramUpper RootX Energy X A B

    end % Loop for different sample
    a=a+2;

end % Loop for different Load
clear i j a
```

```

load('Faulty.mat')
a=2;

for i=1:4; % Loop for different Load

    for j = 1:40; Loop for different sample

        % open the file
        file_name=Faulty{i,j};
        data = load(file_name);
        A = struct2cell(data);
        B= cell2mat(A);

        % ----- Calculation of Statistical Feature based on Time domain ----- %
        X=B (:,2);
        RMS = rms(X);
        RSSQ = rssq(X); % Root-sum-of-squares level
        KURTOSIS = kurtosis(X);
        SKEWNESS = skewness(X);
        Mean = mean(X); % mean
        Variance = moment(X,2); % variance
        PtoP = peak2peak(X); % Peak-to-Peak
        PtoRMS = peak2rms(X); % CrestFactor
        PAPR = ((max(X))^2)/((rms(X))^2); % Peak-to-average power ratio(dB)
        ShapeFactor = rms(X)/mean(X);
        ImpulseFactor = max(abs(X))/mean(X);
        RootX= abs(X.^0.5);
        MarginFactor = max(abs(X))/(sum(RootX)/N)^2; %N:lenght X
        Energy = sum(X.^2);

        ResultRMS(j,a) = RMS; % 1
        ResultRSSQ(j,a) = RSSQ; % 2
        ResultKurtosis(j,a) = KURTOSIS; % 3
        ResultSkewness(j,a) = SKEWNESS; % 4
        ResultMean (j,a) = Mean; % 5
        ResultVariance (j,a) = Variance; % 6
        ResultPtoP(j,a) = PtoP; % 7
        ResultPtoRMS(j,a) = PtoRMS; % 8
        ResultPAPR(j,a) = PAPR; % 9
        ResultShapeFactor(j,a) = ShapeFactor; % 10
        ResultImpulseFactor(j,a) = ImpulseFactor; % 11
        ResultMarginFactor(j,a) = MarginFactor; % 12
        ResultEnergy(j,a) = Energy; % 13

        clear RMS RSSQ KURTOSIS SKEWNESS Mean MOMENT2
        clear PtoP PtoRMS PAPR ShapeFactor ImpulseFactor MarginFactor HistogramLower
        clear HistogramUpper RootX Energy X A B

    end % Loop for different sample
    a=a+2;

end % Loop for different Load
clear i j a

```

Time Domain Analysis based on Envelope Signal

```

load('Healthy.mat')
a=1;
for i=1:4; % Loop for different Load

    for j = 1:40; Loop for different sample

        % open the file
        file_name=Healthy{i,j};
        data = load(file_name);
        A = struct2cell(data);
        B= cell2mat(A);

        % ----%Calculation of Statistical Feature based on Time - Envelope ----- %
        P=B (:,2);
        [up,lo]=envelope (P);
        X=up;
        N = length(X); % N: number of row in X
        RMS = rms(X);
        RSSQ = rssq(X); % Root-sum-of-squares level
        KURTOSIS = kurtosis(X);
        SKEWNESS = skewness(X);
        Mean = mean(X);
        Variance = moment(X,2); % variance
        PtoP = peak2peak(X);
        PtoRMS = peak2rms(X); % CrestFactor or peak-to-RMS ratio
        LogDectect = exp(mean(log(abs(X))));
        PAPR = ((max(X)^2)/((rms(X))^2); % peak-to-average power ratio(dB)
        ShapeFactor = rms(X)/mean(X);
        ImpulseFactor = max(abs(X))/mean(X);
        RootX= abs((X.^0.5));
        MarginFactor = max(abs(X))/(sum(RootX)/N)^2;
        Energy = sum(X.^2);

        ResultRMS(j,a) = RMS; % 1
        ResultRSSQ(j,a) = RSSQ; % 2
        ResultKurtosis(j,a) = KURTOSIS; % 3
        ResultSkewness(j,a) = SKEWNESS; % 4
        ResultMean (j,a) = Mean; % 5
        ResultVariance (j,a) = Variance; % 6
        ResultPtoP(j,a) = PtoP; % 7
        ResultPtoRMS(j,a) = PtoRMS; % 8
        ResultPAPR(j,a) = PAPR; % 9
        ResultShapeFactor(j,a) = ShapeFactor; % 10
        ResultImpulseFactor(j,a) = ImpulseFactor; % 11
        ResultMarginFactor(j,a) = MarginFactor; % 12
        ResultEnergy(j,a) = Energy; % 13

        clear RMS RSSQ KURTOSIS SKEWNESS Mean MOMENT2
        clear PtoP PtoRMS PAPR ShapeFactor ImpulseFactor MarginFactor
        clear RootX LogDectect Energy X N P up lo A B

    end % Loop for different sample

a=a+2;

end % Loop for different Load
clear i j w a

```



```

load('Faulty.mat')
a=2;

for i=1:4; % Loop for different Load

    for j = 1:40; Loop for different sample

        % open the file
        file_name=Faulty{i,j};
        data = load(file_name);
        A = struct2cell(data);
        B= cell2mat(A);

        % ----% Calculation of Statistical Feature based on Time - Envelope ----- %
        P=B(:,2);
        [up,lo]=envelope(P);
        X=up;
        N = length(X); % N:number of row in X
        RMS = rms(X);
        RSSQ = rssq(X); % Root-sum-of-squares level
        KURTOSIS = kurtosis(X);
        SKEWNESS = skewness(X);
        Mean = mean(X);
        Variance = moment(X,2); % variance
        PtoP = peak2peak(X);
        PtoRMS = peak2rms(X); % CrestFactor
        LogDectect = exp(mean(log(abs(X))));
        PAPR = ((max(X)^2)/((rms(X))^2); % peak-to-average power ratio(dB)
        ShapeFactor = rms(X)/mean(X);
        ImpulseFactor = max(abs(X))/mean(X);
        RootX= abs(X.^0.5);
        MarginFactor = max(abs(X))/(sum(RootX)/N)^2;
        Energy = sum(X.^2);

        ResultRMS(j,a) = RMS; % 1
        ResultRSSQ(j,a) = RSSQ; % 2
        ResultKurtosis(j,a) = KURTOSIS; % 3
        ResultSkewness(j,a) = SKEWNESS; % 4
        ResultMean(j,a) = Mean; % 5
        ResultVariance(j,a) = Variance; % 6
        ResultPtoP(j,a) = PtoP; % 7
        ResultPtoRMS(j,a) = PtoRMS; % 8
        ResultPAPR(j,a) = PAPR; % 9
        ResultShapeFactor(j,a) = ShapeFactor; % 10
        ResultImpulseFactor(j,a) = ImpulseFactor; % 11
        ResultMarginFactor(j,a) = MarginFactor; % 12
        ResultEnergy(j,a) = Energy; % 13

        clear RMS RSSQ KURTOSIS SKEWNESS Mean MOMENT2
        clear PtoP PtoRMS PAPR ShapeFactor ImpulseFactor MarginFactor
        clear RootX Energy X N A B P up lo

    end % Loop for different sample

a=a+2;

end % Loop for different Load

clear i j a

```

Anova and Post-Hoc Analysis

```
X= ResultEnergy(:); % The feature that need to be test
[p,tbl,stats,terms] = anovan(X,{Load2 MotorCondition2},'model','full','varnames',{'Load',
'MotorCondition'});
results = multcompare((stats),'CType','tukey-kramer','alpha',0.05,'Dimension',[1 2]);
% ++++++ Input ++++++
% We can additionally set the alpha level using the 'alpha' function followed
% by our alphavalue (in this case, 0.05).
% 'ctype' is then used to specify what type of test we want to use.
% Additionally, we can substitute in:
% 'hsd' or 'tukey-kramer' for the Tukey's honest significant difference criterion.
% 'lsd' for Tukey's least significant difference procedure.
% 'dun-sidak' which uses critical values from the t-distribution after an adjustment for
% multiple comparisons proposed by Dunn and proved accurate by Sidak (hence, DunnSidak).
% 'scheffe' which uses critical values from Scheffe's S-procedure, derived from the Fdistribution.
% ++++++ Output ++++++
% "The return value COMPARISON is a matrix with one row per comparison and six columns.
% Columns 1-2 are the indices of the two samples being compared.
% Columns 3-5 are a lower bound, estimate, and upper bound for their difference.
% The fourth column shows the difference between the estimated group means.
% The third and fifth columns show the lower and upper limits for 95% confidence intervals for the
true mean difference.
% Column 6 is the p-value for each individual comparison.
```

Time-Frequency Domain Analysis with Anova test

```

load('Healthy.mat')
load('Faulty.mat')
load('Motherwavelet102.mat')
load('MotorCondition1.mat') %for Anova
load('Load1.mat') %for Anova
load('ResultTable.mat') %for Anova
load('Folder.mat') %for Anova
load('MAT.mat') %for Anova

CD{1,1}={'Type'};
CD{1,2}={'LevelDec.'};
for g=1:20;
    CD{1,g+2}={ResultTable{1,g}};
end
clear g

Level= input('Enter Number of Level>');

for motherorder = 1:102; %Wavelet packet calculation based on different mother wavelet
    a=1; %for matrix of feature

    for i=1:4; % Loop for different Load

        for j = 1:40; Loop for different sample

            % open the Healthy file
            file_name_H=Healthy{i,j};
            dataH = load(file_name_H);
            AH = struct2cell(dataH);
            BH= cell2mat(AH);
            DH=BH(:,2);

            % wavelet analysis for Healthy

            [CH,LH]= wavedec(DH ,Level,Motherwavelet125{1,motherorder});
            cDLevelH = detcoef(CH,LH,Level);
            DLevelH = wrcoef('d',CH,LH,Motherwavelet125{1,motherorder},Level

            % ----- Statistical Features calculation for Healthy ----- %
            % ----- based on reconstruct signal at detail of level ----- %

            XH=DLevelH;
            NH = length(XH); % N:number of row in X
            Entropyshannon = wentropy(XH,'shannon');
            Entropylogenergy = wentropy(XH,'log energy');

            ResultEntropyshannon (j,a) = Entropyshannon;
            ResultEntropylogenergy (j,a) = Entropylogenergy;

            clear file_name_H dataH AH BH DH
            clear CH LH cDLevelH DLevelH
            clear XH NH Entropyshannon Entropylogenergy

        end % Loop for different sample
    end
end

```

```

%-----Faulty - 40 Sample-----%

a=a+1;

for j = 1:40; Loop for different sample

% open the file
file_name_F=Faulty{i,j};
dataF = load(file_name_F);
AF = struct2cell(dataF);
BF= cell2mat(AF);
DF=BF(:,2);

% wavelet analysis

[CF,LF]= wavedec(DF ,Level,Motherwavelet125{1,motherorder});
cDLevelF = detcoef(CF,LF,Level);
DLevelF = wrcoef('d',CF,LF,Motherwavelet125{1,motherorder},Level);

% ----- Statistical Features calculation for Faulty ----- %
% ----- based on reconstruct signal at detail of level ----- %

XF=DLevelF;
NF = length(XF);      % N:number of row in X
Entropyshannon = wentropy(XF,'shannon');
Entropylogenergy = wentropy(XF,'log energy');

ResultEntropyshannon (j,a) = Entropyshannon;
ResultEntropylogenergy (j,a) = Entropylogenergy;

clear file_name_F dataF AF BF DF
clear CF LF cDLevelF DLevelF
clear XF NF Entropyshannon Entropylogenergy

end % Loop for different sample

a=a+1;
end % Loop for different Load

%%%%%%%%%-----Anova and Post-Hoc Test-----%%%%%%%%%
for n=1:3;
file_name_A=ResultTable{1,n};
save(file_name_A,file_name_A)
dataA = load(file_name_A);
DeleteSaveFile = strcat(Folder,file_name_A,MAT);
delete(DeleteSaveFile);
AA = struct2cell(dataA);
BA= cell2mat(AA);

k=1;
for i=1:2:8;
for j=1:40;
DA(k,:)=BA(j,i);
k=k+1;
end
end

for i=2:2:8;

```

```

    for j=1:40;
        DA(k,:)=BA(j,i);
        k=k+1;
    end
end

[p,Atbl,stats,terms] = anovan(DA,{MotorCondition1 Load1},'model','full','varnames',
{'MotorCondition','Load'},'display','off');
PostHoc_Results = multcompare((stats),'CType','tukey-kramer','alpha',0.05,'Dimension',[1 2],
'Display','off');

p_value(1,1)=cell2mat(Atbl(2,7)); %anovan(MotorCondition)
p_value(2,1)=cell2mat(Atbl(3,7)); %anovan(Load)
p_value(3,1)=cell2mat(Atbl(4,7)); %anovan(Intraction)
p_value(4,1)=PostHoc_Results(1,6);
p_value(5,1)=PostHoc_Results(14,6);
p_value(6,1)=PostHoc_Results(23,6);
p_value(7,1)=PostHoc_Results(28,6);

if all(p_value < 0.05)
    q(motherorder,n)=1;
else
    q(motherorder,n)=0;
end

CD{motherorder+1,1}={Motherwavelet125{1,motherorder}};
CD{motherorder+1,n+2}=q(motherorder,n);

clear i j p stats terms PostHoc_Results file_name_A DeleteSaveFile
clear dataA DA BA AA Atbl p_value

end

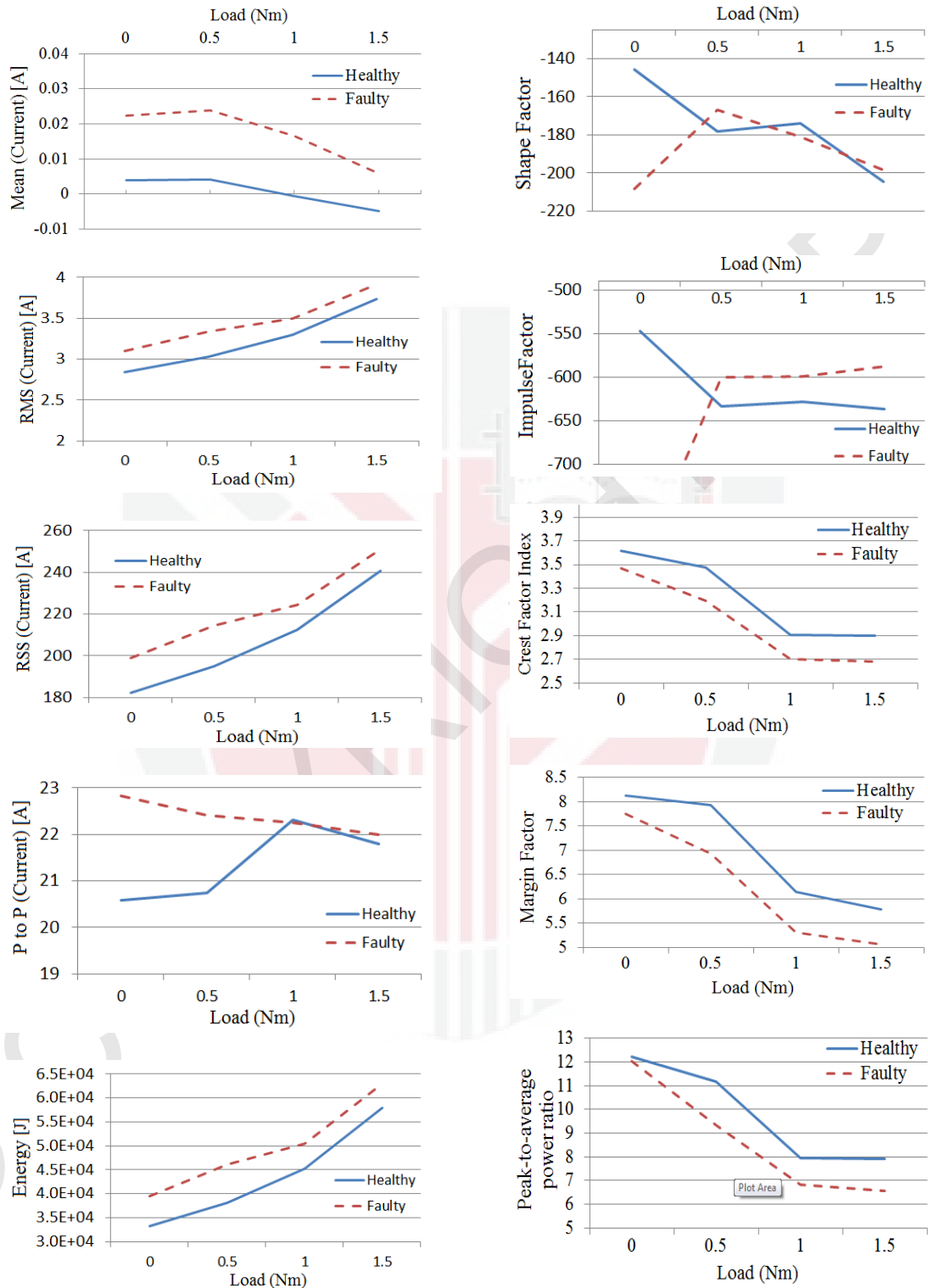
clear ResultEntropyshannon ResultEntropylogenergy

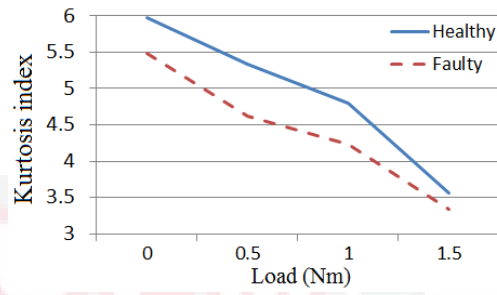
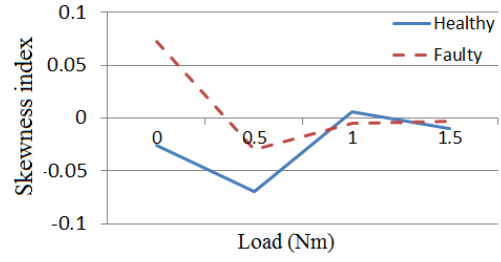
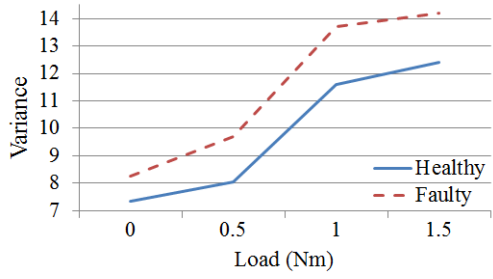
end % Loop for different Mother wavelet
clear k a Level q n

```

APPENDIX F

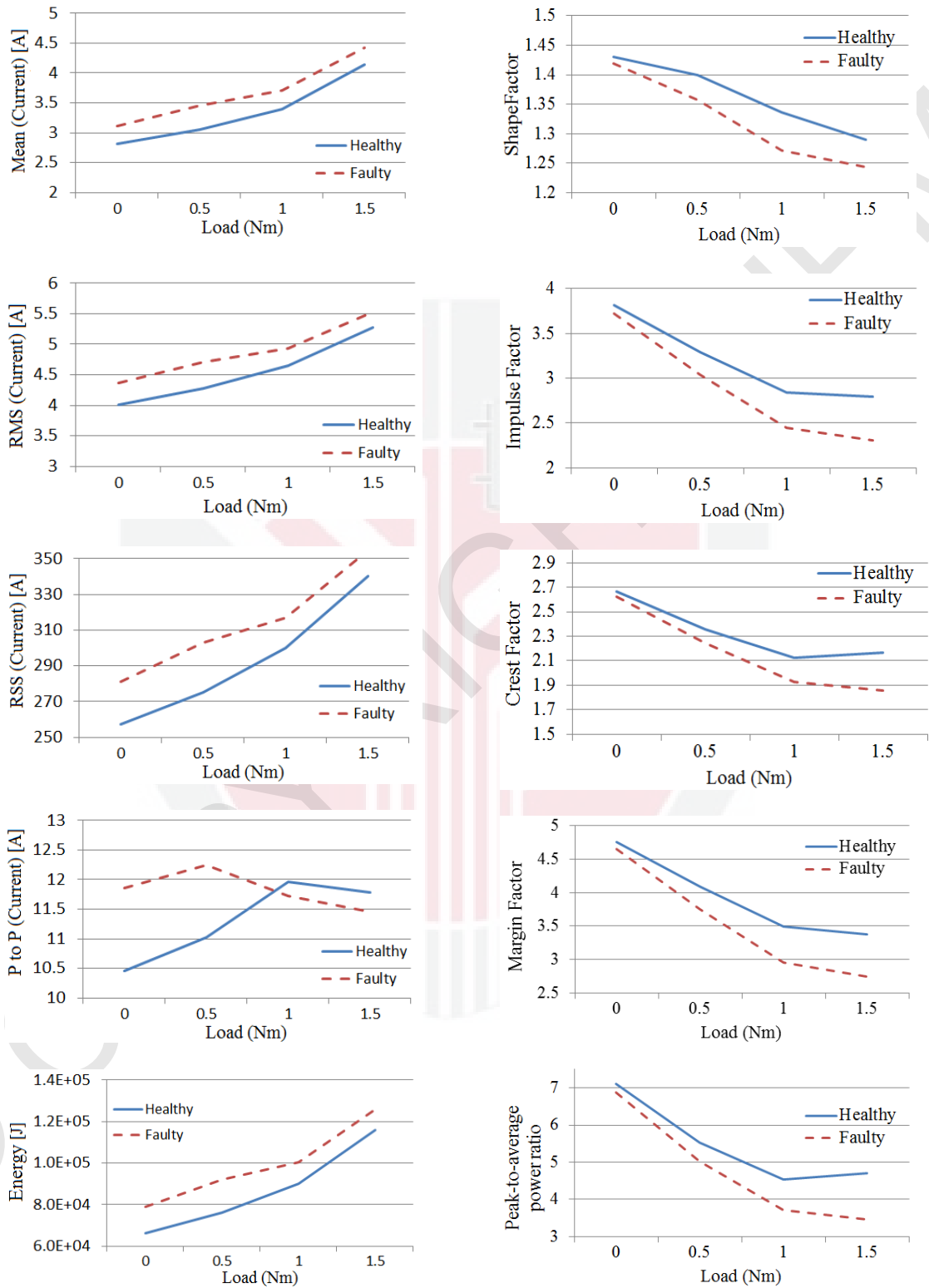
Simulation Result in Time Domain Analysis

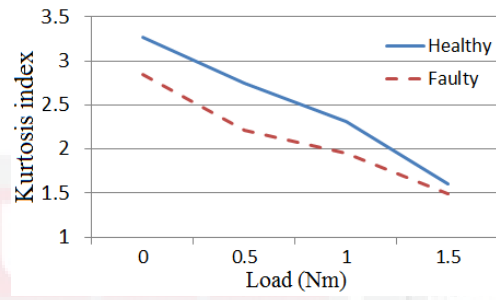
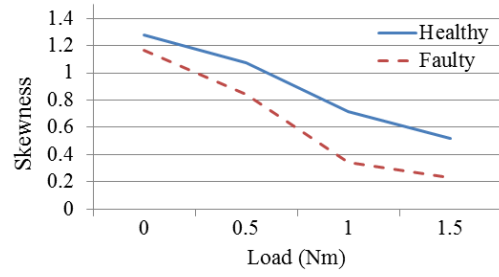
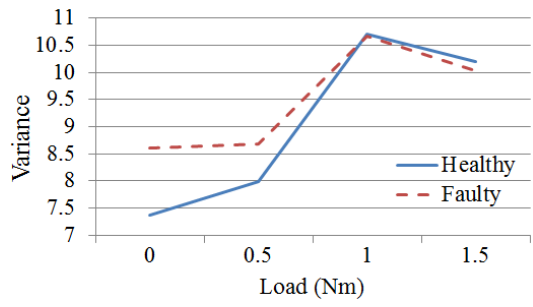




APPENDIX G

Simulation Result for Time Domain Analysis based on Envelope Signal





APPENDIX H

The result of features evaluation in approximation of level 6 using simulation data

Mother Wavelet	Features		Mother Wavelet	Features	
	Shannon Entropy	Log Energy Entropy		Shannon Entropy	Log Energy Entropy
'dmey'	-	-	'sym5'	-	Y
'haar'	-	-	'sym6'	-	Y
'db1'	-	-	'sym7'	-	Y
'db2'	-	-	'sym8'	-	Y
'db3'	-	-	'sym9'	-	Y
'db4'	-	Y	'sym10'	-	Y
'db5'	-	Y	'sym11'	-	Y
'db6'	-	Y	'sym12'	-	Y
'db7'	-	Y	'sym13'	-	Y
'db8'	-	Y	'sym14'	-	Y
'db9'	-	Y	'sym15'	-	Y
'db10'	-	Y	'sym16'	-	Y
'db11'	-	Y	'sym17'	-	Y
'db12'	-	Y	'sym18'	-	Y
'db13'	-	Y	'sym19'	-	Y
'db14'	-	Y	'sym20'	-	-
'db15'	-	Y	'coif1'	-	-
'db16'	-	Y	'coif2'	-	-
'db17'	-	Y	'coif3'	-	Y
'db18'	-	Y	'coif4'	-	Y
'db19'	-	Y	'coif5'	-	Y
'db20'	-	Y	'bior1.1'	-	-
'db21'	-	Y	'bior1.3'	-	-
'db22'	-	Y	'bior1.5'	-	-
'db23'	-	Y	'bior2.2'	-	-
'db24'	-	Y	'bior2.4'	-	-
'db25'	-	Y	'bior2.6'	-	-
'db26'	-	Y	'bior2.8'	-	-
'db27'	-	Y	'bior3.1'	-	Y
'db28'	-	Y	'bior3.3'	-	Y
'db29'	-	Y	'bior3.5'	-	Y
'db30'	-	-	'bior3.7'	-	Y
'db31'	-	-	'bior3.9'	-	-
'db32'	-	-	'bior4.4'	-	-
'db33'	-	-	'bior5.5'	-	-
'db34'	-	-	'bior6.8'	-	-
'db35'	-	-	'rbio1.1'	-	-
'db36'	-	-	'rbio1.3'	-	-
'db37'	-	-	'rbio1.5'	-	-
'db38'	-	-	'rbio2.2'	-	Y
'db39'	-	-	'rbio2.4'	-	Y
'db40'	-	-	'rbio2.6'	-	Y
'db41'	-	-	'rbio2.8'	-	Y
'db42'	-	-	'rbio3.1'	-	Y
'db43'	-	-	'rbio3.3'	-	Y
'db44'	-	-	'rbio3.5'	-	Y
'db45'	-	-	'rbio3.7'	-	Y
'sym1'	-	Y	'rbio3.9'	-	Y
'sym2'	-	Y	'rbio4.4'	-	-
'sym3'	-	Y	'rbio5.5'	-	-
'sym4'	-	Y	'rbio6.8'	-	-

**The result of features evaluation in Detail of level 7
using simulation data**

Mother Wavelet	Features		Mother Wavelet	Features	
	Shannon Entropy	Log Energy Entropy		Shannon Entropy	Log Energy Entropy
'dmey'	-	Y	'sym5'	-	Y
'haar'	-	-	'sym6'	-	Y
'db1'	-	-	'sym7'	-	Y
'db2'	-	-	'sym8'	-	Y
'db3'	-	-	'sym9'	-	Y
'db4'	-	-	'sym10'	-	Y
'db5'	-	-	'sym11'	-	Y
'db6'	-	-	'sym12'	-	Y
'db7'	-	Y	'sym13'	-	Y
'db8'	-	Y	'sym14'	-	Y
'db9'	-	Y	'sym15'	-	Y
'db10'	-	Y	'sym16'	-	Y
'db11'	-	Y	'sym17'	-	-
'db12'	-	Y	'sym18'	-	-
'db13'	-	Y	'sym19'	-	-
'db14'	-	Y	'sym20'	-	-
'db15'	-	Y	'coif1'	-	Y
'db16'	-	Y	'coif2'	-	Y
'db17'	-	Y	'coif3'	-	Y
'db18'	-	Y	'coif4'	-	Y
'db19'	-	Y	'coif5'	-	Y
'db20'	-	Y	'bior1.1'	-	-
'db21'	-	Y	'bior1.3'	-	-
'db22'	-	Y	'bior1.5'	-	-
'db23'	-	Y	'bior2.2'	-	Y
'db24'	-	Y	'bior2.4'	-	Y
'db25'	-	Y	'bior2.6'	-	Y
'db26'	-	Y	'bior2.8'	-	Y
'db27'	-	Y	'bior3.1'	-	Y
'db28'	-	Y	'bior3.3'	-	Y
'db29'	-	Y	'bior3.5'	-	Y
'db30'	-	Y	'bior3.7'	-	Y
'db31'	-	Y	'bior3.9'	-	Y
'db32'	-	Y	'bior4.4'	-	Y
'db33'	-	-	'bior5.5'	-	Y
'db34'	-	-	'bior6.8'	-	Y
'db35'	-	-	'rbio1.1'	-	-
'db36'	-	-	'rbio1.3'	-	-
'db37'	-	-	'rbio1.5'	-	-
'db38'	-	-	'rbio2.2'	-	Y
'db39'	-	-	'rbio2.4'	-	Y
'db40'	-	-	'rbio2.6'	-	Y
'db41'	-	-	'rbio2.8'	-	Y
'db42'	-	-	'rbio3.1'	-	Y
'db43'	-	-	'rbio3.3'	-	Y
'db44'	-	-	'rbio3.5'	-	Y
'db45'	-	-	'rbio3.7'	-	Y
'sym1'	-	Y	'rbio3.9'	-	Y
'sym2'	-	Y	'rbio4.4'	-	Y
'sym3'	-	Y	'rbio5.5'	-	Y
'sym4'	-	Y	'rbio6.8'	-	Y

**The result of features evaluation in approximation of level 7
using simulation data**

Mother Wavelet	Features		Mother Wavelet	Features	
	Shannon Entropy	Log Energy Entropy		Shannon Entropy	Log Energy Entropy
'dmey'	-	Y	'sym5'	-	Y
'haar'	-	-	'sym6'	-	Y
'db1'	-	-	'sym7'	-	-
'db2'	-	Y	'sym8'	-	-
'db3'	-	Y	'sym9'	-	-
'db4'	-	Y	'sym10'	-	-
'db5'	-	Y	'sym11'	-	-
'db6'	-	Y	'sym12'	-	-
'db7'	-	Y	'sym13'	-	-
'db8'	-	Y	'sym14'	-	-
'db9'	-	-	'sym15'	-	-
'db10'	-	-	'sym16'	-	-
'db11'	-	-	'sym17'	-	-
'db12'	-	-	'sym18'	-	-
'db13'	-	-	'sym19'	-	-
'db14'	-	-	'sym20'	-	-
'db15'	-	-	'coif1'	-	-
'db16'	-	-	'coif2'	-	-
'db17'	-	-	'coif3'	-	-
'db18'	-	-	'coif4'	-	-
'db19'	-	-	'coif5'	-	-
'db20'	-	-	'bior1.1'	-	-
'db21'	-	-	'bior1.3'	-	-
'db22'	-	-	'bior1.5'	-	-
'db23'	-	-	'bior2.2'	-	-
'db24'	-	-	'bior2.4'	-	-
'db25'	-	-	'bior2.6'	-	-
'db26'	-	-	'bior2.8'	-	-
'db27'	-	-	'bior3.1'	-	Y
'db28'	-	-	'bior3.3'	-	Y
'db29'	-	-	'bior3.5'	-	Y
'db30'	-	-	'bior3.7'	-	Y
'db31'	-	-	'bior3.9'	-	Y
'db32'	-	-	'bior4.4'	-	Y
'db33'	-	-	'bior5.5'	-	Y
'db34'	-	-	'bior6.8'	-	-
'db35'	-	-	'rbio1.1'	-	Y
'db36'	-	-	'rbio1.3'	-	Y
'db37'	-	-	'rbio1.5'	-	Y
'db38'	-	-	'rbio2.2'	-	Y
'db39'	-	-	'rbio2.4'	-	Y
'db40'	-	-	'rbio2.6'	-	Y
'db41'	-	-	'rbio2.8'	-	Y
'db42'	-	-	'rbio3.1'	-	-
'db43'	-	-	'rbio3.3'	-	-
'db44'	-	-	'rbio3.5'	-	-
'db45'	-	-	'rbio3.7'	-	-
'sym1'	-	-	'rbio3.9'	-	-
'sym2'	-	-	'rbio4.4'	-	-
'sym3'	-	Y	'rbio5.5'	-	-
'sym4'	-	Y	'rbio6.8'	-	-

BIODATA OF STUDENT

Mohammad Rezazadeh Mehrjou was born in Tehran, Iran. He got his B.Sc. degree in Electrical Power Engineering from Islamic Azad University, South Tehran branch. After B.Sc. graduating he started to work as Electrical Engineering of the quality control department of Pars Switch Board Company, Iran. After one year he got a job offer to work as Supervisor of Technical Office in South Pars Gas Field. He continued his corporation with Gas and Oil field as well as Refinery for about 5 years. At 2007, he decided to continue his study and started Master of Science in Department of Electrical Engineering Universiti Putra Malaysia. He got his M.Sc. degree in Electrical Power Engineering from University Putra Malaysia at 2011, currently; he is pursuing PhD degree in Department of Electrical and Electronic Engineering, Faculty of Engineering, Universiti Putra Malaysia. His research was under financial support provided by the Ministry of Higher Education Malaysia with project number of FRGS: 5524356 entitled “Intelligent fault detection scheme for line start permanent magnet synchronous motors”. He is also got a Special Graduate Research Allowance from Ministry of high education Malaysian during his PhD. His research interests include electrical motors, fault detection and condition monitoring techniques.

LIST OF PUBLICATIONS

Book Chapter

M.R.Mehrjou, et al., Wavelet-based Analysis of MCSA for Fault Detection in Electrical Machine, InTech, Wavelet Transform and Some of Its Real-World Applications, ISBN 978-953-51-2230-2, 2015.

Journal

M.R. Mehrjou, et al., Evaluation of Wavelet-Functions for Broken Rotor Bar Detection of Induction Machine using Coefficient-Related Features, *International Journal of Applied Electronics in Physics and Robotics*, 1(1) 2013. (Index-Cited Publication)

M. Karami, N. Mariun, M.R. Mehrjou, MZAMAb Kadir, N Mison, MA Mohd Radzi, Static Eccentricity Fault Recognition in Three-Phase Line Start Permanent Magnet Synchronous Motor Using Finite Element Method. *Mathematical Problems in Engineering*, 2014. (ISI-Q2)

M.R. Mehrjou, et al., Wireless Sensors System for Broken Rotor bar Fault Monitoring using Wavelet Analysis, *IOP Conference Series: Materials Science and Engineering (MSE)*, 99 (1), 2015. (Index-Scopus)

M.R. Mehrjou, et al., Analysis of Statistical Features based on Start-up Current Envelope for Broken Rotor Bar Fault Detection in Line Start Permanent Magnet Synchronous Motor, *Electrical Engineering*, (ISI-Q3)

S. Zolfaghari, S.B.M. Noor, M.H. Marhaban, N. Mariun, M.R. Mehrjou, Broken Rotor Bar Fault Detection in No Load Condition Based on Wavelet Packet Signature Analysis. *International Journal of Control Theory and Applications*, 2016. (Index-Cited Publication)

M.R. Mehrjou, et al., Broken Rotor Bar Fault Detection of Line Start Permanent Magnet Synchronous Motor using Binary Logistic Statistical Method. *Journal of the Chinese Institute of Engineers*, 2017. (ISI-Q4)

J. C. Quiroz, N. Mariun, M. R. Mehrjou, M. Izadi, N. Mison, M.A.M. Radzi, Fault Detection of Broken Rotor Bar in LS-PMSM Using Random Forests. *Measurement*, 2017, Under review (ISI-Q2)

M.R. Mehrjou, et al., A New Method for Broken Rotor Bar Fault Detection in Line Start Permanent Magnet Synchronous Motors under No-Load Condition. *Journal of Mechanical Science and Technology*, Under review (ISI-Q3)

Conference

M.R.Mehrjou, et al., Performance analysis of line-start permanent magnet synchronous motor in presence of rotor fault. *IEEE Student Conference*

- on In Research and Development (SCORed, 2014), Malaysia, pp. 1-4, (Index-Cited Publication).
- M.R.Mehrjou, et al., Statistical Features Analysis of Transient Current Signal for Broken Bars Fault Detection in LS-PMSMs. IEEE The International Conference on Smart Instrumentation, Measurement and Application (ICSIMA, 2015), Putrajaya, Malaysia. (Index-Cited Publication)
- M.R.Mehrjou, et al., Broken Rotor Bar Detection in LS-PMSMs Based on Statistical Features Analysis of Start-up Current Envelope. IEEE The International Conference on Smart Instrumentation, Measurement and Application (ICSIMA, 2015), Putrajaya, Malaysia. (Index-Cited Publication)
- M.R.Mehrjou, et al., A Survey of Broken Rotor Bar Detection Using PT and HT in Squirrel Cage Electrical Machine. IEEE Student Conference on Research and Development (SCORed, 2015). Kuala Lumpur, Malaysia. (Index-Cited Publication)
- M. Izadi, N. Mariun, M.R. Mehrjou, M.Z.A. Ab Kadir, N. Mison, M.A.M. Radzi, Broken Rotor Bar Fault Detection in Line Start Permanent Magnet Synchronous Motor Using Transient Current Signal. IEEE International Conference on Automatic Control and Intelligent Systems, 2016. (Index-Cited Publication)
- S. Zolfaghari, S.B. Mohd Noor, M.H. Marhaban, N. Mariun, M.R. Mehrjou, Broken Rotor Bar Fault Detection in No Load Condition Based on Wavelet Packet Signature Analysis. International Conference on Electrical & Electronic Technology (2016)



UNIVERSITI PUTRA MALAYSIA

STATUS CONFIRMATION FOR THESIS / PROJECT REPORT AND COPYRIGHT

ACADEMIC SESSION : _____

TITLE OF THESIS / PROJECT REPORT :

Broken Rotor Bar Fault Detection in Line start-Permanent Magnet Synchronous Motors

NAME OF STUDENT : Mohammad Rezazadeh Mehjoei

I acknowledge that the copyright and other intellectual property in the thesis/project report belonged to Universiti Putra Malaysia and I agree to allow this thesis/project report to be placed at the library under the following terms:

- 1. This thesis/project report is the property of Universiti Putra Malaysia.
- 2. The library of Universiti Putra Malaysia has the right to make copies for educational purposes only.
- 3. The library of Universiti Putra Malaysia is allowed to make copies of this thesis for academic exchange.

I declare that this thesis is classified as :

*Please tick (v)

CONFIDENTIAL

(Contain confidential information under Official Secret Act 1972).

RESTRICTED

(Contains restricted information as specified by the organization/institution where research was done).

OPEN ACCESS

I agree that my thesis/project report to be published as hard copy or online open access.

This thesis is submitted for :

PATENT

Embargo from _____ until _____
(date) (date)

Approved by:

Norman Mariun

Mohjoei
(Signature of Student)
New IC No/ Passport No.:
X95385806
Date : 29,05,2017

(Signature of Chairman of Supervisory Committee)
Name: **PROFESSOR IR. DR. NORMAN MARIUN**
Head
Date : **Centre of Advanced Power and Energy Research (CAPER)**

[Note : If the thesis is CONFIDENTIAL or RESTRICTED, please attach the letter from the organization/institution with period and reasons for confidentiality.

Universiti Putra Malaysia
43400 UPM Serdang
Selangor Malaysia